University of Alberta

De novo design of alpha-helical coiled-coils
and beta-sheet cyclic antimicrobial peptides

by

Darin Lindsay Lee ©

A thesis submitted to the Faculty of Graduate Studies and Research in partial
fulfillment of the requirements for the degree of Doctor of Philosophy

Department of Biochemistry

Edmonton, Alberta
Fall 2003

National Library
of Canada

Acquisitions and
Bibliographic Services

395 Wellington Street
Ottawa ON K1A 0N4
Canada

Bibliothèque nationale
du Canada

Acquisisitons et
services bibliographiques

395, rue Wellington
Ottawa ON K1A 0N4
Canada

Your file Votre référence
ISBN: 0-612-88010-9
Our file Notre référence
ISBN: 0-612-88010-9

The author has granted a non-exclusive licence allowing the National Library of Canada to reproduce, loan, distribute or sell copies of this thesis in microform, paper or electronic formats.

L'auteur a accordé une licence non exclusive permettant à la Bibliothèque nationale du Canada de reproduire, prêter, distribuer ou vendre des copies de cette thèse sous la forme de microfiche/film, de reproduction sur papier ou sur format électronique.

The author retains ownership of the copyright in this thesis. Neither the thesis nor substantial extracts from it may be printed or otherwise reproduced without the author's permission.

L'auteur conserve la propriété du droit d'auteur qui protège cette thèse. Ni la thèse ni des extraits substantiels de celle-ci ne doivent être imprimés ou aturement reproduits sans son autorisation.

In compliance with the Canadian Privacy Act some supporting forms may have been removed from this dissertation.

Conformément à la loi canadienne sur la protection de la vie privée, quelques formulaires secondaires ont été enlevés de ce manuscrit.

While these forms may be included in the document page count, their removal does not represent any loss of content from the dissertation.

Bien que ces formulaires aient inclus dans la pagination, il n'y aura aucun contenu manquant.

Canada

University of Alberta

Library Release Form

Name of Author: Darin Lindsay Lee

Title of Thesis: De novo design of alpha-helical coiled-coils and beta-sheet cyclic antimicrobial peptides

Degree: Doctor of Philosophy

Year this Degree Granted: 2003

Permission is hereby granted to the University of Alberta Library to reproduce single copies of this thesis and to lend or sell such copies for private, scholarly or scientific research purposes only.

The author reserves all other publication and other rights in association with the copyright in the thesis, and except as herein before provided, neither the thesis nor any substantial portion thereof may be printed or otherwise reproduced in any material form whatever without the author's prior written permission.

Date: August 14, 2003.

University of Alberta

Faculty of Graduate Studies and Research

The undersigned certify that they have read, and recommend to the Faculty of Graduate Studies and Research for acceptance, a thesis entitled *De novo design of alpha-helical coiled-coils and beta-sheet cyclic antimicrobial peptides* submitted by Darin Lindsay Lee in partial fulfillment of the requirements for the degree of Doctor of Philosphophy.

Dr. Robert S. Hodges
(supervisor)

Dr. Brian D. Sykes

Dr. Luis Agellon

Dr. Randall T. Irvin

Dr. Tom Alber
(external examiner)

Date: Aug 12, 2003

This thesis is dedicated to

my grandmother, Laura Suey Ying Chan

my parents, Julie Cho Lee and Kan Cecil Lee

and my brother, Rodney Christopher Lee

Abstract

Our laboratory has investigated the relationship between amino acid sequence and stability requirements for peptide folding into two-stranded α-helical coiled-coil structures, a common structural motif in many naturally occurring proteins. In particular, we examined a 14-residue 'consensus trigger sequence' that was found in several different coiled-coil sequences, as it relates to folding and stability. We demonstrated that the presence of a 'consensus trigger sequence' does not guarantee folding of two-stranded coiled-coils, and is not essential for folding but rather, any sequence that stabilizes coiled-coil structure beyond a minimum threshold level will suffice. The high-resolution X-ray crystal structure of a *de novo*-designed coiled-coil that lacks the 'consensus trigger sequence' reveals numerous stabilizing factors including a complex interchain ion-pairing and hydrogen-bonding network across a destabilizing central asparagine residue located in the hydrophobic core of the structure, as well as stabilization through hydrophobic interactions of leucine residues located at the hydrophobic interface (positions ***e*** and ***g*** of the heptad repeat, $[\boldsymbol{abcdefg}]_n$).

We have also performed structure-activity studies on 14-residue cyclic cationic peptides to elucidate the key design features responsible for their selective toxicity towards microbial organisms *vs.* mammalian cells, *i.e.* a high therapeutic index. Based on the structural template of GS14, an amphipathic (nonpolar and polar residues localized to opposite faces of the molecule) β-sheet cyclic cationic peptide, a diastereomeric analog with D-Lys at position 4 (peptide GS14K4) showed greatly improved microbial specifity with little toxicity to human red blood cells over GS14 (Kondejewski *et al.* 1999, J. Biol. Chem 274: 13181-92) and was selected to carry out further studies. The D-Lys was

positioned on the nonpolar face (*vs.* L-Lys on the polar face in GS14), disrupting β-sheet structure and decreasing peptide amphipathicity.

Using the GS14K4 template, we investigated the effect of hydrophobicity on microbial specificity by altering the amino acid sequence composition of the residues comprising the nonpolar face. Analogs that were less hydrophobic than GS14K4 had alanine residues substituted for the three valine and three leucine residues found in the native sequence, while more hydrophobic analogs had phenylalanine residues substituted for tyrosine and/or leucine residues subtituted for valines. Increased hydrophobicity tended to increase both antimicrobial and hemolytic activity, while decreased hydrophobicity decreased both antimicrobial and hemolytic activity relative to GS14K4.

A novel method that we call "temperature profiling in reversed-phase chromatography" has been used to identify self-association of our 14-residue peptides in aqueous solution. The technique consists of analyzing peptides on a reversed-phase HPLC column at discrete temperature intervals over a range of 5 to 80°C. Loading onto the reversed-phase matrix concentrates the sample and promotes intermolecular interactions causing self-association. We hypothesize that self-association can be observed by an increase in HPLC retention time with increased temperature, and that larger increases in retention times indicate a greater extent of self-association. By studying a series of linear and cyclic peptide analogs, we show that high and low degrees of self-association, as monitored by this technique, are undesirable for optimal microbial specificity in these peptides. The most efficacious peptide, GS14K4, showed an intermediate degree of self-association as noted by the transition temperature, T_p, of 20°C; in comparison, the least efficacious peptide, GS14 had a transition temperature of 55°C.

Acknowledgments

I thank the University of Alberta, the Alberta Heritage Foundation for Medical Research, and the Natural Sciences and Engineering Research Council of Canada for financial support during my Ph. D studies.

I sincerely appreciate the members of the Hodges lab and its associated institutions for their invaluable technical support: Lorne Burke, Michael Carpenter, Marc Genest, Leslie Hicks, Jennifer Labrecque, Robert Luty, Anthony Mehok, Janine Mills, Kimio Oikawa, Paul Semchuk, Elsi Vacano, and Isabelle Werner – many thanks to each of you. The efforts of our collaborators in the Bob Hancock laboratory (Jon-Paul Powers and Susan Farmer, University of British Columbia) and the Michael Vasil laboratory (Adriana Vasil, University of Colorado Health Sciences Center) are also greatly appreciated.

To the postdoctoral and full-time research associates for their expertise and insight in helping me to overcome difficult trials in the course of my research: Paul Cachia, Stephen Lu, Colin Mant, and Brian Tripet – you kept my projects afloat even when my peptides sank (to the bottom of my centrifuge tubes).

A special thanks goes to the leaders who defined my postgraduate experience. To my supervisor, Bob Hodges: you gave me the freedom to juggle my athletic and pedagogical passions along with the responsibilities of research, and for that I will always be grateful. I am also indebted to Terry Danyluk for allowing me to briefly masquerade as a 'mature' student-athlete. Both men have firsthand knowledge of the value of combining sport and academics in student education, and that is why I especially appreciate and respect them: for their personal success in these areas, and for their continuing support of others who share their desire.

Table of Contents

Page

Chapter 1A: Introduction to coiled-coils

1-1. The protein folding problem....1
1-2 Importance of studying the protein folding problem....4
1-3. Protein stability....5
1-4. The coiled-coil as a model protein structural motif....6
1-5. Coiled-coils in *de novo* protein design....9
1-6. Intrinsic sequence-dependent factors influencing coiled-coil stability, specificity, oligomerization state, and orientation....10
1-7. Coiled-coil packing irregularities....14
1-8. Double mutant cycle analysis....14
1-9. Coiled-coil prediction programs....17
1-10. Two-state model for coiled-coil folding....18
1-11. Trigger sequences....20
1-12. References....23

Chapter 1B: Introduction to antimicrobial peptides

1-13. The antibiotic era and the development of antibiotic resistance....30
1-14. Discovery of antimicrobial peptides....33
1-15. Antimicrobial peptide mechanisms of action....36
1-16. Drawbacks to peptide therapeutics....39
1-17. Large-scale industrial peptide production....39
1-18. Gramicidin S....40
1-19. References....45

Chapter 2: Materials and methods

2-1. Materials....50
2-2. Linear peptide synthesis, purification and analysis....51
2-3. Peptide cyclization, deformylation, and purification....55
2-4. Circular dichroism spectroscopy and equilibrium unfolding measurements....56
2-5. Thermodynamic analysis....58
2-6. Crystallization, data collection and processing....62
2-7. Model building and refinement....63
2-8. Calculation of solvent-accessible surface area....64
2-9. Sedimentation equilibrium analytical ultracentrifugation....64
2-10. Measurement of antibacterial and antifungal activity (MIC assays)....65
2-11. Measurement of hemolytic activity....66
2-12. Displacement of dansyl-polymyxin from LPS....66

2-13. Permeabilization of outer membranes to NPN 68
2-14. Di-$SC_3(5)$ release assay 68
2-15. Curve fits for RP-HPLC temperature profiles 69
2-16. Analytical reversed-phase analysis of peptides 70
2-17. References 70

Chapter 3: Trigger sequences in the folding of α-helical coiled-coils

3-1. Introduction 73
3-2. Results 77
3-3. Discussion 100
3-4. References 104

Chapter 4: X-ray crystal structure of a GCN4/cortexillin I hybrid coiled-coil analog

4-1. Introduction 109
4-2. Results 111
4-3. Discussion 135
4-4. Conclusions 138
4-5. References 139

Chapter 5: Optimization of microbial specificity through modulation of hydrophobicity of cyclic antimicrobial peptides

5-1. Introduction 143
5-2. Results 145
5-3. Discussion 162
5-4. Conclusions 166
5-5. References 166

Chapter 6: Alteration of microbial specificity through enantiomeric substitutions of cyclic antimicrobial peptides

6-1. Introduction 171
6-2. Results 174
6-3. Discussion 190
6-4. References 196

Chapter 7: A novel method for measuring self-association of small amphipathic molecules

7-1. Introduction 200
7-2. Results 202
7-3. Discussion 226
7-4. Conclusions 232
7-5. References 232

Appendix I - Structure-activity relationships in cyclic beta-sheet antimicrobial peptides

I-1. Introduction.. 238
I-2. Improvement of synthesis methodology for cyclic peptides.................... 244
I-3. Improvement of aqueous solubility of cyclic peptides............................ 247
I-4. Development of NMR methodology to evaluate structure of cyclic β-sheet peptides.. 247
I-5. Investigation of methods for evaluating antimicrobial activity of cyclic peptides.. 248
I-6. Effect of ring size in cyclic gramicidin S analogs in dissociating hemolytic and antibacterial activity... 250
I-7. Dissociation of antimicrobial and hemolytic activities using diastereomeric substitutions which alter amphipathicity......................... 259
I-8. NMR structures of cyclic peptides... 263
I-9. Modulation of hydrophobicity of the GS14K4 nonpolar face................. 269
I-10. Other studies... 277
I-11. Conclusions.. 283
I-12. References.. 283

Table List

Table **Page**

3-1. CD spectroscopy and sedimentation equilibrium results for peptides used in this study 83
3-2. Thermodynamic data for peptides used in this study 86
3-3. Thermodynamic contribution of amino acid substitutions to coiled-coil stability 87
3-4. Predicted relative contributions of interactions to coiled-coil stability 88
3-5. Predicted and experimentally derived relative coiled-coil stabilities of peptides used in this study 89

4-1. Data collection and refinement statistics 115
4-2. Biophysical characterization of hybrid peptide and analogs 131
4-3. Urea denaturation data 133
4-4. Contributions of α-helix propensity, hydrophobic and electrostatic interactions to coiled-coil stability 134

5-1. Peptide sequences, physical properties and biological activities of peptides used in this study 146
5-2. Activity of GS14K4 hydrophobicity analogs against Gram-negative microorganisms 156
5-3. Antifungal and Gram-positive activity of GS14K4 hydrophobicity analogs 160

6-1. Circular dichroism data for GS14 analogs 179
6-2. HPLC retention times for GS14X4 peptides 181
6-3. Biological activity of GS14 analogs against yeast and Gram-negative bacteria 185
6-4. Biological activity of GS14 analogs against Gram-positive bacteria 186

7-1. HPLC data for peptides used in the temperature profiling study 208
7-2. Biophysical data and biological activity for representative peptides 216

Appendix 1

1. Antibacterial and antifungal activity of gramicidin S and analogs in agar-based and liquid-based assays 249
2. Peptides used in structure-activity studies of gramicidin S analogs 253
3. Comparison of biological activity of GS, GS14, GS14K4, and GS14K4 V3/A3 against Gram-negative microorganisms 275
4. Comparison of biological activity of GS, GS14, GS14K4, and GS14K4 V3/A3 against Gram-positive microorganisms 276

Figure list

Figure **Page**

1-1. Double mutant cycle analysis.......... 16
1-2. Design and preparation of N-terminal and C-terminal deletion constructs from cortexillin I.......... 21
1-3. Carpet and barrel-stave models of antimicrobial peptide permeation of lipid bilayers.......... 37

3-1. Comparison of peptide sequences in this study with the consensus trigger sequence proposed by Kammerer *et al.*.......... 78
3-2. Amino acid sequences of the peptides used in the trigger sequence study.......... 80
3-3. End view of possible parallel homodimeric α-helical coiled-coils, viewed from the N-terminus.......... 81
3-4. Far-UV CD spectra of representative peptides.......... 82
3-5. Concentration dependence of helicity in representative peptides.......... 96
3-6. Thermal unfolding curves for coiled-coil peptides.......... 98
3-7. Influence of Asn15 on coiled-coil stability.......... 102

4-1. Amino acid sequences of peptides used in this study.......... 112
4-2. End-on view of the hybrid peptide analog, viewed from N- to C-terminus.......... 114
4-3. Space filling representation of the GCN4/cortexillin Hybrid 2 structure.......... 116
4-4. Cross-sectional view of the region surrounding the Asn 15 (**a**) core in Hybrid 2..... 118
4-5. Cross-sectional comparison of **g-a** packing and **d-e** packing of leucines in the hydrophobic core of the hybrid peptide analog, viewed from N-terminus to C-terminus.......... 120
4-6. Comparison of the region around the central Asn (**a**) in Hybrid 2 (Panel A) and GCN4 (Panel **B**) coiled-coils.......... 123
4-7. Coiled-coil pitch and coiled-coil radius plotted against the residue number for the Hybrid 2 and the GCN4-p1 peptide.......... 127
4-8. CD spectra of the peptide K19E obtained at 20° C in 50 mM phosphate, 100 mM KCl, pH 7.0 buffer (benign).......... 129
4-9. Chemical unfolding curves of the Hybrid 2 peptide and analogs.......... 130

5-1. CD spectra of GS14 and GS14K4 hydrophobicity analogs.......... 148
5-2. Correlation between predicted relative hydrophobicity and observed RP-HPLC retention times of GS14K4 analogs.......... 151
5-3. Correlation between peptide hydrophobicity and LPS-binding affinity in GS14K4 analogs.......... 152
5-4. Permeabilization of *E. coli* UB1005 cells to NPN.......... 153
5-5. Relationship between hydrophobicity and hemolytic activity of GS14K4 analogs.......... 155

5-6. Antimicrobial activity and microbial specificity of GS14K4 hydrophobicity analogs against Gram-negative microorganisms 158
5-7. Antimicrobial activity and microbial specificity of GS14K4 hydrophobicity analogs against Gram-positive microorganisms and yeast 161

6-1. Sequences of GS14X4 peptides 175
6-2. Representations of GS14X4 analogs 176
6-3. Representative circular dichroism spectra of GS14X4 peptides 178
6-4. Reversed-phase HPLC separation of the 14-residue cyclic peptides with L- and D-amino acid substitutions at position 4 182
6-5. Biological activity of GS14X_D4 peptides 187
6-6. Comparison of biological activity and hydrophobicity of GS14X_D4 peptides 189

7-1. Sequences of peptides used in the temperature profiling study 203
7-2. NMR structures and Connolly surface representations of GS14 and GS14K4 peptides 206
7-3. Proposed mechanisms of temperature profiling by RP-HPLC 213
7-4. Far-UV CD spectra for cyclic and linear GS14 and GS14K4 peptides 215
7-5. Normalized RP-HPLC temperature profiles of cyclic and linear GS14 and GS14K4 peptides 218
7-6. Normalized RP-HPLC temperature profiles of GS14 X4 peptides 221
7-7. Normalized RP-HPLC temperature profiles of GS14K4 and hydrophobicity analogs 223
7-8. RP-HPLC elution of representative GS14 and GS14K4 analogs 224

Appendix 1

1. Model of gramicidin S based on high-resolution ^{1}H-NMR structural analysis 241
2. Synthesis scheme of cyclic β-sheet peptides 246
3. Proposed β-sheet structures of gramicidin S ring-size analogs (6, 8, 10, 12, 14 and 16 residues), assuming that all analogs adopt the β-sheet conformation 251
4. Far-UV circular dichroism spectra of GS ring-size analogs and displacement by GS ring-size analogs of fluorescent dansyl-polymyxin B bound to *E. coli* lipopolysaccharide 258
5. CD spectra of GS14 and representative GS14 diastereomers and reversed-phase HPLC separation of GS14 and single residue substitution diastereomers 261
6. Correlation between amphipathicity and hemolytic activity in GS14 diastereomers and correlation between amphipathicity and LPS binding affinity in GS14 diastereomers 262
7. NMR structures of GS14, GS14K4, and GS14 K3L4 264
8. Connolly surface representations of the average structures of GS14, GS14K4, and GS14 K3L4 calculated from the NMR ensemble 267

9. Correlation between peptide hydrophobicity and LPS-binding affinity in GS14K4 hydrophobicity analogs........271
10. Antimicrobial activity and microbial specificity of GS14K4 hydrophobicity analogs against Gram-negative microorganisms........273
11. Antimicrobial activity and microbial specificity of GS14K4 hydrophobicity analogs against Gram-positive microorganisms and yeast....... 274
12. Model of the ^{19}F-labelled analog based on the structure of gramicidin S and proposed structure and flat alignment of the analog in liquid-crystalline DMPC bilayers........ 279
13. Temperature profiles in reversed-phase chromatography of cyclic peptides GS14, GS14K4, and the linear peptide GS14K4 lin and reversed-phase elution profiles of GS14K4 lin, GS14K4, and GS14 at 80°C........ 282

Abbreviations List

AMP, antimicrobial peptide

AUC, analytical ultracentrifugation

Boc, N^{α} *tert*-butyloxycarbonyl

BOP, benzotriazol-1-yloxytris(dimethylamino)phosphonium hexafluorophosphate

BSA, bovine serum albumin

CCCP - carbonylcyanide-*m*-chlorophenylhydrazone

CD, circular dichroism

CDI: 1,1′-carbonyl-diimidazole

CFU, colony forming units

Clip170: cytoplasmic linker protein 170

CMBT, 5-chloro-2-mercaptobenzothiazole

DCM, dichloromethane

DIEA, *N,N*-diisopropylethylamine

diSC$_3$(5): 3,3′-dipropylthiadicarbocyanine iodide

DMF, dimethylformamide

DPX, dimethylaminonapthalenesulfonyl (dansyl)-polymixin B

EDT, ethanedithiol

FTIR, Fourier-transform infrared spectroscopy

GCN4, general control of amino acid biosynthesis protein N4

GS, gramicidin S

GS14, a *de novo* designed 14-residue cyclic peptide related to GS

HBTU, 2-(1H-benzotriazole-1-yl) – 1,1,3,3 tetramethyluronium hexafluorophosphate

HEPES, 4-(2-hydroxyethyl)-1-piperazineethanesulfonic acid

HOBt, *N*-hydroxybenzotriazole

HPLC, high performance liquid chromatography

LB, Luria broth

LPS, lipopolysaccharide

MALDI-MS, matrix assisted laser desorption ionization mass spectrometry

MHB, Mueller Hinton broth

MIC, minimal inhibitory concentration

NMP, 1-methyl-2-pyrrolidinone

NMR, nuclear magnetic resonance

NOE, nucelar Overhauser effect

NPN, *N*-phenyl-1-naphthylamine

PAM, 4-hydroxymethylphenylacetamidomethyl

PAGE, polyacrylamide gel electrophoresis

PEG, polyethylene glycol

PyBOP, benzotriazole-1-yl-oxy-tris-pyrrolidino-phosphonium hexafluorophosphate

RBC, red blood cell

rmsd, root-mean-square deviation

RP-HPLC, reversed-phase high performance liquid chromatography

SPPS, solid-phase peptide synthesis

TFA, trifluoroacetic acid

TFE, 2,2,2-trifluoroethanol

TI, therapeutic index

Tpr, translocated promoter region

UV, ultraviolet

Amino acid nomenclature

Name	*Abbreviation*
Glycine	G, Gly
Nonpolar	
Alanine	A, Ala
Cysteine	C, Cys
Isoleucine	I, Ile
Leucine	L, Leu
Methionine	M, Met
Proline	P, Pro
Valine	V, Val
Aromatic	
Phenylalanine	F, Phe
Tryptophan	W, Trp
Tyrosine	Y, Tyr
Uncharged polar	
Asparagine	N, Asn
Glutamine	Q, Gln
Serine	S, Ser
Threonine	T, Thr
Charged polar	
Aspartic acid	D, Asp
Glutamic acid	E, Glu
Histidine	H, His
Lysine	K, Lys
Ornithine	O, Orn
Arginine	R, Arg

Chapter 1A. Introduction to coiled-coils.

Chapter 1-1. The protein folding problem. The protein folding problem can be divided into two major parts: establishing rules for the prediction of the final three-dimensional protein structure from primary sequence information, and the determination of the kinetic pathways from unfolded to folded (or folded to unfolded) states. The manner in which the primary amino acid sequence dictates the overall three-dimensional fold of a protein has been an area of extensive study over the past several decades (Plaxco et al. 1998; Hammarstrom et al. 2000; Daggett et al. 2003). The Anfinsen hypothesis, which states that the primary amino acid sequence determines the three-dimensional structure of proteins, was proposed after numerous demonstrations that globular proteins such as ribonuclease and staphylococcal nuclease were able to refold into the same native structure after being denatured and then returned to their starting environmental conditions (Anfinsen 1973).

The other aspect of the protein folding problem related to the kinetics of folding/unfolding pathways is summarized by Levinthal's paradox (Levinthal 1969). If a protein must sample all possible configurations in conformational space to select the final fold, there is an apparent paradox between the time it would take for an amino acid sequence to sample (longer than the lifetime of the universe) and the actual time span observed for protein folding (microseconds to seconds). Clearly, proteins do not sample all conformational space but exhibit stages of folding where the progression to the final folded state involves certain configurations that are held while other regions continue to sample conformational space. The current view of protein folding has progressed from the idea of an unfolded protein passing through a single intermediate structure before adopting the final folded (native) structure, to an energy landscape (or folding funnel) model. All protein molecules in solution are thought of as an ensemble and treated in a statistical manner, where individual molecules can follow different folding pathways yet lead to the same final folded structure. Experimentally observed thermodynamically stable protein folds that are intermediate between the native structure and the denatured state (folding intermediates) are explained as a significant fraction of the total protein ensemble that followed a kinetic pathway that led to conformation resulting in a local energy minimum (a protein in a 'kinetic trap').

What makes both parts of the protein folding problem so difficult to answer is the fact that both local interactions (residues in close proximity along the primary sequence) and nonlocal interactions (residues in close physical proximity in the final folded structure but distant in the primary sequence) contribute to the stability of the final folded state. The prediction of secondary structure (*i.e.* α-helices, β-sheets, or loops) has been developed using computer programs with only short sequence windows that evaluate local interactions. However, the secondary structure of such short sequences is also dependent on the surrounding environment, i.e. nonlocal interactions, as the same sequence has been shown to adopt either an α-helix or β-sheet depending on the protein (referred to as "chameleon sequences" (Minor et al. 1996; Mezei 1998) or "structural cassettes" (Kwok et al. 1998)).

In terms of folding kinetics, the relative order of local secondary structure and nonlocal tertiary structure formation is an area of active debate. Some of the models explaining the protein folding pathway include the framework model (Baldwin et al. 1999), where secondary structure formation precedes tertiary structure; the hydrophobic collapse model

(Dill 1985), where the hydrophobic residues collapse into the core before the formation of secondary structure; and the nucleation-condensation model (Daggett et al. 2003), which attempts to unify preexisting models by explaining that the importance of preformed secondary structure and hydrophobic collapse in the folding pathway or a particular protein is dependent on the degree of stabilization that tertiary structures provide to secondary structures. For example, proteins with early preformed secondary structure in agreement with the framework model would be described by the nucleation-condensation model as having stable secondary structure with little stabilization required by hydrophobic interactions.

The protein folding problem is studied through a combination of experimental and theoretical techniques. Experimental analysis usually involves the thermodynamic and/or kinetic characterization of the folding and unfolding of model proteins and mutants (Daggett et al. 2003) using techniques such as differential scanning calorimetry (Izbarra-Molero et al. 2001; Dragan et al. 2002), circular dichroism (CD) spectroscopy, fluorescence spectroscopy, and nuclear magnetic resonance (NMR) spectroscopy (Holtzer et al. 1997; van Mierlo et al. 2000). Special devices are also typically required in order to observe folding/unfolding kinetics at the millisecond timescale, such as stopped flow, continuous flow, or quenched flow mixers; more rapid nonmixing techniques include infrared nanosecond and picosecond temperature jumps for the refolding of cold-denatured proteins. Importantly, these studies are complemented by the three-dimensional structural determination of crystallized proteins and/or proteins in solution by NMR spectroscopy (Wuthrich et al. 2001), which allows comparison of results from the biophysical techniques with 3-D atomic coordinate data. Theoretical techniques for folding pathways include molecular dynamics simulations of protein unfolding kinetics, typically on nanosecond to microsecond time scales. These simulations are limited by the tremendous amount of computer processing time required even for small timescales (nanoseconds), even though the fastest times for proteins to unfold from the native state occur on a much larger (microsecond) timescale. Other theoretical techniques include computer modelling of 3-D protein structures based on sequence homology and identity to proteins whose structures have already been solved (Dill et al. 1997). Modelling requires less time than a full structural determination by X-ray crystallography or NMR spectroscopy, although the model cannot be verified until the structure has been experimentally determined.

Chapter 1-2. Importance of studying the protein folding problem. A greater understanding of the forces contributing to protein folding has relevant biomedical and industrial applications. These include fundamental knowledge of prion-type diseases and pathologies associated with misfolded proteins and peptides (amyloid pathologies such as Alzheimer's, Parkinson's, Huntington's, and Creutzfeld-Jacob disease) which could possibly lead to treatments that inhibit, disrupt, or abolish protein aggregation (Temussi et al. 2003). The accumulation and availability of enormous amounts of genomic data has also fueled the structural genomics initiative (Burley et al. 2002). The goal of structural genomics is to solve the 3-D structures of large numbers of proteins, in the belief that after a critical number of structures are solved, the structure of many protein sequences can be accurately predicted based on similarity or homology to a protein whose structure has already been determined. Three-dimensional protein structures are important in the drug development process in the design or selection of molecules from a chemical library that would likely bind to the target protein (Schmid 2002). The design of proteins *de novo* with new functions (Martin et al. 2000; Bolon et al. 2002) and the proper refolding of insoluble recombinant proteins (inclusion bodies) in the biotechnology industry are other applications which hold future promise (Clark 2001). Also, a better understanding of the factors influencing protein folding and stability allows existing proteins with known functions to be engineered for different conditions, e.g. enhanced thermostability or altered functional pH ranges.

Chapter 1-3. Protein stability. Along with protein folding, researchers also study protein stability. While "protein stability" is a broad term that is used to describe several areas, including the *in vitro* stability of the fold against various denaturants (heat, chemicals or pressure), *in vivo* stability against enzyme degradation, and industrial stability related to shelf life (*i.e.* how long a protein formulation can remain in its native fold before undergoing aggregation, hydrolysis, chemical decomposition or other modification such as oxidation), our laboratory specifically examines *in vitro* protein and peptide stability under reversible conditions. For example, mutant proteins with minor changes compared to the native sequence can possess the same overall fold as the native structure, yet the protein stability to denaturant may be drastically different. We investigate how factors such as amino acid sequence or other structural modifications (disulfide bonds and lactam bridges, for example) influence the folding and unfolding equilibria of proteins and peptides. By comparing the stability of mutants or analogs *vs.* native molecules, we can identify the thermodynamic contribution that specific residues or interactions between residues make to protein or peptide stability.

The *in vitro* stability of a protein fold is generally expressed in terms of the change in the state functions for the reaction, including Gibbs free energy in transitioning from the folded to unfolded state (ΔG_u) under a given set of conditions, e.g. at a specified temperature, pressure, protein concentration, and buffer condition. The ΔG_u value could also be explained as the amount of energy required to completely unfold a protein under specified conditions, generally standard state (25°C, 1 atmosphere, 1 M protein/peptide concentration in buffer of specified pH and composition). We study this stability by denaturing the protein with heat, urea, or guanidium chloride and monitoring changes in structure using spectroscopic techniques such as CD and fluorescence (Talaga et al. 2000).

The major sequence-dependent factors influencing protein stability involve the presence of structural biases in the unfolded ensemble (e.g., restrictions due to the disulfide bonds between Cys residues), the burial and packing of hydrophobic residues away from bulk solvent (hydrophobic collapse), and the stabilization of secondary through secondary structure propensity effects, ionic interactions, and hydrogen bonding. Independent of the sequence, stability is also influenced by peptide or protein concentration, pH, temperature, and the nature of the environment (aqueous or in the presence of organic solvent, ion composition and salt concentration).

Chapter 1-4. The coiled-coil as a model protein structural motif. The α-helical coiled coil is a model structural motif used by our laboratory and others to study protein folding and stability. Two to five right-handed helices (clockwise turns from N- to C-terminal) form a superhelix with a left-handed twist around the coiled-coil axis. The major source of stability that favors the association of the helices comes from the continuous interface of predominantly hydrophobic residues (leucine, isoleucine, methionine, and valine) found lengthwise along the surface where each helix contacts an adjacent one. The side-chains of amino acids along this hydrophobic core are arranged into a "knobs-into-holes packing". In other words, the side-chains from one helix pack side-by-side with the side-chains from the opposite helix (Crick 1953; O'Shea et al. 1989). The first coiled-coil protein to have its amino acid sequence determined was the two-stranded tropomyosin (Sodek et al. 1972). Manual examination of the tropomyosin sequence revealed a repeating pattern of hydrophobic residues, commonly referred to as the "heptad repeat" or "hydrophobic repeat". At every first and fourth position in a seven-residue pattern, hydrophobic residues occurred at higher frequency, hence the '3-4' (N X X N X X X N X X N XXX... where N is a non-polar residue) or '4-3' (NXXXNXXNXXXNXX...) hydrophobic repeat (denoted **abcdefg**, where positions **a** and **d** contain hydrophobes). The residues at positions **a** and **d** comprise the hydrophobic core that contacts adjacent helices. Structural predictions based on the hydrophobic repeat were confirmed in 1991 by the first high-resolution X-ray crystal structure of a two-stranded coiled-coil region in the yeast transcription factor, GCN4, which showed the **a** and **d** residues buried in the helix-helix contact surface (O'Shea et al. 1991).

There are many reasons why the coiled-coil is a model structure for studying protein folding and stability. The coiled-coil structure possesses secondary structure (α-helical), tertiary structure (secondary structure stabilized by nonlocal interactions, in this case the left-handed supercoiled twist of helices) and quaternary structure (discrete subunits associating together), which means that it contains the same levels of hierarchy observed in naturally occurring globular proteins. Like globular proteins, the coiled-coil motif also contains buried hydrophobic residues shielded from aqueous solvent in the core, which are a major source of stability. At the same time, solubility is generally excellent because coiled-coils possess hydrophilic and charged residues exposed to solvent; therefore, they do not aggregate or precipitate in aqueous solution, a phenomenon observed with amphipathic β-sheet structures (Jelokhani-Niaraki et al. 2001). (For example, tropomyosin has the highest charge density of any known protein making it extremely soluble). Also, the coiled-coil structure can become virtually 100% helical in aqueous solution due to the shielding of hydrophobic residues from bulk solvent (in contrast with monomeric amphipathic α-helices which are never completely helical due to significant end-fraying at N- and C-termini), and the biophysical structural characterization is well understood by techniques such as CD (Hodges 1996; Kohn et al. 1998). The helical secondary structure possesses a far-UV spectrum with local minima at 208 and 222 nm. After the transition from α-helical coiled-coil to the unstructured state, the ellipticity value at 222 nm becomes close to zero. Thus, an unfolding curve can be constructed and protein stability can be determined by measuring the change in mean residue molar ellipticity at this wavelength as a function of denaturant concentration. The repetitive nature of the heptad repeat allows one to design coiled-coils containing essentially the same repeated seven residue sequence, and to introduce multiple amino acid substitutions at equivalent sites in the heptad repeat to enhance the magnitude of the substitution effect. Assuming that the substitution sites are all equivalent, one can then divide by the total number of substitution sites to determine the stability contribution of a single amino acid to the coiled-coil at a given heptad position. The relatively small minimum length requirement of two heptads for a stable folded molecule (Burkhard et al. 2002) means that short coiled-coils can be studied that are more sensitive to amino acid substitutions than longer sequences. There is flexibility in the choice of synthesis methods for coiled-coils; relatively short sequences (less than fifty amino acids) are suitable for solid –phase peptide synthesis methodology, while larger sequences can be expressed as recombinant peptides in bacteria or made by solid-phase chemistry in shorter segments and subsequently ligated to make the full-length segment. Coiled-coils are also found in regions of many proteins found in nature, e.g. viral fusion proteins, motor proteins, and DNA binding proteins, so that one can select a sequence either by *de novo* design or based on the sequence of a natural coiled-coil.

The coiled-coil is a minimalist structural motif that is relatively simple in its design, synthesis, and characterization. Therefore, it is used to understand fundamental principles of protein folding which would be more difficult to study in native globular proteins due to the complex nature of the stabilizing interactions. While it cannot reveal all types of stabilizing contributions to protein folding, it facilitates the establishment of general rules for protein folding and stability, which should subsequently allow more complex model proteins to be developed and studied that may represent the behavior of native globular proteins more accurately in the future.

Chapter 1-5. Coiled-coils in *de novo* protein design. Knowledge of coiled-coil folding and stability has been applied to the *de novo* design of peptides with new or improved functions. The intermolecular interactions between the strands of coiled-coil heterodimers allow each strand to act as a tag in purification and detection systems; heterodimers have been used in biosensor systems, *in vivo* drug delivery vehicles, and purification of expressed proteins by affinity chromatography (Hodges 1996; Yu 2002).

Other designed coiled-coils include a retro- version of GCN4 with the N-to C-terminal sequence order reversed (Mittl et al. 2000), right-handed coiled-coils (Harbury et al. 1998; Sia et al. 2001) and coiled-coils with enhanced stability from fluorinated aliphatic residues in the hydrophobic core (Tang et al. 2001). These diverse examples of the protein design process using coiled-coils demonstrate the utility of the structural motif (Burkhard et al. 2001).

Chapter 1-6. Intrinsic sequence-dependent factors influencing coiled-coil stability, specificity, oligomerization state and orientation. Although there are many sequence-dependent factors influencing coiled-coil stability, the most important is the nature of the residues in the hydrophobic core positions. Stability coefficients for residues in the **a** and **d** positions have been determined, and while as a group hydrophobic residues are generally more stabilizing than polar residues, there are stability differences between residues at positions **a** and **d** among the hydrophobes, with Ile and Val β-branched residues the most preferred at position **a** (Harbury et al. 1993; Zhu et al. 1993; Wagschal et al. 1999a; Acharya et al. 2002) and Leu the most preferred residue at position **d** (Moitra et al. 1997; Tripet et al. 2000). The preferences are due to differences in side-chain packing effects between Leu and the β-branched Ile and Val residues. At position **a**, the C_α-C_β bond vector points away from the hydrophobic core such that beta-branched amino acids such as isoleucine increases the packing efficiency; in position **d**, the C_α-C_β bond vector points towards the hydrophobic core such that the non-beta-branched leucine packs more efficiently there. Therefore, although Leu and Ile are isomeric residues with the same intrinsic hydrophobicity, they can affect coiled-coil stability differently due to the differences in side-chain packing at positions **a** and **d** (Harbury et al. 1993; Harbury et al. 1994; Kohn et al. 1998).

In two-stranded coiled-coils, other factors that influence stability include the types of amino acid residues in positions **e** and **g** of the heptad repeat. Positions **e** and **g** flank the hydrophobic core such that **g** to **e′** (i.e., i to i′ + 5) side-chain interactions between helices (interchain interactions) are possible. Residues at these positions in a two-stranded coiled-coil reside in an environment that is neither fully solvent-exposed nor solvent-excluded. While different groups disagree as to the extent that ionic interactions contribute to coiled-coil stability (Lavigne et al. 1996), oppositely charged residues *e.g.* Lys/Glu, Arg/Glu at the aforementioned positions can increase stability (Zhou et al. 1994a) through a combination of hydrophobic effects, van der Waals forces, hydrogen bonding and/or ion pairing, while similar charged pairs such as ionized Glu/Glu′ can decrease stability (Kohn et al. 1995b). Stabilizing hydrogen bonding effects have also been observed, between interchain Gln-Gln′ pairs, as well as stabilizing hydrophobic effects in uncharged Glu-Glu′ pairs (Kohn et al. 1995a). Other less common interchain electrostatic interactions include i to i′ + 1 and i to i′ + 4 ion pairs observed in the cortexillin I crystal structure (Burkhard et al. 2000). Increasing chain length also tends to increase stability (Lau et al. 1984; Su et al. 1994); there is a minimal chain length requirement of three heptads (containing six hydrophobes at **a** and **d** positions) for model coiled-coils containing an excellent hydrophobic core (Ile at all **a** positions and Leu at all **d** positions), i to i + 3 and i to i + 4 intrachain electrostatic attractions, and i to i′ + 5 interchain electrostatic attractions (Su et al. 1994). However, other *de novo*-designed coiled-coils were able to fold with as little as two heptads by adding additional stabilizing interactions (Burkhard et al. 2002).

Factors that stabilize individual α-helices also influence coiled-coil stability, such as intrachain i to i + 3 and i to i + 4 interactions (charged-charged, H-bonding, charged-aromatic, charged-polar); N-terminal and C-terminal capping residues; hydrophobic staples ; and helix dipoles (Baldwin et al. 1999). Designed and naturally occurring coiled-coil structures also vary in oligomerization state (Harbury et al. 1994; Beck et al. 1997; Wagschal et al. 1999b; Tripet et al. 2000; Burkhard et al. 2001), chain orientation (parallel or antiparallel relative to N- and C-termini) (Monera et al. 1993; Monera et al. 1996; Oakley et al. 1998) and hetero- or homo-specificity (Lumb et al. 1995; Lavigne et al. 1998). How does the amino acid sequence influence each of these characteristics of coiled-coils? For oligomerization states, although the presence of polar residues in the hydrophobic core decreases coiled-coil stability, they can influence oligomerization states; for example, asparagine and lysine (Campbell et al. 2002) at position **a** favors dimer formation while glutamine has been shown to form trimers in GCN4 analogs (Gonzalez et al. 1996b; Eckert et al. 1998). Hydrophobic residues along the hydrophobic core and/or interface (**e** and **g** positions) make a large contribution to stability but can make the sequence more permissive to higher order oligomerization beyond the dimeric form, e.g. trimers (Harbury et al. 1993; Harbury et al. 1994) because of increased numbers of possible packing configurations in the hydrophobic core (Gonzalez et al. 1996a). Interchain ionic interactions can also influence oligomerization state, as in the case of an arginine involved in an Arg-Glu ion pair (in the trimeric cartilage matrix protein) changing oligomerization to tetramer when switched to glutamine (Beck et al.

1997). In general, coiled-coil sequences with larger hydrophobic surfaces promote higher order self-association.

Coiled-coil helix orientation is controlled primarily by ionic forces favoring either the parallel or antiparallel arrangement. In antiparallel coiled-coils, the N-terminal for each strand is associated with the C-terminal of the opposite strand, in contrast with the parallel orientation where the N-termini of every helix are localized together at one end of the coiled-coil and the C-termini are localized at the opposite end. At positions **a** and **d**, the hydrophobic core 'knobs-into-holes' packing in antiparallel coiled-coils is **a** to **d′** and **d** to **a′** *vs.* **a** to **a′** and **d** to **d′** in parallel coiled-coils. At positions **e** and **g**, the interactions at the hydrophobic interface in antiparallel coiled-coils are **g** - **g′** and **e** - **e′** rather than **g** - **e′** in the parallel orientation; electrostatic **g-e′** repulsions and attractive **g** - **g′** and **e** - **e′** ion pairs can favor the antiparallel arrangement due to attractive forces specific to a particular orientation (Monera et al. 1994; Myszka et al. 1994). Also, buried polar residues (Oakley et al. 1998).or the location of Ala residues in the hydrophobic core (Monera et al. 1996) can confer specificity to antiparallel orientation.

Like the ionic forces controlling coiled-coil orientation, a similar rationale exists for hetero- vs. homospecificity of strand association. Homostranded coiled-coils have identical sequences in all associated helices, while heterostranded coiled-coils have different sequences in each helix. The Hodges group specifies heterodimerization using an approach similar to the Kim group's peptide 'Velcro' (Graddis et al. 1993; O'Shea et al. 1993; Zhou et al. 1994b; Litowski et al. 2002). One strand contains primarily anionic Glu residues and another strand contains primarily cationic Lys residues at positions **e** and **g** to specify the heterodimeric form through a combination of electrostatic repulsions in the parallel homodimer and electrostatic attractions in the parallel heterodimer. The same reasoning is also observed in the **a** and **d** positions, e.g. a Lys repulsion at position **a** disfavors homodimers in leucine zippers (Acharya et al. 2002). However, repulsive electrostatic forces in heterodimers are sometimes tolerated, as observed by the Alber group in comparing designed *vs. in vivo* selected heterodimeric coiled-coils (Arndt et al. 2002). In addition to controlling oligomerization by specifying the dimeric state, asparagine at position **a** can also confer homotypic specifity over heterospecificity (Campbell et al. 2002).

Chapter 1-7. Coiled-coil packing irregularities. Most coiled-coils in naturally occurring proteins contain short sequence regions that interrupt the classical 4-3 hydrophobic repeat. These regions are known as stutters, stammers, and skips (Lupas 1996). Stutters are caused by an omission of three residues (the same as an insertion of four residues, e.g. 3-4-3-4-4-3-4-3-4...) in the heptad pattern, causing disruption of core packing and a local underwinding of the helix supercoil, leading to an increased coiled-coil radius (Strelkov et al. 2002). In contrast, stammers are caused by an omission of four residues and leads to overwinding of the superhelix, e.g., 3-4-3-3-4-3-4... (Brown et al. 1996). Skips are caused by an extra residue inserted in the heptad repeat, which changes the helix geometry by introducing a wider turn locally in the helix, e.g. 3-4-(3+1)-4-3-4-3-4... or 3-4-3-(4+1)-3-4....

Chapter 1-8. Double mutant cycle analysis. Although measuring the stability difference between a wild-type protein and a mutant with a single amino acid change can give the relative stability contribution of the single amino acid, this method cannot identify what forces account for this stability difference. Double mutant cycle analysis is a tool to determine the energetic contribution of a particular interacting pair of amino acids (Serrano et al. 1990). It involves the thermodynamic analysis of the wild-type (native) molecule as well as three mutants (or 'analogs' in the case of synthetic peptides): two with a single amino acid substitution, e.g., a substitution at position X in Mutant 1 and position Y in Mutant 2, and one with double amino acid substitutions at both positions X and Y in Mutant 3 (Figure 1-1). By determining ΔG for the wild-type, two single mutants and a double mutant, one can calculate ΔΔG for the interaction energy between the residue pairs. This analysis has often been employed to study the stability contributions of salt bridges in proteins and peptides, and was used to examine the strength of Glu/Lys′ interchain **g-e′** salt bridges in the coiled-coil described in Chapter 4. However, there are two key assumptions that are made when using this technique (Serrano et al. 1990; Makhatadze et al. 2003). One assumption is that the structure of the single and double mutants are not significantly different from the native structure, or that the structural changes cancel in the thermodynamic cycle. The second assumption is that there are no interactions between the sites in the singly or doubly substituted mutants or analogs. If either assumption is not valid, it is possible that factors other than ion pairing contribute to the differences in stability between the native and mutant proteins.

The first assumption of no significant structural changes in mutants can be rationalized based on the location of the substitution sites, e.g. a surface salt bridge that should not disrupt hydrophobic core packing upon mutation, and also confirmed with structural data, as the Fersht group did with a buried Arg/Asp salt bridge in barnase (Vaughan et al. 2002). As a control to validate that the coupling energy between the pair equals the electrostatic contribution and that no other stabilizing effects contribute to the ΔΔG value,

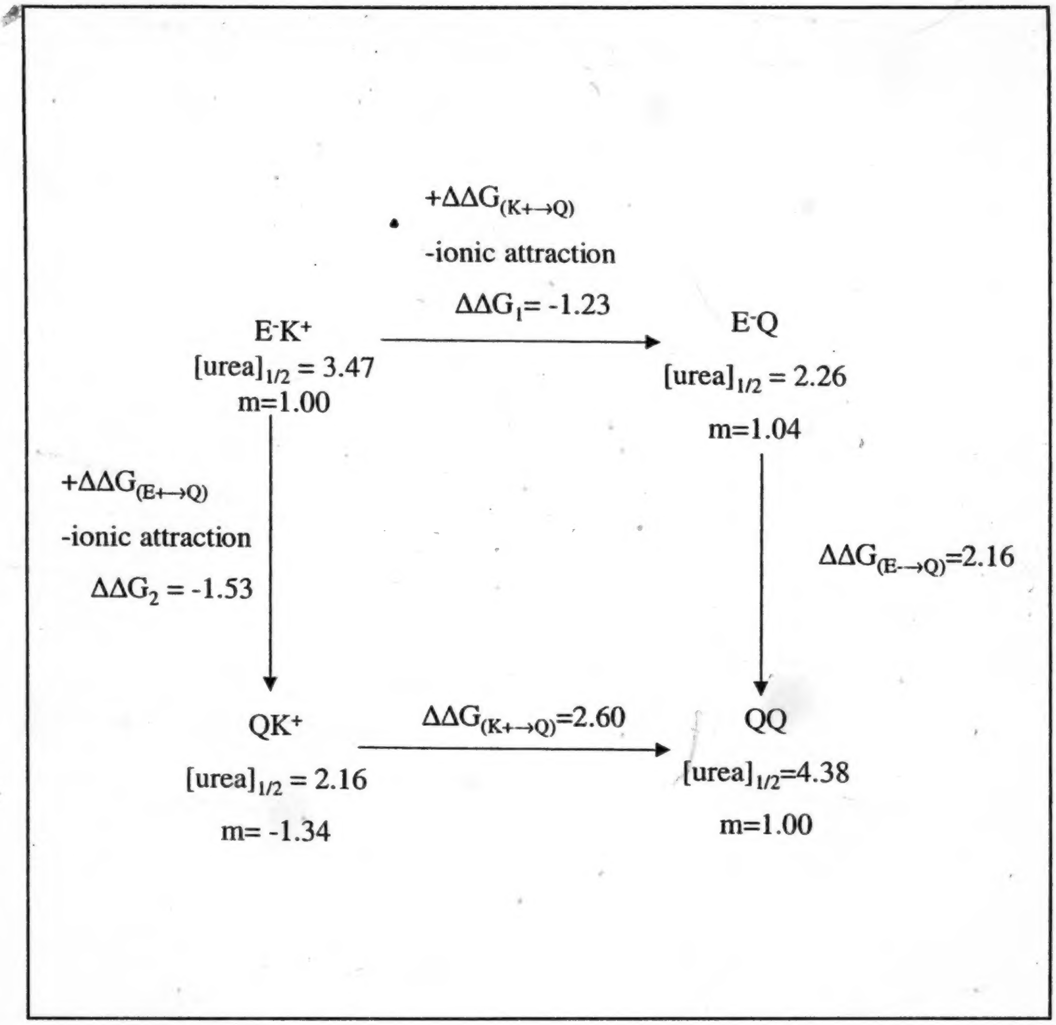
+ΔΔG(K+→Q)
-ionic attraction
ΔΔG1= -1.23
E-K+
[urea]1/2 = 3.47
m=1.00
E-Q
[urea]1/2 = 2.26
m=1.04
+ΔΔG(E+→Q)
-ionic attraction
ΔΔG2 = -1.53
ΔΔG(E-→Q)=2.16
QK+
[urea]1/2 = 2.16
m= -1.34
ΔΔG(K+→Q)=2.60
QQ
[urea]1/2=4.38
m=1.00

Fig. 1-1. Double mutant cycle analysis for the estimation of the net contribution of the interchain ionic attraction to coiled-coil stability (figure and legend adapted from Zhou et al. 1994a). A positive value means an increase in stability in the direction of the arrow. The values of $[\text{urea}]_{1/2}$ and m were determined in 0.1 M KCl, 50 mM PO_4 buffer at pH 7 at 20°C. ΔΔG was calculated by multiplying the difference of $[\text{urea}]_{1/2}$ with the average slope ($\Delta\Delta G=\Delta[\text{urea}]_{1/2}*\langle m\rangle$) (Serrano et al., 1990).

one can determining the stabilities of each protein in low and high salt (e.g., 1 M) conditions. Since high salt tends to screen electrostatic attractions, the effect of electrostatic effects between charged pairs in the native protein are nullified, leaving only the remaining nonelectrostatic effects in the stability determination. Therefore, the stability contributions of the single mutants should be additive in high salt, i.e. the ΔΔG value between the native protein and each of the single mutants should add up to the same value as the ΔΔG value between the native protein and the double mutant.

The second assumption of no interactions between substitution sites in the double mutant is justified by the choice of a small amino acid in the substitutions. Typically alanine is chosen for its small methyl side-chain and lack of polar groups that could potentially form hydrogen bonds.

Chapter 1-9. Coiled-coil prediction programs.

One of the goals of the Hodges laboratory has been to quantitatively determine the contribution of amino acids to coiled-coil folding and stability at various positions along the heptad repeat in order to predict coiled-coil regions in protein sequences. Numerous coiled-coil prediction programs exist to specifically identify two-stranded and/or three-stranded coiled-coils; these include COILS (Lupas et al. 1991); STABLECOIL (Tripet et al. 2001); PairCoil (Berger et al. 1995) and programs derived from it including MultiCoil (Wolf et al. 1997), LearnCoil (Berger et al. 1997), and LearnCoil-VMF (Singh et al. 1999). As well, another program called 2ZIP specifically identifies leucine zippers, which are parallel coiled-coil dimers that contain a characteristic leucine residue in seven-residue intervals at position **d** of the heptad repeat (Bornberg-Bauer et al. 1998). The window size is generally at least 28 residues in length as four heptads was considered to be the minimum chain length required for coiled-coil formation at the time that the programs were developed (Lau et al. 1984).

PairCoil established pairwise residue correlations for a database of known two-stranded coiled-coils. For example, positive pairwise correlations were made between I_aL_d (Ile at position **a** and Leu at position **d**) and, to a lesser degree, V_aL_d, while negative correlations were made with the L_aL_d pair. These correlations were then used to score a general set of protein sequences in the Protein Data Bank to evaluate the program's ability to correctly identify coiled-coils. The advantage of PairCoil over the COILS program is that pairwise residue correlations eliminated false positive identifications of α-helical proteins predicted by COILS to be coiled-coil structures. Modifications to PairCoil in the Kim group led to the development of MultiCoil (which predicts two- and three-stranded coiled-coils), LearnCoil (which uses an iterative approach to scoring sequences), and LearnCoil-VMF (which identifies three-stranded coiled-coils in viral membrane fusion proteins).

While the programs in the previous paragraph assign coiled-coil scores based on the statistical occurrence of residues in the heptad repeat, STABLECOIL uses experimentally determined values for coiled-coil stability at positions **a** and **d** and α-helix propensity to calculate stability scores for regions along a protein sequence. Rather than giving an overall score, it indicates regions of relatively high and low coiled-coil stability along the sequence. The accuracy of the programs was tested against constructed databases of protein sequences with solved structures known to contain coiled-coils. As a negative control, programs were also tested against databases containing protein sequences lacking coiled-coil structures.

obtained at the level of individual amino acids. Changes in tryptophan emission fluorescence indicate changes in the polarity of the surrounding environment at the level of the individual aromatic side-chain packing, whereas changes in far-UV circular dichroism at 222 nm indicate a change of helical secondary structure at the level of protein backbone conformation (van Mierlo et al. 2000). Having three-dimensional structural information on the coiled-coil also supports the claim of a fully folded structure before denaturation takes place.

A peptide based on the coiled-coil sequence of GCN4 exhibits two-state unfolding as observed by thermal and urea denaturations monitored by CD spectroscopy and differrential scanning calorimetry (Izbarra-Molero et al. 2001). Part of this GCN4 sequence was used to design the GCN4/cortexillin I hybrid analogs described in Chapters 3 and 4. However, the unfolding curves of some proteins are not best fit to a two-state model. Multiple transitions were observed by additional reductions in slope terms, as described in a GCN4 coiled-coil analog (Asn moved from the central location in position 16**a** to the previous heptad at position 9**a**) that appeared to best fit a three-state model (Zhu et al. 2001).

Chapter 1-11. Trigger sequences. Although the presence of hydrophobic residues at positions **a** and **d** in the heptad repeat make a major contribution to the stability of the coiled-coil fold, some protein sequences containing the hydrophobic repeat do not form coiled-coils without a key region dubbed the 'trigger' sequence (Figure 1-2) (Kammerer et al. 1998; Steinmetz et al. 1998; Frank et al. 2000; Wu et al. 2000). Deletion analysis of the coiled-coil regions of cortexillin I, human macrophage scavenger receptor, and intermediate filaments revealed a lack of folding in the absence of the 'trigger sequence'.

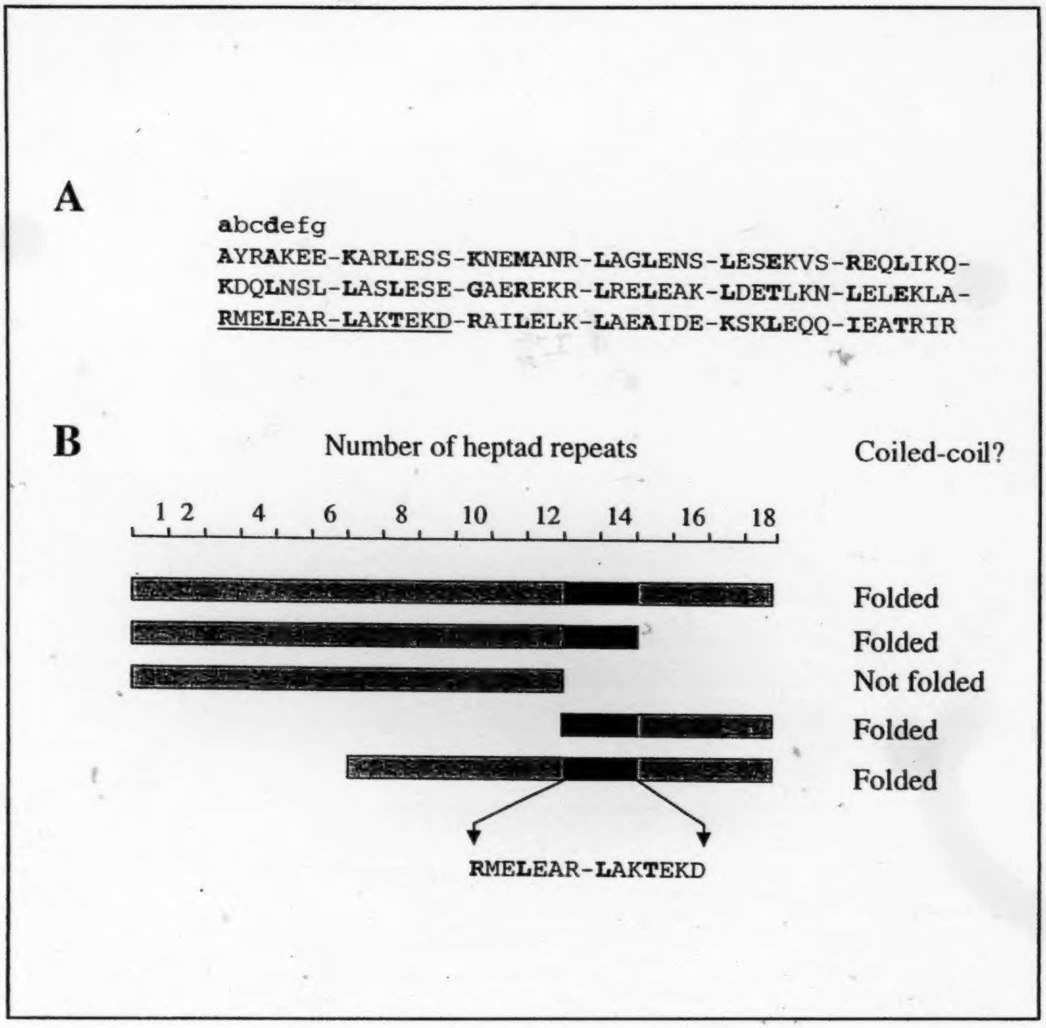
A
abcdefg
AYRAKEE-KARLESS-KNEMANR-LAGLENS-LESEKVS-REQLIKQ-
KDQLNSL-LASLESE-GAEREKR-LRELEAK-LDETLKN-LELEKLA-
RMELEAR-LAKTEKD-RAILELK-LAEAIDE-KSKLEQQ-IEATRIR
B
Number of heptad repeats
Coiled-coil?
1 2 4 6 8 10 12 14 16 18
Folded
Folded
Not folded
Folded
Folded
RMELEAR-LAKTEKD

Fig. 1-2. Design and preparation of N- and C-terminal deletion constructs from cortexillin I (abbreviated as Ir; figure and legend adapted from Steinmetz *et al.* 1998). **(A)** Amino acid sequence of Ir. Heptad repeats were assigned according to the COILS algorithm (Lupas *et al.*, 1991) and are shown in blocks of seven amino acid residues denoted abcdefg. Residues at heptad positions **a** and **d** are indicated in bold. The amino acid trigger site crucial for coiled-coil formation is underlined. **(B)** Schematic representation of Ir and various fragments thereof. The sizes of the polypeptide chain fragments are denoted on top by numbers of heptad repeats. The trigger site for coiled-coil formation is marked as a black box.

Also, designed 31-residue peptides with an excellent hydrophobic core (2 Val, 5 Leu, 1 Met and 1 Asn) did not fold into coiled-coils unless a 13-residue 'trigger sequence' was present (Kammerer et al. 1998). The 'trigger sequence' idea was further extended to other two-stranded coiled-coils as a 13-residue 'consensus trigger sequence' that may serve as a local region of high stability to facilitate folding, as it contains many potential interhelical and intrahelical ion pair stabilizing elements.

Chapter 3 addresses the trigger sequence idea as it relates to a consensus sequence used to screen coiled-coil databases. We addressed the necessity of a consensus trigger sequence in the folding of two-stranded coiled-coils by studying a series of designed sequences containing stable hydrophobic residues in the core positions, with small incremental differences in coiled-coil stability. We determined the increase in stability required to get a nonfolding peptide with a good hydrophobic core to fold into a coiled-coil, even without the presence of a 'consensus trigger sequence'.

Chapter 4 describes the X-ray crystal structure of a designed two-stranded coiled-coil peptide (a GCN4/cortexillin I hybrid analog listed in Chapter 3 as Peptide 7) lacking the consensus trigger sequence, as well as the thermodynamic analysis of alanine-substituted peptide analogs. The coiled-coil structure of the hybrid analog reveals stabilizing interactions responsible for the fold, with different ion pairing and hydrogen-bonding interactions *vs.* the native GCN4 X-ray structure (O'Shea et al. 1991). We also determined the stability contributions of leucine residues at positions **e** and **g** relative to alanine, whose quantitative thermodynamic contributions at these positions had been previously unreported, and identified a unique stabilizing hydrogen bonding-salt bridge complex across the central buried polar asparagine residues that is not present in the native GCN4 X-ray structure.

Chapter 1-12. References

Acharya, A., Ruvinov, S.B., Gal, J., Moll, J.R. and Vinson, C. 2002. A heterodimerizing leucine zipper coiled coil system for examining the specificity of a position interactions: amino acids I, V, L, N, A, and K. *Biochemistry* **41:** 14122-14131.

Anfinsen, C.B. 1973. Principles that govern the folding of protein chains. *Science* **181:** 223-230.

Arndt, K.M., Pelletier, J.N., Muller, K.M., Pluckthun, A. and Alber, T. 2002. Comparison of in vivo selection and rational design of heterodimeric coiled coils. *Structure* **10:** 1235-1248.

Baldwin, R.L. and Rose, G.D. 1999. Is protein folding hierarchic? I. Local structure and peptide folding. *Trends Biochem Sci* **24:** 26-33.

Beck, K., Gambee, J.E., Kamawal, A. and Bachinger, H.P. 1997. A single amino acid can switch the oligomerization state of the alpha- helical coiled-coil domain of cartilage matrix protein. *EMBO J.* **16:** 3767-3777.

Berger, B. and Singh, M. 1997. An iterative method for improved protein structural motif recognition. *J. Comput. Biol.* **4:** 261-273.

Berger, B., Wilson, D.B., Wolf, E., Tonchev, T., Milla, M. and Kim, P.S. 1995. Predicting coiled coils by use of pairwise residue correlations. *Proc. Natl. Acad. Sci. U. S. A.* **92:** 8259-8263.

Bolon, D.N., Voigt, C.A. and Mayo, S.L. 2002. De novo design of biocatalysts. *Curr. Opin. Chem. Biol.* **6:** 125-129.

Bornberg-Bauer, E., Rivals, E. and Vingron, M. 1998. Computational approaches to identify leucine zippers. *Nucleic Acids Res.* **26:** 2740-2746.

Brown, J.H., Cohen, C. and Parry, D.A. 1996. Heptad breaks in alpha-helical coiled coils: stutters and stammers. *Proteins* **26:** 134-145.

Burkhard, P., Ivaninskii, S. and Lustig, A. 2002. Improving coiled-coil stability by optimizing ionic interactions. *J. Mol. Biol.* **318:** 901-910.

Burkhard, P., Kammerer, R.A., Steinmetz, M.O., Bourenkov, G.P. and Aebi, U. 2000. The coiled-coil trigger site of the rod domain of cortexillin I unveils a distinct network of interhelical and intrahelical salt bridges. *Structure Fold. Des.* **8:** 223-230.

Burkhard, P., Stetefeld, J. and Strelkov, S.V. 2001. Coiled coils: a highly versatile protein folding motif. *Trends Cell Biol.* **11:** 82-88.

Burley, S.K. and Bonanno, J.B. 2002. Structuring the universe of proteins. *Annu. Rev. Genomics Hum. Genet.* **3:** 243-262.

Campbell, K.M., Sholders, A.J. and Lumb, K.J. 2002. Contribution of buried lysine residues to the oligomerization specificity and stability of the fos coiled coil. *Biochemistry* **41:** 4866-4871.

Clark, E.D. 2001. Protein refolding for industrial processes. *Curr. Opin. Biotechnol.* **12:** 202-207.

Crick, F.H.C. 1953. The packing of α-helices: simple coiled-coils. *Acta Crystallog.* **6:** 689-697.

Daggett, V. and Fersht, A.R. 2003. Is there a unifying mechanism for protein folding? *Trends Biochem. Sci.* **28:** 18-25.

Dill, K.A. 1985. Theory for the folding and stability of globular proteins. *Biochemistry* **24:** 1501-1509.

Dill, K.A. and Chan, H.S. 1997. From Levinthal to pathways to funnels. *Nat. Struct. Biol.* **4:** 10-19.

Dragan, A.I. and Privalov, P.L. 2002. Unfolding of a lecuine zipper is not a simple two-state transition. *J. Mol. Biol.* **321:** 891-908.

Eckert, D.M., Malashkevich, V.N. and Kim, P.S. 1998. Crystal structure of GCN4-pIQI, a trimeric coiled coil with buried polar residues. *J Mol Biol* **284:** 859-865.

Frank, S., Lustig, A., Schulthess, T., Engel, J. and Kammerer, R.A. 2000. A distinct seven-residue trigger sequence is indispensable for proper coiled-coil formation of the human macrophage scavenger receptor oligomerization domain. *J. Biol. Chem.* **275:** 11672-11677.

Gonzalez, L., Jr., Brown, R.A., Richardson, D. and Alber, T. 1996a. Crystal structures of a single coiled-coil peptide in two oligomeric states reveal the basis for structural polymorphism. *Nat. Struct. Biol.* **3:** 1002-1009.

Gonzalez, L., Jr., Woolfson, D.N. and Alber, T. 1996b. Buried polar residues and structural specificity in the GCN4 leucine zipper. *Nat. Struct. Biol.* **3:** 1011-1018.

Graddis, T.J., Myszka, D.G. and Chaiken, I.M. 1993. Controlled formation of model homo- and heterodimer coiled coil polypeptides. *Biochemistry* **32:** 12664-12671.

Hammarstrom, P. and Carlsson, U. 2000. Is the unfolded state the Rosetta Stone of the protein folding problem? *Biochem. Biophys. Res. Commun.* **276:** 393-398.

Harbury, P.B., Zhang, T., Kim, P.S. and Alber, T. 1993. A switch between two-, three-, and four-stranded coiled coils in GCN4 leucine zipper mutants. *Science* **262:** 1401-1407.

Harbury, P.B., Kim, P.S. and Alber, T. 1994. Crystal structure of an isoleucine-zipper trimer. *Nature* **371:** 80-83.

Harbury, P.B., Plecs, J.J., Tidor, B., Alber, T. and Kim, P.S. 1998. High-resolution protein design with backbone freedom. *Science* **282:** 1462-1467.

Hodges, R.S. 1996. De novo design of alpha-helical proteins: basic research to medical applications. *Biochem. Cell. Biol.* **74:** 133-154.

Holtzer, M.E., Lovett, E.G., d'Avignon, D.A. and Holtzer, A. 1997. Thermal unfolding in a GCN4-like leucine zipper: 13C alpha NMR chemical shifts and local unfolding curves. *Biophys J* **73:** 1031-1041.

Izbarra-Molero, B., Makhatadze, G.I. and Matthews, C.R. 2001. Mapping the energy surface for the folding reaction of the coiled-coil peptide GCN4-p1. *Biochemistry* **40:** 719-731.

Jelokhani-Niaraki, M., Prenner, E.J., Kondejewski, L.H., Kay, C.M., McElhaney, R.N. and Hodges, R.S. 2001. Conformation and other biophysical properties of cyclic antimicrobial peptides in aqueous solutions. *J. Pept. Res.* **58:** 293-306.

Kammerer, R.A., Schulthess, T., Landwehr, R., Lustig, A., Engel, J., Aebi, U. and Steinmetz, M.O. 1998. An autonomous folding unit mediates the assembly of two-stranded coiled coils. *Proc Natl Acad Sci U S A* **95:** 13419-13424.

Kohn, W.D. and Hodges, R.S. 1998. De novo design of alpha-helical coiled-coils and bundles: models for the development of protein-design principles. *Trends Biotechnol.* **16:** 379-389.

Kohn, W.D., Kay, C.M. and Hodges, R.S. 1995a. Protein destabilization by electrostatic repulsions in the two-stranded alpha-helical coiled-coil/leucine zipper. *Protein Sci.* **4:** 237-250.

Kohn, W.D., Monera, O.D., Kay, C.M. and Hodges, R.S. 1995b. The effects of interhelical electrostatic repulsions between glutamic acid residues in controlling the dimerization and stability of two- stranded alpha-helical coiled-coils. *J. Biol. Chem.* **270:** 25495-25506.

Kwok, S.C., Tripet, B., Man, J.H., Chana, M.S., Lavigne, P., Mant, C.T. and Hodges, R.S. 1998. Structural cassette mutagenesis in a de novo designed protein: proof of a novel concept for examining protein folding and stability. *Biopolymers* **47:** 101-123.

Lau, S.Y., Taneja, A.K. and Hodges, R.S. 1984. Synthesis of a model protein of defined secondary and quaternary structure. Effect of chain length on the stabilization and formation of two-stranded alpha-helical coiled-coils. *J. Biol. Chem.* **259:** 13253-13261.

Lavigne, P., Crump, M.P., Gagne, S.M., Hodges, R.S., Kay, C.M. and Sykes, B.D. 1998. Insights into the mechanism of heterodimerization from the 1H-NMR solution structure of the c-Myc-Max heterodimeric leucine zipper. *J Mol Biol* **281:** 165-181.

Lavigne, P., Sonnichsen, F.D., Kay, C.M. and Hodges, R.S. 1996. Interhelical salt bridges, coiled-coil stability, and specificity of dimerization. *Science* **271:** 1136-1138.

Levinthal, C. 1969. How to fold graciously. In *Mossbauer spectroscopy in biological systems: Proceedings of a meeting held at Allerton House, Monticello, Illinois* (J. T. P. DeBrunner and E. Munck, eds.), 22-24, University of Illinois Press, Monticello, Illinois.

Litowski, J.R. and Hodges, R.S. 2002. Designing heterodimeric two-stranded alpha-helical coiled-coils. Effects of hydrophobicity and alpha-helical propensity on protein folding, stability, and specificity. *J. Biol. Chem.* **277:** 37272-37279.

Lumb, K.J. and Kim, P.S. 1995. A buried polar interaction imparts structural uniqueness in a designed heterodimeric coiled coil. *Biochemistry* **34:** 8642-8648.

Lupas, A. 1996. Coiled coils: new structures and new functions. *Trends Biochem. Sci.* **21:** 375-382.

Lupas, A., Van Dyke, M. and Stock, J. 1991. Predicting coiled coils from protein sequences. *Science* **252:** 1162-1164.

Makhatadze, G.I., Loladze, V.V., Ermolenko, D.N., Chen, X. and Thomas, S.T. 2003. Contribution of surface salt bridges to protein stability: guidelines for protein engineering. *J. Mol. Biol.* **327:** 1135-1148.

Martin, L. and Vita, C. 2000. Engineering novel bioactive mini-proteins from small size natural and de novo designed scaffolds. *Curr. Protein Pept. Sci.* **1:** 403-430.

Mezei, M. 1998. Chameleon sequences in the PDB. *Protein Eng.* **11:** 411-414.

Minor, D.L., Jr. and Kim, P.S. 1996. Context-dependent secondary structure formation of a designed protein sequence. *Nature* **380:** 730-734.

Mittl, P.R., Deillon, C., Sargent, D., Liu, N., Klauser, S., Thomas, R.M., Gutte, B. and Grutter, M.G. 2000. The retro-GCN4 leucine zipper sequence forms a stable three-dimensional structure. *Proc. Natl. Acad. Sci. U. S. A.* **97:** 2562-2566.

Moitra, J., Szilak, L., Krylov, D. and Vinson, C. 1997. Leucine is the most stabilizing aliphatic amino acid in the d position of a dimeric leucine zipper coiled coil. *Biochemistry* **36:** 12567-12573.

Monera, O.D., Kay, C.M. and Hodges, R.S. 1994. Electrostatic interactions control the parallel and antiparallel orientation of alpha-helical chains in two-stranded alpha-helical coiled-coils. *Biochemistry* **33:** 3862-3871.

Monera, O.D., Zhou, N.E., Kay, C.M. and Hodges, R.S. 1993. Comparison of antiparallel and parallel two-stranded alpha-helical coiled-coils. Design, synthesis, and characterization. *J. Biol. Chem.* **268:** 19218-19227.

Monera, O.D., Zhou, N.E., Lavigne, P., Kay, C.M. and Hodges, R.S. 1996. Formation of parallel and antiparallel coiled-coils controlled by the relative positions of alanine residues in the hydrophobic core. *J. Biol. Chem.* **271:** 3995-4001.

Myszka, D.G. and Chaiken, I.M. 1994. Design and characterization of an intramolecular antiparallel coiled coil peptide. *Biochemistry* **33:** 2363-2372.

O'Shea, E.K., Klemm, J.D., Kim, P.S. and Alber, T. 1991. X-ray structure of the GCN4 leucine zipper, a two-stranded, parallel coiled coil. *Science* **254:** 539-544.

O'Shea, E.K., Lumb, K.J. and Kim, P.S. 1993. Peptide "Velcro*": design of a heterodimeric coiled coil. *Curr. Biol.* **3:** 658-667.

O'Shea, E.K., Rutkowski, R. and Kim, P.S. 1989. Evidence that the leucine zipper is a coiled coil. *Science* **243:** 538-542.

Oakley, M.G. and Kim, P.S. 1998. A buried polar interaction can direct the relative orientation of helices in a coiled coil. *Biochemistry* **37:** 12603-12610.

Plaxco, K.W., Riddle, D.S., Grantcharova, V. and Baker, D. 1998. Simplified proteins: minimalist solutions to the 'protein folding problem'. *Curr. Opin. Struct. Biol.* **8:** 80-85.

Schmid, M.B. 2002. Structural proteomics: the potential of high-throughput structure determination. *Trends Microbiol.* **10:** S27-S31.

Serrano, L., Horovitz, A., Avron, B., Bycroft, M. and Fersht, A.R. 1990. Estimating the contribution of engineered surface electrostatic interactions to protein stability by using double-mutant cycles. *Biochemistry* **29:** 9343-9352.

Sia, S.K. and Kim, P.S. 2001. A designed protein with packing between left-handed and right-handed helices. *Biochemistry* **40:** 8981-8989.

Singh, M., Berger, B. and Kim, P.S. 1999. LearnCoil-VMF: computational evidence for coiled-coil-like motifs in many viral membrane-fusion proteins. *J. Mol. Biol.* **290:** 1031-1041.

Sodek, J., Hodges, R.S., Smillie, L.B. and Jurasek, L. 1972. Amino-acid sequence of rabbit skeletal tropomyosin and its coiled-coil structure. *Proc. Natl. Acad. Sci. U. S. A.* **69:** 3800-3804.

Steinmetz, M.O., Stock, A., Schulthess, T., Landwehr, R., Lustig, A., Faix, J., Gerisch, G., Aebi, U. and Kammerer, R.A. 1998. A distinct 14 residue site triggers coiled-coil formation in cortexillin I. *EMBO J.* **17:** 1883-1891.

Strelkov, S.V. and Burkhard, P. 2002. Analysis of alpha-helical coiled coils with the program TWISTER reveals a structural mechanism for stutter compensation. *J. Struct. Biol.* **137:** 54-64.

Su, J.Y., Hodges, R.S. and Kay, C.M. 1994. Effect of chain length on the formation and stability of synthetic alpha-helical coiled coils. *Biochemistry* **33:** 15501-15510.

Talaga, D.S., Lau, W.L., Roder, H., Tang, J., Jia, Y., DeGrado, W.F. and Hochstrasser, R.M. 2000. Dynamics and folding of single two-stranded coiled-coil peptides studied by fluorescent energy transfer confocal microscopy. *Proc. Natl. Acad. Sci. U. S. A.* **97:** 13021-13026.

Tang, Y., Ghirlanda, G., Vaidehi, N., Kua, J., Mainz, D.T., Goddard III, W.A., DeGrado, W.F. and Tirrell, D.A. 2001. Stabilization of coiled-coil peptide domains by introduction of trifluoroleucine. *Biochemistry* **40:** 2790-2796.

Temussi, P.A., Masino, L. and Pastore, A. 2003. From Alzheimer to Huntington: why is a structural understanding so difficult? *EMBO J.* **22:** 355-361.

Tripet, B., Wagschal, K., Lavigne, P., Mant, C.T. and Hodges, R.S. 2000. Effects of side-chain characteristics on stability and oligomerization state of a de novo-designed model coiled-coil: 20 amino acid substitutions in position "d". *J. Mol. Biol.* **300:** 377-402.

Tripet, B.T. and Hodges, R.S. 2001. STABLECOIL: An algorithm designed to predict the location and relative stability of coiled-coils in native protein sequences. In *Peptides: The Wave of the Future, Proceedings of the Second International/Seventeenth American Peptide Symposium* (M. Lebl and R. A. Houghten, eds.), 365-366., Kluwer Academic Publishers, San Diego, CA.

van Mierlo, C.P. and Steensma, E. 2000. Protein folding and stability investigated by fluorescence, circular dichroism (CD), and nuclear magnetic resonance (NMR) spectroscopy: the flavodoxin story. *J Biotechnol* **79:** 281-298.

Vaughan, C.K., Harryson, P., Buckle, A.M. and Fersht, A.R. 2002. A structural double-mutant cycle: estimating the strength of a buried salt bridge in barnase. *Acta Crystallog. sect. D* **58:** 591-600.

Wagschal, K., Tripet, B. and Hodges, R.S. 1999a. De novo design of a model peptide sequence to examine the effects of single amino acid substitutions in the hydrophobic core on both stability and oligomerization state of coiled-coils. *J. Mol. Biol.* **285:** 785-803.

Wagschal, K., Tripet, B., Lavigne, P., Mant, C. and Hodges, R.S. 1999b. The role of position a in determining the stability and oligomerization state of alpha-helical coiled coils: 20 amino acid stability coefficients in the hydrophobic core of proteins. *Protein Sci.* **8:** 2312-2329.

Wolf, E., Kim, P.S. and Berger, B. 1997. MultiCoil: a program for predicting two- and three-stranded coiled coils. *Protein Sci.* **6:** 1179-1189.

Wu, K.C., Bryan, J.T., Morasso, M.I., Jang, S.I., Lee, J.H., Yang, J.M., Marekov, L.N., Parry, D.A. and Steinert, P.M. 2000. Coiled-coil trigger motifs in the 1B and 2B rod domain segments are required for the stability of keratin intermediate filaments. *Mol. Biol. Cell* **11:** 3539-3558.

Wuthrich, K. and Riek, R. 2001. Three-dimensional structures of prion proteins. *Adv. Protein Chem.* **57:** 55-82.

Yu, Y. 2002. Coiled-coils: stability, specificity, and drug delivery potential. *Adv. Drug Deliv. Rev.* **54:** 1113-1129.

Zhou, N.E., Kay, C.M. and Hodges, R.S. 1994a. The net energetic contribution of interhelical electrostatic attractions to coiled-coil stability. *Protein Eng.* **7:** 1365-1372.

Zhou, N.E., Kay, C.M. and Hodges, R.S. 1994b. The role of interhelical ionic interactions in controlling protein folding and stability. De novo designed synthetic two-stranded alpha- helical coiled-coils. *J Mol. Biol.* **237:** 500-512.

Zhu, B.Y., Zhou, N.E., Kay, C.M. and Hodges, R.S. 1993. Packing and hydrophobicity effects on protein folding and stability: effects of beta-branched amino acids, valine and isoleucine, on the formation and stability of two-stranded alpha-helical coiled coils/leucine zippers. *Protein Sci.* **2:** 383-394.

Zhu, H., Celinski, S.A., Scholtz, J.M. and Hu, J.C. 2001. An engineered leucine zipper a position mutant with an unusual three- state unfolding pathway. *Protein Sci.* **10:** 24-33.

Chapter 1B. Introduction to antimicrobial peptides

Chapter 1-12. The antibiotic era and the development of antibiotic resistance

A major medical milestone was reached in the late nineteenth century upon the discovery and development of modern antibiotics. The first natural antibiotic, pyocyanase, was discovered in 1888 in bacteria called *Bacillus pyocyaneus* (now called *Pseudomonas aeruginosa*) when E. de Freudenreich tested a solution that stopped growth of other bacteria (Day 2001). The first effective antibacterial compount, Salvarsan, was marketed in 1910. As an indication of the impact they had on humanity, three of the Nobel Prizes in Medicine were awarded to pioneers in antibiotics research: Florey, Chain and Fleming shared the award in 1945 for the discovery and synthesis of penicillin; Domagk won in 1947 for the discovery of the antibiotic from industrial red dye, Prontosil rubrum; and Waksman won in 1952 for discovering streptomycin. Before the large-scale production of antibiotics such as penicillin, bacterial infections were difficult to treat or contain and were a major cause of death worldwide. As more antibiotics were discovered over the following decades, it appeared as though humankind had an abundant supply of effective antimicrobial agents that could adequately control the spread of bacterial infections. Consequently, research into developing new antibiotics dropped precipitously in the latter half of the 20th century.

However, in recent years the pendulum appears to be swinging back in favor of the microbes. The number of microorganisms resistant to one or more antibiotics has been on the rise for the past several decades. Bacteria that are resistant to several different kinds of antibiotics (*i.e.*, multidrug resistant bacteria) have emerged that do not respond even to the antibiotic of last resort, vancomycin. Bacterial strains such as vancomycin-resistant

Enterococcus (VRE), methicillin-resistant *Staphylococcus aureus* (MRSA), and vancomycin-resistant *S. aureus* (VRSA) have appeared in hospitals, causing many to wonder if our current supply of effective antimicrobial agents is on the decline (Heinemann 1999). Clearly there is a growing need to slow the emergence of antibiotic-resistant bacteria, and an increased demand for the development and introduction of novel antimicrobial agents into the drug pipeline.

Development of antibiotic resistance

Mode of action of conventional antibiotics. How do bacteria become antibiotic-resistant? To answer this question, it is imperative to understand the mode of action of conventional antibiotics. Antibiotics kill bacteria in a highly specific fashion, by entering the cell interior and binding to a biomolecule both specific for the microorganism and necessary for cell survival, such as a cell wall component or an enzyme involved in transcription, translation, or intermediary metabolism. The specific molecule targeted by the antibiotic is not present in human cells, so the antibiotic has lower toxicity to the patient. Although killing is not immediate, the interruption of bacterial metabolic processes eventually leads to cell death over the days following the intial antibiotic treatment.

Antibiotic resistance. Antibiotic usage promotes the survival of resistant bacterial strains by killing susceptible strains that would proliferate better than resistant strains under ordinary growth conditions. Unfortunately, the same reason for the high specificity of antibiotics (binding to a specific bacterial molecule) provides a way for bacteria to become resistant to conventional antibiotics. If the mutations in the target reduce drug binding, or the expression of the target molecule increases so that the population of molecules outnumbers the drug, the bacteria can survive antibiotic therapy. At the molecular level, most antibiotic resistance mechanisms act either through exclusion of the drug from the cell by reduction in drug permeability, alteration of the target molecule to decrease antibiotic binding affinity (*e.g.* point mutation of the 50S ribosome to decrease binding of erythromycin), chemical inactivation of the antibiotic (*e.g.* β-lactamases that hydrolyze β-lactam antibiotics such as penicillin and methicillin), physical removal of the antibiotic from the site of action (usually with a transmembrane efflux pump to remove the drug from the cell interior), or overproduction of the target molecule. These resistance mechanisms can develop either through random gene mutation during cell division, chromosomal breakage or rearrangement, or by horizontal gene transfer (Heinemann 1999). In horizontal gene transfer, antibiotic-resistant microorganisms from one type of bacteria pass on genes that code for protein(s) involved in resistance to a different strain (antibiotic-sensitive strain of the same species) or a different species. This transfer allows genetic information conferring resistance to an antibiotic to be shared quickly among various bacterial populations. Surprisingly, gene transfer can also occur in bacteria that cannot divide and may already be dead, but still contain components that allow gene transfer to take place. Some antibiotics can promote this transfer of resistance genes; for example, tetracycline can stimulate the transmission of a transposable element coding for tetracycline resistance by 5- to 100-fold (Torres 1991).

Each class of antibiotics has limited scope in terms of its ability to target different the classes of microorganisms, such as Gram-negative and Gram-positive bacteria. These two categories of bacteria, classified according to their positive or negative staining by crystal violet or methylene blue dye, have markedly different compositions and organizations of their cell walls, with Gram-negative bacteria being surrounded by a double membrane and Gram-positive bacteria enveloped by a single cell membrane coated with a thick peptidoglycan layer (Hancock 1997a). The outer membrane of Gram-negative bacteria acts as a permeability barrier preventing some drugs from entering the cell cytoplasm.

Chapter 1-14. Discovery of antimicrobial peptides

In the latter half of the 20th century, a new class of antimicrobial compounds was discovered in several different types of animals (frogs, moths, bees) as part of their innate immune systems. These compounds were cationic antimicrobial peptides synthesized on the ribosome and expressed by the host organism. Rather than acting on a specific component of bacterial cells, the peptides were thought to act directly on the lipid bilayer in a concentration-dependent manner, exhibiting rapid killing effects (seconds to minutes *vs.* hours for conventional antibiotics) across a broad spectrum of Gram-positive and Gram-negative microorganisms. Because the killing time was so brief and the mode of action was to destabilize the cell wall structure rather than to target specific components of the cell wall, it was thought that bacteria would become less likely to develop resistance against these antimicrobial peptides.

Antimicrobial peptide description

Since the discovery of antimicrobial peptides in the frog skin of *Bombina variegata* in 1970 by Csordas and Michl (Csordas et al. 1970), a large number of peptides have been isolated and characterized from several biological sources (plant and animal sequences are found at http://www.bbcm.univ.trieste.it/~tossi/pag1.html). The definition of an antimicrobial peptide is usually a sequence of amino acids with a molecular weight between 1-5 kDa that exhibits concentration-dependent broad-spectrum bacteriostatic or bacteriocidal activity, generally at micromolar (μM) peptide concentrations. Many of these peptides also possess other functions that will not be discussed here, such as antifungal, anti-endotoxin, antiviral, anticancer, antiparasite, and wound healing properties (Hancock et al. 2000). This definition of antimicrobial peptides does not address toxicity to eukaryotic (*e.g.* mammalian) cells, a fundamental parameter in developing a therapeutic for human use; many peptides classified as "antimicrobial" also have strong hemolytic activity, *i.e.* are toxic to red blood cells (erythrocytes). Antimicrobial peptides can be classified by whether they are produced by the ribosome or made without ribosomes; the peptides made without ribosomes are produced almost exclusively by bacteria, whereas peptides made by ribosomes are found in a variety of organisms of bacterial, plant, and animal nature (Hancock et al. 1999).

Most antimicrobial peptides exhibit a net cationic charge, a large hydrophobic moment, and some type of amphipathicity (a polar face and a nonpolar or hydrophobic face). Some exceptions to these general rules include the anionic peptide, alamethicin (Martin et al. 1976); the hydrophobic channel-forming peptide, gramicidin A (Wallace 1998); and the hydrophilic peptide, androctonin (Hetru et al. 2000). The basic residues in most antimicrobial peptides (AMPs) are thought to promote initial electrostatic interactions between the positively charged peptide and the anionic lipids found in bacterial membrane. These electrostatic interactions may play a role in conferring specificity to bacterial membranes, because the composition of eukaryotic membranes is primarily the zwitterionic (both positively and negatively charged) lipid, phosphatidylcholine. The hydrophobic side-chains of the peptide then become important in associating with the hydrophobic acyl chain region of the lipid bilayer. Changes to the membrane occur as the peptide reaches a critical concentration, resulting in observable differences in parameters such as phase transition temperature, electrochemical potential, membrane permeability, and lipid bilayer flip-flop (Hancock et al. 2002).

Elucidating a mode of action common to all peptides has proven to be a difficult task because they vary greatly in their three-dimensional structure in aqueous solutions as well as in membrane environments. These structures in aqueous solution have been classified into four categories for antimicrobial peptides found in nature: I) the linear α-helical class, II) the linear extended peptides with one overrepresented amino acid, III) the looped structures, and IV) the disulfide-bridged β-strands (Hancock 1997b; Epand et al. 1999; van 't Hof et al. 2001). Epand and Vogel have added groups including cyclic peptides with thioether groups (lantibiotics), lipopeptides terminating in an amino alcohol (peptaibols), and macrocyclic cystine-knotted peptides (Epand et al. 1999). Recently, designed peptides with supramolecular structures, *e.g.* stacked β-sheet cylinders (Fernandez-Lopez et al. 2001) and peptides with unusual helical structure such as a 12-helix (containing β-amino acids and named for the twelve-membered-ring hydrogen bonds in the secondary structure) (Liu et al. 2001; Porter et al. 2002) have been added to this initial structural classification list, and possess the added benefit of higher protease stability. Generally, many antimicrobial peptides possess positive correlations between peptide amphipathicity, hydrophobicity, and hemolytic activity - that is, the most hydrophobic and amphipathic peptides tend to exhibit strong hemolytic activity (Oren et al. 1997; Kondejewski et al. 1999; Avrahami et al. 2001).

Chapter 1-15. Antimicrobial peptide mechanisms of action

What happens to the structure of the bacterial membrane when it interacts with antimicrobial peptides? Studies with model membrane systems have shown that some peptides affect the physical properties of the bilayer, such as curvature (tending to increase positive or negative curvature depending on the peptide), thickness (decreased thickness with increased peptide concentration), and fluidity (Epand 1998). Some peptides can induce membrane fusion among unilamellar vesicles, cause intravesicular aqueous dye release, or promote lipid flip-flop across the bilayer. In bacteria, electron microscopy has also revealed peptide-induced surface morphology changes such as 'blebbing' (Hancock et al. 1999), where projections are observed on the outer surface.

Two prevailing models have been proposed for the appearance of the peptide-lipid complex (Figure 1-3). One of these mechanisms is consistent with observations of pore formation and depolarization of the cell interior, in the 'barrel-stave' model. In this model, peptides form multimeric α-helices oriented perpendicular to the lipid bilayer plane in a bundle. Because of the perpendicular arrangement a pore is formed, causing membrane depolarization. Another proposed mechanism allows the peptide to pass through the outer membrane to the inner membrane of Gram-negative bacteria in a process termed by Hancock as 'self-promoted uptake' (Hancock 1997b; Scott et al. 2000). Such a mechanism is illustrated in the 'carpet' model, where transient pore formation is observed (Shai 1999). In this model, accumulation of peptides parallel to the membrane plane causes detergent-like effects on the lipid bilayer (*i.e.* micelle formation) as the peptides briefly reorient and traverse the membrane, decreasing local peptide concentration on the

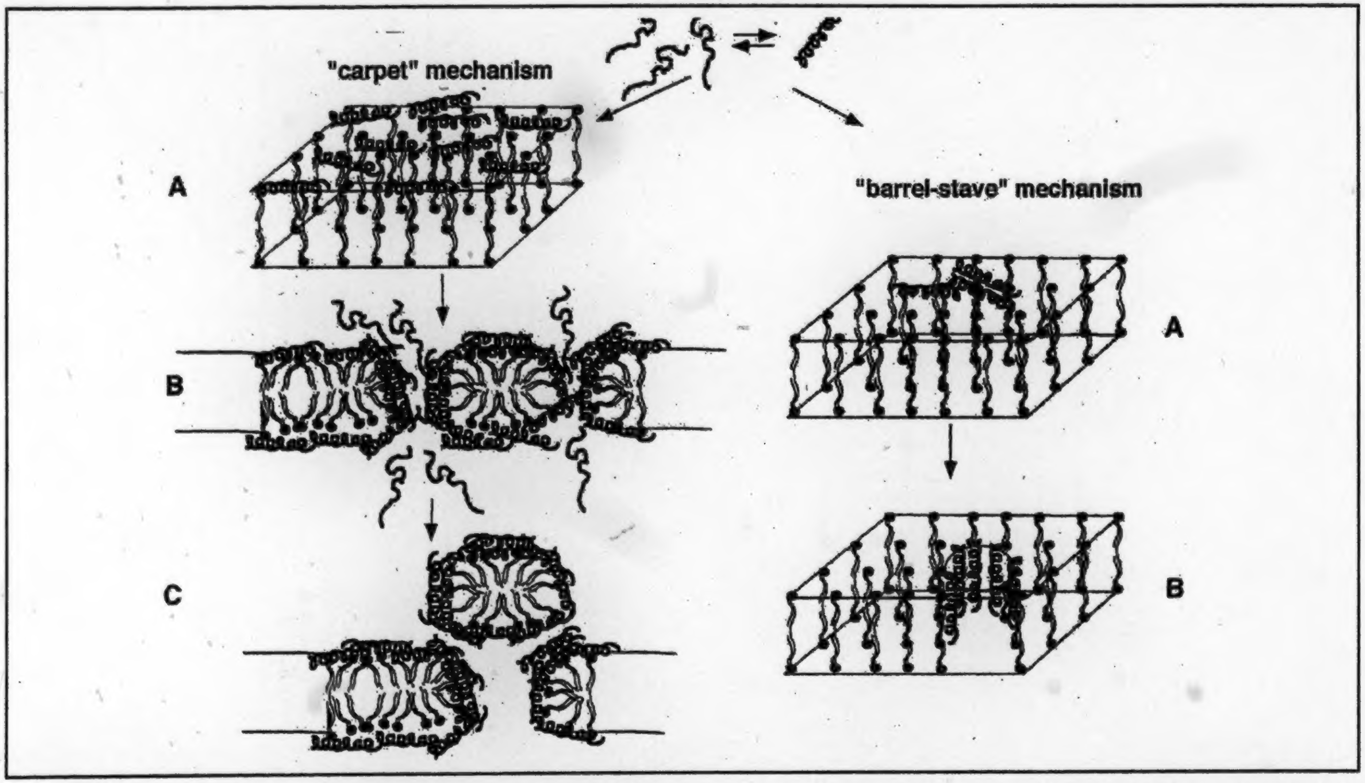

Fig. 1-3. The 'carpet' (left) and 'barrel-stave' (right) models suggested for membrane permeation (figure and legend adapted from Shai 1999). In the 'carpet' model, the peptides are bound to the surface of the membrane with their hydrophobic surfaces facing the membrane and their hydrophilic surfaces facing the solvent (step A). When a threshold concentration of peptide monomers is reached, the membrane goes into pieces (steps B and C). At this stage a transient pore is formed. In the 'barrel-stave' model, peptides first assemble in the surface of the membrane, then insert into the lipid core of the membrane following recruitment of additional monomers.

outer monolayer and eventually stopping pore formation. Peptides oriented perpendicular to the bilayer plane induce local lipid headgroup reorientation such that the headgroups become pointed inwards towards the center of a toroidal pore. In this model, the peptides not only disrupt the electrochemical potential through pore formation but also allow lipid flip-flop since the toroidal pore connects the monolayers. Despite the differences in these proposed modes of action, all antimicrobial peptides share the common trait that they first encounter the bacterial cell wall; this interaction in some way directly or indirectly leads to cell growth inhibition or cell death.

For many years, the most widely held view about the action of antimicrobial peptides was that they acted primarily on the bacterial lipid membrane, to destroy bacteria through membrane destabilization and disruption of the transmembrane electrochemical potential. However, recent work by Hancock *et al.* suggests that during their course of action, some antimicrobial peptides may interact not only with the bacterial cell wall, but also on one or more other cellular targets. These targets may include membrane lipids and/or proteins involved with the functioning of cellular respiration and/or intracellular components including heat shock proteins and polyanions such as DNA and RNA (Hancock et al. 2002). As a result, other components of the adaptive immune system are activated by antimicrobial peptides (Hancock et al. 2000; Zasloff 2002). These additional targets have been the subject of investigation because of observations that complete bacterial lysis was not always observed at the MIC (minimal peptide concentration required to inhibit bacterial growth) (Friedrich et al. 2000). So, the model of membrane destabilization and cell lysis at MIC concentrations (*i.e.* a 'lipid-only' mechanism) was not always supported by experimental results. If additional molecules beyond the lipid bilayer were targeted by antimicrobial peptides, e.g. DNA binding to inhibit transcription, this 'multi-hit' hypothesis might better explain the mode of action of peptides that appear bacteriostatic (rather than bactericidal) at the MIC value.

Chapter 1-16. Drawbacks to peptide therapeutics. There are some fundamental drawbacks to using cationic peptides in place of antibiotics, many of them common to any peptide being developed as a drug. Because an important aspect of the mode of action involves peptide-lipid interactions at the cell wall, there is a lower microbial specificity with antimicrobial peptides (which can interact with lipids in both prokaryotic and eukaryotic cells) *vs.* conventional antibiotics (which specifically interact with biomolecules found only in bacteria and other microbes). Oral bioavailability is low because all peptides and proteins composed of L-amino acids are susceptible to enzymatic proteolysis in the gut. Since the majority of antimicrobial peptides require an overall basic (cationic) charge, the presence of high salt concentrations tends to screen the long-range ionic interactions between peptide and lipid, thus decreasing antimicrobial activity in high salt environments such as the often-infected, mucus-covered lungs of cystic fibrosis patients (Goldman et al. 1997). Still, there are laboratories designing salt-insensitive versions of antimicrobial peptides (Friedrich et al. 1999; Tam et al. 2000) and companies actively engaged in clinical trials with cationic antimicrobial peptides (Zasloff 2002).

Chapter 1-17. Large-scale industrial peptide production. There are tradeoffs involved with each method of peptide production in large-scale quantities for therapeutic applications. The two in common usage are the production of recombinant peptides in a bacterial expression system, and chemical synthesis of peptides using solid-phase or solution-phase methodology. Although the cost of peptide production for commercialization would be reduced by expressing recombinant peptides in bacteria *vs.* chemical synthesis, recombinant methodology has its own limitations in the types of sequences that can be produced by the ribosome, *i.e.* linear sequences with free N- and C-termini containing L-enantiomers of the twenty naturally occurring amino acids. With a recombinant system, the directed formation of specific disulfide bonds in AMPs containing multiple cysteine residues is not possible, whereas with solid-phase peptide chemistry this task is achievable through the appropriate selection of side-chain blocking groups during synthesis. There can also be solubility issues due to peptide self-association/aggregation and the formation of inclusion bodies in a bacterial expression system, especially in the case of highly amphipathic molecules such as cationic antimicrobial peptides.

Chapter 1-18. Gramicidin S

Selection of gramicidin S for structure-activity studies. Our laboratory selected a specific antibiotic, the cyclic antiparallel β-sheet peptide gramicidin S (GS), as the parent molecule on which to base structure-activity studies. Gramicidin S was chosen because it possessed several key features that made it an ideal compound. First, a rigid defined structure (such as the β-sheet in GS) is more amenable to structure-function studies since differences in both the structure and activity of peptide analogs could be easily compared to the parent molecule. Second, its small size should allow easy synthesis and ultimately should require fewer analogs to achieve the desired biological activities (strong antimicrobial activity and weak hemolytic activity) due to the smaller number of theoretical amino acid substitution sites. Third, the cyclic nature of the peptide made it resistant to proteolysis, an important aspect for future drug stability studies *in vivo*. The fourth advantage, from our perspective, was the possibility of a "lipid-only" mechanism, an idea that brought the possibility of achieving microbial specificity based only on differences in lipid composition between microbes and eukaryotic cells.

History of gramicidin S. Gramicidin S is a 10-residue cyclic antiparallel β-sheet peptide isolated as part of a gramicidin complex in 1942 by the French microbiologist, René Dubos. It was found in a 4:1 ratio of gramicidins (A,B, and C) to tyrocidines (another group of cyclic decapeptide antibiotics) but had limited use because in addition to its antimicrobial activity, it also had strong hemolytic activity (Kondejewski et al. 1996a). GS consists of the sequence cyclo-(Val-Orn-Leu-D-Phe-Pro)$_2$, where the aliphatic residues (two valine and two leucine) comprise the nonpolar face, and the two cationic ornithine residues comprise the polar face (See Appendix 1, Fig. 1). The antiparallel β-strands formed by Val-Orn-Leu are connected by two type II′ β-turns at the D-Phe-Pro positions. Intramolecular hydrogen bonding occurs across the strands between the carbonyl oxygen and amide proton of Val and Leu to stabilize the β-sheet structure.

Gramicidin S biosynthesis. Gramicidin S is produced by the Gram-positive bacteria, *Brevibacillus brevis* (formerly called *Bacillus brevis*) (Shida et al. 1996), with a modular multienzyme complex composed of gramicidin S synthetase 1 (GrsA) and gramicidin S synthetase 2 (Grs B) (Marahiel et al. 1997). The complex consists of a total of five modules, one on GrsA and four on GrsB, with each module containing a recognition, attachment, and adenylation (activation) domain; a thiolation domain; and a condensation domain. After an amino acid is recognized and bound, it is adenylated using adenosine triphosphate (ATP) as the substrate. This activation step allows subsequent thiolation to occur to form a thioester attaching the amino acid to the thiolation domain. The condensation domain then links the amino acid or polypeptide to the downstream C-terminal residue on the adjacent module. The module that binds L-Phe is gramicidin S synthetase 1, which also contains an epimerization domain to convert the amino acid to the D-Phe enantiomer before linking it to L-Pro. Gramicidin S synthetase 2 contains four modules that each recognize and bind to a specific amino acid (L-Pro, L-Val, L-Orn, or L-Leu). Synthesis proceeds linearly from N- to C-terminal as the polypeptide is passed to the C-terminal residue (Leenders et al. 1998), starting with D-Phe and ending with L-Leu. Cyclization of two pentapeptides of the sequence D-Phe-Pro-Val-Orn-Leu occurs in a head-to-tail fashion, completing the synthesis.

GS-resistant bacteria. Although there have been relatively few studies conducted on the general likelihood of bacteria developing resistance to antimicrobial peptides (Hancock 1997b; Lohner 2001), bacterial strains resistant to gramicidin S have been cultured and studied *in vitro*. GS-resistant *E. coli* K12S (Gram-negative bacteria) binds large quantities of GS, but the majority is attached to the outer membrane *vs.* the cytoplasmic membrane where depolarization would occur in GS-sensitive *E. coli* (Bulgakova et al. 1990). This observation suggests that sequestering of GS to the outer membrane may be an effective strategy to prevent or inhibit cytoplasmic membrane disruption in Gram-negative bacteria - a barrier to the 'self-promoted uptake' pathway. A GS-resistant strain of *Micrococcus lysodeikticus* (Gram-positive bacteria) was less sensitive to the membrane-disorganizing effects of GS (Bulgakova et al. 1989), and a resistant strain of *Staphylococcus aureus* 209P (Gram-positive) showed a thickened cell wall relative to the antibiotic-sensitive strain (Bulgakova et al. 2000). Thus, it does appear as though bacteria are capable of developing resistance mechanisms to antimicrobial peptides, and that a strategy for GS resistance is through the alteration of the cell wall composition in a way that counteracts the membrane-disruptive action that GS normally exhibits on Gram-positive and Gram-negative bacteria.

Peptide-lipid studies of GS. Many studies have described the interaction of gramicidin S with lipid bilayers (see review by (Prenner et al. 1999b)). The interaction between GS and the lipid membrane has been proposed to first consist of long-range electrostatic interactions between the cationic peptide and the negative charges in the membrane (phosphate head groups in eukaryotic cells, or lipopolysaccharide or peptidoglycan in bacterial cells). Cationic peptides are also attracted by the inside negative electrochemical potential found across the bacterial cytoplasmic membrane (-150 mV). In Gram-negative bacteria, which contain both an outer membrane and an inner cytoplasmic membrane, GS showed poor outer membrane permeabilizing ability and high accumulation at the inner membrane, suggesting a 'self-promoted uptake' pathway where the outer membrane is not greatly perturbed by the peptide as a result of traversal. The electrostatic attraction is followed by partitioning of the hydrophobic side-chains into the nonpolar environment of the membrane lipid acyl chains. Rather than being deeply buried in the hydrophobic core, GS sits at the polar/apolar interfacial region at the bilayer surface (Prenner et al. 1997; Lewis et al. 1999) such that the β-sheet is oriented parallel to the plane of the membrane (Salgado et al. 2001). At a critical peptide concentration transient pore formation occurs, leading to depolarization of the electrochemical potential (inside negative potential becomes less negative) and triggering of events leading to cell death. These events may include decreasing activity of membrane-associated respiratory enzymes, and/or disrupting interactions between lipids and other membrane proteins to disrupt function. However, the depolarization event alone is not the cause for cell death, as maximal depolarization occurs at a peptide concentration below the minimal inhibitory concentration for *Escherichia coli* (Wu et al. 1999). GS has been shown to induce negative curvature stress and promote the formation of nonlamellar phases that have been suggested to play a role in the disruptive effect on membranes (Prenner et al. 1997). The structure of the disrupted peptide-lipid complex is an inverted cubic phase, as determined by X-ray diffraction studies with *Acholeplasma laidlawii* B and *E. coli* membrane lipids (Staudegger et al. 2000). Gramicidin S is also capable of inducing lipid flip-flop between bilayer leaflets and release of an aqueous dye, calcein, in studies with model unilamellar liposomes (Zhang et al. 2001).

The peptide-lipid interactions of GS are highly dependent on the type of lipids studied. Although GS exhibits a preference for binding anionic lipids such as phosphatidylglycerol (PG), cardiolipin (CL), and phosphatidylserine (PS) due to its net cationic charge, the electrostatic interaction is fairly weak and does not confer a large specificity over zwitterionic lipids phosphatidylcholine (PC) and phosphatidylethanolamine (PE) in model membrane systems (Prenner et al. 1999a; Zhang et al. 2001). Perhaps this is not surprising considering that GS does not exhibit high microbial specificity over hemolytic activity (Kondejewski et al. 1996b). However, cholesterol (found only in eukaryotic cells) decreases GS ability to disrupt model membranes (Prenner et al. 2001) which may partially explain the slightly lower disruptive effects of GS on eukaryotic membranes *vs.* bacterial membranes.

The Hodges laboratory has carried out a long-term program to improve biological activity, structurally characterize peptides, and define peptide specificity to microbial membranes of gramicidin S and related peptides. These studies are reviewed in Appendix 1, which serves as a primer that provides a background leading into the work done in Chapters 5 to 7. Chapter 5 describes the effect of modulating nonpolar face hydrophobicity on biological activity and microbial specificity of 14-residue GS14K4 peptides. Chapter 6 describes the effect of introducing a single D- or L-amino acid substitution at position 4 of GS14 on peptide structure, microbial activity, and bacterial cell wall permeability. Chapter 7 introduces a novel method to evaluate the self-association of amphipathic peptides in aqueous solution by conducting a series of reversed-phase HPLC runs over a temperature range of 5 to 80°C.

Although this thesis appears to contain research pertaining to two distinct areas, there are complementary aspects to the sections. Taken together, these studies encompass the two main classes of secondary structure, the helix (in coiled-coil work) and the β-sheet (in the antimicrobial peptide work). Both sections also employ *de novo* design and illustrate two different aims of design approaches. The first section provides new understanding of fundamental aspects of protein folding, and the second section outlines our development of a peptide compound effective against antibiotic-resistant microorganisms and nontoxic to humans at therapeutic dosages.

Chapter 1-19. References

Avrahami, D., Oren, Z. and Shai, Y. 2001. Effect of multiple aliphatic amino acids substitutions on the structure, function, and mode of action of diastereomeric membrane active peptides. *Biochemistry* **40:** 12591-12603.

Bulgakova, V.G., Korolev, P.N., Konoshenko, G.I., Novozhilova, T.I. and Polin, A.N. 1990. [Stability of Escherichia coli to the membranotropic antibiotic gramicidin S]. *Mikrobiologiia* **59:** 702-704.

Bulgakova, V.G., Kostrova, O.M., Sazykina, S., Korolev, P.N. and Polin, A.N. 1989. [Study of the adaptation resistance in bacteria to membrane active polypeptide antibiotics]. *Antibiot Khimioter* **34:** 425-429.

Bulgakova, V.G., Orlova, T.I., Grushina, V.A. and Polin, A.N. 2000. [The study of Staphylococcus aureus strain resistant to actinomycin D]. *Antibiot Khimioter* **45:** 6-11.

Csordas, A. and Michl, H. 1970. Isolation and structure of a haemolytic polypeptide from the defensive secretion of European Bombina species. *Monatsh Chem* **101:** 182-189.

Day, N. 2001. *Killer superbugs: the story of drug-resistant diseases*, Enslow Publishers, Inc., Berkeley Heights, NJ.

Epand, R.M. 1998. Lipid polymorphism and protein-lipid interactions. *Biochem. Biophys. Acta* **1376:** 353-368.

Epand, R.M. and Vogel, H.J. 1999. Diversity of antimicrobial peptides and their mechanisms of action. *Biochim Biophys Acta* **1462:** 11-28.

Fernandez-Lopez, S., Kim, H.S., Choi, E.C., Delgado, M., Granja, J.R., Khasanov, A., Kraehenbuehl, K., Long, G., Weinberger, D.A., Wilcoxen, K.M. and Ghadiri, M.R. 2001. Antibacterial agents based on the cyclic D,L-alpha-peptide architecture. *Nature* **412:** 452-455.

Friedrich, C.L., Scott, M.G., Karunaratne, N., Yan, H., and Hancock, R.E. 2000. Salt-resistant alpha-helical cationic antimicrobial peptides. *Antimicrob Agents Chemother* **43:** 1542-1548.

Friedrich, C.L., Moyles, D., Beveridge, T.J. and Hancock, R.E. 2000. Antibacterial action of structurally diverse cationic peptides on gram- positive bacteria. *Antimicrob Agents Chemother* **44:** 2086-2092.

Goldman, M. J., Anderson, G. M., Stolzenberg, E. D., Kari, U. P., Zasloff, M., and Wilson, J. M. 1997. Human beta-defensin-1 is a salt-sensitive antibiotic in lung that is inactivated in cystic fibrosis. *Cell* **88:** 553-560.

Hancock, R.E. 1997a. The bacterial outer membrane as a drug barrier. *Trends Microbiol* **5:** 37-42.

Hancock, R.E. 1997b. Peptide antibiotics. *Lancet* **349:** 418-422.

Hancock, R.E. and Chapple, D.S. 1999. Peptide antibiotics. *Antimicrob Agents Chemother* **43:** 1317-1323.

Hancock, R.E. and Diamond, G. 2000. The role of cationic antimicrobial peptides in innate host defences. *Trends Microbiol* **8:** 402-410.

Hancock, R.E. and Rozek, A. 2002. Role of membranes in the activities of antimicrobial cationic peptides. *FEMS Microbiol Lett* **206:** 143-149.

Heinemann, J.A. 1999. How antibiotics cause antibiotic resistance. *Drug Discov Today* **4:** 72-79.

Hetru, C., Letellier, L., Oren, Z., Hoffmann, J.A. and Shai, Y. 2000. Androctonin, a hydrophilic disulphide-bridged non-haemolytic anti- microbial peptide: a plausible mode of action. *Biochem J* **345 Pt 3:** 653-664.

Kondejewski, L.H., Farmer, S.W., Wishart, D.S., Hancock, R.E. and Hodges, R.S. 1996a. Gramicidin S is active against both Gram-positive and Gram-negative bacteria. *Int J Pept Protein Res* **47:** 460-466.

Kondejewski, L.H., Farmer, S.W., Wishart, D.S., Kay, C.M., Hancock, R.E. and Hodges, R.S. 1996b. Modulation of structure and antibacterial and hemolytic activity by ring size in cyclic gramicidin S analogs. *J Biol Chem* **271:** 25261-25268.

Kondejewski, L.H., Jelokhani-Niaraki, M., Farmer, S.W., Lix, B., Kay, C.M., Sykes, B.D., Hancock, R.E. and Hodges, R.S. 1999. Dissociation of antimicrobial and hemolytic activities in cyclic peptide diastereomers by systematic alterations in amphipathicity. *J Biol Chem* **274:** 13181-13192.

Leenders, F., Vater, J., Stein, T. and Franke, P. 1998. Characterization of the binding site of the tripeptide intermediate D- Phenylalanyl L-prolyl-L-valine in gramicidin S biosynthesis. *J Biol Chem* **273:** 18011-18014.

Lewis, R.N., Prenner, E.J., Kondejewski, L.H., Flach, C.R., Mendelsohn, R., Hodges, R.S. and McElhaney, R.N. 1999. Fourier transform infrared spectroscopic studies of the interaction of the antimicrobial peptide gramicidin S with lipid micelles and with lipid monolayer and bilayer membranes. *Biochemistry* **38:** 15193-15203.

Liu, D. and DeGrado, W.F. 2001. De novo design, synthesis, and characterization of antimicrobial beta- peptides. *J Am Chem Soc* **123:** 7553-7559.

Marahiel, M.A., Stachelhaus, T. and Mootz, H.D. 1997. Modular peptide synthetases involved in nonribosomal peptide synthesis. *Chem Rev* **97:** 2651-2673.

Martin, D.R. and Williams, R.J. 1976. Chemical nature and sequence of alamethicin. *Biochem J* **153:** 181-190.

Oren, Z., Hong, J. and Shai, Y. 1997. A repertoire of novel antibacterial diastereomeric peptides with selective cytolytic activity. *J Biol Chem* **272:** 14643-14649.

Porter, E.A., Weisblum, B. and Gellman, S.H. 2002. Mimicry of Host-Defense Peptides by Unnatural Oligomers: Antimicrobial beta-Peptides. *J Am Chem Soc* **124:** 7324-7330.

Prenner, E.J., Lewis, R.N., Jelokhani-Niaraki, M., Hodges, R.S. and McElhaney, R.N. 2001. Cholesterol attenuates the interaction of the antimicrobial peptide gramicidin S with phospholipid bilayer membranes. *Biochim Biophys Acta* **1510:** 83-92.

Prenner, E.J., Lewis, R.N., Kondejewski, L.H., Hodges, R.S. and McElhaney, R.N. 1999a. Differential scanning calorimetric study of the effect of the antimicrobial peptide gramicidin S on the thermotropic phase behavior of phosphatidylcholine, phosphatidylethanolamine and phosphatidylglycerol lipid bilayer membranes. *Biochim Biophys Acta* **1417:** 211-223.

Prenner, E.J., Lewis, R.N. and McElhaney, R.N. 1999b. The interaction of the antimicrobial peptide gramicidin S with lipid bilayer model and biological membranes. *Biochim Biophys Acta* **1462:** 201-221.

Prenner, E.J., Lewis, R.N., Neuman, K.C., Gruner, S.M., Kondejewski, L.H., Hodges, R.S. and McElhaney, R.N. 1997. Nonlamellar phases induced by the interaction of gramicidin S with lipid bilayers. A possible relationship to membrane-disrupting activity. *Biochemistry* **36:** 7906-7916.

Salgado, J., Grage, S.L., Kondejewski, L.H., Hodges, R.S., McElhaney, R.N. and Ulrich, A.S. 2001. Membrane-bound structure and alignment of the antimicrobial beta-sheet peptide gramicidin S derived from angular and distance constraints by solid state 19F-NMR. *J Biomol NMR* **21:** 191-208.

Scott, M.G. and Hancock, R.E. 2000. Cationic antimicrobial peptides and their multifunctional role in the immune system. *Crit Rev Immunol* **20:** 407-431.

Shai, Y. 1999. Mechanism of the binding, insertion and destabilization of phospholipid bilayer membranes by alpha-helical antimicrobial and cell non-selective membrane-lytic peptides. *Biochim Biophys Acta* **1462:** 55-70.

Shida, O., Takagi, H., Kadowaki, K. and Komagata, K. 1996. Proposal for two new genera, Brevibacillus gen. nov. and Aneurinibacillus gen. nov. *Int J Syst Bacteriol* **46:** 939-946.

Staudegger, E., Prenner, E.J., Kriechbaum, M., Degovics, G., Lewis, R.N., McElhaney, R.N. and Lohner, K. 2000. X-ray studies on the interaction of the antimicrobial peptide gramicidin S with microbial lipid extracts: evidence for cubic phase formation. *Biochim Biophys Acta* **1468:** 213-230.

Tam, J. P., Lu, Y. A., and Jang, J. L. 2000. Design of salt-insensitive glycine-rich antimicrobial peptides with cyclic tricystine structures. *Biochemistry* **39:** 7159-7169.

van 't Hof, W., Veerman, E.C., Helmerhorst, E.J. and Amerongen, A.V. 2001. Antimicrobial peptides: properties and applicability. *Biol Chem* **382:** 597-619.

Wallace, B.A. 1998. Recent advances in the high resolution structures of bacterial channels: gramicidin A. *J Struct Biol* **121:** 123-141.

Wu, M., Maier, E., Benz, R. and Hancock, R.E. 1999. Mechanism of interaction of different classes of cationic antimicrobial peptides with planar bilayers and with the cytoplasmic membrane of Escherichia coli. *Biochemistry* **38:** 7235-7242.

Zasloff, M. 2002. Antimicrobial peptides of multicellular organisms. *Nature* **415:** 389-395.

Zhang, L., Rozek, A. and Hancock, R.E. 2001. Interaction of cationic antimicrobial peptides with model membranes. *J Biol Chem* **276:** 35714-35722.

Chapter 2: Materials and Methods

Chapter 2-1. Materials

Microbial strains. Strains used in the antimicrobial assays were selected to cover several types of Gram-negative bacteria, Gram-positive bacteria, and fungi. Gram-negative bacteria included wild-type and antibiotic-sensitive strains of *Pseudomonas aeruginosa* (*P. aeruginosa;* strains H187 & H188), *Salmonella typhimurium (S. typhimurium*; strains C587 & C610), and *Escherichia coli (E. coli*; strains UB1005 & DC2*)*. Gram-positive bacteria included wild-type *Staphylococcus epidermidis* (*S. epidermidis*), *Enterococcus faecalis* (*E. faecalis*), and *Corynebacterium xerosis* (*C. xerosis*); wild-type and methicillin-resistant (SAP0017) strains of *Staphylococcus aureus (S. aureus)*; and an environmental isolate of *Bacillus subtilis (B. subtilis)*. The fungal strain was from the yeast *Candida albicans (C. albicans)*.

Materials. All microbial strains were grown on Mueller Hinton broth (MHB) for antibacterial assays, and Luria broth (LB) with no salt for NPN uptake and diSC$_3$(5) assays (Difco Laboratories, Detroit, MI). N$^\alpha$*tert*-butyloxycarbonyl (Boc) amino acids, Boc-Pro-4-hydroxymethylphenylacetamidomethyl (PAM) resin, benzotriazole-1-yl-oxy-tris-pyrrolidino-phosphonium hexafluorophosphate (PyBOP), benzotriazol-1-yloxytris(dimethylamino)phosphonium hexafluorophosphate (BOP), 2-(1H-benzotriazole-1-yl) – 1,1,3,3 tetramethyluronium hexafluorophosphate(HBTU), and *N*-hydroxybenzotriazole (HOBt) were from NovaBiochem (La Jolla, CA), with the exception of Boc-Lys(formyl)-OH from Bachem (Torrance, CA). Trifluoroacetic acid (TFA) was from Halocarbon (River Edge, NJ). Anisole, ethanedithiol (EDT), *N*, *N*-diisopropylethylamine (DIEA), 1,1′-carbonyl-diimidazole (CDI), ninhydrin, polymyxin

B, trifluoroethanol, bovine serum albumin (BSA), carbonylcyanide-*m*-chlorophenylhydrazone (CCCP), *N*-phenyl-1-napthylamine (NPN) and lipopolysaccharide (LPS) from *E. coli* UB1005 were from Sigma Chemical Co. (St. Louis, MO). Dansyl-polymyxin B and 3,3'-dipropylthiadicarbocyanine iodide (diSC$_3$(5)) were from Molecular Probes (Eugene, OR). Glucose, 4-(2-hydroxyethyl)-1-piperazineethanesulfonic acid (HEPES), potassium cyanide, phenol, ammonium acetate, ethyl ether, hydrochloric acid, ethanol, acetonitrile, methanol, dichloromethane (DCM), and dimethylformamide (DMF) were from Fisher Scientific.

Chapter 2-2. Linear peptide synthesis, purification and analysis

This thesis describes two major types of peptide categories with slightly different synthesis strategies. The peptides used in coiled-coil folding studies consisted of linear peptides with N-terminal acetyl and C-terminal amide. The cyclic peptides used in membrane activity studies were first made in the linear form, purified, then subsequently cyclized in solution before final removal of side-chain protecting groups and purification.

All of the amino acid side-chain protecting groups for linear peptides with N-terminal acetyl and C-terminal amides were selected so that they would be removed during cleavage from the resin. However, in the case of peptides intended for cyclization, a formyl group on the lysine side-chain was chosen so that the N$^{\epsilon}$-amino group would remain protected after cleavage. This protection of the lysines increased efficiency of the subsequent head-to-tail cyclization reaction by preventing unwanted cyclization of the linear peptide's carboxy terminus *via* the primary amino group on the lysine side-chain. Removal of the lysine formyl groups was performed only after the cyclization reaction was completed.

Synthesis of the polypeptide chain on a solid resin support consisted of repeated cycles of 1) N-terminal deprotection of Boc protecting groups, 2) resin neutralization, 3) activation and coupling of the next amino acid, and 4) verification of complete coupling. Because each amino acid was added to the free N-terminal of the growing polypeptide chain, synthetic peptides were built from C-terminal to N-terminal, in contrast to the N- to C-terminal order observed during ribosomal biosynthesis of proteins.

Peptides with N-terminal acetyl groups and C-terminal amides in the sequence were synthesized by conventional Boc-amino acid solid-phase peptide synthesis methodology using methylbenzhydrylamine resin, as described previously (Litowski et al. 1999). Boc amino acid side chain protecting groups were Asn(β-xanthyl), Asp(β-cyclohexyl), Glu(O-benzyl), Ser(O-benzyl), and Lys(Nε-2-Cl-benzyloxycarbonyl). For the addition of each Boc-amino acid to the growing polypeptide chain, resin was deprotected 15 minutes with 50% TFA in DCM to remove the Boc group from the N-terminal α-amino group, neutralized with 5% DIEA in DCM, washed with DMF, and coupled with 0.4 mmol of Boc-amino acid pre-activated with 0.4 mmol HBTU, 0.4 mmol HOBt, and 0.5 mmol (1.2x molar excess) DIEA dissolved in DMF (0.5 M Boc-amino acid solution). Couplings were monitored for completion by a qualitative ninhydrin test (Kaiser et al. 1970) but were typically complete after 30 minutes. After completion of synthesis, resin was neutralized with 10:90 (v/v) DIEA:DMF, and N-terminal amino groups were acetylated with 25:75 (v/v) acetic anhydride:DCM.

Although Boc-L-Lys(formyl)-OH was commercially available, the Boc-D-Lys(formyl)-OH enantiomer was unavailable and was synthesized in our laboratory by derivatizing the side-chain of Boc-D-Lys-OH. Formic acid (20 mmol) dissolved in 10 ml acetonitrile was added dropwise to 20 mmol of 1,1′-carbonyl-diimidazole (CDI) in 20 ml acetonitrile at 0°C in a round bottom flask. The solution was allowed to stir at room temperature for 15 minutes for activation of formic acid. Activated formate ester was added to 20 mmol Boc-D-Lys-OH (5 g) dissolved in acetonitrile/water, and allowed to stir for 1 hr at room temperature. Completeness of the reaction was monitored by reversed-phase high performance liquid chromatography (RP-HPLC). Solvent was removed by rotary evaporation. The resulting oil was dissolved in ethyl acetate, transferred to a separatory funnel, and washed three times with water acidified to pH 2 with potassium hydrogen sulfate ($KHSO_4$). Remaining water was dried with magnesium sulfate, and the ethyl acetate was filtered into another round bottom flask, where the solvent was removed by rotary evaporation. Finally, the mixture was dissolved in a minimal volume of ethyl acetate and recrystallized in cold hexane, or dissolved in DMF to 1 mg/ml and purified by preparative RP-HPLC. Purity was determined by analytical RP-HPLC.

Peptides intended for cyclization were first synthesized as linear peptides with free N- and C-termini by solid-phase peptide synthesis using standard Boc chemistry (Litowski et al., 1999). Boc- amino acid side-chain protecting groups were L-Asn(β-xanthyl), D-Lys(formyl), L-Lys(formyl), D-Tyr(O-benzyl), and L-Tyr(O-benzyl). Boc-Pro-PAM resin (0.1 mmol) was used as the starting material. For the addition of each Boc-amino acid to the growing polypeptide chain, resin was deprotected 15 minutes with 50% TFA in DCM to remove the Boc group from the N-terminal α-amino group, neutralized with 5% DIEA in DCM, and coupled with 0.4 mmol of Boc-amino acid pre-activated with 0.4 mmol HBTU, 0.4 mmol HOBt, and 0.5 mmol (1.2x molar excess) DIEA dissolved in DMF (0.5 M Boc-amino acid solution). Couplings were monitored for completion by a qualitative ninhydrin test (Kaiser et al. 1970) but were typically complete after 30 minutes.

The Kaiser test for reactive amines involves a ninhydrin reaction at 120°C. Reaction between ninhydrin, hydrindantin and free primary amines yields a blue/purple resin color (Ruhemann's Purple; λ_{max}=570 nm), and reaction with secondary amines, *e.g.* proline, gives an orange color (λ_{max}=440 nm). Both positive results indicate incomplete Boc-amino acid coupling. The absence of free amines yields a yellow color (negative result). Reagent A was 5 g ninhydrin in 100 ml ethanol, reagent B was 80 g liquified phenol in 20 ml ethanol, and reagent C was 2 ml of 1 mM potassium cyanide in 98 ml pyridine. To test the coupling reaction for completeness, 50 µl of each reagent plus a small resin sample were added to a test tube and heated at 120°C for 4-6 minutes. If the Kaiser test was positive, the amino acid was recoupled to the remaining free amino groups on the peptide using a new solution of activated amino acid (Boc-amino acid, HBTU, HOBt and DIEA in DMF) for 30 minutes and the Kaiser test was repeated.

The linear peptides were cleaved from the resin using anhydrous liquid hydrogen fluoride (HF, 20 ml/g resin) containing 10% (v/v) anisole and 1% (v/v) 1,2-ethanedithiol for 1 h at -4°C. HF was removed under reduced pressure, and peptides were precipitated and washed with cold ethyl ether, extracted with 0.05% trifluoroacetic acid (v/v) in 50% aqueous acetonitrile, and purified by RP-HPLC (Wagschal et al. 1999). Linear crude peptides were purified on a Beckman System Gold HPLC, using a Brownlee Aquapore RP-300 column, 250 x 7.0 mm I.D. Peptides were eluted using a linear gradient (0 – 50% B) at 0.25% B/min, where A=0.05% aqueous TFA, B=0.05% TFA in acetonitrile. The flow rate was 2 ml/min. Elution profiles were monitored at 230 nm or 280 nm, depending on the absence or presence of aromatic amino acid side-chains (e.g., D-Tyr). Peptide purity was verified by analytical reversed-phase HPLC and mass spectrometry on a Fisons VG Quattro triple quadrupole mass spectrometer (Manchester, England) or Kratos Analytical MALDI-MS (Manchester, England) using a CMBT matrix. Analytical RP-HPLC was determined on a Zorbax 300 SB-C_8 column (150 X 2.1 mm I.D., 5 μm particle size, 300 Å pore size; Rockland Technologies, Wilmington, DE) using a Hewlett Packard 1100 chromatograph at 25°C with a linear AB gradient and a gradient rate of 1% B/min (where solvent A was 0.05% aqueous TFA and solvent B was 0.05% TFA in acetonitrile) at a flow rate of 0.25 ml/min. Peaks were detected by absorbance at 210 nm.

Chapter 2-3. Peptide cyclization, deformylation, and purification

Peptides intended for cyclization were synthesized as linear peptides by the solid-phase method with Boc-amino acids, cleaved from PAM resin, and purified as described above (Kondejewski et al. 1996). Pure linear peptides were then cyclized with 5 molar equivalents (eq.) of DIEA, 3 eq. PyBOP and 3 eq. HOBt in DMF at 2 mg/ml peptide concentration. Aliquots of the cyclization reaction were monitored at 1 hr. intervals by analytical RP-HPLC, and the reaction was typically complete after 3 hrs. DMF was removed by rotary evaporation, and the mixture was deformylated in 20% HCl in methanol (2 mg peptide/ml) at 40°C for 12 hours. Solvent was removed by rotary evaporation, and the peptide was solubilized in aqueous acetonitrile (up to 40% depending on peptide solubility) for HPLC purification. Cyclized peptides were purified with a 0.25% B/min linear AB gradient, with the starting and ending compositions dependent on peptide solubility (elution conditions ranged from 20-70%B where solvent

A was 0.05% aqueous TFA and solvent B was 0.05% TFA in acetonitrile), flow rate 2 ml/min. Purified fractions were lyophilized to a dry powder.

Chapter 2-4. Circular dichroism spectroscopy and equilibrium unfolding measurements

CD measurements were obtained on a JASCO J-720 Spectropolarimeter at 5°C (Easton, MD, USA) using 'J700 for Windows Standard Measurement software', Version 1.10.00 running on a Pentium II under Windows 98 (4.10.2222A), or on a JASCO J-810 Spectropolarimeter at 20°C (Easton, MD, USA) using Spectra Manager™ software, Version 1.10.00 running on a Pentium III under Windows 2000. Temperature was controlled in a Lauda Model RMS-6 water bath (Brinkman Instruments, Rexdale, Canada). Data were collected at 0.1 nm intervals at 5°C or 20°C from 190 to 250 nm for wavelength scans, with the average of 4 or 8 scans reported. In the analysis of linear peptides (Chapters 3 and 4), benign CD buffer was 50 mM potassium phosphate, 100 mM potassium chloride, pH 7; or 5 mM sodium phosphate, 150 mM sodium chloride, pH 7.4. In the analysis of peptides in Chapters 5 to 7, benign buffer was 5 mM sodium acetate, pH 5.5. Peptide concentrations used in Chapter 7 were approximately 30 μM as determined by amino acid analysis or UV absorbance at 280 nm ($\varepsilon = 2840\ \mathrm{cm^{-1}\ M^{-1}}$ from two D-Tyr residues) of stock solutions. In the case of both linear and cyclic peptides, analyses were performed in benign buffer in the presence or absence of 50% (v/v) TFE. Ellipticity was reported as mean residue molar ellipticity ($[\theta]$) in $\mathrm{deg{\bullet}cm^2{\bullet}dmol^{-1}}$ using the following equation:

$$[\theta] = \theta(\mathrm{MRW})/(10lc)$$

where θ is the ellipticity in millidegrees, MRW is the mean residue weight (molecular weight divided by number of residues), l is the optical path length of the cell in cm, and c is the peptide concentration in mg/ml. Alternatively, for ease of use the equation can be rearranged to the following form:

$$[\theta] = \theta/(10nc_M l)$$

where θ is the ellipticity in millidegrees, n is the number of residues in the peptide or protein, c_M is the peptide concentration in mol/L, and l is the optical path length of the cell in cm. This form of the equation allows direct entry of ellipticity (in millidegrees) and concentration (in M) values obtained from experiment, without requiring the mean residue weight calculation.

Concentration dependence scans of linear peptides (Chapter 3) were performed by measuring the mean residue ellipticity at 222 nm at 5°C, using peptide concentrations ranging from 5 to 1470 μM. For the concentration dependence scans of peptide K19E (Chapter 4), scans from 190 to 250 nm were performed in 50 mM potassium phosphate, 100 mM potassium chloride, pH 7 at 20°C using concentrations ranging from 4 μM to 2592 μM, and quartz cells and plates with path lengths ranging from 0.005 cm to 1 cm.

Thermal denaturation data were obtained from 5°C to 85°C in 0.1 cm cells at ~100 μM peptide concentration in 5 mM sodium phosphate, 150 mM NaCl, pH 7.4 buffer (Chapter 3). Urea denaturation data were obtained by monitoring the ellipticity at 220 nm of peptide solutions in a 0.02 cm quartz cell at 20°C (Chapter 4). Aliquots of ~10 mg/ml peptide stock solution were diluted with the appropriate amount of CD buffer (50 mM phosphate, 100 mM KCl, pH 7) and 10 M urea solution in CD buffer. Solutions were allowed to equilibrate overnight at room temperature to give final urea concentrations ranging from 0 to 8 M in 0.5 M intervals and ~400 uM peptide concentration. Concentrations of peptide solutions were determined by amino acid analysis on a Beckman model 6300 analyzer (San Ramon, CA).

For each peptide analyzed by urea or thermal denaturation, ellipticity values were converted to fraction folded values, using the equation

$$f_f = ([\theta]_o - [\theta]_u)/([\theta]_n - [\theta]_u)$$

where f_f is the fraction of the population folded, $[\theta]_o$ is the observed mean residue molar ellipticity at a given urea concentration or temperature, $[\theta]_u$ is the peptide mean residue molar ellipticity in the fully unfolded state, and $[\theta]_n$ is the peptide mean residue molar ellipticity in the native (fully folded) state. For each peptide, the $[\theta]_n$ value was assumed to be the same as $[\theta]_o$ at 0 M or 5 °C, and the $[\theta]_u$ value was assumed to be $[\theta]_o$ at 8 M or 85 °C. However, for the hybrid 2 peptide (Chapter 4), the shape of the denaturation curve did not indicate complete unfolding at 8 M urea and 85 °C and so the $[\theta]_u$ value of -4000 deg cm^2 $dmol^{-1}$ was obtained from the other peptides in the series that did appear to approach a minimal $[\theta]_u$ value at 8 M urea.

Chapter 2-5. Thermodynamic analysis

For the analysis of coiled-coil folding/unfolding equilibria, we operated under the assumption of co-operative, reversible two-state folding. Also, in the case of peptide analogs, we operated under the assumption that the native conformations were the same for all analogs and the unfolded conformations were all the same amongst the analogs.

Fits for thermal denaturation curves in Chapter 3 were calculated using an in-house fitting method (Lavigne et al. 1998). The method first establishes native and unfolded baselines for each individual denaturation curve. For each temperature T in the curve, a spectroscopic value is assigned (in this case, mean residue molar ellipticity) that corresponds to the condition when all peptide molecules in solution are either in the native structure ($[\theta]_{222,N}(T)$) or in the fully unfolded conformation ($[\theta]_{222,U}(T)$). By definition, every data point from the denaturation curve is located somewhere between $[\theta]_{222,N}(T)$ and $[\theta]_{222,U}(T)$ at any given temperature. Then, all data points on the denaturation curve are converted from mean residue molar ellipticity to the fraction of the total peptide population that is unfolded at temperature T ($f_U(T)$). The change in CD signal at 222 nm at temperature T was fit to a two-state unfolding curve based on the following equation (Shortle et al. 1988):

$$[\theta]_{222,o}(T)=(1-f_U(T)) \bullet [\theta]_{222,N}(T) + f_U(T) \bullet [\theta]_{222,U}(T)$$

where $[\theta]_{222,o}(T)$ is the observed mean residue molar ellipticity at 222 nm at temperature T, $[\theta]_{222,N}(T)$ is the mean residue molar ellipticity of the fully folded (native) molecule at temperature T, $[\theta]_{222,U}(T)$ is the mean residue molar ellipticity of the fully unfolded (denatured) molecule at temperature T, and $f_U(T)$ is the fraction of peptide in the unfolded state at temperature T.

To determine $f_U(T)$, the previous equation was rearranged to give

$$f_U(T)=([\theta]_{222,o}(T)-[\theta]_{222,N}(T))/([\theta]_{222,U}(T)-[\theta]_{222,N}(T))$$

The T_m was obtained as the temperature showing the maximum value in the plot of the first derivative of the $f_u(T)$ *vs.* temperature plot. The rationale is that since the slope value of the denaturation curve is lowest when close to the fully folded and unfolded states and gets larger towards the transition midpoint, the slope (positive in the case of $f_u(T)$ *vs.* T) should have a maximum value at the transition midpoint temperature, T_m. The T_m is needed for the next iterative cycle in the curve fitting method.

After obtaining $f_U(T)$ from the experimental data, the change in free energy of unfolding at temperature T was approximated by the following equation using an iterative approach:

$$\Delta G_U(T)=\Delta H_u^\circ(T_m)\bullet(1-T/T_m)+\Delta C_{p,u}\bullet(T-T_m)-T\bullet\ln(T/T_m)$$

where T_m is the transition midpoint temperature, $\Delta H_u^\circ(T_m)$ is the change in molar enthalpy at T_m, and $\Delta C_{p,u}$ is the change in molar heat capacity. The values for $\Delta H_u^\circ(T_m)$ and $\Delta C_{p,u}$ were approximated and the resultant $\Delta G_U(T)$ values were used to obtain fitted $P_u(T)$ values in the following equation:

$$P_u(T)=(\exp(-\Delta G_u(T)/RT))/(1+\exp(-\Delta G_u(T)/RT))$$

The fitted $P_u(T)$ values were then compared to the experimentally obtained $P_u(T)$ values, and the $\Delta H_u^\circ(T_m)$ and $\Delta C_{p,u}$ were varied over subsequent iterative cycles until there was close agreement between the fitted and experimental $P_u(T)$ values over the entire temperature range.

However, $\Delta G_U(T)$ is dependent on peptide concentration. In order to normalize all results to 1 M peptide concentration (denaturation was performed with μM peptide concentrations), the molar Gibbs free energy change of unfolding at temperature T ($\Delta G^\circ_U(T)$) was determined using the equation for a monomer to dimer equilibrium (Yu et al. 1999):

$$\Delta G_u^\circ(T) = \Delta H_u^\circ(T_m) \bullet (1-T/T_m) + \Delta C_{p,u}(T - T_m) - T(R \bullet \ln 3.32[N] + \Delta C_{p,u} \bullet \ln (T/T_m))$$

where $\Delta H_u^\circ(T_m)$ is the change in molar enthalpy at the unfolding transition midpoint temperature T_m, $\Delta C_{p,u}$ is the change in molar heat capacity, R is the ideal gas constant, and N is the dimer peptide concentration in mol/L.

Also, to determine T_m at 1 mol/L peptide concentration, the following equation was used:

$$\partial(\ln[N])/\partial(1/T_m)=-\Delta H^\circ(T_m)/((n-1)*R)$$

where [N] is the dimeric peptide concentration, $\Delta H_u^\circ(T_m)$ is the standard state change in enthalpy at T_m, n=2 for a homodimeric reaction, and R is the ideal gas constant, $1.9872*10^{-3}$ kcal•mol^{-1}K^{-1} (Yu et al., 1999). This equation gives a straight line that can be used to extrapolate T_m at 1 M concentration, given the fact that we had previously determined T_m at a lower peptide concentration.

The stability contribution of a specific amino acid substitution or set of substitutions was calculated as the difference in the standard state change in free energy of unfolding at a reference temperature of 50°C ($\Delta\Delta G^\circ_U(50^\circ)$). For a given substitution or set of substitutions A, the general equation is

$$\Delta\Delta G^\circ_U(50^\circ)_X = \Delta G^\circ_U(50^\circ)_{X+Y} - \Delta G^\circ_U(50^\circ)_Y$$

where Y represents all other amino acid substitution(s) in addition to those in X. For example, in determining the stability contribution of the substitutions S6A, S13A, S27A, let X = S6A, S13A, S27A and let Y = E19K, D20A. Thus, $\Delta\Delta G^\circ_U(50^\circ)_{S6A,\ S13A,\ S27A}$ = $\Delta G^\circ_U(50^\circ)_{E19K,\ D20A,\ S6A,\ S13A,\ S27A} - \Delta G^\circ_U(50^\circ)_{E19K,\ D20A}$ (Chapter 3).

For each urea denaturation curve in Chapter 4, the midpoint of the unfolding curve ($[\text{urea}]_{1/2}$), the slope of the linear portion of the transition (*m*), and the stability contribution of hybrid 2 relative to the analog ($\Delta\Delta G_u^{obs}$), were determined as described previously (Santoro et al. 1988; Serrano et al. 1989). The linear extrapolation equation for the free energy change in unfolding as a function of denaturant concentration is

$$\Delta G_u([\text{urea}])=\Delta G_u^{H2O}+m[\text{urea}]$$

where ΔG_u^{H2O} is the free energy change in the absence of denaturant, *m* is the slope of the line obtained from plotting ΔG_u([urea]) values near the transition midpoint, and [urea] is the urea concentration (Santoro et al. 1988). ΔG_u([urea]) is calculated by

$$\Delta G_u([\text{urea}]) = -RT\ln K_u$$

where R is the ideal gas constant, T is the temperature in Kelvin, and K_u is the equilibrium constant between folded and unfolded peptide at a given urea concentration. In non-disulfide-bridged coiled-coils, stability increases with increasing peptide concentration, thus the fraction of folded peptide (and thus the equilibrium constant) is concentration-dependent (Zhou et al. 1992). The equation for determining K_u is given by

$$K_u=2[N]\ f_u^2/f_f$$

where [N] is the concentration of monomeric peptide, f_u is the fraction of unfolded peptide, and f_f is the fraction of folded peptide.

The change in the observed ΔG_u is given by the equation

$$\Delta\Delta G_u^{obs}=([\text{urea}]_{1/2,A} - [\text{urea}]_{1/2,B})*(m_A+m_B)/2)\text{(Serrano et al. 1989)}$$

where $[\text{urea}]_{1/2,A}$ is the urea concentration at the transition midpoint for peptide A, $[\text{urea}]_{1/2,B}$ is the urea concentration at the transition midpoint for peptide B, and m_A and m_B are the respective slopes for peptides A and B obtained from the previous equation, $\Delta G_u([\text{urea}])=\Delta G_u^{H2O}+m[\text{urea}]$.

Chapter 2-6. Crystallization, data collection and processing

Crystals of the hybrid 2 peptide (Chapter 4) were grown in 24-well Falcon plates by vapor diffusion using the hanging-drop method (McPherson 1982). The 1 ml well solution contained 0.1–0.2 M ammonium acetate, 30% PEG_{4000} and 0.1 M sodium acetate buffer at pH 4.6. The 4 µl drop contained 2 µl peptide at a concentration of 20 mg/ml and

2 µl of well solution. Crystals grew within 2 days to dimensions up to 0.3 x 0.3 x 0.5 mm^3. The crystals belong to the space group $C222_1$ with unit cell dimensions a = 18.098 Å, b = 117.287 Å and c = 22.209 Å and contain one monomer in the asymmetric unit (Table 4-1).

The X-ray diffraction data set from the peptide crystals was collected at 100 K on the X11 beam-line (EMBL, DESY Hamburg) at a wavelength of λ=0.8033 Å. The data set was processed and scaled using DENZO and SCALEPACK (Otwinowski et al. 1997), respectively.

Chapter 2-7. Model building and refinement

The structure of hybrid 2 (Chapter 4) was determined by molecular replacement methods using the program AMoRe (Navaza 1994). A polyalanine model of a 30-residue long coiled-coil fragment based on the structure of the GCN4 coiled-coil (RSCB accession code 2zta) was used as a search model. The model of the peptide was refined with the program SHELXL (Sheldrick et al. 1996) including anisotropic B-factor refinement to an R-factor of 17.9% and R-free calculated with 10% of the data set aside prior to refinement of 21.7%, at a resolution of 1.17 Å. R.m.s. deviations from ideality in bond lengths and angles are 0.009 Å and 1.8°, respectively (Table 4-1). The final model comprises one monomer, comprised of residues 3-31, and 32 water molecules in the asymmetric unit. The first two residues at the N-terminus appeared to be disordered in the crystal structure and displayed no interpretable electron density. The side-chains of residues Leu 8, Ser 10 and Asn 15 were modeled in two alternative conformations. The overall quality of the model was good as judged by the low R values, the low deviations from stereochemical ideality, and the perfect appearance of the Ramachandran diagram with all residues in the most favored α-helical regions according to the program PROCHECK (Laskowsky et al. 1993). Graphical representations were performed using Insight II (Accelrys Inc., San Diego, CA).

Chapter 2-8. Calculation of solvent-accessible surface area

Solvent-accessible surface area is generally calculated by theoretically rolling a "probe sphere" with the radius of a water molecule (1.4 Å) along the surface of a protein or peptide (Richards 1971; Connolly 1983). The accessible surface is the sum of two types of surfaces: the contact surface in which the probe sphere contacts single protein atoms (displayed as a convex surface on the protein), and the reentrant surface in which the probe sphere touches more than one atom simultaneously (displayed as a saddle or torus).

Models for L7A and L26A were built by modifying the PDB file for the hybrid 2 peptide to substitute alanine residues for leucines (Chapter 4). Accessible surface areas were calculated using GETAREA 1.1 (www.scsb.utmb.edu/getarea) (Fraczkiewicz et al. 1998). The program receives input in Cartesian coordinates in the Protein Data Bank format, producing output that includes the calculated solvent-accessible surface area for each amino acid in the protein or peptide. The value is expressed as a percent ratio, relative to the average solvent-accessible surface area for residue X in the random coil tripeptide Gly-X-Gly, in an ensemble of 30 random conformations. Residues are reported as solvent exposed if the ratio is above 50%, and buried if the ratio is less than 20%.

Chapter 2-9. Sedimentation equilibrium analytical ultracentrifugation

Sedimentation equilibrium experiments were performed at 5°C on a Beckman XL-I analytical ultracentrifuge with Rayleigh interference and absorbance optics (Wagschal et al. 1999). Peptides were dissolved and dialyzed in centrifugation buffer (20 mM potassium phosphate, 100 mM potassium chloride, pH 7) at 4°C overnight at 1-2 mg/ml stock peptide concentrations. Concentrations of peptide solutions were determined by amino acid analysis on a Beckman model 6300 analyzer (San Ramon, CA) or by Rayleigh interference. A 100 μl aliquot of each sample was loaded at three different concentrations into a six-sector charcoal-filled Epon cell and spun for 48 hours at three rotor speeds (34 000, 38 000, and 42 000 rpm for peptides in Chapter 3; and 42 000, 46 000, and 50 000 rpm for peptides in Chapter 4). The partial specific volume of each peptide and the density of the solvent were calculated with the program SEDNTERP v. 1.05 (Hayes et al. 1998). By spinning each sample at three rotor speeds and three concentrations, the oligomerization state was determined by globally fitting the data to the best self-association model (*e.g.* single species dimer, monomer-dimer, monomer-trimer, *etc.*) obtained with the program NONLIN v. 1.06 (Yphantis 1991).

Chapter 2-10. Measurement of antibacterial and antifungal activity (MIC assays*)*

Antibacterial assays were performed using the modified microtitre dilution method for cationic antimicrobial peptides, as described by Hancock et al. (http://cmdr.ubc.ca/bobh/MIC.htm). Notably in this method, rather than using polystyrene microtitre plates that have been shown to bind cationic peptides and influence results, polypropylene microtitre plates were used. Bacteria were grown overnight at 37°C and diluted in Mueller Hinton Broth (MHB) to give 2 – 7 x 10^5 colony forming units/ml. Peptides were dissolved and diluted in 0.01% acetic acid, 0.2% bovine serum albumin. Bacterial aliquots of 100 μl were incubated 18-24 hrs at 37°C with 11 μl peptide (2-96 μg/ml final concentration) in MHB. MIC (Minimum Inhibitory Concentration) was defined as the minimum peptide or antibiotic concentration required to completely inhibit bacterial growth over 24 hours, as determined by visual inspection of 96-well plates.

Chapter 2-11. Measurement of hemolytic activity

Freshly collected human blood with heparin was centrifuged to remove the buffy coat, and the erythrocytes, i.e. red blood cells (RBC), were washed three times in 0.85% saline and stored at 4°C. The hemolytic activity for each peptide was determined by making two-fold serial dilutions of the peptide sample in a round bottom microtiter plate to a final volume of 100μl, and adding 100μl of washed human erythrocytes in a 1% suspension based on packed cell volume. Concentrations of peptide stock solutions were determined by amino acid analysis on a Beckman model 6300 analyzer (San Ramon, CA). Plates were incubated for 2 or 24 hours at 37°C and the minimal peptide concentration for complete RBC lysis (determined visually) was considered to be the hemolytic activity for that peptide, reported in μg/ml. There was never greater than a two-fold change in activity for any peptide from 2 hours to 24 hours. A negative control was determined from samples of 200 μl of 1% RBC with no peptide present.

Chapter 2-12. Displacement of dansyl-polymyxin from LPS

Dansyl-polymyxin (DPX) displacement from *Pseudomonas aeruginosa* lipopolysaccharide (LPS) was measured to determine the binding of the affinity of the peptides to LPS as described previously (Moore et al. 1986). DPX exhibited fluorescence when bound to LPS, such that a decrease in fluorescence was observed upon addition of peptide. Briefly, peptides were titrated into stirred cuvettes containing 3 μg of LPS per ml and 2.5 μM dansyl-polymyxin (approximately 90% saturation of LPS binding sites) in 2 ml of 5 mM sodium HEPES buffer, pH 7.0, and the decrease in fluorescence was recorded. The fluorescence (excitation λ 350 nm, emission λ 420 nm) was measured as a function of peptide concentration to calculate percent displacement of DPX, where the percent displacement was calculated using the following equation:

$$\%\ \text{DPX displacement} = F_{obs}/F_0 * 100$$

where F_{obs} is the observed fluorescence at a given peptide concentration, and F_0 is the fluorescence of dansyl-polymyxin bound to LPS in the absence of peptide. Peptide binding affinities were obtained by extrapolating to the x-intercept in plots of (% DPX displacement)$^{-1}$ against (peptide concentration)$^{-1}$, which gave highly correlated ($R>0.99$) straight lines with positive slopes. A plot of the inverse of the percent inhibition as a function of the inverse of inhibitor concentration gave a value for I_{50}, the inhibitor concentration resulting in 50% displacement of dansyl-polymyxin from LPS (-1/x intercept).

It is important to note that this assay was later discontinued by our laboratory due to numerous issues surrounding assay reproducibility and accuracy. In an attempt to develop an alternative assay to measure peptide-lipid binding affinity, we investigated isothermal titration calorimetry and surface plasmon resonance. Although we obtained accurate and reproducible results with both polymyxin B and GS14K4 using isothermal titration calorimetry (data not shown), many of the peptides in Chapter 6 were insoluble at the concentrations required for titration (mg/ml) and this method was also abandoned. Since surface plasmon resonance required the smallest peptide quantities and lowest concentrations (μg/ml), our laboratory is now attempting to optimize this method to determine binding affinities of peptides to lipopolysaccharide monolayers coated on the surface of the biosensor chip.

Chapter 2-13. Permeabilization of outer membranes to NPN

The ability of peptides to increase outer membrane permeability of Gram-negative bacteria was determined by measuring incorporation of the fluorescent dye 1-*N*-phenylnapthylamine (NPN) into the outer membrane of *E. coli* UB1005 (Loh et al. 1984). Permeabilization studies were carried out as described previously (Hancock et al. 1993; Ono et al. 1987). Briefly, *Escherichia coli* UB1005 cells were suspended in 5 mM sodium HEPES buffer, pH 7.0, containing 5 mM glucose and 5 mM carbonyl cyanide *m*-chlorophenylhydrazone. NPN was added to 2 mL of cells in a quartz cuvette to give a final concentration of 10 μM and the background fluorescence recorded (excitation λ 350 nm, emission λ 420 nm). Aliquots of peptide were added to the cuvette and fluorescence recorded as a function of time until there was no further increase in fluorescence.

As outer membrane permeability is increased by addition of peptide, NPN incorporated into the membrane causes an increase in fluorescence. Values were converted to % NPN uptake using the equation

$$\% \text{ NPN uptake} = (F_{obs}-F_0)/(F_{100}-F_0)*100$$

where F_{obs} is the observed fluorescence at a given peptide concentration, F_0 is the initial fluorescence of NPN with *E. coli* cells in the absence of peptide, and F_{100} is the fluorescence of NPN with *E. coli* cells upon addition of 10 μg/ml polymyxin B, which is used as a positive control in this assay because of its strong outer membrane permeabilizing properties (Hancock et al. 1984). The peptide concentration leading to 50% NPN uptake was reported as the P_{50} value.

Chapter 2-14. Di-SC$_3$(5) release assay

To measure the ability of peptides to disrupt the electrochemical potential across the bacterial cytoplasmic membrane, the release of the membrane-associated probe, diSC$_3$(5), from *E. coli* DC2 cells was monitored by fluorescence spectroscopy as described previously (Wu et al. 1999). Fluorescence of the dye is quenched upon initial incorporation into the cytoplasmic membrane; as peptide is added, the membrane is depolarized (inside becomes less negative) and the dye is released into the aqueous medium, resulting in increased fluorescence (Sims et al. 1974). The *E. coli* mutant DC2 strain was used because its increased outer membrane permeability allows the dye to be incorporated into the inner cytoplasmic membrane. Luria broth was inoculated with an overnight culture of cells, grown at 37°C to mid-logarithmic phase (OD$_{600}$ 0.5-0.6) and pelleted in a centrifuge. The cells were washed with 5 mM HEPES, pH 7.2, 5 mM glucose buffer and resuspended in the same buffer to OD$_{600}$ ~0.05. Addition of aliquots of 0.4 μM DiSC$_3$(5) was monitored at 670 nm until reduction of fluorescence due to quenching was maximal. Potassium chloride was added to a final concentration of 100 mM to equilibrate the cytoplasmic and external K$^+$ concentrations. Suspensions of 2 ml were added to a 1 cm quartz cuvette and the fluorescence was continuously monitored (excitation λ 622 nm, emission λ 670 nm) upon addition of peptide on a Perkin Elmer model LS-50B.

Chapter 2-15. Curve fits for RP-HPLC temperature profiles

Temperature profiling data (Chapter 7) were fit to either a first-order nonlinear least-squares equation, a fourth-order polynomial, or a smooth fit using Kaleidagraph v. 3.52 (Synergy Software, Reading PA). Transition temperature values (T$_p$) were defined as the temperatures at which the maximum retention times were experimentally observed, i.e., in 5°C increments, and were not determined by maxima obtained from fitted curves. If more accurate data are required, we recommend that the analysis be performed in 3°C increments from 5°C to 80°C if sample quantity and run time are not limiting factors.

Chapter 2-16. Analytical reversed-phase analysis of peptides

Peptides in Chapter 7 were analyzed on an Agilent 1100 Series liquid chromatograph (Little Falls, DE, USA). Runs were performed on a Zorbax 300SB-C8 column (2.1 mm I.D. x 150 mm, 300 Å pore size, 5 µm particle size) from Agilent Technologies using a linear AB gradient (0.5% B/min) and a flow rate of 0.35 ml/min, where solvent A is 0.05% aqueous trifluoroacetic acid (TFA), pH 2 and solvent B is 0.05% TFA in acetonitrile. Analyses were performed in 5°C increments, from 5°C to 80°C.

Chapter 2-17. References

Connolly, M.L. 1983. *J Applied Cryst* **16:** 548-553.

Fraczkiewicz, R. and Braun, W. 1998. Exact and efficient analytical calculation of the accessible surface areas and their gradients for macromolecules. *J Comp Chem* **19:** 319-333.

Hancock, R.E. and Farmer, S.W. 1993. Mechanism of uptake of deglucoteicoplanin amide derivatives across outer membranes of *Escherichia coli* and *Pseudomonas aeruginosa*. *Antimicrob Agents Chemother* **37:** 453-456.

Hancock, R.E. and Wong, P.G. 1984. Compounds which increase the permeability of the *Pseudomonas aeruginosa* outer membrane. *Antimicrob Agents Chemother* **26:** 48-52.

Kaiser, E., Colescott, R.L., Bossinger, C.D. and Cook, P.I. 1970. Color test for detection of free terminal amino groups in the solid- phase synthesis of peptides. *Anal Biochem* **34:** 595-598.

Kondejewski, L.H., Farmer, S.W., Wishart, D.S., Kay, C.M., Hancock, R.E. and Hodges, R.S. 1996. Modulation of structure and antibacterial and hemolytic activity by ring size in cyclic gramicidin S analogs. *J Biol Chem* **271:** 25261-25268.

Laskowsky, R.A., MacArthur, M.W., Moss, D.S. and Thornton, J.M. 1993. PROCHECK: a program to check the stereochemical quality of protein structures. *J Appl Cryst* **26:** 283-291.

Lavigne, P., Crump, M.P., Gagne, S.M., Hodges, R.S., Kay, C.M. and Sykes, B.D. 1998. Insights into the mechanism of heterodimerization from the 1H-NMR solution structure of the c-Myc-Max heterodimeric leucine zipper. *J Mol Biol* **281:** 165-181.

Litowski, J.R., Semchuk, P.D., Mant, C.T. and Hodges, R.S. 1999. Hydrophilic interaction/cation exchange chromatography for the purification of synthetic peptides from closely related impurities: serine side-chain acetylated peptides. *J Peptide Res* **54:** 1-11.

Loh, B., Grant, C. and Hancock, R.E. 1984. Use of the fluorescent probe 1-N-phenylnaphthylamine to study the interactions of aminoglycoside antibiotics with the outer membrane of Pseudomonas aeruginosa. *Antimicrob Agents Chemother* **26:** 546-551.

McPherson, A. 1982. *Preparation and analysis of protein crystals*, John Wiley and Sons, Inc, New York.

Moore, R.A., Bates, N.C. and Hancock, R.E. 1986. Interaction of polycationic antibiotics with Pseudomonas aeruginosa lipopolysaccharide and lipid A studied by using dansyl-polymyxin. *Antimicrob Agents Chemother* **29:** 496-500.

Navaza, J. 1994. AMoRE: An automated package for molecular replacement. *Acta Cryst* **A50:** 157-163.

Ono, S., Lee, S., Kodera, Y., Aoyagi, H., Waki, M., Kato, T. and Izumiya, N. 1987. Environment-dependent conformation and antimicrobial activity of a gramicidin S analog containing leucine and lysine residues. *FEBS Lett* **220:** 332-336.

Otwinowski, Z. and Minor, W. 1997. Processing of X-ray diffraction data collected in oscillation mode. In *Methods Enzymol* (C. W. Carter and R. M. Sweet, eds.), 307-326, Academic Press, Inc., New York.

Santoro, M.M. and Bolen, D.W. 1988. Unfolding free energy changes determined by the linear extrapolation method. 1. Unfolding of phenylmethanesulfonyl alpha-chymotrypsin using different denaturants. *Biochemistry* **27:** 8063-8068.

Serrano, L. and Fersht, A.R. 1989. Capping and alpha-helix stability. *Nature* **342:** 296-299.

Sheldrick, G.M. and Schneider, T.R. 1996. SHELXL: High resolution refinement. In *Methods Enzymol* (C. W. Carter and R. M. Sweet, eds.), 319-343, Academic Press, Inc., New York.

Shortle, D., Meeker, A.K. and Freire, E. 1988. Stability mutants of staphylococcal nuclease: large compensating enthalpy-entropy changes for the reversible denaturation reaction. *Biochemistry* **27:** 4761-4768.

Sims, P.J., Waggoner, A.S., Wang, C.H. and Hoffman, J.F. 1974. Studies on the mechanism by which cyanine dyes measure membrane potential in red blood cells and phosphatidylcholine vesicles. *Biochemistry* **13:** 3315-3330.

Wagschal, K., Tripet, B., Lavigne, P., Mant, C. and Hodges, R.S. 1999. The role of position a in determining the stability and oligomerization state of alpha-helical coiled coils: 20 amino acid stability coefficients in the hydrophobic core of proteins. *Protein Sci* **8:** 2312-2329.

Wu, M. and Hancock, R.E. 1999. Interaction of the cyclic antimicrobial cationic peptide bactenecin with the outer and cytoplasmic membrane. *J Biol Chem* **274:** 29-35.

Yu, Y.B., Lavigne, P., Kay, C.M. and Hodges, R.S. 1999. Contribution of translational and rotational entropy to the unfolding of a dimeric coiled-coil. *J Phys Chem B* **103:** 2270-2278.

Zhou, N.E., Zhu, B.Y., Kay, C.M. and Hodges, R.S. 1992. The two-stranded alpha-helical coiled-coil is an ideal model for studying protein stability and subunit interactions. *Biopolymers* **32:** 419-426.

Chapter 3: Are trigger sequences essential in the folding of two-stranded α-helical coiled-coils?

A version of this chapter has been published. Lee, D. L., Lavigne, P., and Hodges, R. S. 2001. Journal of Molecular Biology. 306: 539-553.

Chapter 3-1. Introduction

The protein folding problem remains one of the most challenging problems in biochemistry. How does the primary amino acid sequence dictate the three-dimensional tertiary and quaternary structures of proteins in solution? Despite intensive work addressing this question, the capability of predicting three-dimensional protein structures based on protein sequence information alone has not yet emerged. The ability to predict structure from sequence will have tremendous value in applications including *de novo* protein design, protein engineering, and for protein sequences identified by recent genomic and proteomic initiatives.

A minimalistic structural motif well suited to protein folding studies is the two-stranded α-helical coiled-coil. Two amphipathic α-helices form a rod-like structure by coiling around each other into a left-handed superhelix stabilized by continuous interhelical contacts between the hydrophobic faces of the helices. In the case of the two-stranded coiled-coil, the hydrophobic positions were identified at regular intervals in a 4-3 (or 3-4) hydrophobic repeat (Sodek et al. 1972), where positions ***a*** and ***d*** in the heptad repeat, denoted by $(\boldsymbol{abcdefg})_n$, represent hydrophobic amino acids. The ***a*** and ***d*** side chains in the hydrophobic core pack against each other in a "knobs-into-holes" fashion predicted by

Crick (Crick 1953) and verified by the first high resolution X-ray crystal structure of a two-stranded coiled-coil in the yeast transcription factor, GCN4 (O'Shea et al. 1991). Diversity within this motif is observed in the helix orientation (parallel or antiparallel), oligomerization state (two to five helices), and oligomerization specificity (homo- or hetero-oligomerization) (Hodges 1996; Kohn et al. 1998a; Micklatcher et al. 1999; Woolfson et al. 1995). The appeal of the two-stranded α-helical coiled-coil motif in studying protein folding lies in its simplicity. It contains only one type of secondary structure, the α-helix, and only two α-helices are required to introduce tertiary and quaternary structure. Because it can autonomously fold with a relatively short sequence (as short as three heptads) (Lau et al. 1984; Lumb et al. 1994; Su et al. 1994), peptides and analogs containing amino acid substitutions can be rapidly synthesized and characterized, with the magnitude of substitution effects augmented by the short sequence length. The burial of hydrophobic surfaces between helices of the coiled-coil mimics the burial of interhelical hydrophobic side chains in globular proteins, thus providing a model protein with folding characteristics similar to native coiled-coils and globular proteins. In other words, all of the non-covalent interactions involved in stabilizing a given protein fold are involved in stabilizing two-stranded α-helical coiled-coils.

Numerous studies of helices, coiled-coils and globular proteins have led to an understanding of the factors affecting coiled-coil and protein stability in general, including polypeptide chain length (Fairman et al. 1995; Lau et al. 1984; Lumb et al. 1994; Su et al. 1994), stability contributions from residues in the hydrophobic core (***a*** and ***d***) positions (Tripet et al. 2000; Wagschal et al. 1999a; Wagschal et al. 1999b), side chain van der Waals packing effects (Eriksson et al. 1992), side chain rotational entropy (Yu et al. 1999), interchain and intrachain electrostatic interactions (Kohn et al. 1995a, 1998b; Yu et al. 1996; Zhou et al. 1994a), side chain helical propensities (O'Neil et al. 1990; Zhou et al. 1994b), helix dipole effects (Sali et al. 1988), N- and C-terminal helix capping effects (Aurora et al. 1998; Lu et al. 1999), and several different types of intrahelical side-chain:side-chain interactions (Baldwin et al. 1999; Huyghues-Despointes et al. 1997; Smith et al. 1998). Of these effects, the burial of the hydrophobic core is one of the major contributors to coiled-coil stability (Hodges 1992; Talbot et al. 1982). Recently, an intriguing study by Kammerer *et al.* (Kammerer et al. 1998) demonstrated that the stability of the hydrophobic core alone is not always a reliable determinant of protein folding. A 31-residue sequence based on sequences from the two-stranded parallel coiled-coil domains of the yeast transcriptional activator GCN4 and the actin-bundling protein *Dictyostelium discoideum* cortexillin I failed to dimerize even though it contained a stable hydrophobic core. Kammerer *et al.* proposed that a 'trigger sequence' exists within the coiled-coil domains of GCN4 and cortexillin I that is essential for their self-assembly. The idea was first proposed as a possible explanation to why truncated versions of the coiled-coil regions in cortexillin I and myosin II failed to fold (Steinmetz et al. 1998; Trybus et al. 1997). In cortexillin I, only deletion constructs containing a 14-residue sequence (Arg 311-Arg324) dimerized. This sequence was dubbed the 'trigger sequence' because of its necessity in triggering folding, and was later identified in two-stranded coiled-coil domains of other proteins including the oligomerization domain of GCN4, kinesin, myosin, tropomyosin, Tpr and Clip170. As a result, a 13-residue 'consensus trigger sequence' (**xxLExchxcxccx**, where x is any amino acid, L is leucine, E is glutamic acid, c is a charged residue and h is a hydrophobic residue), was introduced based on its identification in these proteins, and was hypothesized to nucleate the folding pathway of coiled-coils through collision of pre-formed α-helical structure (Kammerer et al. 1998). The X-ray crystal structure of the 18-heptad coiled-coil in the cortexillin I oligomerization domain revealed numerous salt bridges stabilizing the trigger site, suggesting that the trigger site possibly induces folding by increasing dimer stability via electrostatic interactions (Burkhard et al. 2000). Similarly, the identification of a 7-residue trigger sequence in the three-stranded human macrophage scavenger receptor coiled-coil domain further supported the idea of a trigger sequence stabilizing the coiled-coil in order to allow the folding process to take place (Frank et al. 2000).

In this study, we addressed the question of whether a consensus trigger sequence is essential for folding to occur. Is there something unique about trigger sequences that causes folding, or can any sequence achieve the same result if it increases the stability of the coiled-coil beyond a threshold value? Starting with a peptide sequence that had a stable hydrophobic core but failed to form a two-stranded homodimeric parallel coiled-coil, we attempted to induce folding through a variety of amino acid substitutions that increased overall coiled-coil stability. We used a hybrid sequence from the coiled-coil regions of GCN4 and cortexillin I that did not contain any consensus trigger sequence, to demonstrate that peptide folding could be induced by amino acid substitutions without the presence of a consensus trigger sequence. Because we were investigating only the effect of sequence-dependent parameters on folding and stability, other factors including peptide chain length, peptide concentration, pH, and ionic strength were kept constant in this study. By varying combinations of helical propensity, interchain electrostatics, intrachain electrostatics, and hydrophobicity outside the hydrophobic core, we have shown that a specific 'trigger sequence' is not essential for coiled-coil formation. Instead, we conclude that any sequence that increases overall coiled-coil stability beyond a threshold level under given conditions allows folding to occur.

Chapter 3-2. Results

Peptide Design

Of fundamental importance to our study was the design of a coiled-coil sequence (referred to as peptide 1 or parent peptide) that was not stable enough on its own to fold into a two-stranded α-helical coiled-coil, but contained a sequence of hydrophobic residues at the ***a*** and ***d*** positions that are known to form stable two-stranded coiled-coils in native sequences. For example, a 31-residue peptide from the coiled-coil region of GCN4 (Fig. 3-1) is known to form a stable two-stranded α-helical coiled-coil with a T_m of 53°C (Kammerer et al. 1998). Positions ***a*** and ***d*** contain 8 large hydrophobes (4 Leu, 3 Val, 1 Met) known to make significant contributions to the stability of coiled-coils (Moitra et al. 1997; Tripet et al. 2000; Wagschal et al. 1999b). The only exception to the excellent hydrophobic core in GCN4 is an Asn residue at position ***a*** in the centre of the sequence. Asparagine is a polar residue buried in the hydrophobic core of the wild-type GCN4 sequence (O'Shea et al. 1991) to specify dimerization versus higher order oligomerization (Gonzalez et al. 1996a; Gonzalez et al. 1996b; Gonzalez et al. 1996c; Harbury et al. 1993). Thus, our design goal was to maintain a central asparagine at an ***a*** position and an identical hydrophobic core for all the analogs of the parent sequence.

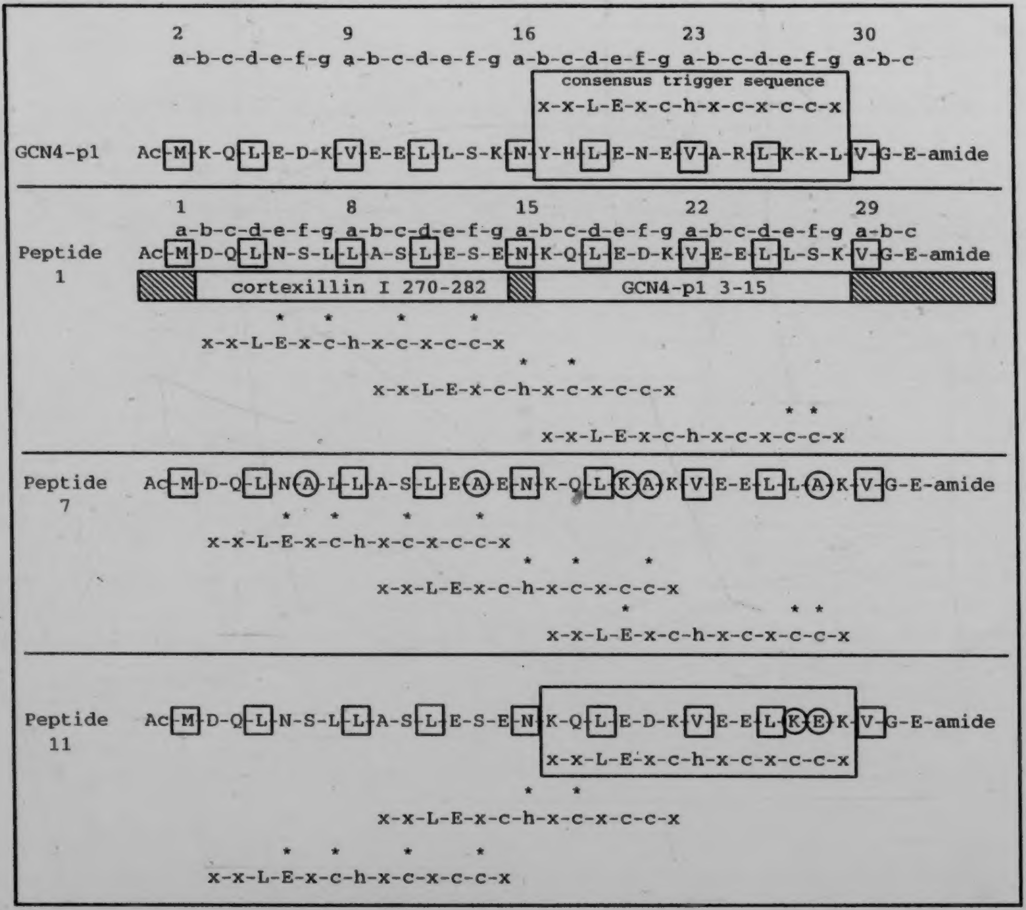
2 9 16 23 30
a-b-c-d-e-f-g a-b-c-d-e-f-g a-b-c-d-e-f-g a-b-c-d-e-f-g a-b-c
consensus trigger sequence
x-x-L-E-x-c-h-x-c-x-c-c-x
GCN4-p1
Ac-M-K-Q-L-E-D-K-V-E-E-L-L-S-K-N-Y-H-L-E-N-E-V-A-R-L-K-K-L-V-G-E-amide
1 8 15 22 29
a-b-c-d-e-f-g a-b-c-d-e-f-g a-b-c-d-e-f-g a-b-c-d-e-f-g a-b-c
Peptide 1
Ac-M-D-Q-L-N-S-L-L-A-S-L-E-S-E-N-K-Q-L-E-D-K-V-E-E-L-L-S-K-V-G-E-amide
cortexillin I 270-282
GCN4-p1 3-15
* * * *
x-x-L-E-x-c-h-x-c-x-c-c-x
* *
x-x-L-E-x-c-h-x-c-x-c-c-x
* *
x-x-L-E-x-c-h-x-c-x-c-c-x
Peptide 7
Ac-M-D-Q-L-N-A-L-L-A-S-L-E-A-E-N-K-Q-L-K-A-K-V-E-E-L-L-A-K-V-G-E-amide
* * * *
x-x-L-E-x-c-h-x-c-x-c-c-x
* * *
x-x-L-E-x-c-h-x-c-x-c-c-x
* * *
x-x-L-E-x-c-h-x-c-x-c-c-x
Peptide 11
Ac-M-D-Q-L-N-S-L-L-A-S-L-E-S-E-N-K-Q-L-E-D-K-V-E-E-L-K-E-K-V-G-E-amide
x-x-L-E-x-c-h-x-c-x-c-c-x
* *
x-x-L-E-x-c-h-x-c-x-c-c-x
* * * *
x-x-L-E-x-c-h-x-c-x-c-c-x

Figure 3-1. Comparison of peptide sequences in this study with the consensus trigger sequence proposed by Kammerer *et al.* (Kammerer et al. 1998). The 13-residue consensus trigger sequence is xxLExchxcxccx, where x is any amino acid, c is a charged residue, L is leucine, E is glutamic acid, and h is a hydrophobic residue. Boxes indicate residues involved in the hydrophobic core between the helices during coiled-coil formation (positions ***a*** and ***d*** of the heptad repeat ***abcdefg***). Circles indicate amino acid substitutions relative to peptide 1, the parent sequence (see Fig. 3-2). Asterisks above the consensus sequence indicate amino acid differences between the consensus trigger sequence and the peptide sequence. Top, the sequence of a 33-residue peptide from the coiled-coil region of wild-type GCN4 (GCN4-p1) (O'Shea et al. 1991) showing the position of the consensus trigger sequence (Kammerer et al. 1998). Second panel, comparison of peptide 1 with the consensus sequence shown in the three possible registrations along the length of the parent sequence. The sequence for peptide 1 was derived from coiled-coil regions of the actin-bundling protein cortexillin I and the yeast transcription factor GCN4 (open rectangles). Hatched rectangles indicate the sequence of the coiled-coil region of GCN4-p1 (residues 2-32, numbered 1-31 in peptides from this study) used as a framework in which to insert the 13-residue sequences from cortexillin I (270-282) and GCN4-p1 (4-16). Alignments of peptide 7 and peptide 11 (Fig. 3-2) with the consensus trigger sequence are shown in the third and fourth panels.

Kammerer *et al.* used a GCN4/cortexillin I hybrid coiled-coil sequence that failed to fold but contained a hydrophobic core sequence similar to wild-type GCN4, where the only difference was a leucine replacing a valine residue at an ***a*** position (Kammerer et al. 1998). This single substitution was not expected to have a significant effect on coiled-coil stability (Wagschal et al. 1999b). Similarly, in this study we used a 31-residue GCN4/cortexillin I hybrid sequence for our parent peptide that kept the same amino acids in position ***a*** and ***d*** as the Kammerer peptide (Figs. 3-2 and 3-3, top). The parent was largely an unfolded monomer, as determined by far-UV CD spectroscopy (Fig. 3-4A), and sedimentation equilibrium (Table 3-1). Although the parent peptide did not fold, it was represented as a folded coiled-coil in a helical wheel diagram to indicate the location of potential electrostatic repulsions if the parent were to adopt a parallel two-stranded coiled-coil conformation (Fig. 3-3, top).

The other goal in the design of the parent was to choose a sequence that did not match the 13-residue 'consensus trigger sequence' proposed by Kammerer *et al.* (Kammerer et al. 1998). Our parent sequence differed from the consensus trigger sequence in the three regions of the 31-residue parent sequence where the consensus sequence could possibly be placed: N-terminal (2-14), central (9-21), and C-terminal (16-28) (Fig. 3-1). Since only 7 of the 13 residues in the consensus trigger sequence designate specific residues (xx**LE**x**ch**x**c**x**cc**x), the peptide sequences chosen for this study contain departures from the trigger sequence in at least 2 of 7 possible sites (≥ 28% difference). Substitutions in peptide analogs were made in the positions ***e***, ***f***, and ***g*** to raise the stability of the peptide via numerous approaches, including modification of 1) electrostatic interactions, 2) α-helical propensities of amino acids, and 3) hydrophobic interactions outside the core ***a***

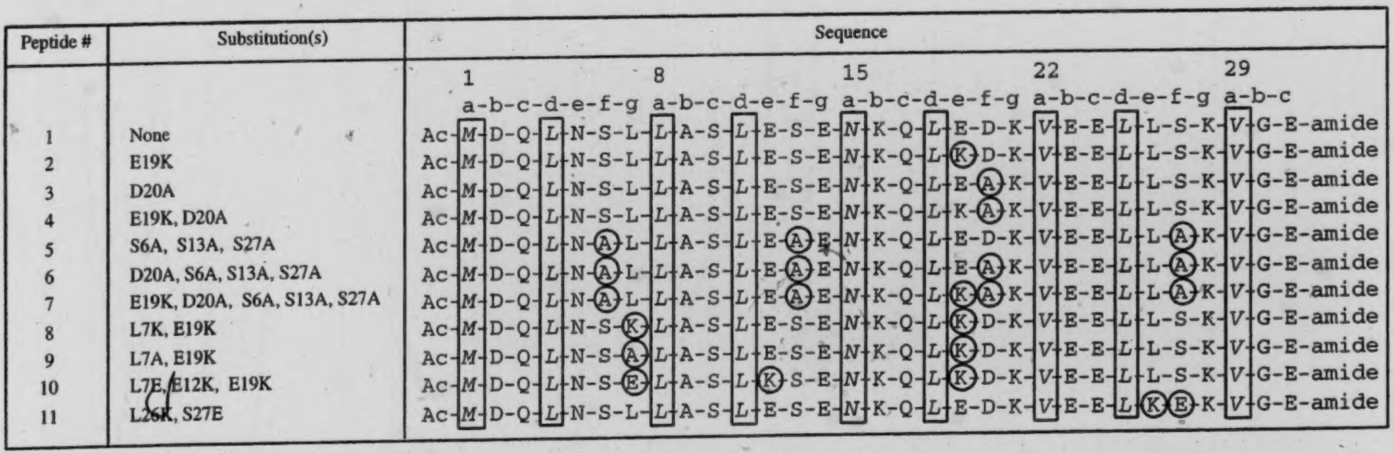

Peptide #	Substitution(s)	Sequence
		1 8 15 22 29
		a-b-c-d-e-f-g a-b-c-d-e-f-g a-b-c-d-e-f-g a-b-c-d-e-f-g a-b-c
1	None	Ac-*M*-D-Q-*L*-N-S-L-*L*-A-S-*L*-E-S-E-*N*-K-Q-*L*-E-D-K-*V*-E-E-*L*-L-S-K-*V*-G-E-amide
2	E19K	Ac-*M*-D-Q-*L*-N-S-L-*L*-A-S-*L*-E-S-E-*N*-K-Q-*L*-K-D-K-*V*-E-E-*L*-L-S-K-*V*-G-E-amide
3	D20A	Ac-*M*-D-Q-*L*-N-S-L-*L*-A-S-*L*-E-S-E-*N*-K-Q-*L*-E-A-K-*V*-E-E-*L*-L-S-K-*V*-G-E-amide
4	E19K, D20A	Ac-*M*-D-Q-*L*-N-S-L-*L*-A-S-*L*-E-S-E-*N*-K-Q-*L*-K-A-K-*V*-E-E-*L*-L-S-K-*V*-G-E-amide
5	S6A, S13A, S27A	Ac-*M*-D-Q-*L*-N-A-L-*L*-A-S-*L*-E-A-E-*N*-K-Q-*L*-E-D-K-*V*-E-E-*L*-L-A-K-*V*-G-E-amide
6	D20A, S6A, S13A, S27A	Ac-*M*-D-Q-*L*-N-A-L-*L*-A-S-*L*-E-A-E-*N*-K-Q-*L*-E-A-K-*V*-E-E-*L*-L-A-K-*V*-G-E-amide
7	E19K, D20A, S6A, S13A, S27A	Ac-*M*-D-Q-*L*-N-A-L-*L*-A-S-*L*-E-A-E-*N*-K-Q-*L*-K-A-K-*V*-E-E-*L*-L-A-K-*V*-G-E-amide
8	L7K, E19K	Ac-*M*-D-Q-*L*-N-S-K-*L*-A-S-*L*-E-S-E-*N*-K-Q-*L*-K-D-K-*V*-E-E-*L*-L-S-K-*V*-G-E-amide
9	L7A, E19K	Ac-*M*-D-Q-*L*-N-S-A-*L*-A-S-*L*-E-S-E-*N*-K-Q-*L*-K-D-K-*V*-E-E-*L*-L-S-K-*V*-G-E-amide
10	L7E, E12K, E19K	Ac-*M*-D-Q-*L*-N-S-E-*L*-A-S-*L*-K-S-E-*N*-K-Q-*L*-K-D-K-*V*-E-E-*L*-L-S-K-*V*-G-E-amide
11	L26K, S27E	Ac-*M*-D-Q-*L*-N-S-L-*L*-A-S-*L*-E-S-E-*N*-K-Q-*L*-E-D-K-*V*-E-E-*L*-K-E-K-*V*-G-E-amide

Figure 3-2. Amino acid sequences of the peptides used in this study. All peptides were N-terminal acetylated and C-terminal amidated. Peptides are named according to their amino acid substitutions in the parent peptide (peptide 1). Substitutions are indicated by the residue number and one-letter amino acid code, e.g. E19K corresponds to an analog with a glutamic acid (E) to lysine (K) substitution at position 19. Circles denote substituted amino acids. Boxes indicate residues involved in the hydrophobic core between the helices during coiled-coil formation (positions ***a*** and ***d*** of the heptad repeat, ***abcdefg***).

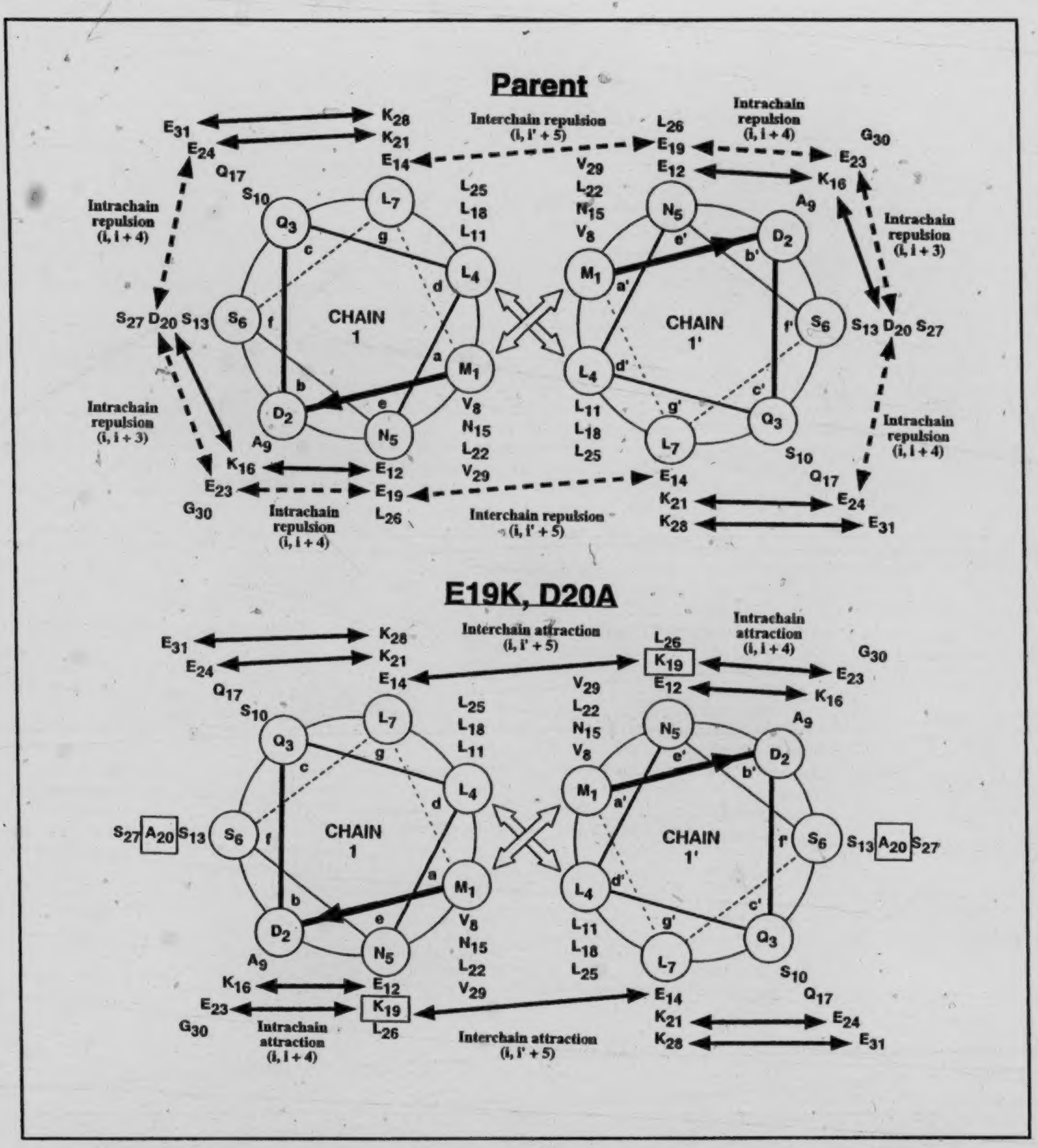
Parent
Interchain repulsion (i, i' + 5)
Intrachain repulsion (i, i + 4)
Intrachain repulsion (i, i + 3)
CHAIN 1
CHAIN 1'
E31 E24 Q17 S10 Q3
K28 K21 E14
L7 L4 M1 D2 N5 S6
L25 L18 L11
V29 L22 N15 V8
L26 E19 E12
G30 E23 K16 A9
S27 D20 S13
a b c d e f g
a' b' c' d' e' f' g'
L11 L18 L25
Interchain repulsion (i, i' + 5)
E19K, D20A
Interchain attraction (i, i' + 5)
Intrachain attraction (i, i + 4)
K19
A20

Figure 3-3. End view of possible parallel homodimeric α-helical coiled-coils, viewed from the N-terminus. Top, the parent peptide sequence (peptide 1) and below, the analog E19K, D20A (peptide 4, Fig. 3-2). Open two-headed arrows denote hydrophobic interactions between residues *a* to *a′* and *d* to *d′* in the hydrophobic core. Dashed two-headed arrows denote putative electrostatic repulsions (intrachain and interchain) between similarly charged residues. Solid two-headed arrows denote putative electrostatic attractions between oppositely charged residues. Substitutions at positions 19 and 20 are boxed for peptide E19K, D20A.

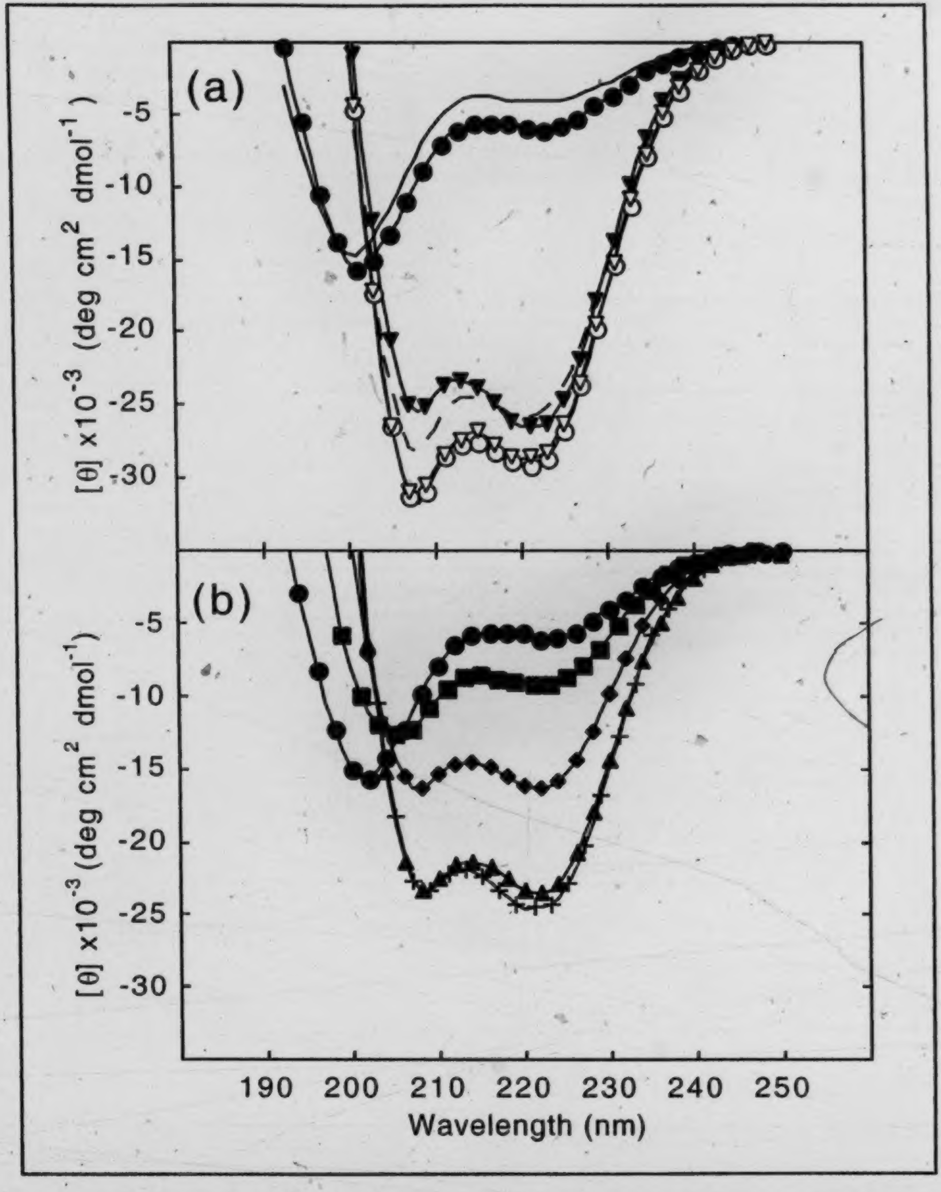

Figure 3-4. Far-UV CD Spectra of representative peptides. (a): Peptides L26K, S27E (solid line), parent (●) and D20A, S6A, S13A, S27A (▼) were in benign buffer (5 mM sodium phosphate, 150 mM NaCl, pH 7.4); peptides L26K, S27E (dashed line), parent (O) and peptide D20A, S6A, S13A, S27A (▽) were in equal volumes of benign buffer and 50% TFE at 5°C (see Fig 2 for sequences). Peptide concentrations were 250, 206, 203 and 203 μM. (b): Parent peptide (●), D20A (■), S6A, S13A, S27A (◆), E19K (▲), and E19K, D20A, S6A, S13A, S27A (+) in 5 mM sodium phosphate, 150 mM NaCl, pH 7.4 buffer at 5°C (See Fig. 3-2 for sequences). Peptide concentrations were 206, 237, 220, 323, and 176 μM.

Table 3-1. CD spectroscopy and sedimentation equilibrium results for peptides used in this study

Peptide	Substitution(s)	$[\theta]_{222}$[a]		$[\theta]_{222}/[\theta]_{208}$[b]		% helix[c]	MW_{obs}[d]	MW_{calc}[e]
		benign	TFE	benign	TFE			
1	None	-6200	-29000	0.62	0.91	18	4202 (M-D)	3532
2	E19K	-23500	-27700	1.00	0.92	68	7493 (D)	3529
3	D20A	-9300	-25000	0.80	0.92	27	4147 (M-D)	3488
4	E19K, D20A	-27100	-27700	1.04	0.92	79	6977 (D)	3487
5	S6A, S13A,S27A	-15400	-27500	1.00	0.92	45	4931 (M-D)	3484
6	D20A, S6A, S13A, S27A	-26500	-28500	1.04	0.92	77	6618 (D)	3438
7	E19K, D20A, S6A, S13A, S27A	-24400	-27300	1.05	0.92	71	6698 (D)	3439
8	L7K, E19K	-25100	-27100	1.02	0.94	73	6691 (D)	3544
9	L7A, E19K	-17100	-25400	0.92	0.90	50	5957 (M-D)	3487
10	L7E, E12K, E19K	-26300	-27500	1.03	0.89	76	7178 (D)	3544
11	L26K, S27E	-4100	-25600	0.51	0.91	12	n.d.[†]	3589

[a] Mean residue ellipticity of CD spectra at 222 nm in benign buffer (5 mM PO_4, 150 mM NaCl, pH 7.4) and in equal volumes of benign buffer and 2,2,2-trifluoroethanol (TFE). Peptide concentrations ranged from 176 to 323 μM and spectra were measured at 5°C.

[b] Ratio of mean residue ellipticity at 222 nm and 208 nm in the same solvents used in a.

[c] Percent helix calculated from $[\theta]_{222}$ where 100% helical content was based on the equation $[\theta]_H^n=[\theta]_H^\infty(1-k/n)$. $[\theta]_H^\infty$ is -37400 degrees•cm^2•$dmol^{-1}$ for a helix of infinite length, n is the number of residues in the helix and k is a wavelength-dependent constant (2.5 at 222 nm). For a 31-residue peptide, the theoretical value for 100% helix was -34,384.

[d] Observed molecular weight as determined by sedimentation equilibrium. Data was best fit to a monomer (M), dimer (D), or monomer to dimer equilibrium (M-D).

[e] Calculated molecular weight of the monomeric 31-residue peptide.

[†] n.d., not determined.

and ***d*** positions. Substitutions were not confined to a particular region along the length of the peptide and were located at positions 6, 7, 12, 13, 19, 20, and 27 in various analogs (Fig. 3-2). The position of these substitutions emphasize that raising stability anywhere in the sequence can help to induce folding without the necessity of introducing a specific 'consensus trigger sequence'. These substitutions also did not bring the sequences in closer agreement with the consensus trigger sequence (see peptide 7, Fig. 3-1). In addition, we designed a peptide (with only two changes to the parent sequence) that introduces the consensus trigger sequence to show that the presence of the trigger sequence does not guarantee the folding and formation of the coiled-coil (peptide 11, Figs. 3-1 and 3-2).

Removal of Electrostatic Repulsions

The effect of electrostatic interactions in stabilizing coiled-coils remains controversial (Hendsch et al. 1994, 1999; Lavigne et al. 1996; Lumb et al. 1995; O'Shea et al. 1993). Nevertheless, in the X-ray crystal structures of both coiled-coil regions of GCN4 and cortexillin I, interchain ionic interactions have been observed between side chains in ***g*** and ***e′*** positions (i, i′+5) while intrachain ionic interactions within α-helices have been observed between i, i+3 positions and i, i+4 positions (Burkhard et al. 2000; O'Shea et al. 1991). With our analogs we have measured the effect of removing the classical interchain and intrachain electrostatic repulsions on coiled-coil folding and stability. Examination of the parent peptide revealed possible interchain repulsions between acidic residues Glu14 and Glu19′, intrachain i, i+3 repulsions between Asp20-Glu23, and intrachain i, i+4 repulsions between Glu19-Glu23 and Asp20-Glu24 (Fig. 3-3, top). One or a combination of these interactions may have destabilized the parent peptide to prevent significant folding, as observed by CD spectroscopy and sedimentation equilibrium studies (Peptide 1, Table 3-1; Fig. 3-4A). Thus, we examined the effect of removing the interchain electrostatic repulsion with the E19K substitution, and the effect of removing the intrachain electrostatic repulsion with the D20A substitution (peptide E19K, D20A; Fig. 3-3, bottom).

E19K

The E19K substitution on its own eliminated the Glu-Glu′ (***g-e′***) repulsion between residues 14 and 19 and also added a Glu-Lys′ (***g-e′***) interchain attraction in the middle of the sequence (Peptide 2, Fig. 3-2). In addition, this substitution also removed an intrachain i, i+4 Glu-Glu repulsion and added an intrachain i, i+4 Lys-Glu attraction between residues 19 and 23. This single substitution resulted in a significant increase in folding (Table 3-1, Fig. 3-4B). The far-UV CD spectra, $[\theta]_{222}/[\theta]_{208}$ ratio in benign buffer, and sedimentation equilibrium data were characteristic of results observed for a two-stranded coiled-coil (positive band at 190 nm, local minima at 208 and 222 nm; $[\theta]_{222}/[\theta]_{208}$ ratio >1; MW_{app} approximately double the calculated monomer MW). Previous work determined the contribution to coiled-coil stability from elimination of a Glu-Glu′ interchain repulsion to be 0.45 kcal•mol^{-1} (Kohn et al. 1995b), and the addition of a Glu-Lys′ interchain attraction to be 0.37 kcal•mol^{-1} (Zhou et al. 1994a). The experimentally derived increase in stability for the E19K substitution relative to the parent peptide, 2.89 kcal mol^{-1}, determined by the difference in molar free energies of unfolding between peptide 6 and peptide 7 (Tables 3-2 and 3-3), closely matched the predicted stability increase of 2.84 kcal mol^{-1} (Tables 3-4 and 3-5).

Table 3-2. Thermodynamic data for peptides used in this study

Substitution(s)	[Peptide][a] (μM)	Experimental T_m[b] (°C)	$T_{m, 1M}$[c] (°C)	$\Delta H°(T_m)$[d] (kcal•mol^{-1})	$\Delta C_{p,u}$[e] (kcal•mol^{-1}K^{-1})	$\Delta G_u°(50°)$[f] (kcal•mol^{-1})
E19K, D20A, S6A, S13A, S27A	88	70	149	34	0.40	7.43
E19K, D20A	115	56	144	28	0.45	5.98
L7E, E12K, E19K	117	40	131	25	0.44	4.63
E19K	128	37	120	17	0.55	4.55
D20A, S6A, S13A, S27A	121	40	122	27	0.42	4.54
L7K, E19K	106	38	125	26	0.50	4.34
S6A, S13A, S27A	110 (876)*	34*	85	30*	0.50*	2.41*
L7A, E19K	158 (1054)*	40*	92	30*	0.50*	3.02*

[a] Peptide concentration (monomer).

[b] Experimentally determined temperature at which the first derivative of the magnitude of the slope in the thermal denaturation curve reaches maximum at peptide concentrations shown. Asterisks (*) indicates peptides that had thermodynamic parameters obtained at higher concentrations (shown in parentheses) to increase accuracy of the determination of T_m and other parameters.

[c] T_m calculated at 1 M peptide concentration (monomer). Values were calculated using the equation $\partial(\ln[N])/\partial(1/T_m) = -\Delta H°(T_m)/((n-1)*R)$, where [N] is the dimer concentration, $\Delta H°(T_m)$ is the standard state change in enthalpy at T_m, n=2 for a homodimeric reaction, and R is the ideal gas constant, $1.9872*10^{-3}$ kcal•mol^{-1}K^{-1} (Yu *et al.* 1999a).

[d] Change in molar enthalpy at T_m.

[e] Change in molar heat capacity, obtained from curve fit.

[f] Change in Gibbs free energy of unfolding at a reference temperature of 50°C, 1 M peptide concentration.

Table 3-3. Thermodynamic contribution of amino acid substitutions to coiled-coil stability

Substitution	Ionic attractions[a]	Ionic repulsions[b]	Helical propensity	Hydrophobicity at ***g***[c]	$\Delta\Delta G_u°(50°)$ peptide[d] (kcal•mol^{-1})	Substitutions per coiled-coil[e]	$\Delta\Delta G_u°(50°)$ substitution[f] (kcal•mol^{-1})
E19K	↑	↓	↑	-	2.89	2	1.45
D20A	↓	↓	↑	-	1.43	2	0.71
S6A, S13A, S27A	-	-	↑	-	1.45	6	0.24
L7K	↑	-	↓	↓	-0.21	2	-0.10
L7A	-	-	↑	↓	-1.53	2	-0.76
K7A	↓	-	↑	↑	-1.32	2	-0.66
K7E, E12K	-†	-	-	-	0.29	2†	0.15†

[a] Change in the number of ionic attractions (interchain or intrachain) caused by substitution.

[b] Change in the number of ionic repulsions (interchain or intrachain) caused by substitution

[c] Change in the hydrophobicity at heptad repeat position ***g*** caused by substitution.

[d] Stabilizing effect of substitution(s) on the change in molar free energy of peptide unfolding at 50°C.

[e] Number of substitutions in a two-stranded α-helical coiled-coil.

[f] Stabilizing effect of a single substitution on the change in molar Gibbs free energy of unfolding at 50°C.

† K7E, E12K substitutions are a change in orientation of the salt bridge from K-E to E-K and are counted as a single substitution.

Table 3-4. Predicted relative contributions of interactions to coiled-coil stability

Peptide	α-helical propensity[a] (kcal•mol^{-1})	i, i+4 intrachain[b] (kcal•mol^{-1})	i, i′+5 interchain[c] (kcal•mol^{-1})	Leu at ***e*** or ***g***[d] (kcal•mol^{-1})	Stability coefficients at ***a*** and ***d***[e] (kcal•mol^{-1})	Total score[f] (kcal•mol^{-1})	$\Delta\Delta G_u°$ relative to parent per peptide chain[g] (kcal•mol^{-1})	$\Delta\Delta G_u°$ relative to parent per coiled-coil[h] (kcal•mol^{-1})
E19K, D20A, S6A, S13A, S27A	6.46	0.6	0.37	1.38	31.16	39.97	2.74	5.48
GCN4p-wt[†]	5.57	0.4	0.74	0.69	31.78	39.18	1.95	3.90
E19K, D20A	5.51	0.6	0.37	1.38	31.16	39.02	1.79	3.58
E19K	5.14	0.6	0.37	1.38	31.16	38.65	1.42	2.84
D20A, S6A, S13A, S27A	6.26	0.2	-0.45	1.38	31.16	38.55	1.32	2.64
L7K, E19K	5.08	0.6	0.74	0.69	31.16	38.27	1.04	2.08
S6A, S13A, S27A	5.89	0.2	-0.45	1.38	31.16	38.18	0.95	1.90
L7A, E19K	5.21	0.6	0.37	0.69	31.16	38.03	0.80	1.60
L7E, E12K, E19K	5.08	0.2	0.74	0.69	31.16	37.87	0.64	1.28
D20A	5.32	0.2	-0.45	1.38	31.16	37.61	0.38	0.76
Parent	4.94	0.2	-0.45	1.38	31.16	37.23	0.00	0.00
L26K, S27E	3.88	-0.2	-0.90	0.69	31.16	34.63	-2.60	-5.20

[a] Sum of the α-helical propensity $\Delta\Delta G_u$ values relative to glycine for residues in positions ***bcefg*** in each peptide sequence. Values of the α-helical propensities in a monomeric α-helix (Zhou et al. 1994b) were divided by two to obtain helix propensities for amino acids in a two-stranded coiled-coil (Kwok et al. 1999).

[b] Sum of the i, i+4 intrachain electrostatic contributions to stability in each peptide sequence. A value of 0.2 kcal•mol^{-1} was used for attractions (Zhou et al. 1993) and –0.2 kcal•mol^{-1} was used for repulsions (Kohn et al. 1995b).

[c] Sum of the i, i′+5 interchain electrostatic ***g-e′*** contributions to stability in each peptide sequence. A value of 0.37 kcal•mol^{-1} was used for Glu-Lys or Lys-Glu attractions (Zhou et al. 1994a) and –0.45 kcal•mol^{-1} was used for interchain repulsions (Kohn et al. 1995b).

[d] Sum of the contributions to stability from the hydrophobic effect of Leu at positions ***e*** or ***g*** in the hydrophobic interface. A value of 0.69 kcal•mol^{-1} was used based on results obtained from this study.

[e] Sum of the stability coefficients from residues in the ***a*** and ***d*** positions in each peptide sequence (Tripet et al. 2000; Wagschal et al. 1999b).

[f] Sum of $\Delta\Delta G_u$ values in columns a to e.

[g] $\Delta\Delta G_u$ relative to the parent stability score, calculated as $\Delta\Delta G_u$ = total score of selected peptide – total score of parent peptide.

[h] $\Delta\Delta G_u$ for the coiled-coil, calculated as the $\Delta\Delta G_u$ per peptide chain x 2 chains per coiled-coil.

[†] Peptide 31-mer from the coiled-coil region of wild-type GCN4 containing the ‘consensus trigger sequence’ (Kammerer et al. 1998).

Table 3-5. Predicted and experimentally derived relative coiled-coil stabilities of peptides used in this study

Peptide	Predicted $\Delta\Delta G_u°(50°)^a$ (kcal•mol^{-1})	Experimentally derived $\Delta\Delta G_u°(50°)^b$ (kcal•mol^{-1})	$T_{m,\,100\,\mu M}{}^c$ (°C)
E19K, D20A, S6A, S13A, S27A	5.48	5.77	71
GCN4p-wt	3.90	n.d.[d]	53[e]
E19K, D20A	3.58	4.32	55
E19K	2.84	2.89	34
D20A, S6A, S13A, S27A	2.64	2.88	39
L7K, E19K	2.08	2.68	38
L7E, E12K , E19K	1.28	2.97	39
S6A, S13A, S27A	1.90	1.45	21
L7A, E19K	1.60	1.36	25
D20A	0.76	1.43	n.d.[d]
Parent	0.00	0.00	n.d.[d]

[a] Relative predicted stability of peptides based on side chain stability coefficients in positions ***a*** and ***d*** in kcal•mol^{-1} as calculated in Table 3-4.

[b] Experimentally derived peptide stability relative to the parent peptide, based on $\Delta\Delta G_u°(50°)$ values in Table 3-3.

[c] Transition midpoint of peptides at concentrations corrected to exactly 100 µM in 150 mM NaCl, 5 mM PO_4, pH 7.4. Values were calculated using the equation $\partial(\ln[N])/\partial(1/T_m) = -\Delta H°(T_m)/((n-1)*R)$, where [N] is the peptide dimer concentration, $\Delta H°(T_m)$ is the standard state change in enthalpy at experimental T_m, n=2 for a homodimeric reaction, and R is the ideal gas constant (Yu et al. 1999a). Peptides listed above the dashed line exhibited significant folding at 100 µM peptide concentration.

[d] Not determined.

[e] T_m value of a 31-mer peptide from the coiled-coil region of wild-type GCN4 (Kammerer et al. 1998) determined at 75 µM peptide concentration in 150 mM NaCl, 5 mM sodium phosphate buffer, pH 7.4.

D20A

The D20A substitution replaced an Asp with an Ala at an *f* position near the middle of the sequence (Fig. 3-2). Asp20 has potential anionic intrachain repulsions with Glu23 and Glu24 and a potential intrachain attraction with Lys16 (Fig. 3-3, top). Substitution of Asp20 by Ala was expected to affect not only intrachain electrostatic interactions, but also to raise stability via alanine's higher α-helical propensity (O'Neil et al. 1990; Zhou et al. 1994b). This substitution alone did not induce significant α-helical content (Table 3-1, Fig. 3-4B), but D20A combined with the E19K substitution resulted in an increase in T_m from 34°C to 55°C between peptides E19K and E19K, D20A at 100 μM concentration (Table 3-5). Our experimentally derived value for the stability contribution from D20A, 1.43 kcal•mol^{-1}, was greater than the predicted value of 0.76 kcal•mol^{-1} by 0.67 kcal•mol^{-1} per coiled-coil (Table 3-5).

Helical Propensity

Only one set of substitutions (S6A, S13A, S27A) specifically examined the effects of increased helical propensity on coiled-coil folding and stability in the parent peptide in the absence of other effects. Because of its small nonpolar methyl side chain (-CH_3), alanine will not provide additional steric, hydrogen bonding, or electrostatic interactions with neighboring side chains, such that any changes in peptide stability can be attributed strictly to helical propensity differences between serine and alanine.

The three serine residues that were switched to alanine were selected for three reasons. 1) The serines were located along the entire length of the sequence and were not localized to a specific region, e.g. N-terminal or C-terminal. By making substitutions spread along the whole length of the sequence, we wanted to show that increased local stability was not the only way to induce protein folding, a strategy one observes with insertion of a 'trigger sequence'. 2) All serines were at ***f*** positions, away from the hydrophobic core ***a*** and ***d*** positions and away from the hydrophobic interface ***e*** and ***g*** positions. Therefore, the locations for the substitutions would not influence either the packing or the hydrophobicity of the hydrophobic core and/or interface. 3) Serine has a relatively low helical propensity versus alanine (O'Neil et al. 1990; Zhou et al. 1994b).

The S6A, S13A, S27A substitutions increased the fraction of folded molecules within the total population of peptide molecules, but could not induce the entire population to fold at 110 μM peptide concentration (Fig. 3-4B, Table 3-1). A second denaturation was performed at 876 μM to increase folding and stability to accurately calculate the T_m at 100 μM peptide concentration (21°C, Table 3-5). The energetic contribution of the Ser to Ala substitutions was obtained by subtracting the change in Gibbs free energy of unfolding values for the two peptides E19K, D20A, S6A, S13A, S27A and E19K, D20A (Table 3-2). The overall contribution to stability was calculated to be 1.45 $kcal \bullet mol^{-1}$, or 0.24 $kcal \bullet mol^{-1}$ per Ser to Ala substitution (six substitutions in the coiled-coil), assuming that each serine along the sequence contributed equally to stability, i.e. no positional dependence to stability (Table 3-3).

Hydrophobicity Effects

The burial of nonpolar residues is generally accepted as one of the principal forces driving the folding of protein tertiary structure (Hodges 1992; Talbot et al. 1982). In two-stranded coiled-coils, burial of hydrophobes occurs at ***a*** and ***d*** positions; thus, residues at these locations are a major contributor to coiled-coil stability through hydrophobic and packing effects (Hodges 1996; Tripet et al. 2000; Wagschal et al. 1999b; Yu et al. 1999). However, we did not alter the composition of the hydrophobic core in our analogs because the core residues of the parent sequence were already strongly stabilizing hydrophobes, having similar stabilizing contributions as core residues observed in wild-type GCN4 coiled-coils (O'Shea et al. 1991; Tripet et al. 2000; Wagschal et al. 1999b).

How did the hydrophobic effect at the ***g-e′*** positions compare to the interchain electrostatic contribution to folding and stability? We specifically examined the stability contribution of the residues at position 7 (***g*** position). A subset of three peptides was constructed, all containing the E19K substitution to induce folding but with different amino acids at position 7 (Leu, Lys or Ala; peptides 2, 8, and 9 in Fig. 3-2). In the parent peptide, position 7 contained a hydrophobic residue (Leu) and position 12 contained an acidic residue (Glu). Replacement of the Leu7 with Lys7 eliminated a hydrophobe from the ***g*** position, but introduced an interchain electrostatic Lys-Glu′ attraction across the interface (peptides 2 and 8, Fig. 3-2). This substitution was carried out to increase stability in a similar manner to the E19K, via attractive Glu-Lys ion pairing. Thus, the peptide L7K, E19K results in four ***g-e′*** interchain electrostatic attractions per coiled-coil (two attractions between Lys and Glu at positions 7 and 12, and two attractions between Glu and Lys at positions 14 and 19). However, both peptides E19K and L7K, E19K folded to a similar extent and had similar stabilities, indicating that the hydrophobic Leu7 contributed to folding and stability to approximately the same extent as the Lys7-Glu12′ salt bridge (peptides 2 and 8, Table 3-1 and Table 3-2). To further demonstrate the importance of the Leu as a stabilizing hydrophobe in position ***g***, peptide E19K ($T_{m,\,100\,\mu M}$ = 34°C) had an increase in α-helical content and greater stability relative to peptide L7A, E19K ($T_{m,\ 100\ \mu M}$ = 25°C) as observed by a T_m difference of 9°C (Table 3-5). The net destabilizing effect of L7A indicated that the loss of hydrophobicity and packing effects from the Leu at position ***g*** is more detrimental to folding than the stabilizing effect of increasing helical propensity from switching Leu to Ala. The difference in helical propensity between Ala and Leu was reported as 0.15 kcal•mol^{-1} for a single-stranded amphipathic α-helix (Zhou et al. 1994b), but Kwok *et al.* reported that the helical propensity contribution to stability in coiled-coils is approximately half the value in monomeric helices (Kwok et al. 1999). Taking the helical propensity value for a Leu to Ala substitution as 0.075 kcal•mol^{-1} (0.15 kcal•mol^{-1}÷ 2) and subtracting this from the 0.76 kcal•mol^{-1} for the L7A substitution gave the hydrophobic effect for a Leu at position ***g***, 0.69 kcal•mol^{-1}. This value was greater than the stabilizing interchain electrostatic effects from the Lys7-Glu12 salt bridge (0.53 kcal•mol^{-1}) in L7K, E19K by 0.16 kcal•mol^{-1} per chain.

Hydrophobic effects from burial of nonpolar residues have been previously shown to be stabilizing relative to a buried salt bridge triad in the Arc repressor protein and in a hybrid LexA/Jun protein (Schmidt-Dorr et al. 1991; Waldburger et al. 1995). Computational analysis of the GCN4 coiled-coil also indicated that the proximity of charged residues to the hydrophobic core (positions ***a*** and ***d***) resulted in a desolvation penalty for the formation of ion pairs at the ***e*** and ***g*** positions (Hendsch et al. 1999). The results of these studies support the view that hydrophobic side chains at the flanking ***e*** and ***g*** positions of two-stranded coiled-coils are stabilizing relative to ion pairs.

Orientation of Interchain Electrostatics

Other analogs examined the effect of orientation of electrostatics at the ***g-e′*** interface between residues 7 and 12 (Leu7 and Glu12 in the parent sequence). Peptides L7K, E19K and L7E, E12K, E19K (peptides 8 and 10, Fig. 3-2) both contained the Glu-Lys salt bridge between positions 14 and 19, with another salt bridge between positions 7 and 12 in either the Glu-Lys (peptide 10) or Lys-Glu (peptide 8) orientation. Peptides 8 and 10 exhibited similar folding and thermostabilities, with % helix values of 73% and 76%, and $T_{m,\ 100\ \mu M}$ values of 38°C and 39°C, respectively (Table 3-1 and Table 3-5). Our data is in agreement with previous work that determined that the orientation of the Glu-Lys′ ion pair in peptide L7E, E12K, E19K is slightly more stable versus the Lys-Glu′ orientation in peptide L7K, E19K (Kohn et al. 1998b).

Oligomerization State

Residues in the both the ***a*** and ***d*** positions can affect the oligomerization state of coiled-coils. Studies with the coiled-coil region of GCN4 indicate that an asparagine located in the ***a*** position of the hydrophobic core is important in maintaining the dimeric state. Substitution of the asparagine with glutamine, longer by a single methylene group, gives a mixture of dimers and trimers (Gonzalez et al. 1996c). The crystal structure of the GCN4 coiled-coil showed that the asparagine hydrogen bonds with the asparagine in the hydrophobic core of the other coiled-coil strand and disfavors the trimer configuration through side chain packing effects (O'Shea et al. 1991). Other substitutions in the ***a*** and ***d*** positions with leucine, isoleucine, and valine produced dimers, trimers and tetramers (Harbury et al. 1993).

The oligomerization domains from GCN4 and cortexillin I both form parallel homodimeric coiled-coils. Because we wanted to confer the dimeric form for all analogs and ensure a 2monomer⇔dimer equilibrium folding pathway without higher order oligomers, we kept the asparagine in the ***a*** position in our hybrid sequence. All peptides in the study were analyzed by sedimentation equilibrium at different peptide concentrations and rotors speeds and the apparent molecular weights were globally fit to either a dimer, or distribution of monomer-dimer forms (Table 3-1). Thus, substitutions in positions ***e*** and ***g*** did not appear to confer oligomerization states in our peptide analogs higher than the dimeric form.

The extent of oligomerization was concentration-dependent in all peptides, with dimers favored at higher concentrations according to the law of mass action (Fig. 3-5). Consistent with the far-UV circular dichroism results, the peptides that exhibited significant folding (peptides 2, 4, 6, 7, 8, 10, Table 3-1) were best fit to dimers at the concentrations analyzed (~200 μM), indicating that nearly the entire population of molecules had folded into two-stranded coiled-coils. The parent (peptide 1) and peptides 3 (D20A), 4 (S6A, S13A, S27A) and 9 (L7A, E19K) were best fit to a monomer-dimer equilibrium, supporting the CD spectroscopy results indicating a partial population of folded dimers in equilibrium with unfolded monomers. This is based on the two-state unfolding model, i.e. molecules in an all-or-none 2monomer⇔dimer equilibrium with unfolded monomer or folded coiled-coil dimer, with some disorder at the N- and C-termini caused by end-fraying. In support of this model, we observed co-operative denaturation curves consistent with two-state unfolding, and recooling of peptides to 5°C

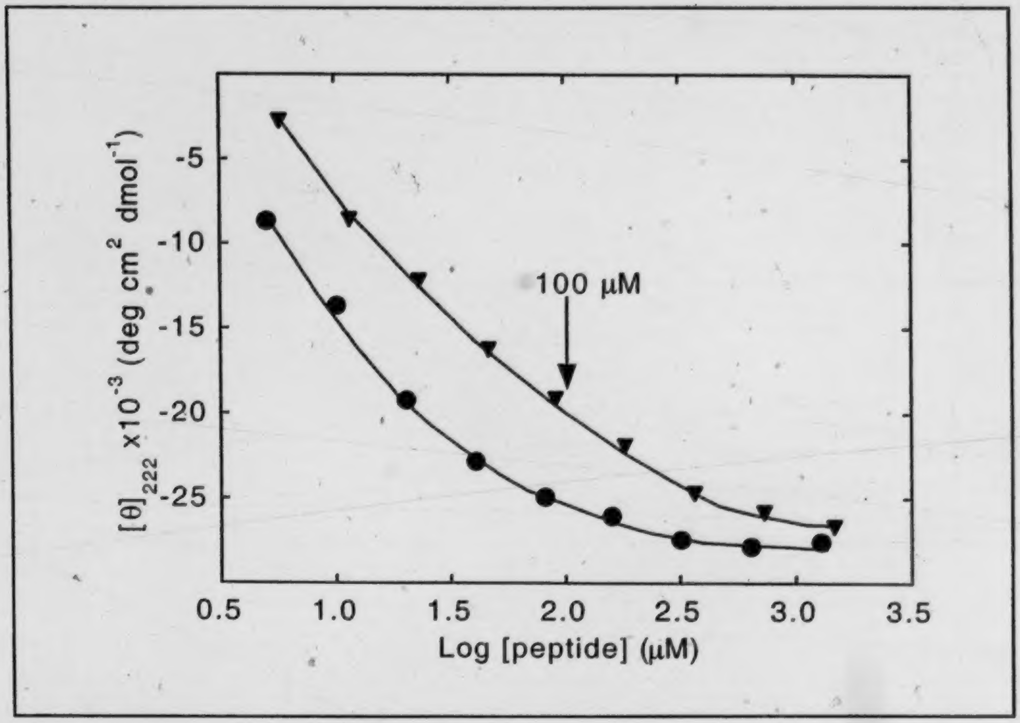

Figure 3-5. Concentration dependence of helicity in representative peptides. Plot of mean residue ellipticity at 222 nm versus the logarithm of the monomer peptide concentration for peptide S6A, S13A, S27A (▲) and peptide D20A, S6A, S13A, S27A (●) in 5 mM sodium phosphate, 150 mM NaCl, pH 7.4 buffer at 5°C (see Fig. 3-2 for sequences).

after thermal melting gave molar ellipticities similar to those obtained before denaturation (data not shown).

Coiled-Coil Stability

Although both external and internal (sequence-dependent) factors affect coiled-coil stability, we chose to examine only how the variation of internal parameters 1) interchain electrostatic effects, 2) intrachain electrostatic effects, 3) helical propensity, and 4) hydrophobicity outside the hydrophobic core ***a*** and ***d*** positions influenced coiled-coil folding and stability.

Protein stability is usually determined based on measuring changes in folding at increasing levels of denaturant such as urea, guanidium hydrochloride, or heat. Although urea and guanidium hydrochloride are often selected for chemical denaturation, we chose thermal denaturation of our peptides because this technique can be used to monitor unfolding of proteins with lower stabilities, such as the coiled-coil peptides used in this study. Between temperatures of 5°C and 85°C, we observed a broad range of stabilities for different peptides, with $T_{m,\ 100\ \mu M}$ values ranging between 21 and 71°C (Table 3-5). A reference temperature of 50°C was chosen to report the change in molar free energy of unfolding, $\Delta G_u°(T_{ref})$, because this temperature was close to the middle of the range of $T_{m,\ 100\ \mu M}$ values for peptides in this study. Molar ellipticity data collected at 222 nm is consistent with a reversible, co-operative two-state helix-coil transition (Fig. 3-6A, 6B). The $\Delta G_u°(50°)$ values were then used to calculate $\Delta\Delta G_u°(50°)$, the contribution to stability for specific effects or substitutions at 50°C (Table 3-3). Because the parent peptide did not fold, we could not calculate the $\Delta\Delta G_u°(50°)$ for substitutions by simply taking the

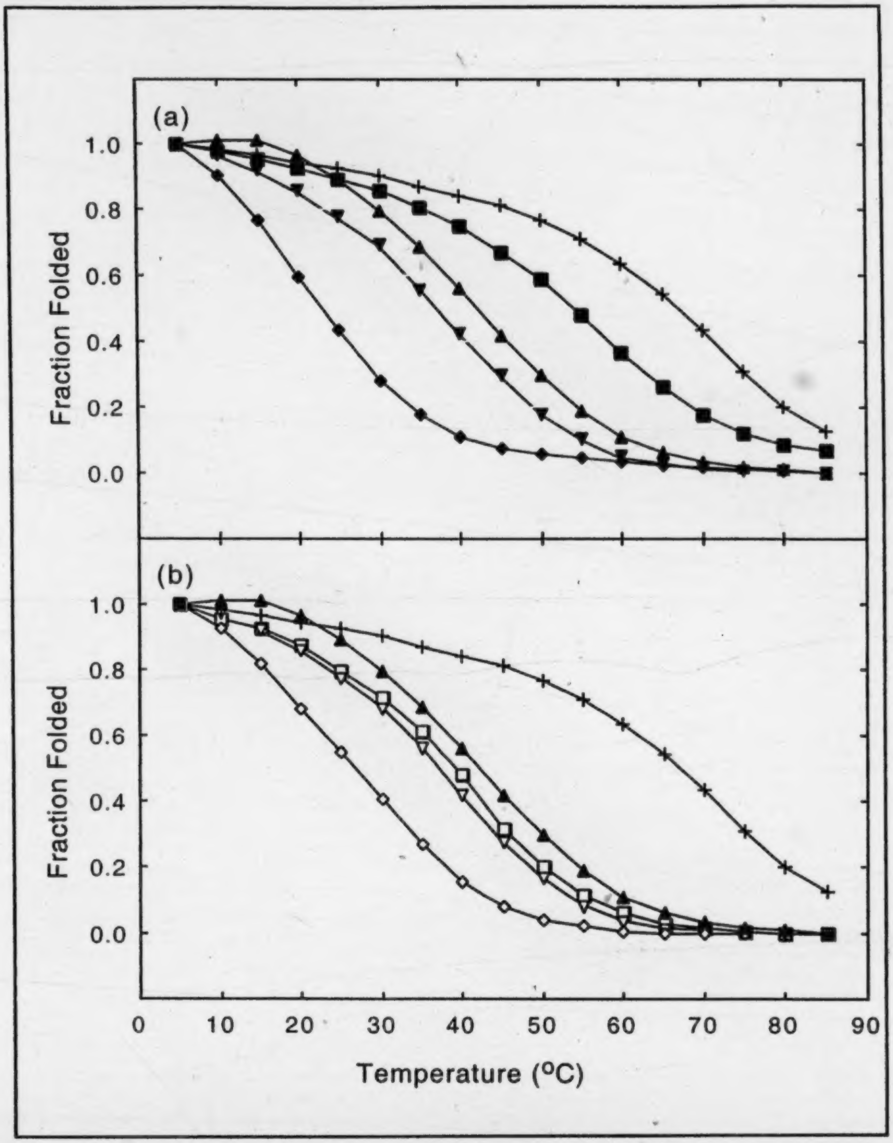

Figure 3-6. Thermal unfolding curves for coiled-coil peptides. Representative plots of fraction folded at given temperatures. Fraction folded is $([\theta]-[\theta]_u)/([\theta]_f-[\theta]_u)$, where $[\theta]$ is the observed molar ellipticity, $[\theta]_u$ is the molar ellipticity of the unfolded peptide and $[\theta]_f$ is the molar ellipticity of the folded peptide. (a) Peptides S6A, S13A, S27A (◆), D20A, S6A, S13A, S27A (▼), E19K (▲), E19K, D20A (■), and E19K, D20A, S6A, S13A, S27A (+). (b) E19K analogs. Peptides L7A, E19K (◊), L7K, E19K (▽), L7E, E12K, E19K (□), E19K (▲), and E19K, D20A, S6A, S13A, S27A (+). Data was collected from 5 to 85°C at 5° intervals in benign buffer (5 mM sodium phosphate, 150 mM NaCl, pH 7.4). Peptide concentrations ranged from 88 to 158 μM.

difference between unfolding energies of the analog and the parent peptides, $\Delta G_u°(T_{ref})_{analog}$-$\Delta G_u°(T_{ref})_{parent}$.. Instead, we determined the change in unfolding energy for an analog containing the sum of several substitutions that stabilized the coiled-coil (peptides 4 and 7, Fig. 3-2) and then determined $\Delta\Delta G_u°(50°)$ values for substitutions by taking the difference in $\Delta G_u°(T_{ref})$ between peptides 4 or 7 and lesser substituted analogs (see Materials and Methods). Thus, we were able to calculate $\Delta\Delta G_u°(T_{ref})$ for substitutions without directly measuring the stability of the parent peptide.

The changes in stability as indicated by $\Delta\Delta G_u°(50°)$ values correlated well with the increase in folding as measured by far-ultraviolet CD spectroscopy in benign conditions (Tables 3-1 and 3-3, Fig. 3-4B). Taken together, the order of relative stability contributions to coiled-coil folding from the interactions examined in this study are interchain ionic attractions + loss of interchain ionic repulsions from Glu to Lys substitution > Ala to Leu at ***g*** > Glu-Lys′ (***g-e′***) ion pair > Lys-Glu′ (***g-e′***) ion pair > loss of intrachain electrostatic effects + Asp to Ala gain in helical propensity > Ser to Ala gain in helical propensity > re-orientation of Lys-Glu′ (***g-e′***) salt bridges.

The prediction of relative contributions of various interactions to coiled-coil stability of the parent are reported in Table 3-4, in the order of decreasing stability. The residues comprising the hydrophobic core (***a*** and ***d*** positions) were the major contributor to overall stability, adding >31 kcal•mol^{-1} to stability relative to alanine (Tripet et al. 2000; Wagschal et al. 1999b). However, this contribution was the same in all GCN4/cortexillin I peptides as the hydrophobic core was kept the same in all sequences. The single Leu to Val difference in the ***a*** position of wild-type GCN4 was predicted to increase its stability over the GCN4/cortexillin hybrids by 1.24 kcal•mol^{-1} per coiled-coil (Wagschal et al.

1999b). The greatest differences in predicted stability among the GCN4/cortexillin I peptides came from differences in helical propensity and interchain electrostatic interactions. A difference of 3.04 kcal•mol^{-1} per coiled-coil (2x1.52 kcal•mol^{-1}) was predicted between the helical propensity scores of the individual helices of E19K, D20A, S6A, S13A, S27A (6.46 kcal•mol^{-1}) and the parent peptide (4.94 kcal•mol^{-1}), while a 2.38 kcal•mol^{-1} difference per coiled-coil (2x1.19 kcal•mol^{-1}) was predicted between peptides with the most (0.74 kcal•mol^{-1}) and least (-0.45 kcal•mol^{-1}) stabilizing interchain electrostatic effects per helix.

Table 3-5 showed a general agreement between the predicted contributions to stability reported in Table 3-4 and the experimentally derived stability contributions obtained from thermal denaturation of peptides in this study. Listed in the order of decreasing experimentally derived stability, the peptides can be grouped into three general categories: very stable and folded, stable and folded, and unstable and not fully folded. Very stable peptides had transition midpoint values at 100 μM above 50°C, stable peptides had $T_{m,\ 100\ \mu M}$ values between 34° and 40°C, and unstable peptides had $T_{m,\ 100\ \mu M}$ values at or below 25°C. The largest difference between predicted and experimentally derived stability contributions was for peptide L7E, E12K, E19K, with a difference of 1.69 kcal•mol^{-1} per coiled-coil (2.97 - 1.28 kcal•mol^{-1}, Table 3-5). It may be possible that some intrachain repulsions predicted to destabilize this peptide do not occur, but even taking this into account does not explain the discrepancy.

Chapter 3-3. Discussion

We have demonstrated here that it is not necessary to have a consensus trigger sequence for the folding of two-stranded α-helical coiled-coils. We deliberately avoided including the trigger sequence in the peptides used in this study to demonstrate that although the sequence may be necessary for folding in cortexillin I and GCN4, the formation of two-stranded coiled-coils is not solely dependent on the presence of a trigger sequence. Instead, we have hypothesized that folding depends on the overall stability of the entire sequence. Thus, the trigger sequence may simply be a method that nature has developed to raise the local sequence stability and in turn increase the overall sequence stability past a threshold level needed for coiled-coil folding. Kammerer *et al.* previously introduced the 'trigger sequence' as a way to explain why deletion mutants from the dimeric coiled-coil region of cortexillin I would not fold into coiled-coils unless a specific 14-residue 'trigger sequence' (Arg311-Arg324) was present (Kammerer et al. 1998). The high-resolution crystal structure of cortexillin I showed that 5 interchain ion pairs and 4 intrachain ion pairs stabilized the trigger sequence, and that the trigger sequence was the most stable region of the coiled-coil (Burkhard et al. 2000). In contrast, the crystal structure did not contain any interhelical or intrahelical ion pairs in Asp270-Glu282, the region of cortexillin I incorporated into our cortexillin I/GCN4 parent peptide.

Perhaps the addition of a stabilizing region compensates for regions of lower stability simply by increasing the overall stability of a sequence. Does this stabilizing region need to be near the regions of lower stability, or concentrated in the form of a 'trigger sequence?' Based on our results from peptide S6A, S13A, S27A, the answer seems to be no. The computer program STABLECOIL (Tripet et al. 2001) predicted the region surrounding the central asparagine at an ***a*** position to be destabilized (Fig. 3-7), a result

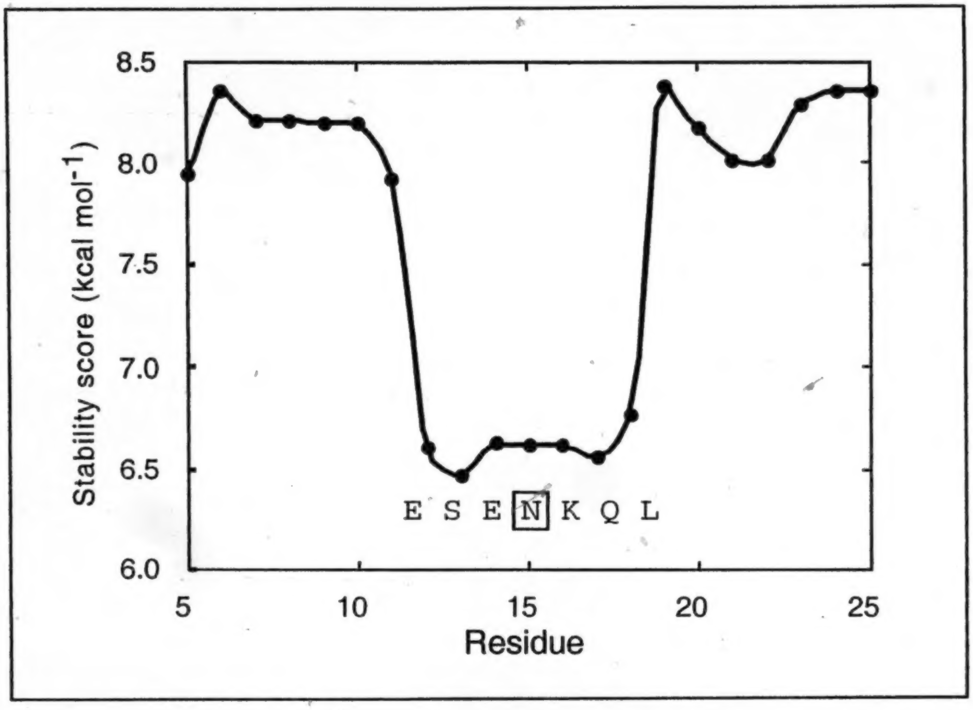

Figure 3-7. Influence of Asn15 on coiled-coil stability. Prediction of coiled-coil stability using STABLECOIL (Tripet et al. 2001). Scores were assigned to 7-residue windows along the sequence of the parent peptide based on helical propensity values for residues at positions ***b,c,e,f***, and ***g*** (Zhou et al. 1994b) and stabilities for residues at positions ***a*** and ***d*** (Tripet et al. 2000; Wagschal et al. 1999b). The residue number on the horizontal axis corresponds to the amino acid in the centre of the 7-residue window. Upper case letters indicate one letter amino acid code for the parent sequence, with Asn15 boxed to highlight its predicted destabilizing effect.

supported by NMR spectroscopy studies of GCN4 and GCN4-like coiled-coils (Holtzer et al. 1997). However, S6A, S13A, S27A contained substitutions along the entire length of the sequence and was still able to induce folding even though two of the substitutions at Ser6 and Ser27 were not near the Asn15. Although we assumed that each serine contributed equally to coiled-coil stability, it would be interesting to determine whether the serine closer to Asn15 (Ser13) was a greater contributor to stability versus the serines further from the middle of the sequence (Ser6 and Ser27).

Based upon our results in this study, we hypothesize that sequences must have proper stabilizing interactions in order to fold into a two-stranded coiled-coil, but these interactions are not confined to a specific trigger sequence. Therefore, one cannot simply include a trigger sequence and expect folding to occur without closer examination of the many sequence-dependent interactions governing coiled-coil folding. In further support of this hypothesis, we designed a peptide that contained the consensus trigger sequence and did not form a two-stranded coiled-coil (peptide 11, Figs. 3-1 and 3-4A; Table 3-1). This clearly demonstrated that the consensus trigger sequence itself is not adequate for the folding of two-stranded coiled-coils if there is insufficient stability in the trigger sequence region. In this case, peptide 11 is predicted not to fold because of the interchain and intrachain electrostatic repulsions introduced by the L26K and S27E substitutions (Table 3-4). In general, trigger sequences are simply one way to increase overall stability to achieve coiled-coil folding. Though they are not essential to induce folding, they could be important in nature's design to regulate the timing of folding during ribosomal protein synthesis. The concentrated higher local stability of the trigger sequence could also be an important way to allow conformational change in coiled-coils to affect protein-protein interactions. The regions of higher local stability could compensate for other regions of lower local stability to maintain the overall folded coiled-coil state, yet the structure of these lower stability coiled-coil regions could be more easily disrupted to possibly interact with other proteins.

Chapter 3-4. References

Aurora, R. and Rose, G.D. 1998. Helix capping. *Protein Sci* **7:** 21-38.

Baldwin, R.L. and Rose, G.D. 1999. Is protein folding hierarchic? I. Local structure and peptide folding. *Trends Biochem Sci* **24:** 26-33.

Burkhard, P., Kammerer, R.A., Steinmetz, M.O., Bourenkov, G.P. and Aebi, U. 2000. The coiled-coil trigger site of the rod domain of cortexillin I unveils a distinct network of interhelical and intrahelical salt bridges. *Structure Fold Des* **8:** 223-230.

Crick, F.H.C. 1953. The packing of α-helices: simple coiled-coils. *Acta Crystallog* **6:** 689-697.

Eriksson, A.E., Baase, W.A., Zhang, X.J., Heinz, D.W., Blaber, M., Baldwin, E.P. and Matthews, B.W. 1992. Response of a protein structure to cavity-creating mutations and its relation to the hydrophobic effect. *Science* **255:** 178-183.

Fairman, R., Chao, H.G., Mueller, L., Lavoie, T.B., Shen, L., Novotny, J. and Matsueda, G.R. 1995. Characterization of a new four-chain coiled-coil: influence of chain length on stability. *Protein Sci* **4:** 1457-1469.

Frank, S., Lustig, A., Schulthess, T., Engel, J. and Kammerer, R.A. 2000. A distinct seven-residue trigger sequence is indispensable for proper coiled-coil formation of the human macrophage scavenger receptor oligomerization domain. *J Biol Chem* **275:** 11672-11677.

Gonzalez, L., Jr., Brown, R.A., Richardson, D. and Alber, T. 1996a. Crystal structures of a single coiled-coil peptide in two oligomeric states reveal the basis for structural polymorphism. *Nat Struct Biol* **3:** 1002-1009.

Gonzalez, L., Jr., Plecs, J.J. and Alber, T. 1996b. An engineered allosteric switch in leucine-zipper oligomerization. *Nat Struct Biol* **3:** 510-515.

Gonzalez, L., Jr., Woolfson, D.N. and Alber, T. 1996c. Buried polar residues and structural specificity in the GCN4 leucine zipper. *Nat Struct Biol* **3:** 1011-1018.

Harbury, P.B., Zhang, T., Kim, P.S. and Alber, T. 1993. A switch between two-, three-, and four-stranded coiled coils in GCN4 leucine zipper mutants. *Science* **262:** 1401-1407.

Hendsch, Z.S. and Tidor, B. 1994. Do salt bridges stabilize proteins? A continuum electrostatic analysis. *Protein Sci* **3:** 211-226.

Hendsch, Z.S. and Tidor, B. 1999. Electrostatic interactions in the GCN4 leucine zipper: substantial contributions arise from intramolecular interactions enhanced on binding. *Protein Sci* **8:** 1381-1392.

Hodges, R.S. 1992. Unzipping the secrets of coiled-coils. *Curr Biol* **2:** 122-124.

Hodges, R.S. 1996. De novo design of alpha-helical proteins: basic research to medical applications. *Biochem Cell Biol* **74:** 133-154.

Holtzer, M.E., Lovett, E.G., d'Avignon, D.A. and Holtzer, A. 1997. Thermal unfolding in a GCN4-like leucine zipper: ^{13}C alpha NMR chemical shifts and local unfolding curves. *Biophys J* **73:** 1031-1041.

Huyghues-Despointes, B.M. and Baldwin, R.L. 1997. Ion-pair and charged hydrogen-bond interactions between histidine and aspartate in a peptide helix. *Biochemistry* **36:** 1965-1970.

Kammerer, R.A., Schulthess, T., Landwehr, R., Lustig, A., Engel, J., Aebi, U. and Steinmetz, M.O. 1998. An autonomous folding unit mediates the assembly of two-stranded coiled coils. *Proc Natl Acad Sci U S A* **95:** 13419-13424.

Kohn, W.D. and Hodges, R.S. 1998a. De novo design of alpha-helical coiled-coils and bundles: models for the development of protein-design principles. *Trends Biotechnol* **16:** 379-389.

Kohn, W.D., Kay, C.M. and Hodges, R.S. 1995a. Protein destabilization by electrostatic repulsions in the two-stranded alpha-helical coiled-coil/leucine zipper. *Protein Sci* **4:** 237-250.

Kohn, W.D., Kay, C.M. and Hodges, R.S. 1998b. Orientation, positional, additivity, and oligomerization-state effects of interhelical ion pairs in alpha-helical coiled-coils. *J Mol Biol* **283:** 993-1012.

Kohn, W.D., Monera, O.D., Kay, C.M. and Hodges, R.S. 1995b. The effects of interhelical electrostatic repulsions between glutamic acid residues in controlling the dimerization and stability of two- stranded alpha-helical coiled-coils. *J Biol Chem* **270:** 25495-25506.

Kwok, S.C., Mant, C.T. and Hodges, R.S. 1999. Effects of alpha-helical and beta-sheet propensities of amino acids on protein stability. In *Peptides 1998: Proceedings of the Twenty-Fifth European Peptide Symposium* (S. Bajusz and F. Hudecz, eds.), 34-35, Akademiai Kiado, Budapest.

Lau, S.Y., Taneja, A.K. and Hodges, R.S. 1984. Synthesis of a model protein of defined secondary and quaternary structure. Effect of chain length on the stabilization and formation of two-stranded alpha-helical coiled-coils. *J Biol Chem* **259:** 13253-13261.

Lavigne, P., Sonnichsen, F.D., Kay, C.M. and Hodges, R.S. 1996. Interhelical salt bridges, coiled-coil stability, and specificity of dimerization. *Science* **271:** 1136-1138.

Lu, M., Shu, W., Ji, H., Spek, E., Wang, L. and Kallenbach, N.R. 1999. Helix capping in the GCN4 leucine zipper. *J Mol Biol* **288:** 743-752.

Lumb, K.J., Carr, C.M. and Kim, P.S. 1994. Subdomain folding of the coiled coil leucine zipper from the bZIP transcriptional activator GCN4. *Biochemistry* **33:** 7361-7367.

Lumb, K.J. and Kim, P.S. 1995. Measurement of interhelical electrostatic interactions in the GCN4 leucine zipper. *Science* **268:** 436-439.

Micklatcher, C. and Chmielewski, J. 1999. Helical peptide and protein design. *Curr Opin Chem Biol* **3:** 724-729.

Moitra, J., Szilak, L., Krylov, D. and Vinson, C. 1997. Leucine is the most stabilizing aliphatic amino acid in the d position of a dimeric leucine zipper coiled coil. *Biochemistry* **36:** 12567-12573.

O'Neil, K.T. and DeGrado, W.F. 1990. A thermodynamic scale for the helix-forming tendencies of the commonly occurring amino acids. *Science* **250:** 646-651.

O'Shea, E.K., Klemm, J.D., Kim, P.S. and Alber, T. 1991. X-ray structure of the GCN4 leucine zipper, a two-stranded, parallel coiled coil. *Science* **254:** 539-544.

O'Shea, E.K., Lumb, K.J. and Kim, P.S. 1993. Peptide "Velcro*": design of a heterodimeric coiled coil. *Curr Biol* **3:** 658-667.

Sali, D., Bycroft, M. and Fersht, A.R. 1988. Stabilization of protein structure by interaction of alpha-helix dipole with a charged side chain. *Nature* **335:** 740-743.

Schmidt-Dorr, T., Oertel-Buchheit, P., Pernelle, C., Bracco, L., Schnarr, M. and Granger-Schnarr, M. 1991. Construction, purification, and characterization of a hybrid protein comprising the DNA binding domain of the LexA repressor and the Jun leucine zipper: a circular dichroism and mutagenesis study. *Biochemistry* **30:** 9657-9664.

Smith, J.S. and Scholtz, J.M. 1998. Energetics of polar side-chain interactions in helical peptides: salt effects on ion pairs and hydrogen bonds. *Biochemistry* **37:** 33-40.

Sodek, J., Hodges, R.S., Smillie, L.B. and Jurasek, L. 1972. Amino-acid sequence of rabbit skeletal tropomyosin and its coiled-coil structure. *Proc Natl Acad Sci U S A* **69:** 3800-3804.

Steinmetz, M.O., Stock, A., Schulthess, T., Landwehr, R., Lustig, A., Faix, J., Gerisch, G., Aebi, U. and Kammerer, R.A. 1998. A distinct 14 residue site triggers coiled-coil formation in cortexillin I. *EMBO J* **17:** 1883-1891.

Su, J.Y., Hodges, R.S. and Kay, C.M. 1994. Effect of chain length on the formation and stability of synthetic alpha-helical coiled coils. *Biochemistry* **33:** 15501-15510.

Talbot, J.A. and Hodges, R.S. 1982. Tropomyosin: a model protein for studying coiled-coil and alpha-helix stabilization. *Acc Chem Res* **15:** 224-230.

Tripet, B., Wagschal, K., Lavigne, P., Mant, C.T. and Hodges, R.S. 2000. Effects of side-chain characteristics on stability and oligomerization state of a de novo-designed model coiled-coil: 20 amino acid substitutions in position "d". *J Mol Biol* **300:** 377-402.

Tripet, B.T. and Hodges, R.S. 2001. STABLECOIL: An algorithm designed to predict the location and relative stability of coiled-coils in native protein sequences. In *Peptides: The Wave of the Future, Proceedings of the Second International/Seventeenth American Peptide Symposium* (M. Lebl and R. A. Houghten, eds.), 365-366, Kluwer Academic Publishers, San Diego, CA.

Trybus, K.M., Freyzon, Y., Faust, L.Z. and Sweeney, H.L. 1997. Spare the rod, spoil the regulation: necessity for a myosin rod. *Proc Natl Acad Sci U S A* **94:** 48-52.

Wagschal, K., Tripet, B. and Hodges, R.S. 1999a. De novo design of a model peptide sequence to examine the effects of single amino acid substitutions in the hydrophobic core on both stability and oligomerization state of coiled-coils. *J Mol Biol* **285:** 785-803.

Wagschal, K., Tripet, B., Lavigne, P., Mant, C. and Hodges, R.S. 1999b. The role of position a in determining the stability and oligomerization state of alpha-helical coiled coils: 20 amino acid stability coefficients in the hydrophobic core of proteins. *Protein Sci* **8:** 2312-2329.

Waldburger, C.D., Schildbach, J.F. and Sauer, R.T. 1995. Are buried salt bridges important for protein stability and conformational specificity? *Nat Struct Biol* **2:** 122-128.

Woolfson, D.N. and Alber, T. 1995. Predicting oligomerization states of coiled coils. *Protein Sci* **4:** 1596-1607.

Yu, Y., Monera, O.D., Hodges, R.S. and Privalov, P.L. 1996. Investigation of electrostatic interactions in two-stranded coiled- coils through residue shuffling. *Biophys Chem* **59:** 299-314.

Yu, Y.B., Lavigne, P., Privalov, P.L. and Hodges, R.S. 1999. The measure of interior disorder in a folded protein and its contribution to stability. *J Am Chem Soc* **121:** 8443-8449.

Zhou, N.E., Kay, C.M. and Hodges, R.S. 1994a. The net energetic contribution of interhelical electrostatic attractions to coiled-coil stability. *Protein Eng* **7:** 1365-1372.

Zhou, N.E., Monera, O.D., Kay, C.M. and Hodges, R.S. 1994b. Alpha-helical propensities of amino acids in the hydrophobic face of an amphipathic alpha-helix. *Protein Peptide Letters* **1:** 114-119.

Zhou, N.E., Zhu, B.-Y., Kay, C.M. and Hodges, R.S. 1993. Importance of intra-chain ionic interactions in stabilizing alpha-helices in proteins. In *Peptides: Biology and Chemistry (Proceedings of the 1992 Chinese Peptide Symposium)* (Y.-C. Du and Y.-S. Zhang, eds.), 217-220, Escom Science Publishers, Leiden, the Netherlands.

Chapter 4: Unique stabilizing interactions identified in the two-stranded α-helical coiled-coil: Crystal structure of a cortexillin I/GCN4 hybrid coiled-coil peptide

A version of this chapter has been published. Lee, D. L., Ivaninskii, S., Burkhard, P., and Hodges, R. S. 2003. Protein Science 12:1395-1405.

Chapter 4-1. Introduction

The rodlike α-helical coiled-coil is one of the simplest yet most common structural motifs occurring in proteins. Consisting of two to five α-helices twisted into a left-handed supercoil, the occurrence of this structure is well documented, occurring in a wide variety of proteins including motor proteins, DNA binding proteins, extracellular proteins, and viral fusion proteins (Burkhard et al. 2001; Kohn et al. 1997; Lupas 1996). The presence of a continuous interface of hydrophobic amino acids along the length of the helices provides a major source of stability to the fold as the hydrophobes pack in a knobs-into-holes fashion shielded from the bulk solvent (Crick 1953). The pattern of repeating hydrophobic residues at positions **a** and **d** of the heptad repeat (denoted ***abcdefg***) that are responsible for coiled-coil formation was first identified by Hodges *et al.* (Hodges et al. 1972) from the amino acid sequence of tropomyosin. This 3-4 or 4-3 hydrophobic repeat allows for the prediction of coiled-coils based on statistical occurrence of residues in these positions (Berger et al. 1997; Berger et al. 1995; Singh et al. 1999; Wolf et al. 1997), and more recently, with STABLECOIL, an algorithm based on experimentally derived stability data (Tripet et al. 2000; Tripet et al. 2001; Wagschal et al. 1999). However, deletion and/or mutational analysis of some protein sequences (such as GCN4, cortexillin I, macrophage scavenger receptor and intermediate filament chains) has revealed that the presence of heptad repeats does not always guarantee the formation of coiled-coil structure (Frank et al. 2000; Kammerer et al. 2001; Lee et al. 2001; Steinmetz et al. 1998; Wu et al. 2000). The absence of a key region of only one or two heptads (dubbed the 'trigger sequence') prevented folding, while its presence induced folding of the coiled-coil structure. We previously took a 31-residue peptide that did not fold even with an excellent hydrophobic core, and then introduced stabilizing amino acid substitutions to induce dimeric coiled-coil folding without matching a proposed 'consensus trigger sequence' to prove that such a sequence is not necessary for coiled-coil folding (Lee et al. 2001). While trigger sequences may be important for folding in naturally occurring coiled-coils of substantial length, we proposed that any sequence with enough stability above a critical threshold will fold, whether the stability is distributed evenly along the coiled-coil sequence or concentrated heavily in distinct regions. Thus, the ability to induce coiled-coil folding is not limited to a consensus trigger sequence, but should belong to any peptide sequence with sufficient individual helix and/or coiled-coil stability (Burkhard et al. 2002; Burkhard et al. 2000b).

Here we have determined the crystal structure for the most stable folded peptide from our previous study, which did not contain a 'consensus trigger sequence'. This stable peptide contained potentially stabilizing design elements over the nonfolding sequence, including increased helix propensity, elimination of ionic repulsions and introduction of ionic attractions. These stabilizing elements are identified in the 1.17 Å crystal structure. We also quantify the previously unreported stability contribution of three interactions using thermodynamic analysis of urea denaturation curves of peptide analogs: a unique complex hydrogen bonding - electrostatic network involving i to i′ + 5 electrostatic interactions and hydrogen bonding interactions with Asn in the hydrophobic core, and hydrophobic packing of leucine residues at positions **e** (d-e′ interaction) and **g** (g-a′ interaction).

Chapter 4-2. Results

Peptide design

Our previous results showed that the native peptide (Hybrid 1) did not fold, even though it had an excellent hydrophobic core (Fig. 4-1) (Lee et al. 2001). This sequence was based primarily on the coiled-coil regions of the transcription factor, GCN4, and the actin bundling protein, cortexillin I. The N-terminal (residues 2 to 14) contains cortexillin I 270-282 (Burkhard et al. 2000a), while the C-terminal (residues 16-28) contains GCN4-p1 residues 3 to 15 (O'Shea et al. 1991). Both segments were inserted into the GCN4-p1 sequence 2-32, labelled as 1-31 in Fig. 4-1. In the middle of this peptide sequence, residue 15 is a polar asparagine (**a** position) buried in the hydrophobic core. Polar residues in core **a** and **d** positions reduce coiled-coil stability (Akey et al. 2001; Tripet et al. 2000; Wagschal et al. 1999; Zhu et al. 2000) *versus* more hydrophobic amino acids, but asparagine was left in the GCN4 template to specify dimerization over higher order oligomerization states such as trimers or tetramers (Harbury et al. 1993). This central asparagine is analogous to the central Asn observed in the coiled-coil structure of GCN4-p1 (O'Shea et al. 1991).

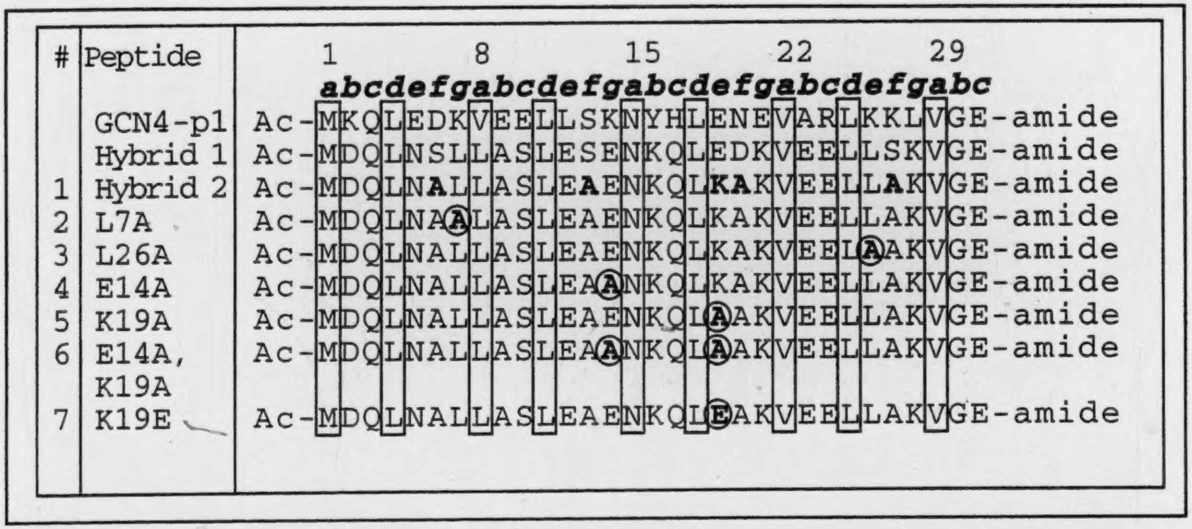

#	Peptide	1 8 15 22 29 **abcdefgabcdefgabcdefgabcdefgabc**
	GCN4-p1	Ac-MKQLEDKVEELLSKNYHLENEVARLKKLVGE-amide
	Hybrid 1	Ac-MDQLNSLLASLESENKQLEDKVEELLSKVGE-amide
1	Hybrid 2	Ac-MDQLN**A**LLASLE**A**ENKQL**KA**KVEELL**A**KVGE-amide
2	L7A	Ac-MDQLNA**A**LASLEAENKQLKAKVEELLAKVGE-amide
3	L26A	Ac-MDQLNALLASLEAENKQLKAKVEEL**A**AKVGE-amide
4	E14A	Ac-MDQLNALLASLEA**A**NKQLKAKVEELLAKVGE-amide
5	K19A	Ac-MDQLNALLASLEAENKQL**A**AKVEELLAKVGE-amide
6	E14A, K19A	Ac-MDQLNALLASLEA**A**NKQL**A**AKVEELLAKVGE-amide
7	K19E	Ac-MDQLNALLASLEAENKQL**E**AKVEELLAKVGE-amide

Figure 4-1. Sequences of peptides used in this study. Peptides are denoted by one letter code and are labelled peptides 1 to 7. The sequence of GCN4-p1 (O'Shea et al. 1991) residues 2-32 is shown for comparison, where Met 2 of GCN4-p1 is labelled residue 1. Hybrid 1 is a GCN4-cortexillin I hybrid that did not fold into a coiled-coil, while Hybrid 2 formed a stable coiled-coil (Lee et al. 2001). The **a** and **d** positions of the heptad repeat **abcdefg** are boxed. Bolded residues indicate amino acid substitutions in Hybrid 2 relative to Hybrid 1. The circled and bolded residues in peptides 2 to 7 indicate amino acid substitutions relative to the Hybrid 2 peptide sequence. The residues 2-14 in the Hybrid 1 sequence are from cortexillin I residues 270-282 and residues 16-28 contain GCN4-p1 2-14, where both segments are inserted into the GCN4 template 1-31.

Because Hybrid 1 did not fold, we introduced amino acid substitutions into Hybrid 1 that would induce folding independently of a 'consensus trigger sequence'. The result was Hybrid 2, whose structure was determined in this manuscript. Hybrid 2 exhibited increased coiled-coil folding and stability over Hybrid 1 because of five amino acid substitutions: S6A, S13A, D20A, S27A, and E19K. Hybrid 2 contains four alanine residues in the **f** positions (A6, A13, A20, and A27) not found in GCN4 or cortexillin I, in order to increase α-helix propensity (Fig. 4-2). Also, a lysine replaced a glutamic acid at position 19 (**e** position), which eliminated a potential i to i′ - 5 ionic repulsion with Glu 14′ (**g′** position) in the original nonfolding peptide, and could instead form a potential interhelical i to i′ - 5 salt bridge across the hydrophobic interface (Fig. 4-2).

Overall fold

The x-ray crystal structure of Hybrid 2 (Table 4-1) is a parallel two-stranded coiled-coil (Fig. 4-3). The dimer of the coiled-coil is built up from an internal two-fold crystal symmetry element. Two core residues at the dimer interface (Leu 8 and Asn 15), each in **a** positions of the heptad repeat, show two rotamer conformations (Figs. 4-4 and 4-5). Asn 15 adopts the two most preferred rotamer conformations (Lovell et al. 2000) with $\chi 1/\chi 2$ torsion angles of -82° /14° and 169°/-90°, respectively. In contrast with the two-fold symmetry observed in Hybrid 2, the crystal structure of another coiled-coil, GCN4-p1 (O'Shea et al. 1991) (sequence in Fig. 4-1) does not show two-fold symmetry but still shows Asn 15 in two different conformations (in and out).

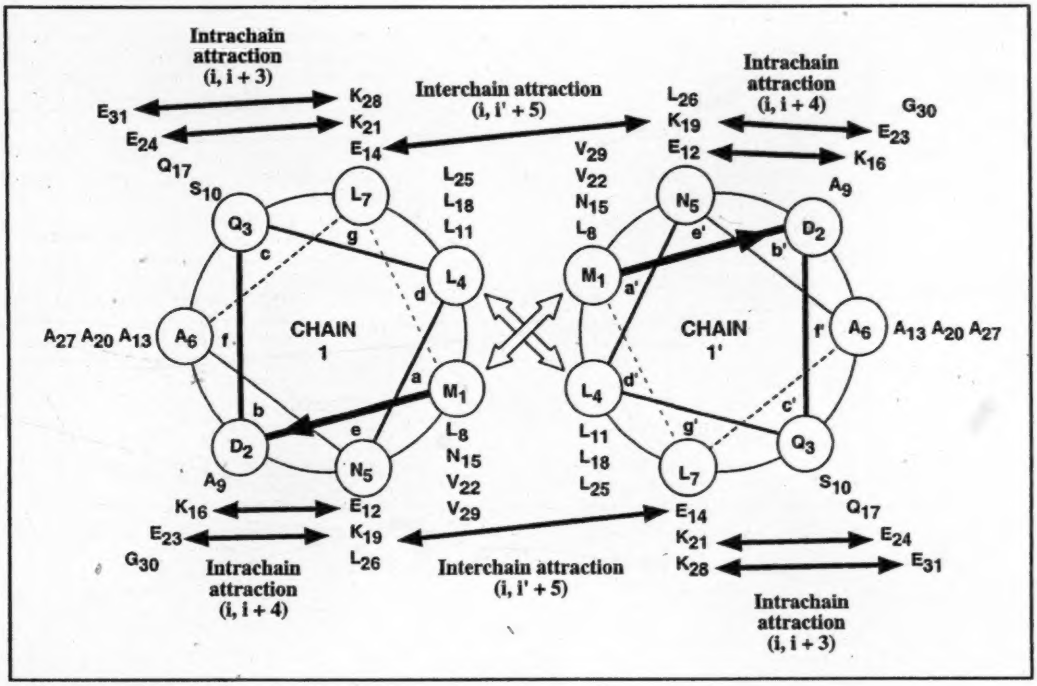
Intrachain attraction (i, i + 3)
E_{31}
E_{24}
Q_{17}
S_{10}
K_{28}
K_{21}
E_{14}
Interchain attraction (i, i' + 5)
L_{26}
K_{19}
E_{12}
Intrachain attraction (i, i + 4)
G_{30}
E_{23}
K_{16}
A_9
L_{25}
L_{18}
L_{11}
V_{29}
V_{22}
N_{15}
L_8
Q_3
L_7
g
c
L_4
d
A_{27} A_{20} A_{13}
A_6
f
CHAIN 1
a
M_1
b
e
D_2
N_5
N_5
e'
D_2
b'
M_1
a'
CHAIN 1'
f'
A_6
A_{13} A_{20} A_{27}
L_4
d'
c'
g'
Q_3
L_7
L_8
N_{15}
V_{22}
V_{29}
L_{11}
L_{18}
L_{25}
A_9
K_{16}
E_{23}
G_{30}
E_{12}
K_{19}
L_{26}
Intrachain attraction (i, i + 4)
Interchain attraction (i, i' + 5)
E_{14}
K_{21}
K_{28}
S_{10}
Q_{17}
E_{24}
E_{31}
Intrachain attraction (i, i + 3)

Figure 4-2. End-on view of the hybrid peptide analog, viewed from N- to C-terminus. Solid arrows denote predicted interchain (i to i′ + 5) and intrachain (i to i + 3; i to i + 4) ion pairing between residues. Open arrows denote the hydrophobic interactions between residues **a** and **a′** or **d** and **d′**.

Table 4-1. Data collection and refinement statistics

Space group		$C222_1$
Unit cell	a, b, c (Å)	18.098, 117.287, 22.209
	α, β, γ (°)	90, 90, 90
Monomers / au		1
Data collection statistics		
Resolution (Å)		1.17
Observed reflections		263880
Unique reflections		8183
Completeness (%)		97.8
R_{sym}*		0.037
Refinement statistics		
R factor (%)¶		17.9
R_{free} (%)¶		21.7
Mean B factor protein atoms (Å^2)		15.1
Mean B factor water atoms (Å^2)		31.3
rmsd bond distances (Å)#		0.009
rmsd bond angles (°)#		1.8

*$R_{\mathrm{sym}} = \Sigma | I - \langle I \rangle | / \Sigma I$.

¶R factor$= \Sigma | |F_{\mathrm{obs}}| - |F_{\mathrm{calc}}| | / \Sigma |F_{\mathrm{calc}}|$.

#Root-mean-square deviation.

Figure 4-3. Space filling representation of the GCN4/cortexillin Hybrid 2 structure. Residues in positions **a** and **d** along the hydrophobic core are displayed in orange and green, respectively, with the exception of Asn 15 (**a** position) in light blue. Leu 7 (**g**) and Leu 26 (**e**) side chains are displayed in yellow. Glu 14 (**g**) and Lys 19′ (**e′**) side chains are displayed in red and dark blue, with the i to i′ + 5 interchain interaction shown in white.

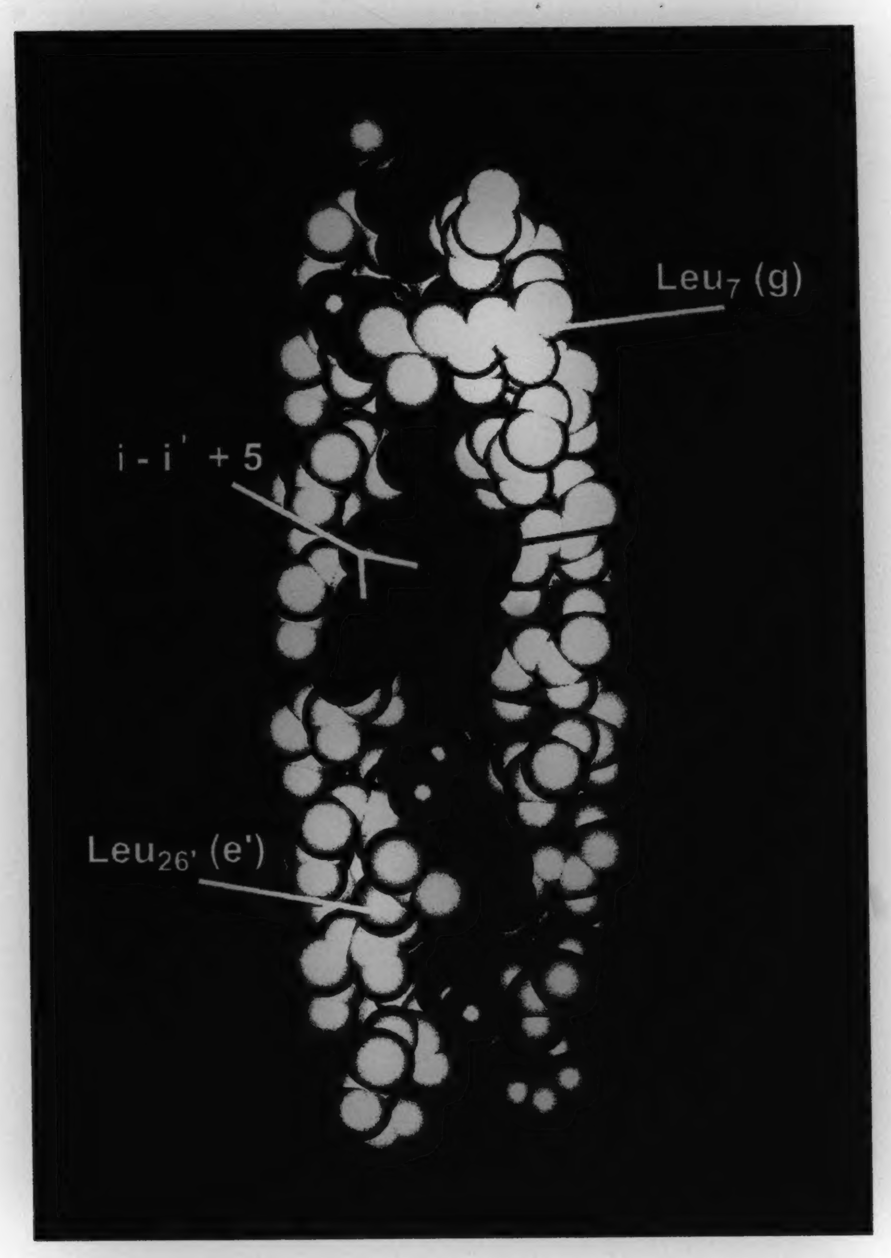
Leu₇ (g)
i - i' + 5
Leu₂₆' (e')

Figure 4-4. Cross-sectional view of the region surrounding the Asn 15 **(a)** core in Hybrid 2. Hydrogen bonds are denoted by dashed yellow lines. Oxygen atoms are red; nitrogen atoms are blue. The C_α helix backbone is shown in white (ribbon representation). The two interconverting conformers of Asn 15 and Asn 15′ ('in' or 'out') are inside the pink boxes of panels A and B. Panel A: Asn 15 is 'in' (lower helix); Asn 15′ is 'out' (upper helix). Panel B: Asn 15 'is 'out' (lower helix); Asn 15′ is 'in' (upper helix).

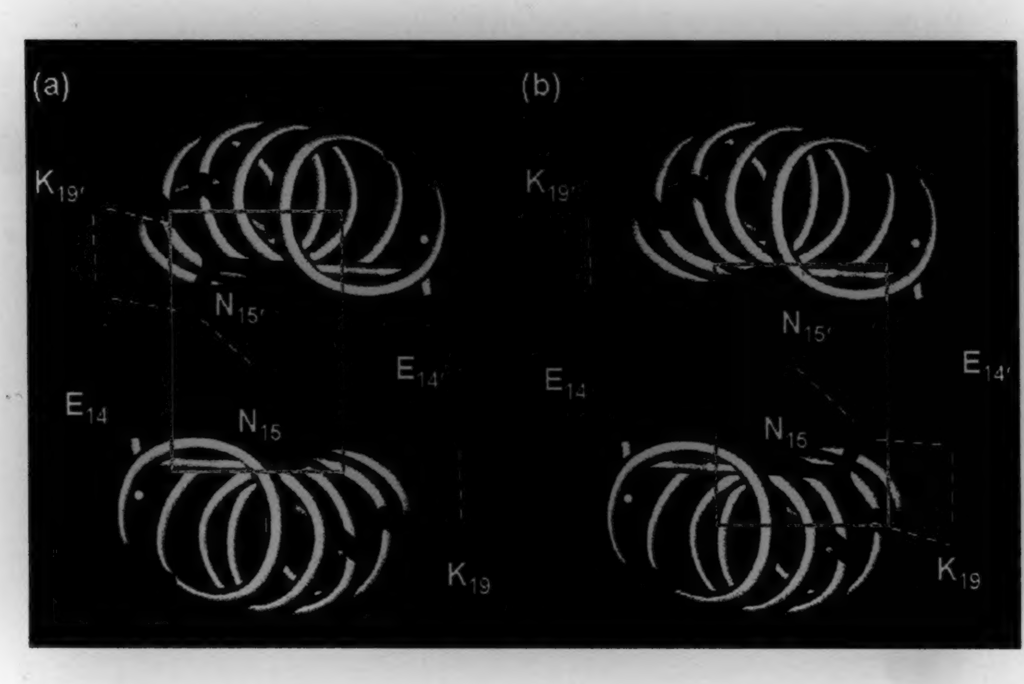
(a)
$K_{19'}$
$N_{15'}$
$E_{14'}$
E_{14}
N_{15}
K_{19}
(b)
$K_{19'}$
$N_{15'}$
E_{14}
$E_{14'}$
N_{15}
K_{19}

Figure 4-5. Cross-sectional comparison of **g-a** packing and **d-e** packing of leucines in the hydrophobic core of the hybrid peptide analog, viewed from N-terminus to C-terminus. The C_α helix backbone is shown as white sticks, while hydrogen atoms are depicted as white balls. Panels A and B, Leu 7 **(g)** and Leu 7′ **(g′)** side chains are shown in yellow; Leu 8 **(a)** and Leu 8′ **(a′)** side chains are shown in orange. The two conformations of Leu 8 **(a)** and Leu 8′ **(a′)**, labelled from left to right, are **a)** 'out/in and **b)** 'in/out'. Panel C, packing of Leu 25 **(d)** (green) and Leu 26 **(e)** (yellow) in the hydrophobic interface.

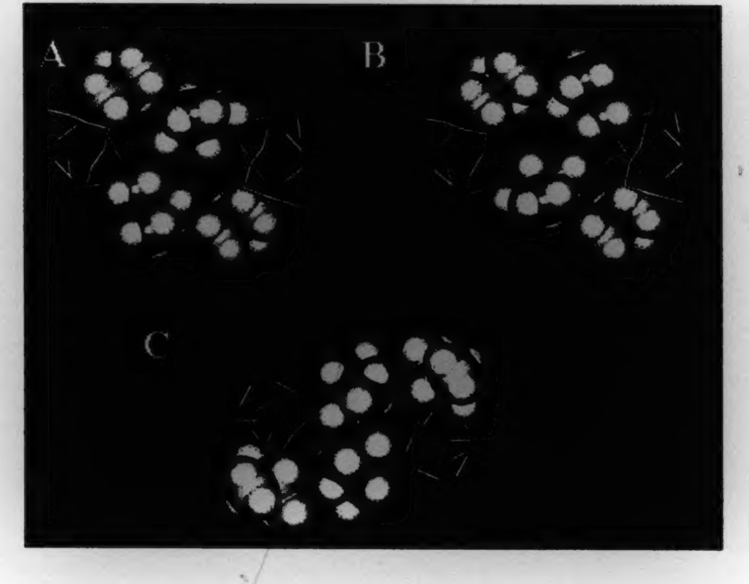
A
B
C

Interactions in the Asn 15 core region

The two asparagines in core **a** positions (Asn 15 and Asn 15′), together with the two Glu (14 and 14′) and two Lys (19 and 19′) residues, form an extended network of hydrogen bonds with a total of five (four interhelical and one intrahelical) hydrogen bonds not previously observed in the structures of coiled-coils (Fig. 4-4). The amide and carbonyl groups of the two Asn 15 side-chains are 3.1 Å apart from each other. The $N_{\delta 2}$ atom from asparagine with the 'out' conformation also forms a 2.8 Å hydrogen bond with the carboxyl group oxygen of Glu 14 (Fig. 4-4a) and Glu 14′ (Fig. 4-4b). Glu 14 - Lys 19′ and Glu 14′ - Lys 19 form the two interhelical salt bridges with an N_ζ to $O_{\epsilon 1}$ distance of 3.2 Å on both sides of the coiled-coil. The lone intrahelical hydrogen bond occurs between the O_δ of Asn 15 in the 'out' conformation and the N_ζ of Lys 19.

In the GCN4-p1 coiled-coil, there is an interchain electrostatic interaction on only one side of the coiled-coil with an interatomic distance of 3.7 Å. But, there is no interaction with the nearest Asn residue in the hydrophobic core. On the other side of GCN4-p1, the side-chains of Lys and Glu are 6.1 Å apart (Fig. 4-6b) and thus are too far apart to interact with each other, or with Asn 15 (indicated by the red X's in Fig. 4-6b). This can be explained by the fact that in the GCN4-p1 peptide, the charged residues are in opposite positions, and due to the stereochemical restraints, the favorable hydrogen bonding pattern as observed in the Hybrid 2 structure cannot form. This is a clear indication that the configuration with Glu in the **g** position and Lys in the **e'** position (as it is in Hybrid 2) is more stabilizing to the coiled-coil than the opposite arrangement, if Lys is in the **g** position and Glu is in the **e'** position (as it is in the GCN4-p1 coiled-coil).

Figure 4-6. Comparison of the region around the central Asn (a) in Hybrid 2 (Panel A) and GCN4 (Panel B) coiled-coils. The numbering of residues in GCN4 have been aligned to the hybrid sequence in Fig. 4-1. Oxygen atoms are red; nitrogen atoms are blue. Hydrogen bonds are denoted by dashed yellow lines. The C_α helix backbone is shown in white (ribbon representation). Solid yellow lines with a red 'x' denote a lack of noncovalent bonding between atoms.

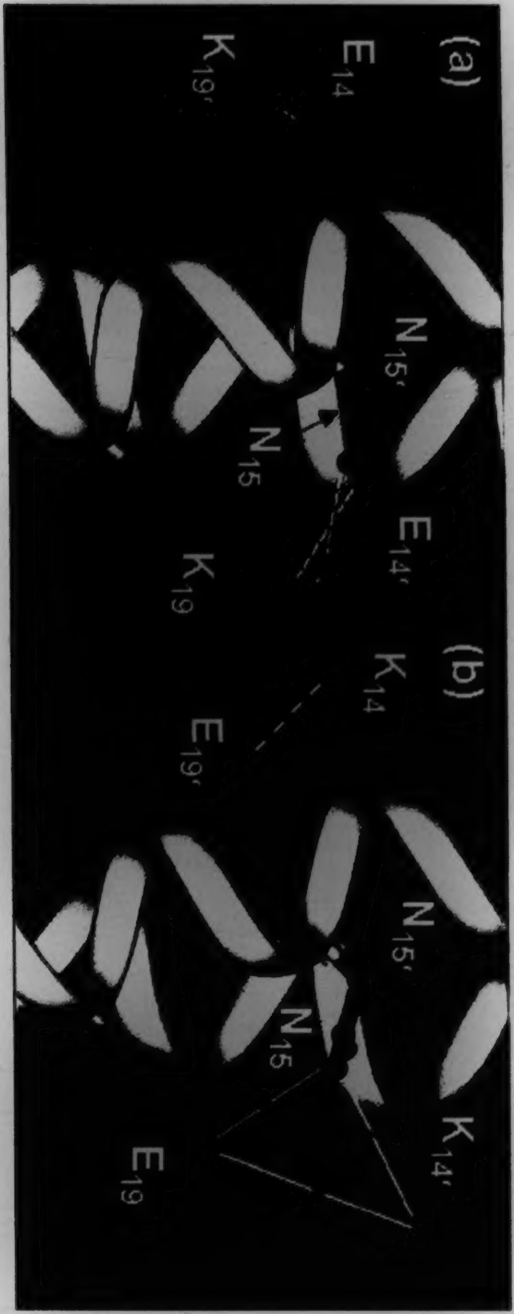
(a)
E_{14}
$K_{19'}$
$N_{15'}$
N_{15}
$E_{14'}$
K_{19}
(b)
K_{14}
$E_{19'}$
$N_{15'}$
N_{15}
$K_{14'}$
E_{19}

Crystal contacts

Surprisingly, none of the proposed intrahelical salt bridges are formed in the crystal. Instead, all residues thought to form such interactions are involved in crystal lattice contacts. Lys 21 and Glu 24 (potential i to i + 3 ion pair) form salt bridges with the residues Glu 24 and Lys 21 from a symmetry related molecule; the distance between these residues is approximately 4 Å. Glu 12 is involved in an interaction with Asn 15 of a symmetry related molecule, and does not form an i to i + 4 intrahelical salt bridge with Lys 16. Glu 23 forms a salt bridge with Lys 28 from a symmetry related molecule, despite the possibility that these residues could each form intrahelical salt bridges with Lys 19 (i to i + 4) and Glu 31 (i to i + 3), respectively. Also, three hydrophobic alanine residues in **b** and **f** positions - Ala 6(**f**), Ala 9(**b**), and Ala 13(**f**) - pack against identical residues from a crystallographically related molecule. Thus, crystal packing forces may disrupt intrachain interactions that would be very important in solution, in favor of intermolecular interactions in the crystal.

Comparison with GCN4

The peptide backbone can be superimposed upon the GCN4-p1 coiled-coil dimer, giving an rmsd of 0.71 Å for C_α atoms from residues 3 to 30. The largest differences in the positions of the C_α backbone atoms occur at the N-terminus. In contrast, the C_α atoms of the C-terminal portion of the coiled-coil (residues 15-29) can be superimposed with an rmsd of only 0.36 Å. Hybrid 2 has a leucine residue in an N-terminal **a** position (Leu 8) compared to a smaller valine residue in GCN4-p1 that may explain the difference in the C_α backbone between GCN4-p1 and Hybrid 2. The C_α-C_α distance between Leu 8 and Leu 8′ at position **a** is 6.3 Å, while in the GCN4-p1 structure the Val 8 and Val 8′ C_α

carbons are separated by 5.5 Å (see Fig. 4-1 for sequences). According to the program TWISTER (Strelkov et al. 2002), the coiled-coil radius of Hybrid 2 increases towards the N-terminus and also the coiled-coil pitch of Hybrid 2 increases, indicating a local unwinding of the coiled-coil (Fig. 4-7): the C_α-C_α distance between the two Leu 4 residues at position **d** gets as high as 8.4 Å, whereas in GCN4-p1 it is only 6.3 Å. Clearly, packing the larger Leu residue instead of Val at position **a** results in the increase in coiled-coil radius, as position 8 has the only residue that is different in the hydrophobic **a** and **d** positions of GCN4-p1 *vs.* Hybrid 2.

Biophysical characterization of peptides

To quantitatively determine the extent that residues in the **e** and **g** positions stabilize the coiled-coil structure of Hybrid 2, we synthesized a set of analogs substituted at various **e** and **g** positions along the sequence (peptides 2 to 7 in Fig. 4-1). We characterized the secondary structure, oligomerization state, and thermodynamic stability of the peptides by circular dichroism (CD), sedimentation equilibrium, and chemical unfolding experiments (Figs. 4-8 and 4-9; Table 4-2). All peptides formed α-helices in benign medium and are fully folded as α-helical coiled-coils based on the following characteristics: high negative molar ellipticity values in benign medium, with double minima at 208 and 222 nm and a maximum at 190 nm; and a high α-helix content such that the addition of 50% trifluoroethanol (TFE) does not significantly increase the α-helix content (determined at 222 nm) (Table 4-2). Furthermore, the ratio of molar ellipticities at 222 nm and 208 nm suggest that all of the peptides studied formed coiled-coils: the

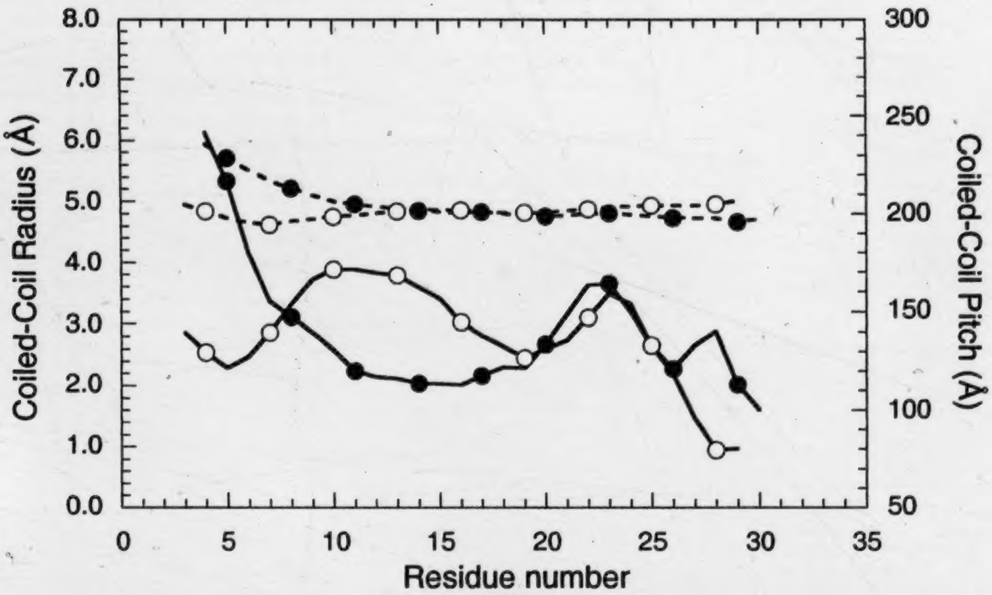

Figure 4-7. Coiled-coil pitch (solid lines) and coiled-coil radius (dashed lines) plotted against the residue number for the Hybrid 2 (●) and the GCN4-p1 peptide (○). The residue number is according to the Hybrid 2 peptide in both sequences, *i.e.* in GCN4-p1 they are shifted by one residue.

$[\theta]_{222}/[\theta]_{208}$ ratio for coiled-coils in benign medium is usually greater than 1.0 (Lau et al. 1984) and this value decreases to 0.90 in the presence of the monomeric helix-inducing solvent, trifluoroethanol. Also, results from sedimentation equilibrium experiments indicated that most of peptides in this study were globally fit to a single dimeric species in benign medium, with observed molecular weights that are approximately double the calculated weight of the monomers (Table 4-2). Peptides E14A and E14A, K19A exhibited higher order oligomerization in benign medium, but when the runs were repeated in 2 M urea (a denaturant concentration high enough to disrupt higher order oligomerization but low enough to not cause significant unfolding of the coiled-coil as shown in Fig. 4-9), they were observed to exist as either a single dimeric species (E14A, K19A) or in a monomer-to-dimer equilibrium (E14A).

By monitoring the folded state of the coiled-coil as a function of denaturant concentration using CD spectroscopy, we obtained values for the urea concentration at the transition midpoint ($[\text{urea}]_{1/2}$), the slope at the transition midpoint (*m*), and the stability contributions for Hybrid 2 relative to less stable analogs ($\Delta\Delta G_u^{obs}$) (Fig. 4-9 and Table 4-3). Peptides were analyzed at ~400 μM concentration to ensure that the total population of the entire set of peptides was essentially fully folded in the absence of denaturant; the effect of peptide concentration on the CD spectra of the least stable peptide in this study, K19E (peptide 7 in Fig. 4-1), is shown in Fig. 4-8. Although K19E shows an increase in negative molar ellipticity from 426 μM to 2600 μM, indicating greater helicity at higher concentrations, it was calculated to be 91% helical at ~400 μM by comparing $[\theta]_{222}$ values in benign conditions and in 50% TFE (Table 4-2).

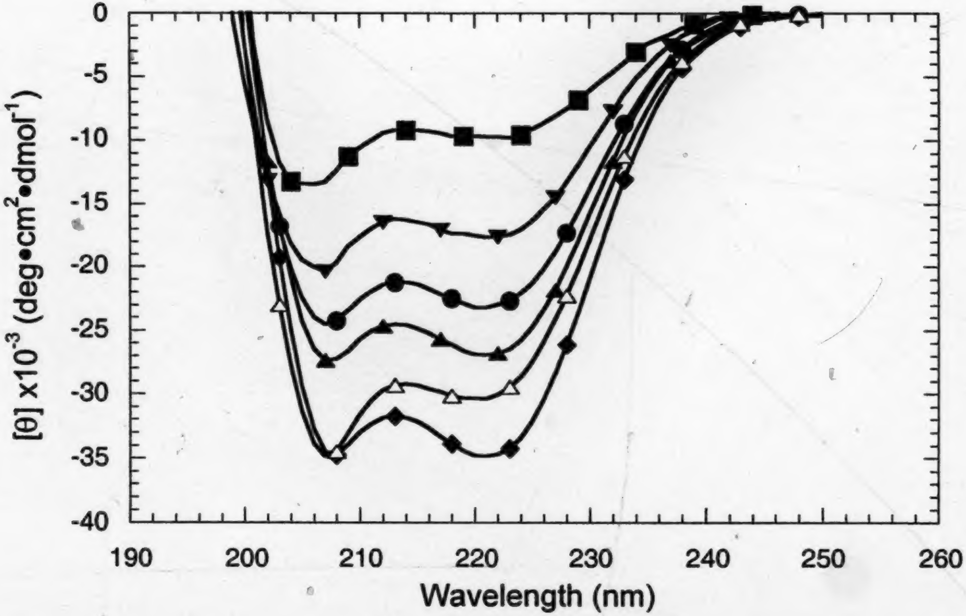

Figure 4-8. CD spectra of the peptide K19E obtained at 20° C in 50 mM phosphate, 100 mM KCl, pH 7.0 buffer (benign). Peptide concentrations were 2592 μM (◆), 432 μM (▲), 86 μM (●), 22 μM (▼) 4 μM (■) and in 1:1 (v:v) benign buffer and TFE at 432 μM (Δ).

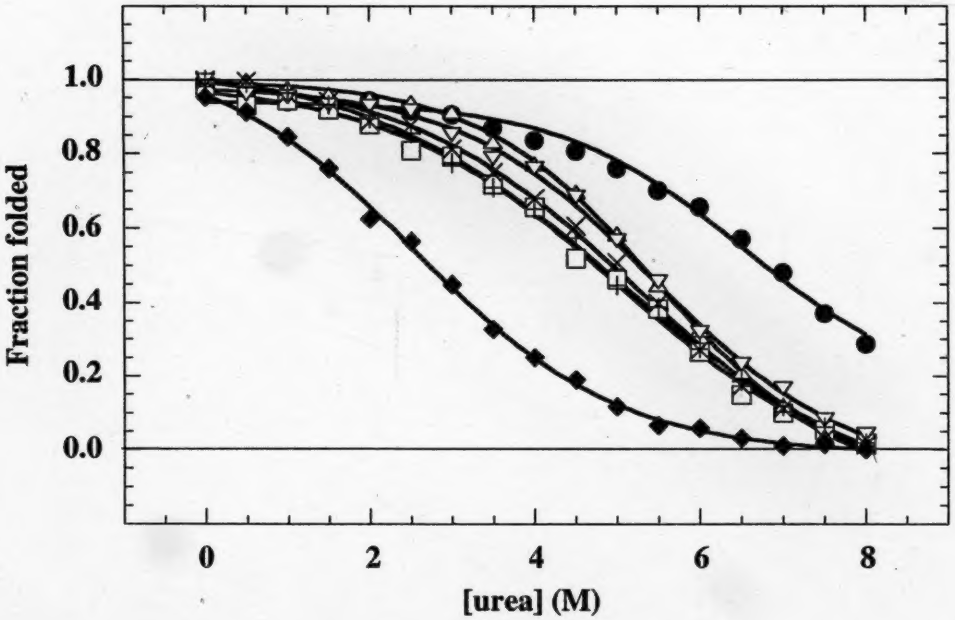

Figure 4-9. Chemical unfolding curves of the Hybrid 2 peptide and analogs. Fraction folded was plotted against denaturant concentration for Hybrid 2 (●) and peptides E14A (∇); K19A (+); L7A (□); L26A (×); E14A, K19A (Δ); and K19E (◆).

Table 4-2. Biophysical characterization of hybrid peptide and analogs

Peptide	$[\theta]_{222}$ (x10^3 deg cm^{2}dmol^{-1})[a]		$[\theta]_{222}/[\theta]_{208}$ benign[b]	$[\theta]_{222}/[\theta]_{208}$ TFE[c]	Percent helix[d]	Helical residues[e]	m_{calc} (Da)[f]	m_{obs} (Da)[g]
	Benign	TFE			Benign			
Hybrid 2	-31.5	-30.6	1.00	0.86	103	33	3439	6698(D)†
L7A	-29.9	-31.8	1.02	0.87	94	29	3397	6556 (D)
L26A	-29.8	-31.1	1.03	0.90	96	30	3397	6266 (D)
E14A	-29.4	-29.7	1.03	0.89	99	31	3381	6162 (M-D)*
K19A	-30.8	-30.3	1.03	0.89	102	32	3382	6383 (D)
E14A, K19A	-31.3	-33.0	1.02	0.89	95	29	3324	6524 (D)*
K19E	-27.7	-30.3	1.01	0.88	91	28	3440	6618 (D)†

[a] Molar ellipticity at 222 nm at 20° C in benign buffer (50 mM potassium phosphate, 100 mM KCl, pH 7.0), 400 μM peptide concentration. For samples containing trifluoroethanol (TFE), the above buffer was diluted 1:1 (v:v) with TFE.

[b] Ratio of molar ellipticities at 222 nm and 208 nm in benign buffer.

[c] Ratio of molar ellipticities at 222 nm and 208 nm in a mixture of 1:1 (v:v) benign buffer and trifluoroethanol.

[d] The percent α-helix was calculated by taking 100% α-helix as the $[\theta]_{222}$ value obtained in 50% TFE (the maximum inducible α-helical structure).

[e] The number of α-helical residues was calculated by multiplying the percent α-helix (Column d) by the number of residues in the polypeptide chain, 31.

[f] Calculated molecular mass of monomeric peptides based on average isotopic masses.

[g] Observed molecular mass based on global fits of sedimentation equilibrium data (see Methods). Data was best fit to a monomer to dimer equilibrium (M-D), or dimer (D). Values labelled with an asterisk (*) were determined in the presence of 2 M urea to eliminate higher order oligomerization observed in benign buffer; peptide E14A was originally fit to a monomer-trimer (MW_{obs} 8087) and E14A, K19A was fit to a monomer-tetramer (MW_{obs} 9896) in benign conditions.

† Previously determined sedimentation equilibrium values (Lee et al. 2001).

All the other peptides were more stable and more helical than K19E (Fig. 4-9) at 400 μM concentration in benign conditions (Table 4-2) . Hybrid 2 was the most stable peptide in this study, so $\Delta\Delta G_u^{obs}$ was reported as a positive value, *i.e.* a stabilizing contribution, by calculating the stability difference of Hybrid 2 over the less stable analog (Table 4-4).

The choice of substituting the residues by alanine to eliminate **g** to **e′** interchain effects such as ionic interactions or hydrophobic interactions also affects another parameter that influences coiled-coil stability: α-helix propensity. Alanine has the highest intrinsic helix propensity among the twenty naturally-occurring amino acids (O'Neil et al. 1990; Blaber et al. 1993; Monera et al. 1995; Myers et al. 1997; Pace et al. 1998) and so the difference in helix propensities between Ala and the substituted residue was applied in the final column of Table 4 as a correction to the stability contribution. Alanine is an ideal residue to carry out substitutions in our case because it does not disrupt the α-helical coiled-coil structure, as it might if one were inserting it into an alternate nonhelical structure (Minor et al. 1994). After correction, the average value for the strength of a **g** to **e′** ion pair was 0.79 kcal mol^{-1} (averaged over the $\Delta\Delta G_u^{obs}$ values of single substitutions E14A; K19A; and double substitutions E14A, K19A). Leucine was not corrected for helix propensity, although its value has previously been shown to be similar to Ala (Pace et al. 1998).

Table 4-3. Urea denaturation data

Peptide[a]	Heptad position[b]	[Peptide] (μM)[c]	$[\text{Urea}]_{1/2}$ (M)[d]	m (kcal $\text{mol}^{-1}\text{M}^{-1}$)[e]	$\Delta\Delta G_u^{obs}$ (kcal mol^{-1})[f]
Hybrid 2	-	341	6.9	0.67	-
L7A	g	350	4.6	0.70	1.58
L26A	e	465	5.0	0.78	1.38
E14A	g	450	5.3	0.88	1.24
K19A	e	316	4.8	0.67	1.41
E14A, K19A	g, e	375	5.3	0.92	1.28
K19E	e	460	2.8	0.85	2.41

[a] The sequences are given in Fig. 1.

[b] The position of the substituted residue within the heptad repeat, ***abcdefg***.

[c] Amino acid analysis of stock peptide solutions was used to determine the total peptide concentration in solutions analyzed by CD spectroscopy.

[d] Denaturant concentration required to achieve a 50% reduction of the folded state or loss of α-helical content as measured by $[\theta]_{222}$.

[e] Slope term in the equation $\Delta G_u([\text{urea}])=\Delta G_u^{H2O}+m[\text{urea}]$, where ΔG_u^{H2O} is the Gibbs free energy change of unfolding in the absence of denaturant (Santoro and Bolen 1988). The ΔG_u^{H2O} value for hybrid 2 was 9.3 kcal mol^{-1}.

[f] $\Delta\Delta G_u^{obs}$ is the observed change in ΔG_u, the free energy change of unfolding, between hybrid 2 and the peptide analog in column 1, and is calculated $\Delta\Delta G_u^{obs}=([\text{urea}]_{1/2,\text{ hybrid 2}}-[\text{urea}]_{1/2,\text{ analog}})*(m_{\text{hybrid 2}}+m_{\text{analog}})/2$ (Serrano and Fersht 1989).

Table 4-4. Contributions of α-helix propensity, hydrophobic and electrostatic interactions to coiled-coil stability

Peptide comparisons More stable coiled-coil	 Less stable coiled-coil	$\Delta\Delta G_u^{obs}$ coiled-coil (kcal mol^{-1})	Description of stabilizing contribution	$\Delta\Delta G_u^{obs}$ per substitution (kcal mol^{-1})	$\Delta\Delta G_u^{obs}$ corrected[d] (kcal mol^{-1})
Hybrid 2	L7A	1.58	Hydrophobic contribution of Leu (**g**) *vs.* Ala	0.79	0.79
Hybrid 2	L26A	1.38	Hydrophobic contribution of Leu (**e**) *vs.* Ala	0.69	0.69
Hybrid 2	E14A	1.24	Electrostatic attraction uncorrected for α-helix propensity	0.62	0.82
Hybrid 2	K19A	1.41	Electrostatic & H-bond attractions uncorrected for α-helix propensity	0.71	0.71
Hybrid 2	E14A, K19A	1.28	Electrostatic & H-bond attractions uncorrected for α-helix propensity	0.64	0.84
E14A, K19A	K19A	0.40[a]	Helix propensity of Ala *vs.* Glu (**g**)	0.20	-
E14A, K19A	E14A	0.00	Helix propensity of Ala *vs.* Lys (**e**)	0.00	-
K19A	K19E	1.52[b]	Removal of electrostatic repulsions uncorrected for α-helix propensity	0.76	0.56
Hybrid 2	K19E	2.41[c]	Removal of electrostatic repulsions and replacement with electrostatic & H-bond attractions	-	-

[a] The α-helix propensity effect of E14 to A14 is calculated from the equation $\Delta\Delta G_u^{obs}$ = ([urea]$_{1/2}$(E14A, K19A) - [urea]$_{1/2}$(K19A)) * ($m_{E14A,\ K19A}$ +m_{K19A})/2 (from Serrano and Fersht 1989).

[b] The stabilizing effects of removing two electrostatic repulsions is calculated from $\Delta\Delta G_u^{obs}$ = ([urea]$_{1/2}$(K19A)-[urea]$_{1/2}$(K19E)*(m_{K19A}+m_{K19E})/2 (from Serrano and Fersht 1989).

[c] Observed values of $\Delta\Delta G_{u,\ coiled\ coil}$=2.41 kcal mol^{-1} can be compared with the calculated corrected values from the loss of two electrostatic repulsions 2*(0.56), plus the gain of the average value for two electrostatic attractions and H-bonding 2*(0.79), =2.70 kcal mol^{-1}.

[d] $\Delta\Delta G_u^{obs}$ corrected is the $\Delta\Delta G_u^{obs}$ per substitution corrected for α-helix propensity effects. The α-helix propensity of Ala compared to Glu is 0.20 kcal mol^{-1}, which means the stabilizing effect of an electrostatic & H-bond attraction is the $\Delta\Delta G_u^{obs}$ value of 0.64 kcal mol^{-1} plus 0.20 kcal mol^{-1} to give 0.84 kcal mol^{-1}.

Interactions of leucine residues at positions e and g

Peptides L7A and L26A contain destabilizing substitutions by replacing leucine residues at positions **g** and **e** respectively with the shorter, less hydrophobic alanine side-chains. L7A reduced stability by 0.79 kcal mol^{-1} while L26A reduced stability by 0.69 kcal mol^{-1} per substitution. Overall, leucine residues at **e** and **g** each contributed 0.7 to 0.8 kcal mol^{-1} to stability relative to alanine, while the interchain Glu-Lys′ salt bridge involved in the hydrogen bonding network contributed 0.8 kcal mol^{-1} to stability after correction for helix propensity.

Chapter 4-3. Discussion

Unlike the **a** and **d** positions in the hydrophobic core, the environment of side-chains located at the **e** and **g** positions in a two-stranded coiled-coil is partially solvent-excluded but also partially solvent-exposed (Fig. 4-2). Therein lies the controversy over the effects of interchain ion pairs located at these positions, as the stabilizing benefit of an electrostatic attraction must outweigh the energy penalty from both desolvation and the presence of charged residues in a hydrophobic environment. Similarly, hydrophobic residues such as the aliphatic chains of leucine and isoleucine, while gaining a favorable energy contribution to stability in the hydrophobic environment may suffer a penalty because of their solvent accessibility at the **e** and **g** positions.

Electrostatic interactions at positions e and g.

In comparison with other values for interchain Glu-Lys′ attractions (ranging from 0.4 to 0.5 kcal mol^{-1}) (Krylov et al. 1998; Zhou et al. 1994) and Glu-Glu′ repulsions (0.45 kcal mol^{-1}) (Kohn et al. 1995) in **g-e′** positions of coiled-coils, our values for each electrostatic effect in this study are approximately double. This difference can be explained by the two hydrogen bonds (Fig. 4-4a) in the Asn core region (one from E14 to N15′, the other from K19′ to N15′) which contribute the added stability.

Hydrophobic residues at positions e and g.

Hydrophobic residues at positions **a** and **d** in the hydrophobic core and their contributions to stability have previously been studied in detail. Here we examined Leu packing and stability at positions **e** and **g**, and found similar stability values in both positions. The side-chain packing of Leu (Fig. 4-5) in both cases are adjacent to another Leu, either **g-a′** (Leu 8) or **d-e′** (Leu 25). Our values of 0.7 and 0.8 kcal mol^{-1} for leucine in positions **e** and **g** are less than half the stability contribution at the **a** and **d** positions (1.75 and 1.90 kcal mol^{-1}) (Tripet et al. 2000; Wagschal et al. 1999). The stability differences between Leu at **a** or **d** *vs.* **e** or **g** positions match the differences in solvent-accessible surface area: after calculating accessible surface area in the Hybrid 2 structure using GETAREA 1.1 (Fraczkiewicz et al. 1998), we observed that Leu 26 and Leu 7 at positions **e** and **g** were 48% exposed to solvent, while Leu 8 and Leu 25 at positions **a** and **d** were only 7% exposed at position **d**, and 9% ('in' conformation) or 20% ('out' conformation) exposed at position **a**. Thus, the more that leucine was shielded from solvent (in positions **a** or **d**), the more it contributed to stability *via* the hydrophobic effect.

How does side-chain packing affect the stability of hydrophobes in positions **e** and **g**? Fig. 4-5 shows the **g-a′** packing of Leu 7 and Leu 8, and the **d-e′** packing of Leu 25 and Leu 26. With two conformations of Leu 8 in each helix of Hybrid 2, two possible combinations for the coiled-coil are shown in panels **A** and **B**: 'out/in' and 'in/out'. These conformations would satisfy both the packing of the hydrophobic core as well as interactions with the neighboring Leu 7 at position **g** and could cause the coiled-coil radius to increase towards the N-terminal as observed. The neighboring Leu 7 (**g**) may stabilize Leu 8 (**a**) in the 'out' conformation, as none of the other hydrophobic residues in **a** or **d** positions (Val or Leu) show more than one rotamer conformation in the X-ray structure. For example, Leu 25 (**d**) and Leu 26 (**e**) adopt a stable packing conformation, where the side-chains at position **d** are densely packed in the hydrophobic core and also make close contact with the side-chains at position **e** (Fig. 4-5C).

If a hydrophobic residue such as leucine at positions **e** and **g** contributes the same amount of stability to a two-stranded coiled-coil as an ion pair, should we expect to see the same statistical occurrence of hydrophobic residues as charged amino acids in these positions? The database of two- and three-stranded coiled-coil proteins from GenBank showed that at positions **e** and **g**, charged residues were heavily favored over hydrophobic residues by over a factor of four: 51.7% of residues at positions **e** and **g** were charged, while only 11.8% were hydrophobic (Lupas et al. 1991). What can explain the preference for charged residues over hydrophobes at these positions? First, having hydrophobes *vs.* polar side-chains at positions **e** and **g** reduces protein solubility in an aqueous environment. Second, hydrophobes at positions **e** and **g** have been shown to affect oligomerization state and allowing higher orders of self-association (trimers and tetramers) (Harbury et al. 1993; Potekhin et al. 1994). So, if one decides to incorporate a relatively small number of hydrophobes in the **e** and **g** positions of *de novo* designed coiled-coils, these residues can increase overall stability but possibly at the cost of reducing solubility and decreasing specificity for the dimeric state. Nevertheless, despite the relatively low occurrence of leucine at positions **e** and **g** in two-stranded coiled-coils, it would not be possible to predict overall protein stability or the variations of stability along the sequence of coiled-coils without understanding the quantitative contributions of the leucine residues at positions **e** and **g**.

Chapter 4-4. Conclusions

The crystal structure of the GCN4/cortexillin I peptide (Hybrid 2) contains key details helping to explain its stability. In addition to the hydrophobic residues found in the core **a** and **d** positions are the alanine residues in the **f** positions, the leucine residues in the **e** and **g** positions of the hydrophobic interface, the interchain ionic Glu-Lys′ salt bridges on both sides of the two central Asn 15 core residues and the complex hydrogen bonding network in the surrounding region. Although structurally similar to GCN4, Hybrid 2 possesses more ionic and hydrogen bonds in the vicinity of the central asparagines (especially at the Asn in the 'out' conformation), and has a larger coiled-coil radius near the N-terminal due to the alternate packing conformers of leucine in an **a** position. Biophysical studies have shown the importance of Glu 14 and Lys 19 in establishing **g-e′** ionic interactions, as well as the contributions of Leu 26 and Leu 7 at positions **e** and **g** to coiled-coil stability. To our knowledge, this work is the first reported biophysical quantification of the stability contributions of **d-e′** or **g-a′** leucine packing in a two-stranded coiled-coil, as well as the first identification of a unique network of hydrogen bonds involved in the ion pairs from **g-e′** and the Asn residues in the hydrophobic core due to the reversed ion pairing compared to GCN4-p1. The results provide further information to assist in the *de novo* design of coiled-coils (Burkhard et al. 2002;

Burkhard et al. 2000b) and understanding the folding and stability of coiled-coils, in ways that do not necessarily require the inclusion of a consensus trigger sequence.

Accession number

Coordinates have been deposited with the Research Collaboratory for Structural Bioinformatics under the accession code 1P9I.

Chapter 4-5. References

Akey, D.L., Malashkevich, V.N. and Kim, P.S. 2001. Buried polar residues in coiled-coil interfaces. *Biochemistry* **40:** 6352-6360.

Berger, B. and Singh, M. 1997. An iterative method for improved protein structural motif recognition. *J Comput Biol* **4:** 261-273.

Berger, B., Wilson, D.B., Wolf, E., Tonchev, T., Milla, M. and Kim, P.S. 1995. Predicting coiled coils by use of pairwise residue correlations. *Proc Natl Acad Sci U S A* **92:** 8259-8263.

Blaber, M., Zhang, X.J. and Matthews, B.W. 1993. Structural basis of amino acid alpha helix propensity. *Science* **260:** 1637-1640.

Burkhard, P., Ivaninskii, S. and Lustig, A. 2002. Improving coiled-coil stability by optimizing ionic interactions. *J Mol Biol* **318:** 901-910.

Burkhard, P., Kammerer, R.A., Steinmetz, M.O., Bourenkov, G.P. and Aebi, U. 2000a. The coiled-coil trigger site of the rod domain of cortexillin I unveils a distinct network of interhelical and intrahelical salt bridges. *Structure Fold Des* **8:** 223-230.

Burkhard, P., Meier, M. and Lustig, A. 2000b. Design of a minimal protein oligomerization domain by a structural approach. *Protein Sci* **9:** 2294-2301.

Burkhard, P., Stetefeld, J. and Strelkov, S.V. 2001. Coiled coils: a highly versatile protein folding motif. *Trends Cell Biol* **11:** 82-88.

Crick, F.H.C. 1953. The packing of α-helices: simple coiled-coils. *Acta Crystallog* **6:** 689-697.

Fraczkiewicz, R. and Braun, W. 1998. Exact and efficient analytical calculation of the accessible surface areas and their gradients for macromolecules. *J Comp Chem* **19:** 319-333.

Frank, S., Lustig, A., Schulthess, T., Engel, J. and Kammerer, R.A. 2000. A distinct seven-residue trigger sequence is indispensable for proper coiled-coil formation of the human macrophage scavenger receptor oligomerization domain. *J Biol Chem* **275:** 11672-11677.

Harbury, P.B., Zhang, T., Kim, P.S. and Alber, T. 1993. A switch between two-, three-, and four-stranded coiled coils in GCN4 leucine zipper mutants. *Science* **262:** 1401-1407.

Hodges, R.S., Sodek, J., Smillie, L.B. and Jurasek, L. 1972. Tropomyosin: amino acid sequence and coiled-coil structure. *Cold Spring Harbor Symp. Quant. Biol.* **37:** 299-310.

Kammerer, R.A., Jaravine, V.A., Frank, S., Schulthess, T., Landwehr, R., Lustig, A., Garcia-Echeverria, C., Alexandrescu, A.T., Engel, J. and Steinmetz, M.O. 2001. An intrahelical salt bridge within the trigger site stabilizes the GCN4 leucine zipper. *J Biol Chem* **276:** 13685-13688.

Kohn, W.D., Kay, C.M. and Hodges, R.S. 1995. Protein destabilization by electrostatic repulsions in the two-stranded alpha-helical coiled-coil/leucine zipper. *Protein Sci* **4:** 237-250.

Kohn, W.D., Mant, C.T. and Hodges, R.S. 1997. Alpha-helical protein assembly motifs. *J Biol Chem* **272:** 2583-2586.

Krylov, D., Barchi, J. and Vinson, C. 1998. Inter-helical interactions in the leucine zipper coiled coil dimer: pH and salt dependence of coupling energy between charged amino acids. *J Mol Biol* **279:** 959-972.

Lau, S.Y., Taneja, A.K. and Hodges, R.S. 1984. Synthesis of a model protein of defined secondary and quaternary structure. Effect of chain length on the stabilization and formation of two-stranded alpha-helical coiled-coils. *J Biol Chem* **259:** 13253-13261.

Lee, D.L., Lavigne, P. and Hodges, R.S. 2001. Are trigger sequences essential in the folding of two-stranded alpha- helical coiled-coils? *J Mol Biol* **306:** 539-553.

Lovell, S.C., Word, J.M., Richardson, J.S. and Richardson, D.C. 2000. The penultimate rotamer library. *Proteins* **40:** 389-408.

Lupas, A. 1996. Coiled coils: new structures and new functions. *Trends Biochem Sci* **21:** 375-382.

Lupas, A., Van Dyke, M. and Stock, J. 1991. Predicting coiled coils from protein sequences. *Science* **252:** 1162-1164.

Minor, D.L., Jr. and Kim, P.S. 1994. Context is a major determinant of beta-sheet propensity. *Nature* **371:** 264-267.

Monera, O.D., Sereda, T.J., Zhou, N.E., Kay, C.M. and Hodges, R.S. 1995. Relationship of sidechain hydrophobicity and alpha-helical propensity on the stability of the single-stranded amphipathic alpha-helix. *J Pept Sci* **1:** 319-329.

Myers, J.K., Pace, C.N. and Scholtz, J.M. 1997. A direct comparison of helix propensity in proteins and peptides. *Proc Natl Acad Sci U S A* **94:** 2833-2837.

O'Neil, K.T. and DeGrado, W.F. 1990. A thermodynamic scale for the helix-forming tendencies of the commonly occurring amino acids. *Science* **250:** 646-651.

O'Shea, E.K., Klemm, J.D., Kim, P.S. and Alber, T. 1991. X-ray structure of the GCN4 leucine zipper, a two-stranded, parallel coiled coil. *Science* **254:** 539-544.

Pace, C.N. and Scholtz, J.M. 1998. A helix propensity scale based on experimental studies of peptides and proteins. *Biophys J* **75:** 422-427.

Potekhin, S.A., Medvedkin, V.N., Kashparov, I.A. and Venyaminov, S. 1994. Synthesis and properties of the peptide corresponding to the mutant form of the leucine zipper of the transcriptional activator GCN4 from yeast. *Protein Eng* **7:** 1097-1101.

Singh, M., Berger, B. and Kim, P.S. 1999. LearnCoil-VMF: computational evidence for coiled-coil-like motifs in many viral membrane-fusion proteins. *J Mol Biol* **290:** 1031-1041.

Steinmetz, M.O., Stock, A., Schulthess, T., Landwehr, R., Lustig, A., Faix, J., Gerisch, G., Aebi, U. and Kammerer, R.A. 1998. A distinct 14 residue site triggers coiled-coil formation in cortexillin I. *EMBO J* **17:** 1883-1891.

Strelkov, S.V. and Burkhard, P. 2002. Analysis of alpha-helical coiled coils with the program TWISTER reveals a structural mechanism for stutter compensation. *J. Struct. Biol.* **137:** 54-64.

Tripet, B., Wagschal, K., Lavigne, P., Mant, C.T. and Hodges, R.S. 2000. Effects of side-chain characteristics on stability and oligomerization state of a de novo-designed model coiled-coil: 20 amino acid substitutions in position "d". *J Mol Biol* **300:** 377-402.

Wagschal, K., Tripet, B., Lavigne, P., Mant, C. and Hodges, R.S. 1999. The role of position a in determining the stability and oligomerization state of alpha-helical coiled coils: 20 amino acid stability coefficients in the hydrophobic core of proteins. *Protein Sci* **8:** 2312-2329.

Wolf, E., Kim, P.S. and Berger, B. 1997. MultiCoil: a program for predicting two- and three-stranded coiled coils. *Protein Sci* **6:** 1179-1189.

Wu, K.C., Bryan, J.T., Morasso, M.I., Jang, S.I., Lee, J.H., Yang, J.M., Marekov, L.N., Parry, D.A. and Steinert, P.M. 2000. Coiled-coil trigger motifs in the 1B and 2B rod domain segments are required for the stability of keratin intermediate filaments. *Mol Biol Cell* **11:** 3539-3558.

Zhou, N.E., Kay, C.M. and Hodges, R.S. 1994. The net energetic contribution of interhelical electrostatic attractions to coiled-coil stability. *Protein Eng* **7:** 1365-1372.

Zhu, H., Celinski, S.A., Scholtz, J.M. and Hu, J.C. 2000. The contribution of buried polar groups to the conformational stability of the GCN4 coiled coil. *J Mol Biol* **300:** 1377-1387.

Chapter 5: Optimization of microbial specificity in cyclic peptides by modulation of hydrophobicity within a defined structural framework

A version of this chapter has been published. Kondejewski, L. H., Lee, D. L., Jelokhani-Niaraki, M., Farmer, S. W., Hancock, R. E. W., and Hodges, R. S. 2002. Journal of Biological Chemistry. 277:67-74.

Chapter 5-1. Introduction

The cationic antimicrobial peptides represent a potentially new class of antibiotics to combat microorganisms that have developed resistance to the traditional antibiotics and as such, their structure-activity relationships have been actively pursued (Hancock 1997; Hancock et al. 1998). While their mode of action is not fully understood, it is well established that these peptides must interact with the plasma membrane of susceptible microorganisms, where either their accumulation in the membrane causes increased permeability and loss of barrier function or they cross the membrane to access cytoplasmic targets (Hancock et al. 1998). Studies with gramicidin S have indicated that this peptide is very membrane active (Zhang et al. 2000a). The concept that the site of action of certain peptides is the cell membrane (as opposed to microbial enzymes) is consistent with observations of rapid (minutes to hours), concentration-dependent action, with the development of resistant microbial strains being reduced or eliminated (Oren et al. 2001). Moreover, some cationic peptides also displayed toxicity to higher eukaryotic cells, an unsurprising result if the target is indeed the cell membrane. Differences in the lipid composition and the membrane potential gradient between prokaryotic and higher eukaryotic cell membranes have been used to explain the differences in specificity of these peptides (Matsuzaki et al. 1995). Since it is believed that killing with peptides like gramicidin S after peptide interaction with membranes, efforts have been made to enhance specificity to provide the greatest discrimination between prokaryotic and higher eukaryotic membranes.

Two major classes of the cationic antimicrobial peptides are the α-helical and the β-sheet peptides (Andreau et al. 1998; Matsuzaki 1999; van 't Hof et al. 2001). The α-helical class (*e.g.* cecropins (Holak et al. 1988), magainins (Bechinger et al. 1992; Zasloff 1987), and melittin (Bazzo et al. 1988)) consists of linear peptides that exist as disordered structures in aqueous media and become helical upon interaction with hydrophobic solvents or phospholipid vesicles. Unlike the α-helical peptides, β-sheet peptides are cyclic peptides constrained in this conformation either by disulfide bonds (tachyplesins (Kawano et al. 1990; Nakamura et al. 1988), protegrins (Harwig et al. 1995; Storici et al. 1993), and polyphemeusins (Miyata et al. 1989; Zhang et al. 2000b)) or by cyclization of the backbone (gramicidin S (Khaled et al. 1978) and tyrocidines (Kuo et al. 1980)).

From structure-activity relationship studies of cationic antimicrobial peptides, a number of factors important for antimicrobial and anti-eukaryotic cell activity have been identified. These fundamentally important characteristics include the presence of both hydrophobic and basic residues, an amphipathic nature which describes the relative positioning of the basic and hydrophobic residues, and secondary structure, either preformed or inducible in lipid-mimicking environments (Hancock 1997; Hancock et al. 1998; Izumiya et al. 1979; Pathak et al. 1995). The difficulty in interpreting results from such studies is that it is difficult to systematically study one variable while holding other variables constant, since sequence changes generally lead to structural changes which affect amphipathicity. Conformationally constrained peptides have the advantage that sequence changes alter conformation to a lesser degree than in their linear counterparts, and thus facilitate the dissection of the relative contributions of each property.

In structure-activity studies on cyclic peptides related to gramicidin S (GS), we have previously found that amphipathicity plays a critical role in defining the scope of biological activities in these peptides (Kondejewski et al. 1996; Kondejewski et al. 1999;

McInnes et al. 2000). Furthermore, it was seen that antimicrobial activity could be dissociated from hemolytic activity and that the differences between these two activities could be maximized by the selection of the appropriate amphipathicity (Kondejewski et al. 1999). It was seen that a high amphipathicity is not desirable in these peptides, as this results in high hemolytic activity coupled with low antimicrobial activity. Through systematic reduction of amphipathicity utilizing enantiomeric substitutions within the framework of the highly amphipathic ß-sheet peptide, GS14 [cyclo(VKLKV*d*-YPLKVKL*d*-YP), where *d*- denotes a D-amino acid], it was possible to define the optimum amphipathicity leading to the highest therapeutic index (Kondejewski et al. 1999). In the present study, we have utilized the structural framework of the GS14 diastereomer possessing the highest therapeutic index, GS14K4 [cyclo(VKL*d*-KV*d*-YPLKVKL*d*-YP)], and have systematically altered the hydrophobicity in order to define the optimal hydrophobicity leading to the greatest antimicrobial activity and specificity within this structural framework.

Chapter 1-2. Results

Peptide design

In a previous study we defined the optimum amphipathicity leading to a high specificity for microorganisms over human erythrocytes through the use of systematic enantiomeric substitutions within the framework of a 14-residue head-to-tail cyclic peptide (Kondejewski et al. 1999). In the present investigation we have attempted to further optimize the biological properties of the diastereomeric peptide possessing the optimum amphipathicity, GS14K4, [cyclo(VKL*d*-KV*d*-YPLKVKL*d*-YP)] by modulation of hydrophobicity. Under the assumption that this "optimum structure" leading to the optimum amphipathicity (relative distribution of hydrophobic and basic residues) is retained, we have systematically replaced the hydrophobic residues in GS14K4 in order to obtain peptides which are either less hydrophobic or more hydrophobic than GS14K4 (Table 5-1). GS14K4 has two D-tyrosines, three leucines, and three valine residues in its

Table 5-1. Peptide sequences, physical properties and biological activities of peptides used in this study

Peptide	Linear Sequence[a]	Retention Time (min)[b]	Predicted Relative Hydrophobicity (min) [c]	LPS binding affinity (μM)[d]	Hemolytic activity (μg/ml) [e]
GS14	VKLKVYPLKVKLYP	49.5	49.6	3	1.5
Y2/F2, V3/L3	LKLKLFPLKLKLFP	46.2	55.3	25	12.5
V3/L3	LKLKLYPLKLKLYP	42.5	47.9	46	25
Y2/F2	VKLKVFPLKVKLFP	42.3	49.9	59	40
GS14K4	VKLKVYPLKVKLYP	38.9	42.5	93	200
V3/A3	AKLKAYPLKAKLYP	32.2	34.4	163	>800
L3/A3	VKAKVYPAKVKAYP	28.6	29.0	243	>800
V3L3/A6	AKAKAYPAKAKAYP	21.7	20.9	291	>800

[a] Linear sequences of cyclic peptides. One-letter amino acid code is used; underlined residues represent D-amino acids.

[b] Retention time on RP-HPLC at 25°C.

[c] Calculated using the HPLC hydrophobicity scale of Sereda *et al.* (1994) with values for Leu, Phe, Val, Tyr, and Ala as 8.5, 7.9, 6.7, 4.2, and 4.0, respectively. Values for Pro and L-Lys were taken from Guo *et al.* (1986) of 2.0 and –2.1, respectively. The value for D-Lys which has been shown to be on the hydrophobic face was taken as –9.2 (Sereda et al. 1994).

[d] Peptide concentration to displace 50% of dansyl-polymyxin B from LPS.

[e] Peptide concentration for 100% lysis of human erythrocytes. The hemolytic activity of GS was 12.5 μg/ml.

sequence that were selected to alter hydrophobicity in the analogs used in this study. Hydrophobicity was increased relative to GS14K4 by replacing two D-Tyr residues with two D-Phe residues (peptide Y2/F2), three Val with three Leu (peptide V3/L3), or a combination of both (peptide Y2/F2, V3/L3). Hydrophobicity was reduced relative to GS14K4 by replacing three Val with three Ala (V3/A3), three Leu with three Ala (L3/A3) or all six hydrophobes with Ala (V3L3/A6).

Peptide structure

CD spectroscopy

The secondary structure of the peptides was evaluated by CD spectroscopy. Similar to GS, GS14 exhibited a CD spectrum with large negative ellipticities at 206 nm and 223 nm (Fig. 5-1) which is indicative of ß-sheet structure in these cyclic peptides (Gibbs et al. 1999; Kondejewski et al. 1996; Kondejewski et al. 1999). This ß-sheet conformation imparts a highly amphipathic nature to GS14 (Kondejewski et al. 1999). The incorporation of a D-Lys residue in the framework of GS14 (GS14K4) resulted in a CD spectrum more characteristic of a disordered structure under aqueous conditions, indicating disruption of both ß-sheet structure and amphipathicity of GS14 (Fig. 5-1A). The nuclear magnetic resonance (NMR) solution structure of GS14K4 has recently been determined in this laboratory. These studies verified the disruption of ordered structure and amphipathicity. They also showed that the structural basis for the decreased amphipathicity of GS14K4 is the placement of D-Lys4 on the hydrophobic face of the molecule (McInnes et al. 2000). All the GS14K4 hydrophobicity analogs, whether less or more hydrophobic, exhibited CD spectra similar to GS14K4, indicating that all possessed a similar disrupted ß-sheet/ß-turn conformation under aqueous conditions.

In the presence of a hydrophobic structure-inducing solvent such as trifluoroethanol, the spectrum of GS14 was greatly enhanced, indicating a stabilization of the ß-sheet structure (Fig. 5-1B). As well, all the GS14K4 hydrophobicity analogs exhibited some inducibility of structure in the presence of TFE. The measured negative ellipticities in

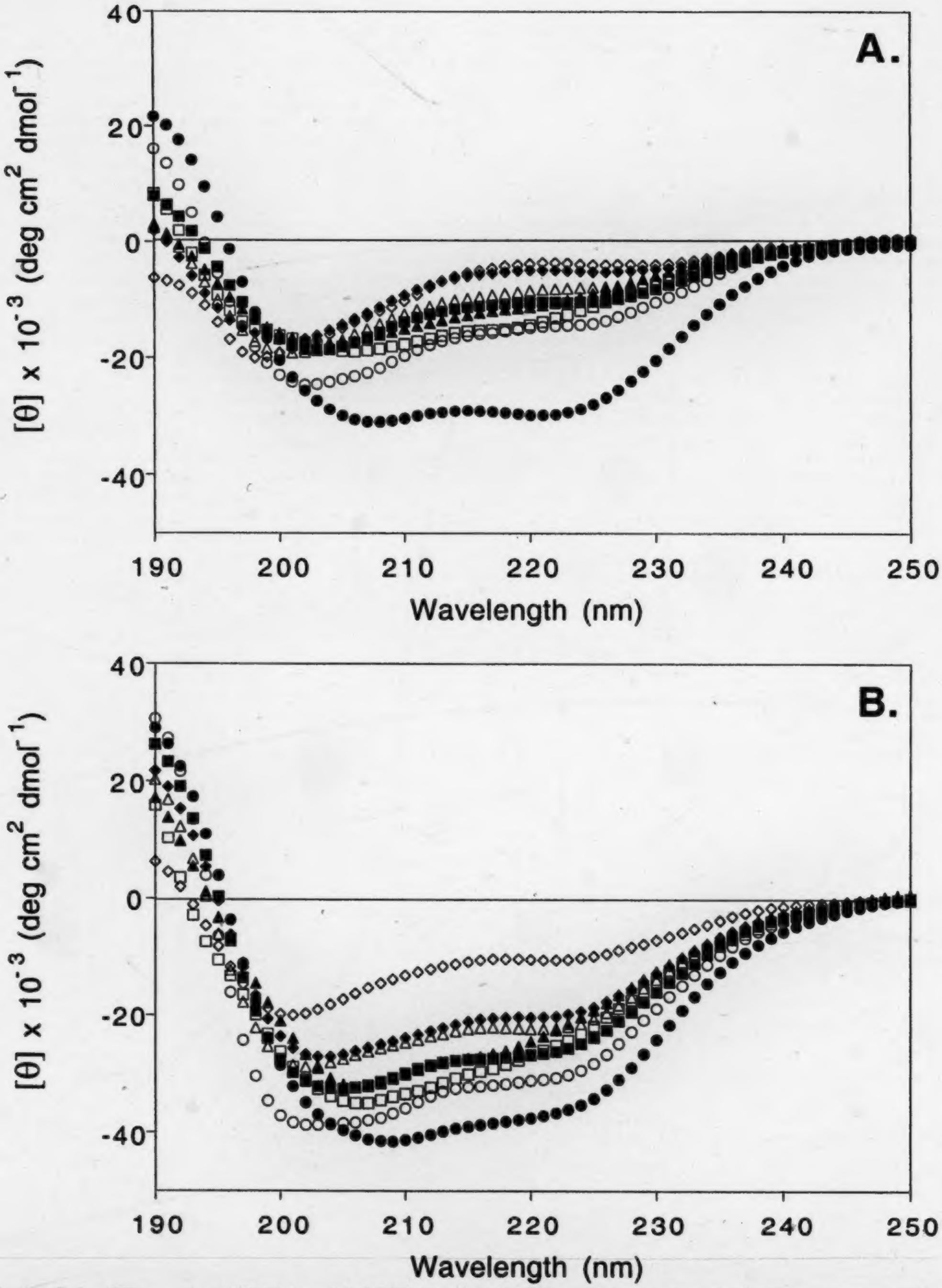

Figure 5-1. CD spectra of GS14 and GS14K4 hydrophobicity analogs. Panel A, CD spectra recorded in 5 mM sodium acetate buffer, pH 5.5, at 20 °C. Samples were GS14 (closed circle); GS14K4 (open circle); Y2/F2 (open square); V3/L3 (closed square); L3/A3, Δ ; Y2/F2, V3/L3 (closed triangle); V3L3/A6 (open diamond); V3/A3 (closed diamond). Panel B, CD spectra recorded in 5 mM sodium acetate buffer, pH 5.5, containing 50% TFE, at 20 °C. Symbols for samples were identical to Panel A.

the presence of TFE showed a correlation with predicted hydrophobicity (Table 5-1) at both 205 nm (R = 0.83) as well as at 220 nm (R=0.80), indicating that the structure of the more hydrophobic analogs was stabilized more efficiently by TFE (data not shown). These findings suggest that TFE-mediated structure induction in these cyclic peptides is a consequence of interactions between the hydrophobic portion of the alcohol with hydrophobic groups present in the peptides. Similar hydrophobic-hydrophobic peptide-alcohol interactions have been noted with melittin, an α-helical peptide (Hirota et al. 1998).

Reversed-phase HPLC analysis

Retention time on reversed-phase HPLC can be used as a measure of peptide hydrophobicity (Guo et al. 1986; Parker et al. 1986); however, it is well known that the formation of a hydrophobic preferred binding domain due to peptide secondary structure can affect peptide interactions with reversed-phase matrices (Krause et al. 1996; Rothemund et al. 1996; Wishart et al. 1996; Zhou et al. 1990). We have shown previously with a complete set of GS14 diastereomers that the observed retention times on RP-HPLC are a measure of peptide amphipathicity in such a homologous series of peptides (Kondejewski et al. 1999; Mant et al. 1998). This can be seen in the comparison of the observed retention times between GS14 and GS14K4 (Table 5-1). Both these peptides have exactly the same composition and sequence and therefore the same intrinsic hydrophobicity, but differ only in structure. The 10.6 minute difference in retention times between GS14 and GS14K4 (49.5 min and 38.9 min, respectively) showed the differences in the ability of the peptides to form a hydrophobic preferred binding domain and at the same time segregate basic residues to the opposite side of the molecule. Retention time differences between these two molecules were therefore a measure of peptide amphipathicity, and showed that GS14K4 has a substantially lower amphipathicity compared to GS14. We have attempted to modulate the hydrophobicity of the present analogs through residue substitutions in the framework of GS14K4 under the assumption that the optimum structural features leading to the optimum amphipathicity present in GS14K4 will also be present in the analogs. As shown in Table 5-1, three of the designed analogs were more hydrophobic than GS14K4 and three analogs were less hydrophobic. A plot of the predicted relative hydrophobicity using RP-HPLC retention time data for the hydrophobicity analogs against their observed retention times (Fig. 5-2) yielded a linear relationship (R=1.0) indicating that all the analogs can present their hydrophobic residues in the same orientation for interaction with the reversed-phase matrix. This correlation suggests that the analogs possessed essentially similar structures in a hydrophobic environment and had a similar relative distribution of hydrophobic and basic residues and only differ in their intrinsic hydrophobicity.

Interaction of peptides with bacterial outer membranes

Interaction with Bacterial Lipopolysaccharide

Cationic antimicrobial peptides interact initially with negatively charged outer membrane lipopolysaccharide (LPS) on the surface of Gram negative bacteria (Hancock 1981; Nicas et al. 1983). The interaction of the GS14K4 analogs with bacterial LPS was investigated by monitoring the displacement of LPS-bound dansyl-polymyxin B by the peptides (Kondejewski et al. 1996; Moore et al. 1986); the measured binding affinities are listed in Table 5-1. There was a direct correlation (R=0.99) between peptide hydrophobicity and LPS-binding affinity (Fig. 5-3) indicating that increased peptide hydrophobicity resulted in higher binding affinity to LPS. Comparison of the LPS binding affinity of GS14 with GS14K4, two peptides which only differed in amphipathicity, shows that amphipathicity also played a large role in modulating binding affinity (Table 5-1).

Permeabilization of Outer Membranes to NPN

Permeabilization of *E. coli* outer membranes by the analogs was monitored using the hydrophobic fluorescent probe *N*-phenyl-1-naphthylmine (NPN). NPN fluorescence is substantially increased when it is incorporated into the hydrophobic bacterial cell

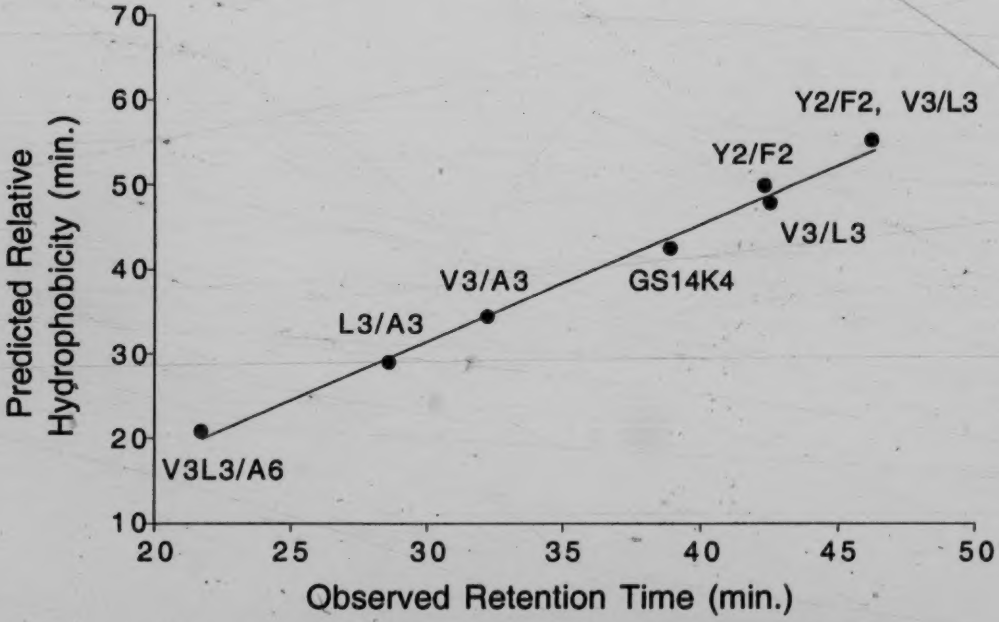

Figure 5-2. Correlation between predicted relative hydrophobicity and observed RP-HPLC retention times of GS14K4 analogs. The predicted RP-HPLC retention times were calculated using the RP-HPLC-derived hydrophobicity scale of Guo *et al.* (Guo et al. 1986) for random coil peptides and the RP-HPLC-derived hydrophobicity scale of Sereda *et al.* (Sereda et al. 1994) for α-helical peptides. The observed retention times were determined on a Zorbax SB-C8 column (150 x 2.1 mm inner diameter; 5-μm particle size; 300 Å pore size) with a linear AB gradient of 1% B/min (where solvent A was 0.05% aqueous trifluoroacetic acid and solvent B was 0.05% trifluoroacetic acid in acetonitrile) at a flow rate of 0.25 ml/min.

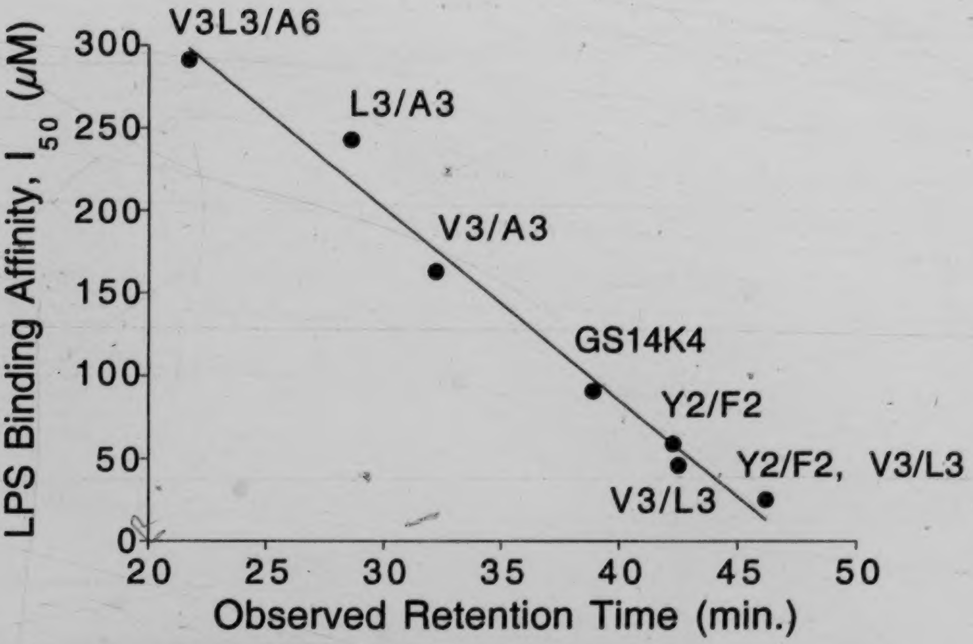

Figure 5-3. Correlation between peptide hydrophobicity and LPS-binding affinity in GS14K4 analogs. The RP-HPLC-derived retention times and LPS-binding affinity listed in Table 5-1 were measured as described under Materials and Methods (Chapter 2).

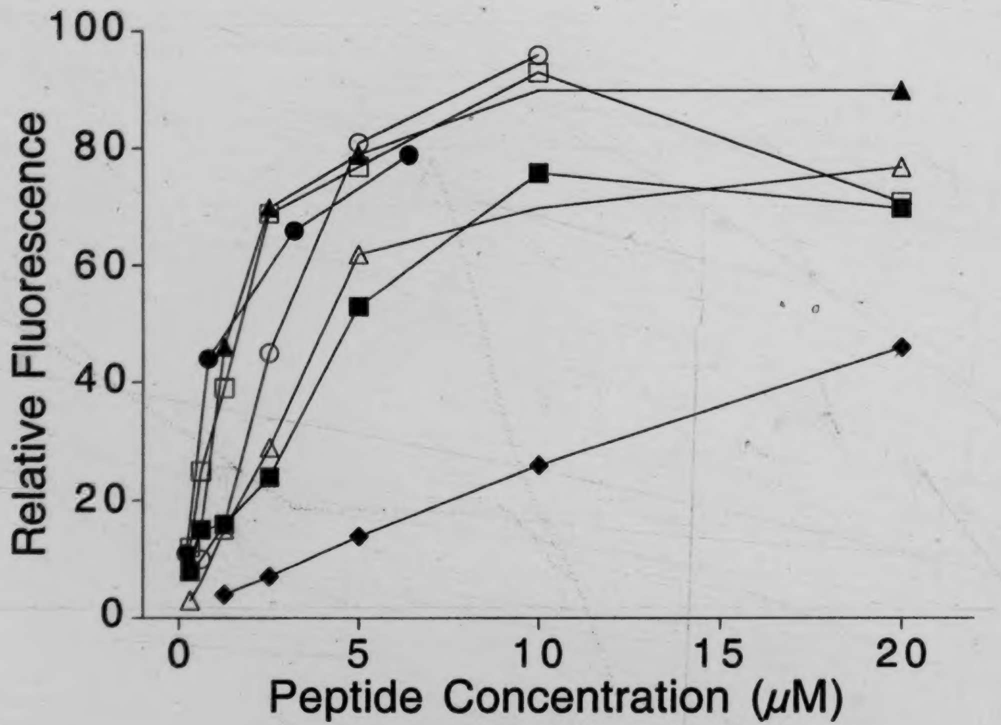

Figure 5-4. Permeabilization of *E. coli* UB1005 cells to NPN. Peptide-mediated outer membrane destabilization was monitored by fluorescence increase due to NPN partitioning into the hydrophobic membrane interior. Samples were GS14K4 (closed circle); V3L3 (open circle); Y2/F2 (open square); Y2/F2, V3/L3 (closed square); L3/A3, Δ ; V3/A3 (closed triangle); V3L3/A6 (closed diamond).

membrane (after permeabilization) compared to its fluorescence in the presence of bacterial cells under non permeabilizing conditions (Loh et al. 1984). Outer membrane destabilization by the GS14K4 hydrophobicity analogs is shown in Fig. 5-4. All the analogs with the exception of the least hydrophobic analog (V3L3/A6) were found to exhibit similar capacities to permeabilize the outer membrane to the hydrophobic probe. Peptide V3L3/A6 was approximately 1/10th as effective at destabilizing the outer membrane as compared to the other analogs.

Biological activities of peptides

Hemolytic activity

The hemolytic activities of the peptides against human erythrocytes were determined as a measure of peptide toxicity towards higher eukaryotic cells (Table 5-1). The hemolytic activity of GS14K4 is considerably lower than that of the parent compound, GS14, due to the decreased amphipathicity of GS14K4 (Kondejewski et al. 1999). The GS14K4 hydrophobicity analogs exhibited a range of hemolytic activities, from that approaching GS14, to greatly decreased hemolytic activity (Table 5-1). There was a correlation between hemolytic activity and RP-HPLC determined hydrophobicities of the analogs (Fig. 5-5), whereby strong hemolytic activity was seen only in those analogs that had retention times greater than 39 min. (*i.e.* greater than that of GS14K4). This suggests that the hemolytic activity of the peptides is strongly influenced by hydrophobicity of the nonpolar face of the molecule. Analogs with hydrophobicities less than GS14K4 exhibited negligible hemolytic activity.

Activity against Gram-negative bacteria

The antimicrobial activities of the peptides against a number of Gram negative microorganisms is shown in Table 5-2, along with a therapeutic index that was calculated as a measure of specificity of the peptides for the microorganism over human erythrocytes. GS14K4 exhibited both high activity against all the microorganisms as well as high specificity, as evident from the high therapeutic indices.

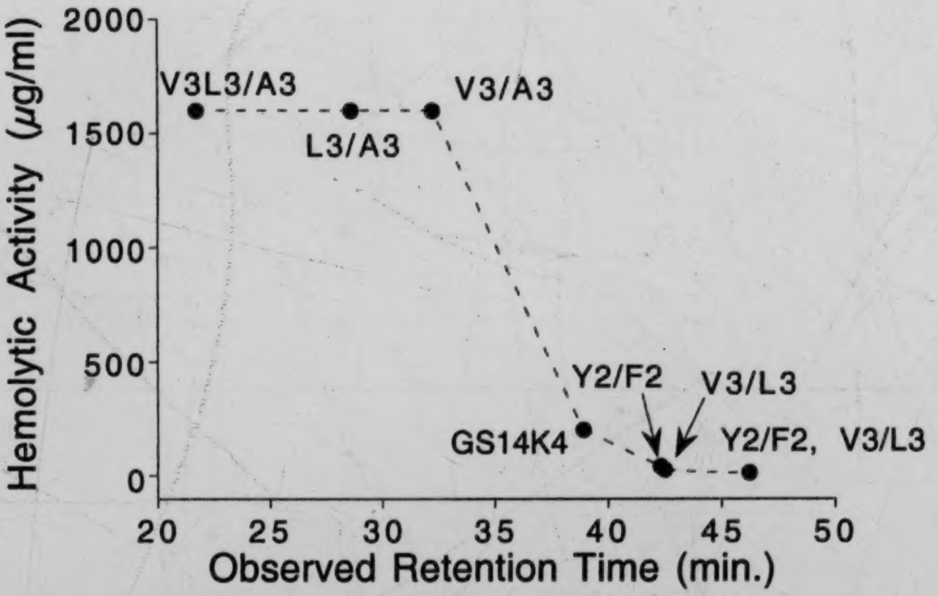

Figure 5-5. Relationship between hydrophobicity and hemolytic activity of GS14K4 analogs. Hemolytic activity and RP-HPLC-derived retention times listed in Table 5-1 were determined as described under Materials and Methods (Chapter 2). Hemolytic activities reported as >800 μg/ml in Table 5-1 are plotted as 1600 μg/ml.

Table 5-2. Activity of GS14K4 hydrophobicity analogs against Gram-negative microorganism

Peptide	Minimal Inhibitory Concentration (μg/mL) and Therapeutic Index[a]											
	P. aeruginosa H187		*P. aeruginosa* H188		*E. coli* UB1005		*E. coli* DC2		*S. typhimurium* C587		*S. typhimurium* C610	
	activity	index	activity	index	activity	index	activity	index	activity	index	activity	index
GS	20	0.6	6.2	2	6.2	2	3.1	4	20	0.6	10	1.3
GS14	>200	<0.01	>200	<0.01	>200	<0.01	200	0.01	>200	<0.01	>200	<0.01
Y2/F2, V3/L3	16	0.8	3.1	4	8.1	1.5	2	6.3	33	0.4	13	1
V3/L3	100	0.3	3.1	8	6.2	4	2.8	8.9	100	0.3	18	1.4
Y2/F2	19	2.7	3.1	16	5.6	8.9	1.5	33	8.1	6.2	3.1	16
GS14K4	25	8	3.1	65	6.2	32	3.1	65	11	18	4.1	49
V3/A3	150	11	18	89	13	128	9	178	38	42	6.2	258
L3/A3	>200	4	100	16	200	8	200	8	>200	4	100	16
V3L3/A6	>200	4	150	11	>200	4	>200	4	>200	4	>200	4

[a] Therapeutic index = hemolytic activity/minimal inhibitory concentration. For the calculation of the therapeutic index, values of 400 μg/ml were used for MIC values reported as >200 μg/ml and values of 1600 μg/ml were used for hemolytic activity values reported as >800 μg/ml. The therapeutic index of the analog with the highest value for each microorganism is shaded. The open box highlights the peptide (GS14K4) with antimicrobial activity within two-fold of the most active peptide against each organism in this study, as well as possessing the second highest therapeutic index. The hemolytic activity of GS was 12.5 μg/ml.

GS14, on the other hand, had essentially no activity against these microorganisms due to its high amphipathicity (Kondejewski et al. 1999; McInnes et al. 2000). Compared to GS14K4, some of the hydrophobicity analogs exhibited similar antimicrobial activities, while others exhibited greatly reduced activity.

We found a correlation between peptide hydrophobicity and antimicrobial activity as shown in Fig. 5-6 for representative Gram negative microorganisms. It was evident that for all the microorganisms there was a dramatic loss of antimicrobial activity below a certain hydrophobicity threshold (approximately 32 min. retention time, analog V3/A3). For most of the microorganisms, this analog represented the hydrophobicity cutoff for the peptides studied. For the majority of microorganisms, there was a limit to the maximum antimicrobial activity, with little further increase in activity obtained with increasing hydrophobicity past approximately 39 min. retention time (analog GS14K4). Interestingly, increasing the peptide hydrophobicity (analog V3/L3) substantially decreased antimicrobial activity against two different Gram negative microorganisms (*P. aeruginosa* H187 and *S. typhimurium* C587, Table 5-2).

Also shown in Table 5-2 and Fig. 5-6 are the therapeutic indices of the analogs for the Gram negative microorganisms. It is clear from these data that there was an optimal hydrophobicity that conferred specificity for all the microorganisms. The highest therapeutic indices for each organism are shaded in Table 5-2 to highlight these differences. Of the analogs studied, V3/A3 possessed the best therapeutic indices and demonstrated an improvement over the therapeutic index of GS14K4. Although the antimicrobial activity of this peptide was reduced compared to GS14K4, the greatly reduced hemolytic activity was the dominating influence on the therapeutic index, resulting in indices that were in the range of 2- to 5-fold greater than those for GS14K4. The analogs with hydrophobicities higher or lower than this optimal peptide (peptides L3/A3 and GS14K4, with retention times of 28.6 min. and 38.9 min., respectively) therefore mark the boundaries of a "therapeutic window", inside of which would be

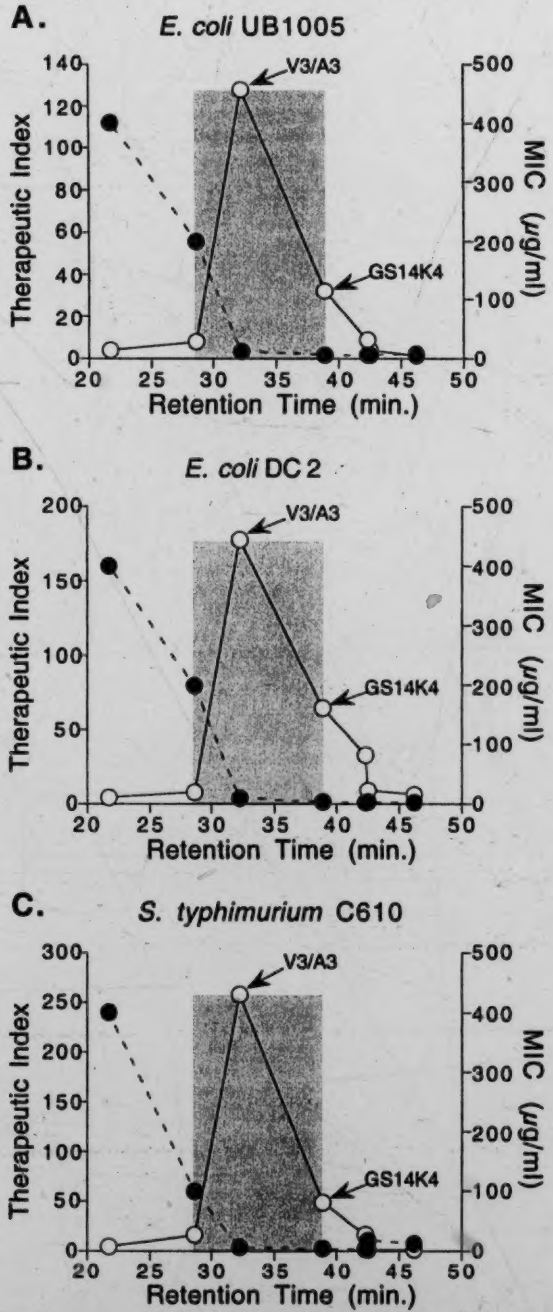

Figure 5-6. Antimicrobial activity and microbial specificity of GS14K4 hydrophobicity analogs against Gram negative microorganisms. The minimal inhibitory concentration (closed circle) and the therapeutic index (open circle) of the GS14K4 analogs shown in Table 5-2 are plotted as a function of peptide hydrophobicity as determined by RP-HPLC (observed retention time, Table 5-1). Plots are for: (A) *E. coli* UB1005; (B) *E. coli* DC2; (C) *S. typhimurium* C610. A value of 400 µg/ml was used for MIC values reported as >200 µg/ml and a value of 1600 µg/ml was used for hemolytic activities reported as >800 µg/ml to allow calculation of the therapeutic index.

predicted to lie the optimal peptide hydrophobicity for this series of peptides against Gram negative microorganisms. The therapeutic windows are shaded in Fig. 5-6. Comparison of the therapeutic indices of the best analog, V3/A3, with those of GS itself shows that V3/A3 possesses therapeutic indices in the range of 20- to 200-fold greater than GS itself and thus represents a significant improvement in specificity. Overall, GS14K4 showed an activity that is near maximum antimicrobial activity (less than a two-fold difference between GS14K4 and the most active compound in this series, L3/A3) and a reasonable therapeutic index among the analogs listed in this study (Table 5-2).

Activity against fungi and Gram-positive bacteria

The activity of the hydrophobicity analogs against a number of Gram positive microorganisms and yeast is shown in Table 5-3. GS14K4 exhibited strong activity against most of the tested microorganisms, coupled with a high therapeutic index. Unlike the case for Gram negative microorganisms where maximum antimicrobial activity reached a plateau at the hydrophobicity level of GS14K4, a number of the more hydrophobic analogs exhibited substantially greater activity against some of the Gram positive microorganisms as well as yeast. In most cases, however, GS14K4 exhibited the highest therapeutic indices due to the increased hemolytic activity of the more hydrophobic analogs. The highest therapeutic indices for each microorganism are shaded. The Y2/F2 peptide (Table 5-3), which increased the hydrophobicity of the two turns, had much better antimicrobial activity than GS14K4 and even with the greater hemolytic activity (Table 5-1), still had the best therapeutic index. Peptide V3/A3, a slightly less hydrophobic peptide than GS14K4, exhibited a 4-fold increase in therapeutic index for *C. xeroses* over GS14K4. As with Gram negative microorganisms above, a similar trend of antimicrobial activity and therapeutic index changes with hydrophobicity changes was seen against Gram positive microorganisms and yeast (Fig. 5-7).

Table 5-3. Antifungal and Gram-positive activity of GS14K4 hydrophobicity analogs

Peptide	Minimal Inhibitory Concentration (μg/mL) and Therapeutic Index[a]													
	S. aureus SAP0017		*S. aureus* K147		*S. epidermidis*		*B. subtilis*		*E. faecalis*		*C. xeroses*		*C. albicans*	
	activity	index	activity	index	activity	index	activity	index	activity	index	activity	index	activity	index
GS	1.5	8.3	1.5	8.3	1.5	8.3	3.1	4	2.8	4.5	0.7	18	3.1	4
GS14	>200	<0.01	>200	<0.01	113	0.01	>200	<0.01	2.3	0.7	6.2	0.2	175	0.01
Y2/F2, V3/L3	9.4	1.3	9.4	1.3	2	6.3	6.2	2	1.5	8.3	1.2	10	3.1	4
V3/L3	13	2	23	1.1	2	13	9.4	2.7	1.5	17	1	25	4	6.3
Y2/F2	8.1	6.2	11	4.4	2.8	18	13	4.4	6.2	8.1	1.4	36	3.1	16
GS14K4	50	4	100	2	2	100	25	8	1.5	133	1.7	118	6.2	32
V3/A3	>200	4	>200	4	50	32	>200	4	>200	4	3.1	520	50	32
L3/A3	>200	4	>200	4	>200	4	>200	4	>200	4	100	16	>200	4
V3L3/A6	>200	4	>200	4	>200	4	>200	4	>200	4	150	10	>200	4

[a] Therapeutic index = hemolytic activity/antibacterial activity. For the calculation of the therapeutic index, values of 400 μg/ml were used for MIC values reported as >200 μg/ml and values of 1600 μg/ml were used for hemolytic activity values reported as >800 μg/ml. The therapeutic index of the analog with the highest value for each microorganism is shaded. The open boxed values highlight the antimicrobial activity of peptides Y2/F2 and GS14K4 which have the highest therapeutic index or second highest therapeutic index for comparison. The hemolytic activity of GS was 12.5 μg/ml.

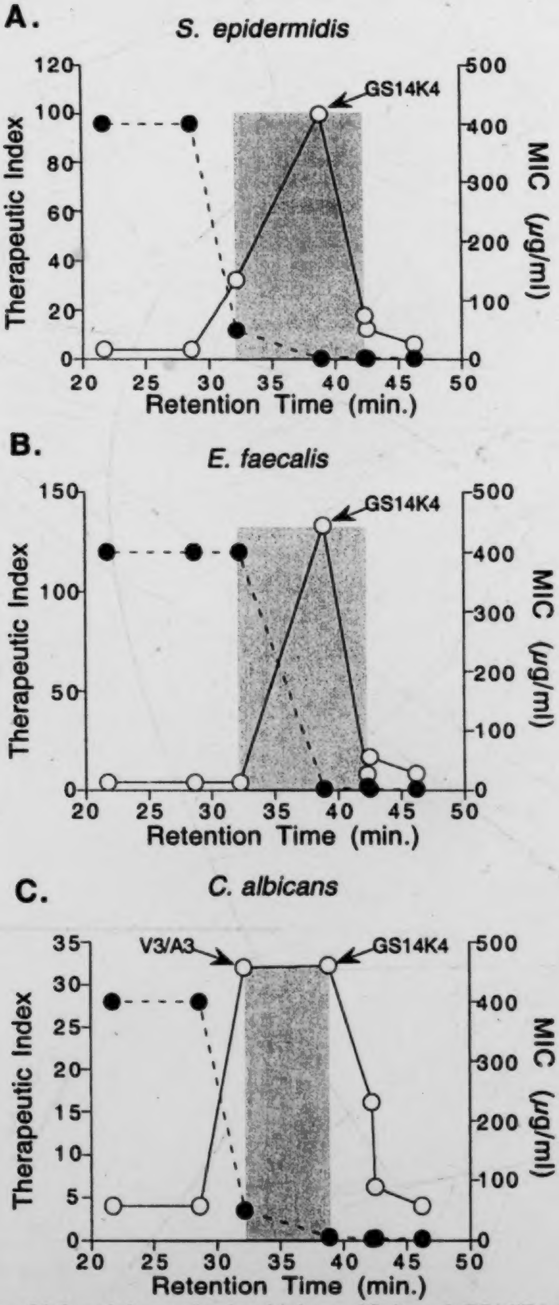

Figure 5-7. Antimicrobial activity and microbial specificity of GS14K4 hydrophobicity analogs against Gram positive microorganisms and yeast. The minimal inhibitory concentration (closed circle) and the therapeutic index (open circle) of the GS14K4 analogs shown in Table 5-3 are plotted as a function of peptide hydrophobicity as determined by RP-HPLC (observed retention time, Table 5-1). Plots are for: (A) *S. epidermidis*; (B) *E. faecalis*; (C) *C. albicans*. A value of 400 μg/ml was used for MIC values reported as >200 μg/ml and a value of 1600 μg/ml was used for hemolytic activities reported as >800 μg/ml to allow calculation of the therapeutic index.

In this case, however, the hydrophobicity threshold was more variable and dependent on the microorganism, but overall the threshold was shifted to slightly higher hydrophobicity values, indicating that a higher hydrophobicity was required for strong activity against Gram positive microorganisms than for Gram negative microorganisms. As with the Gram negative microorganisms, a therapeutic window can be defined, but centered at somewhat higher hydrophobicity values. For the majority of Gram positive microorganisms and yeast, peptides with this optimal hydrophobicity eluted at 39 min. retention time (GS14K4), The analogs with higher or lower retention time (peptides Y2/F2 and V3/A3, with retention times of 42.3 min. and 32.2 min., respectively) marked the boundaries of the optimum hydrophobicity for Gram positive microorganisms and yeast in this series of peptides.

Chapter 5-3. Discussion

The backbone framework of the head-to-tail cyclic peptide, GS14K4, was used as a structural scaffold in the present study in order to optimize hydrophobicity within the amphipathic framework of GS14K4. All hydrophobicity analogs were found to possess similar backbone conformations under aqueous conditions as measured by CD spectroscopy, as well as similar side chain location in a hydrophobic environment as determined by RP-HPLC. Together, these results indicate that the amphipathicity (relative distribution of hydrophobic and basic residues) remained substantially similar in the analogs, and that the analogs differed only in hydrophobicity.

In our previous study, we reported that we could modulate hemolytic activity through structural changes leading to changes in amphipathicity within the framework of GS14 (Kondejewski et al. 1999); this can be seen in the large difference in hemolytic activities between GS14 and GS14K4 (Table 5-1). Here we find that while maintaining the structural changes responsible for decreased amphipathicity, we could further modulate the hemolytic activity of the present peptides by specific residue replacements that either increased or decreased the hydrophobicity of the peptides.

Together, these findings indicate that peptide hydrophobicity drives hemolytic activity. Within the context of a highly amphipathic molecule, there was a high "directed hydrophobicity". Conversely, the present GS14K4 hydrophobicity analogs possessed similar relative distributions of hydrophobic and basic residues, but differed in overall peptide hydrophobicity. Again, there appears to be a threshold hydrophobicity for the "hydrophobic patch" that was responsible for the observed hemolytic activity. Peptides that were less hydrophobic than GS14K4 possessed no hemolytic activity, whereas peptides that were more hydrophobic were considerably more hemolytic than GS14K4. High hydrophobicity would be expected to increase activity of membrane-active peptides, since increased hydrophobicity would be predicted to facilitate partitioning of a greater proportion of the peptide into the membrane. Similar findings relating hydrophobicity and hemolytic activity have been reported in linear α-helical peptides (Dathe et al. 1997; Juvvadi et al. 1996; Wieprecht et al. 1997) as well as other cyclic peptides based on GS (Jelokhani-Niaraki et al. 2000).

As with hemolytic activity, antimicrobial activity was also sensitive to changes in hydrophobicity. Increasing hydrophobicity also tended to result in peptides with a maximal amount of antimicrobial activity depending on the microbial strain tested, usually at the hydrophobicity of GS14K4. A systematic study of hydrophobicity effects on the activity of α-helical antimicrobial peptides has been reported previously (Pathak et al. 1995). Based on amino acid sequence analysis, however, the majority of antimicrobial peptides identified from natural sources are amphipathic, containing hydrophobic regions that may facilitate partitioning into the cell membrane. Antimicrobial peptides with hydrophilic sequences, such as androctonin (Hetru et al. 2000) may act *via* a different mechanism than amphipathic peptides, perhaps by a method that does not directly involve destabilization of the integrity of the membrane lipid bilayer, but alternatively, interacts instead with DNA in the cell nucleus to interfere with transcription processes.

The outer membrane of Gram negative microorganisms is the first cell component which antimicrobial peptides encounter. This barrier must be breached to allow access of the peptides to the inner membrane, in a process sometimes described as 'self-promoted uptake' (Hancock 1997). A major constituent of the outer membrane is lipopolysaccharide (LPS), a negatively charged molecule containing numerous carbohydrate moieties anchored to the membrane by a lipid A molecule. The interaction of the highly amphipathic GS14 peptide with bacterial membranes is relatively strong, approaching the affinity of polymyxin B itself (Kondejewski et al. 1996). Utilizing a complete set of GS14 diastereomers we previously found a correlation between high amphipathicity, increased LPS-binding affinity, and decreased antimicrobial activity (Kondejewski et al. 1999). This observation suggests that high affinity interactions with outer membrane components may sequester peptides to the outer membrane, hinder the movement of the peptides to their presumed site of action on the inner membrane and inhibit peptide accumulation there, thus decreasing antimicrobial activity.

In the present study, we found a direct correlation between peptide hydrophobicity and outer membrane binding affinity (the positive charge distribution is constant in these analogs). Surprisingly, however, these interactions by high hydrophobicity analogs did not appear to impede the activity of the peptides in most cases, although activity against three of the six Gram negative microorganisms tested did decrease with increasing peptide hydrophobicity (peptide V3/L3 is significantly less active than GS14K4 against *P. aeruginosa* H187, *S. typhimurium* C587, and *S. typhimurium* C610). It should be noted that GS14 has LPS binding affinity approximately one order of magnitude higher than the best GS14K4 hydrophobicity analogs (Table 5-1). The GS14K4 analogs have lower amphipathicity due to the disruption of the hydrophobic patch by D-Lys at position 4. It is possible that the amphipathicity of GS14 is too high due to the four lysine residues on the hydrophilic face, which allows high affinity LPS binding and prevents subsequent membrane translocation and destabilization – the peptide may be sequestered in the interfacial region parallel to the plane of the bilayer akin to gramicidin S (Prenner et al. 2001; Prenner et al. 1999) without a change in orientation. In summary, the overall amphipathicity of the GS14K4 high hydrophobicity analogs may be low enough to allow the peptide to partition to the inner membrane, whereas high LPS binding affinity (in the case of GS14), as a result of high amphipathicity, may preclude this partitioning.

The NPN permeabilization studies in Gram negative bacteria reveal important characteristics of the GS14K4 hydrophobicity analogs. Since all peptides except the least hydrophobic analog, V3L3/A6, permeabilized the outer membrane, the results support the idea that this series of peptides must possess a minimal hydrophobicity to penetrate the bacterial outer membrane, move through the periplasmic space and interact with the inner membrane to kill bacteria. Peptide V3L3/A6 could not permeabilize the outer membrane as effectively and thus was not antimicrobial. This model could apply to both Gram positive and Gram negative bacteria as hydrophobic peptide-lipid interactions would certainly be required in both membrane systems to facilitate bacteriocidal effects. Similarly, V3L3/A6 was also not hemolytic, probably because it lacked the minimal hydrophobicity required for partitioning into lipid membranes and for membrane-destabilizing interactions necessary to promote cell lysis.

To maximize therapeutic index, the optimum hydrophobicity will likely differ slightly between target microorganisms, and for other antimicrobial peptides with different structures. Based on therapeutic index values, the peptides L3/A3 and GS14K4, with retention times of 28.6 and 38.9 minutes, respectively, mark the lower and upper hydrophobicity limits of a "therapeutic window", inside of which would be predicted to lie the optimal peptide hydrophobicity for this series of GS14K4 analogs against Gram negative organisms. But against Gram positive organisms, this “therapeutic window” shifts to the higher hydrophobicities between peptides V3/A3 and Y2/F2 (retention times 32.2 min. and 42.3 min. respectively) due to the higher hydrophobicity required for activity against these microorganisms. Designing peptides with smaller incremental changes in hydrophobicity within these therapeutic windows would allow one to arrive at the optimal peptide hydrophobicity for any given microorganism.

Chapter 5-4. Conclusions

Utilizing a rational approach to antimicrobial peptide design, we first identified an appropriate amphipathicity leading to the optimum antimicrobial properties coupled with weak hemolytic activity (GS14K4). Working within this structural framework, we have now further optimized the activities and specificities of these peptides through incremental changes in the intrinsic hydrophobicity of the peptide. These changes in intrinsic hydrophobicity were accomplished through manipulation of the nature of the hydrophobic residues and result in changes in the effective hydrophobicity of the peptides existing in a defined structure. We find that both hemolytic activity and affinity for bacterial outer membranes decreased with decreasing effective hydrophobicity. Through such incremental changes in hydrophobicity we were able to define the limits of an optimal therapeutic window for each microorganism, where both hemolytic and antimicrobial activities are optimized resulting in the greatest specificity. This therapeutic window was found to be at a slightly higher effective hydrophobicity for Gram positive microorganisms compared to Gram negative microorganisms and yeast.

Chapter 5-5. References

Andreau, D. and Rivas, L. 1998. Animal antimicrobial peptides: an overview. *Biopolymers* **47:** 415-433.

Bazzo, R., Tappin, M.J., Pastore, A., Harvey, T.S., Carver, J.A. and Campbell, I.D. 1988. The structure of melittin. A 1H-NMR study in methanol. *Eur J Biochem* **173:** 139-146.

Bechinger, B., Zasloff, M. and Opella, S.J. 1992. Structure and interactions of magainin antibiotic peptides in lipid bilayers: a solid-state nuclear magnetic resonance investigation. *Biophys J* **62:** 12-14.

Dathe, M., Wieprecht, T., Nikolenko, H., Handel, L., Maloy, W.L., MacDonald, D.L., Beyermann, M. and Bienert, M. 1997. Hydrophobicity, hydrophobic moment and angle subtended by charged residues modulate antibacterial and haemolytic activity of amphipathic helical peptides. *FEBS Lett* **403:** 208-212.

Gibbs, A.C., Kondejewski, L.H., Gronwald, W., Nip, A.M., Hodges, R.S. and Wishart, D.S. 1999. Unusual beta-sheet periodicity in small cyclic peptides. *Nature Struct Biol* **5:** 284-288.

Guo, D., Mant, C.T., Taneja, A.K., Parker, J.M.R. and Hodges, R.S. 1986. Prediction of peptide retention times in reversed-phase high-performance liquid chromatography. 1. Determination of retention coefficients of amino acid residues of model synthetic peptides. *J Chromatogr* **359:** 499-517.

Hancock, R.E. 1981. Aminoglycoside uptake and mode of action-with special reference to streptomycin and gentamicin. II. Effects of aminoglycosides on cells. *J Antimicrob Chemother* **8:** 429-445.

Hancock, R.E. 1997. Peptide antibiotics. *Lancet* **349:** 418-422.

Hancock, R.E.W. and Lehrer, R. 1998. Cationic peptides: a new source of antibiotics. *Trends Biotechnol* **16:** 82-88.

Harwig, S.S., Swiderek, K.M., Lee, T.D. and Lehrer, R.I. 1995. Determination of disulphide bridges in PG-2, an antimicrobial peptide from porcine leukocytes. *J Pept Sci* **1:** 207-215.

Hetru, C., Letellier, L., Oren, Z., Hoffmann, J.A. and Shai, Y. 2000. Androctonin, a hydrophilic disulphide-bridged non-haemolytic anti- microbial peptide: a plausible mode of action. *Biochem J* **345 Pt 3:** 653-664.

Hirota, N., Mizuno, K. and Goto, Y. 1998. Group additive contributions to the alcohol-induced alpha-helix formation of melittin: implication for the mechanism of the alcohol effects on proteins. *J Mol Biol* **275:** 365-378.

Holak, T.A., Engstrom, A., Kraulis, P.J., Lindeberg, G., Bennich, H., Jones, T.A., Gronenborn, A.M. and Clore, G.M. 1988. The solution conformation of the antibacterial peptide cecropin A: a nuclear magnetic resonance and dynamical simulated annealing study. *Biochemistry* **27:** 7620-7629.

Jelokhani-Niaraki, M., Kondejewski, L.H., Farmer, S.W., Hancock, R.E., Kay, C.M. and Hodges, R.S. 2000. Diastereoisomeric analogues of gramicidin S: structure, biologicalactivity and interaction with lipid bilayers. *Biochem J* **349 Pt 3:** 747-755.

Juvvadi, P., Vunnam, S., Merrifield, E.L., Boman, H.G. and Merrifield, R.B. 1996. Hydrophobic effects on antibacterial and channel-forming properties of cecropin A-melittin hybrids. *J Pept Sci* **2:** 223-232.

Kawano, K., Yoneya, T., Miyata, T., Yoshikawa, K., Tokunaga, F., Terada, Y. and Iwanaga, S. 1990. Antimicrobial peptide, tachyplesin I, isolated from hemocytes of the horseshoe crab (Tachypleus tridentatus). NMR determination of the beta-sheet structure. *J Biol Chem* **265:** 15365-15367.

Khaled, M.A., Urry, D.W., Sugano, H., Miyoshi, M. and Izumiya, N. 1978. Hydrogen-deuterium substitution and solvent effects on the nitrogen-15 nuclear magnetic resonance of gramicidin S: evaluation of secondary structure. *Biochemistry* **17:** 2490-2494.

Kondejewski, L.H., Farmer, S.W., Wishart, D.S., Kay, C.M., Hancock, R.E. and Hodges, R.S. 1996. Modulation of structure and antibacterial and hemolytic activity by ring size in cyclic gramicidin S analogs. *J Biol Chem* **271:** 25261-25268.

Kondejewski, L.H., Jelokhani-Niaraki, M., Farmer, S.W., Lix, B., Kay, C.M., Sykes, B.D., Hancock, R.E. and Hodges, R.S. 1999. Dissociation of antimicrobial and hemolytic activities in cyclic peptide diastereomers by systematic alterations in amphipathicity. *J Biol Chem* **274:** 13181-13192.

Krause, E., Beyermann, M., Fabian, H., Dathe, M., Rothemund, S. and Bienert, M. 1996. Conformation of a water-soluble beta-sheet model peptide. A circular dichroism and Fourier-transform infrared spectroscopic study of double D-amino acid replacements. *J Peptide Protein Res* **48:** 559-568.

Kuo, M.C. and Gibbons, W.A. 1980. Nuclear Overhauser effect and cross-relaxation rate determinations of dihedral and transannular interproton distances in the decapeptide tyrocidine A. *Biophys J* **32:** 807-836.

Loh, B., Grant, C. and Hancock, R.E. 1984. Use of the fluorescent probe 1-N-phenylnaphthylamine to study the interactions of aminoglycoside antibiotics with the outer membrane of Pseudomonas aeruginosa. *Antimicrob Agents Chemother* **26:** 546-551.

Mant, C.T., Kondejewski, L.H. and Hodges, R.S. 1998. Hydrophilic interaction/cation-exchange chromatography for separation of cyclic peptides. *J Chromatogr A* **816:** 79-88.

Matsuzaki, K. 1999. Why and how are peptide-lipid interactions utilized for self-defense? Magainins and tachyplesins as archetypes. *Biochim Biophys Acta* **1462:** 1-10.

Matsuzaki, K., Sugishita, K., Fujii, N. and Miyajima, K. 1995. Molecular basis for membrane selectivity of an antimicrobial peptide, magainin 2. *Biochemistry* **34:** 3423-3429.

McInnes, C., Kondejewski, L.H., Hodges, R.S. and Sykes, B.D. 2000. Development of the structural basis for antimicrobial and hemolytic activities of peptides based on gramicidin S and design of novel analogs using NMR spectroscopy. *J Biol Chem* **275:** 14287-14294.

Miyata, T., Tokunaga, F., Yoneya, T., Yoshikawa, K., Iwanaga, S., Niwa, M., Takao, T. and Shimonishi, Y. 1989. Antimicrobial peptides, isolated from horseshoe crab hemocytes, tachyplesin II, and polyphemusins I and II: chemical structures and biological activity. *J Biochem (Tokyo)* **106:** 663-668.

Moore, R.A., Bates, N.C. and Hancock, R.E. 1986. Interaction of polycationic antibiotics with Pseudomonas aeruginosa lipopolysaccharide and lipid A studied by using dansyl-polymyxin. *Antimicrob Agents Chemother* **29:** 496-500.

Nakamura, T., Furunaka, H., Miyata, T., Tokunaga, F., Muta, T., Iwanaga, S., Niwa, M., Takao, T. and Shimonishi, Y. 1988. Tachyplesin, a class of antimicrobial peptide from the hemocytes of the horseshoe crab (Tachypleus tridentatus). Isolation and chemical structure. *J Biol Chem* **263:** 16709-16713.

Nicas, T.I. and Hancock, R.E. 1983. Alteration of susceptibility to EDTA, polymyxin B and gentamicin in Pseudomonas aeruginosa by divalent cation regulation of outer membrane protein H1. *J Gen Microbiol* **129:** 509-517.

Parker, J.M., Guo, D. and Hodges, R.S. 1986. New hydrophilicity scale derived from high-performance liquid chromatography peptide retention data: correlation of predicted surface residues with antigenicity and X-ray-derived accessible sites. *Biochemistry* **25:** 5425-5432.

Pathak, N., Salas-Auvert, R., Ruche, G., Janna, M.H., McCarthy, D. and Harrison, R.G. 1995. Comparison of the effects of hydrophobicity, amphiphilicity, and alpha-helicity on the activities of antimicrobial peptides. *Proteins* **22:** 182-186.

Prenner, E.J., Lewis, R.N., Jelokhani-Niaraki, M., Hodges, R.S. and McElhaney, R.N. 2001. Cholesterol attenuates the interaction of the antimicrobial peptide gramicidin S with phospholipid bilayer membranes. *Biochim Biophys Acta* **1510:** 83-92.

Prenner, E.J., Lewis, R.N., Kondejewski, L.H., Hodges, R.S. and McElhaney, R.N. 1999. Differential scanning calorimetric study of the effect of the antimicrobial peptide gramicidin S on the thermotropic phase behavior of phosphatidylcholine, phosphatidylethanolamine and phosphatidylglycerol lipid bilayer membranes. *Biochim Biophys Acta* **1417:** 211-223.

Rothemund, S., Krause, E., Beyermann, M., Dathe, M., Bienert, M., Hodges, R.S., Sykes, B.D. and Sonnichsen, F.D. 1996. Peptide destabilization by two adjacent D-amino acids in single- stranded amphipathic alpha-helices. *Pept Res* **9:** 79-87.

Sereda, T.J., Mant, C.T., Sonnichsen, F.D. and Hodges, R.S. 1994. Reversed-phase chromatography of synthetic amphipathic alpha-helical peptides as a model for ligand/receptor interactions. Effect of changing hydrophobic environment on the relative hydrophilicity/hydrophobicity of amino acid side-chains. *J Chromatogr A* **676:** 139-153.

Storici, P. and Zanetti, M. 1993. A novel cDNA sequence encoding a pig leukocyte antimicrobial peptide with a cathelin-like pro-sequence. *Biochem Biophys Res Commun* **196:** 1363-1368.

van 't Hof, W., Veerman, E.C., Helmerhorst, E.J. and Amerongen, A.V. 2001. Antimicrobial peptides: properties and applicability. *Biol Chem* **382:** 597-619.

Wieprecht, T., Dathe, M., Beyermann, M., Krause, E., Maloy, W.L., MacDonald, D.L. and Bienert, M. 1997. Peptide hydrophobicity controls the activity and selectivity of magainin 2 amide in interaction with membranes. *Biochemistry* **36:** 6124-6132.

Wishart, D.S., Kondejewski, L.H., Semchuk, P.D., Sykes, B.D. and Hodges, R.S. 1996. A method for the facile solid phase synthesis of gramicidin S and its analogs. *Letters Peptide Sci* **3:** 53-60.

Zasloff, M. 1987. Magainins, a class of antimicrobial peptides from Xenopus skin: isolation, characterization of two active forms, and partial cDNA sequence of a precursor. *Proc Natl Acad Sci U S A* **84:** 5449-5453.

Zhang, L., Dhillon, P., Yan, H., Farmer, S. and Hancock, R.E. 2000a. Interactions of bacterial cationic peptide antibiotics with outer and cytoplasmic membranes of Pseudomonas aeruginosa. *Antimicrob Agents Chemother* **44:** 3317-3321.

Zhang, L., Scott, M.G., Yan, H., Mayer, L.D. and Hancock, R.E. 2000b. Interaction of polyphemusin I and structural analogs with bacterial membranes, lipopolysaccharide, and lipid monolayers. *Biochemistry* **39:** 14504-14514.

Zhou, N.E., Mant, C.T. and Hodges, R.S. 1990. Effect of preferred binding domains on peptide retention behavior in reversed-phase chromatography: amphipathic alpha-helices. *Pept Res* **3:** 8-20.

Chapter 6: Effects of single D-amino acid substitutions on disruption of β-sheet structure and hydrophobicity in cyclic 14-residue antimicrobial peptide analogs related to gramicidin S

A version of this chapter has been submitted. Lee, D. L., Powers, J.-P. S., Vasil, M. L., Pflegerl, K., Hancock, R. E. W., and Hodges, R. S. 2003. Journal of Peptide Research.

Chapter 6-1. Introduction

Pathogens that are becoming resistant to conventional antibiotics has emerged as a prominent global health concern, as the number of resistant bacterial strains has increased significantly in the last decades (Lohner et al. 2001). The issue has brought attention to the need for alternative antimicrobial agents that bacteria have not or are unlikely to develop resistance mechanisms against. In the past two decades, a number of naturally occurring cationic antimicrobial peptides have been identified and characterized in a wide range of organisms (Ganz et al. 1998; Hancock et al. 2000; Tossi et al. 2000; van 't Hof et al. 2001). In contrast with conventional antibiotics that specifically inhibit essential molecules such as enzymes involved in cell wall synthesis, transcription or translation, these peptides are thought to directly interact with and disrupt the stability of the microbial membrane (Merrifield 1994). Therefore, killing is rapid (minutes *vs.* hours or days) fairly nonspecific (active against a broad spectrum of Gram-positive and Gram-negative bacteria) and does not produce bacteria resistant to this mode of action (Oren et al. 2001).

Gramicidin S (GS) is an antimicrobial peptide that has been the subject of numerous structure-activity studies (Aarstad et al. 1979; Ando et al. 1983; Balasubramanian 1967;

Conti 1969; Jelokhani-Niaraki et al. 2000; Katsu et al. 1986; Kondejewski et al. 1996b; Tamaki et al. 1996; Tamaki et al. 1995; Yonezawa et al. 1986; Zidovetzki et al. 1988). It is active against both Gram-negative and Gram-positive bacteria (Kondejewski et al. 1996a), but has had limited applications as a therapeutic antimicrobial agent because of its high toxicity to human cells. GS is a cyclic 10-residue β-sheet peptide sharing features common to many antimicrobial peptides, including an overall positive (+2) charge, secondary structure in the membrane, and some degree of amphipathicity (nonpolar and polar faces).

Recently, efforts have been made to design peptides related to gramicidin S that increase specificity towards microbial cells *vs.* eukaryotic cells, based on the differences in membrane lipid composition between prokaryotes and eukaryotes. Attempts have been made to dissociate antimicrobial activity from hemolytic activity by changing parameters such as ring size, β-sheet structure, and amphipathicity (Kondejewski et al. 1996b; Kondejewski et al. 1999; Tamaki et al. 1995). GS analogs of 4 to 14 amino acids were prepared and tested for biological activity. Although a *de novo*-designed peptide, GS14, enabled dissociation between antimicrobial activity and hemolytic activity, the result (poor antimicrobial activity and strong hemolytic activity, *i.e.* a low therapeutic index) was opposite to that desired. Nevertheless, this study demonstrated that it was possible to alter membrane specificity between prokaryotic and eukaryotic cells by sequence manipulation.

In a subsequent study of GS14 analogs, introducing D-enantiomers in the ten β-strand positions that normally contain L-amino acids reversed this specificity profile. These GS14 diastereomers had disrupted β-sheet structure in benign medium and reduced amphipathicity due to positioning of the D-amino acid side-chain on the opposite face of the molecule compared to the L-counterpart. In the absence of structural changes, inversion of the optical center of single amino acids resulted in nonpolar amino acids on the polar face and polar amino acids on the nonpolar face, while maintaining the same overall hydrophobicity as GS14. The peptide with the highest therapeutic index (hemolytic activity/antimicrobial activity) was a GS14 diasteromer with D-Lys substituted at position 4 (GS14K4) (Kondejewski et al. 1999).

In this study, we continue to investigate the effects of enantiomeric substitutions in GS14. Here, we substitute single D-amino acids other than D-Lys at position 4, in an attempt to further increase microbial specificity and reduce hemolytic activity. These substitutions, in addition to disrupting β-sheet structure and affecting amphipathicity, also change the overall peptide hydrophobicity. To determine which of these parameters are responsible for the changes in biological activity, we also studied GS14 peptides with the corresponding L-amino acid at position 4 to compare differences in structure, amphipathicity and activity between D- and L-diastereomers. In addition, we substituted the achiral amino acid glycine at position 4 to examine its effect on disruption of β-sheet structure and biological activity in the absence of a side chain. We find here that all L-substituted peptides maintained a β-sheet structure, and generally have strong hemolytic activity and weak antimicrobial activity. Although the Gly substitution disrupted β-sheet structure, it did not significantly improve hemolytic or antimicrobial activity over the L-substitutions. The D-substitutions disrupted β-sheet structure, with varying improvements in hemolytic and antimicrobial activity. Polar D-substitutions provided the best improvements in therapeutic index, with the D-Lys substituted peptide yielding the highest therapeutic indices in this study against all microorganisms tested. Our work suggests that obtaining GS14 analogs with a high therapeutic index requires a combination of a disrupted β-sheet structure in benign medium that becomes more structured in membranes, reduced amphipathicity relative to GS14, and an optimized overall hydrophobicity.

Chapter 6-2. Results

Peptide Design. The peptide sequences used in this study were based on the GS14 sequence (Kondejewski et al. 1996b), with amino acids substituted at position 4 (Fig. 6-1). GS14 is a cyclic β-sheet peptide possessing high amphipathicity, *i.e.* nonpolar and polar residues are distributed on opposite faces of the molecule (Fig. 6-2, left, (McInnes et al. 2000)). Although GS14 exhibited strong hemolytic activity and weak antimicrobial activity, diastereomers with D-amino acid substitutions at various ring positions disrupted β-sheet structure and decreased amphipathicity, resulting in weaker hemolytic activity and stronger antimicrobial activity, *i.e.* a higher therapeutic index (Kondejewski et al. 1999). Notably, the GS14 diastereomer with D-Lys at position 4 had the highest therapeutic index (GS14K_D4, Fig. 6-1) compared to other diastereomers at other positions in the two strands of the β-sheet. For this reason, we chose to study position 4 diastereomers, substituting D-amino acids covering a broad range of hydrophobicities, to compare structure and activity relationships.

If the GS14X_D4 diasteromers in this study are structurally similar to GS14K_D4 (as we anticipate with a constrained head-to-tail cyclic peptide), the substituted D-amino acids should be positioned on the nonpolar face, disrupt β-sheet structure, and alter both amphipathicity and affect overall hydrophobicity of the nonpolar face (Fig. 6-2, right).

Peptide Name	Sequence
GS14X$_L$4 series	**2 4 6 8 10 12 14**
GS14	cyclo- VKLKV***Y***PLKVKL***Y***P
GS14L$_L$4	cyclo- ---L----------
GS14F$_L$4	cyclo- ---F----------
GS14Y$_L$4	cyclo- ---Y----------
GS14N$_L$4	cyclo- ---N----------
GS14X$_D$4 series	
GS14K$_D$4	cyclo- ---***K***----------
GS14L$_D$4	cyclo- ---***L***----------
GS14F$_D$4	cyclo- ---***F***----------
GS14Y$_D$4	cyclo- ---***Y***----------
GS14N$_D$4	cyclo- ---***N***----------
GS14G4	cyclo- ---G----------

Figure 6-1. Sequences of GS14X4 peptides used in this study, where X is the amino acid substituted at position 4, and the subscript L or D denotes the stereochemistry. One-letter amino acid code is used; bold italicized letters denote D-amino acids. The peptides are cyclized between the α-NH_2 and α-COOH groups.

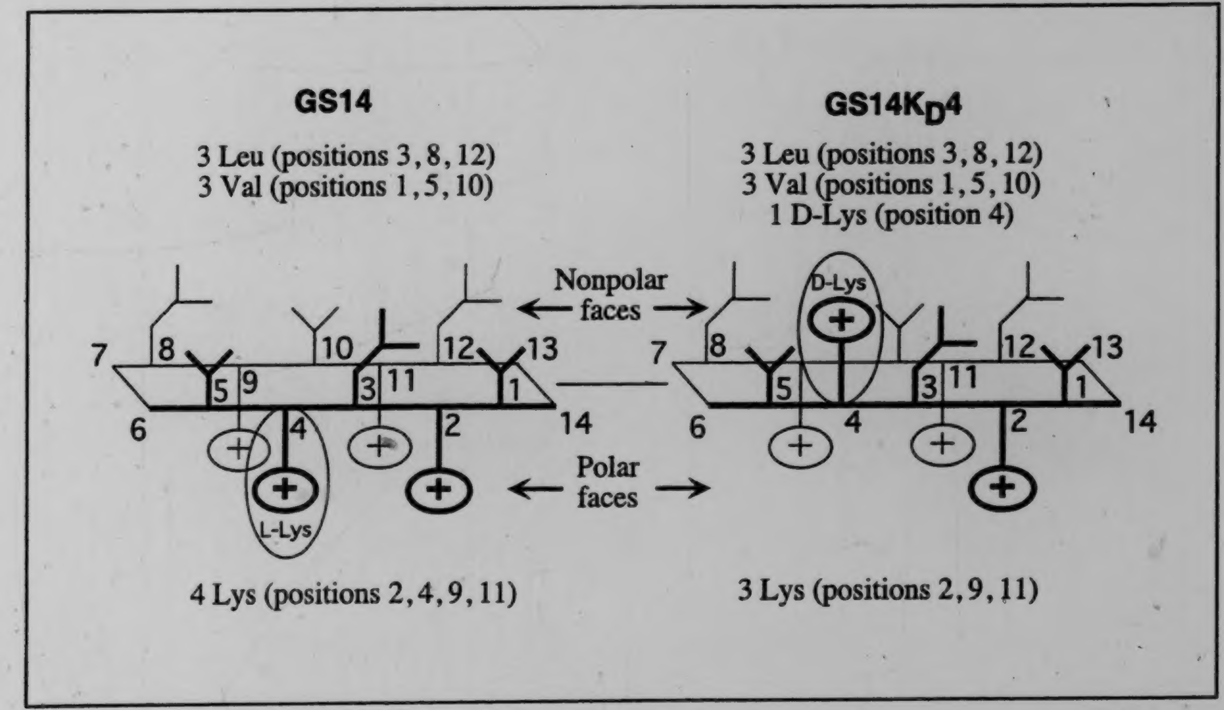
GS14
3 Leu (positions 3, 8, 12)
3 Val (positions 1, 5, 10)
GS14K$_D$4
3 Leu (positions 3, 8, 12)
3 Val (positions 1, 5, 10)
1 D-Lys (position 4)
Nonpolar faces
Polar faces
D-Lys
L-Lys
7
8
5
9
10
3
11
12
13
1
6
4
2
14
4 Lys (positions 2, 4, 9, 11)
3 Lys (positions 2, 9, 11)

Figure 6-2. Representations of GS14X4 analogs. L-amino acid substitutions at position 4 project onto the polar face (left panel), while D-amino acids at position 4 project onto the nonpolar face (right panel). The bold portions of the molecule denote proximity to the viewer.

Furthermore, we predict that GS14X$_L$4 peptides, though differing in hydrophobicity and amphipathicity, will remain β-sheet in a manner consistent with the GS14 structure. In this study, we present data for six amino acid substitutions at position 4 (a total of eleven peptides: five GS14X$_L$4, five GS14X$_D$4, and GS14G4) representing a range of hydrophobicities found among the twenty amino acids. The substitutions include Gly (no side-chain), Lys (polar charged), Asn (polar), Tyr and Phe (aromatic hydrophobes) and Leu (large aliphatic hydrophobe). Our goal is to improve the combined effects of D-amino acids (β-sheet disruption and changes in hydrophobicity and amphipathicity) on biological specificity of these cyclic 14-residue peptides.

CD Spectroscopy. We examined secondary structures of GS14X4 peptides in benign and membrane-mimicking solvents (see Chapter 2 for methods). GS14X$_L$4 peptides form β-sheet structures in benign conditions, as shown by their CD spectra with local minima at 205 and 220 nm (Fig. 6-3, top). The spectra of these peptides are not characteristic of conventional β-sheet spectra. Due to the major contribution of the β-turns to molar ellipticity at ~208 nm, the spectra appear similar to the representative spectrum of an α-helix (Kondejewski et al. 1999). Therefore, an estimate of per cent β-sheet could not be calculated. In 50% trifluoroethanol (TFE), the GS14X$_L$4 peptides became more structured, as indicated by the increase in negative molar ellipticity observed, for example, in GS14L$_L$4 (Fig. 6-3, top, and Table 6-1). The Gly-substituted GS14G4 went from a disrupted β-sheet in benign solution (maxima shifted from 205 nm to ~202 nm and decreased negative molar ellipticity at 220 nm *vs.* GS14L$_L$4 spectrum - Fig. 6-3, panel A) to a more ordered structure in TFE. Similarly, the D-substitutions also disrupted β-sheet structure in benign media and formed a more ordered structure in TFE.

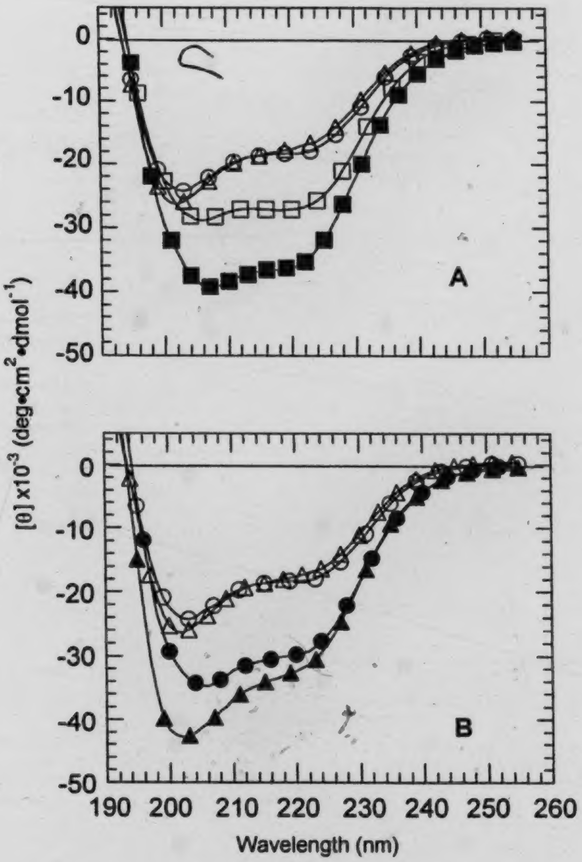

Figure 6-3. Representative circular dichroism spectra of GS14X4 peptides. Panel A: peptides with D-Leu (open triangles), Gly (open circles) and L-Leu (open squares) substituted at position 4 in benign buffer (5 mM sodium acetate, pH 5.5, at 20°C). Closed squares denote the L-Leu peptide in 5 mM sodium acetate, pH 5.5 at 20°C, 50% trifluoroethanol. Panel B: peptides in the presence (closed symbols) and absence (open symbols) of 50% TFE.

Table 6-1. Circular dichroism data for GS14 analogs

Substitution	$[\theta]_{220}$ Benign[2]			$[\theta]_{220}$ 50% TFE[3]			$\Delta[\theta]_{220}$ TFE-benign[4]	
	L	D	Δ(L-D)	L	D	Δ(L-D)	L	D
Leu	-27200	-17600	-9600	-36200	-32300	-3900	-9000	-14700
Phe	-26200	-24100	-2100	-36100	-34000	-2100	-9900	-9900
Tyr	-27300	-23000	-4300	-34200	-29900	-4300	-6900	-6900
Asn	-29600	-11200	-18400	-37300	-23400	-13900	-7700	-12200
Lys	-26300	-14200	-12100	-33600	-27800	-5800	-7300	-13600
Gly	-18400			-29700			-11300	

[1] Amino acid substitution at position 4 of GS14. Side-chain stereochemistry is denoted above columns labelled L and D, with achiral Gly listed between L and D columns.

[2] Peptide mean residue molar ellipticity at 220 nm in benign medium (5 mM sodium acetate, pH 5.5, 20°C. Δ(L-D) is the difference in mean residue molar ellipticity between the L-diastereomer and D-diastereomer.

[3] Peptide mean residue molar ellipticity at 220 nm in 50% trifluoroethanol, 5 mM sodium acetate, pH. 5.5.

[4] Inducible structure, calculated as the difference between molar ellipticities at 220 nm for peptides in 50% TFE and benign conditions.

Differences were observed between GS14G4 and GS14X$_D$4 spectra in TFE at the 205 nm minimum (Fig. 6-3, panel B). In TFE, $[\theta]_{220}$ values were generally similar for L- and D-diastereomers and GS14G4 ranging from –34000 to –27800, with the exception of D-Asn at –23400. The extent of inducible structure ($[\theta]_{220}$ (TFE-benign), Table 6-1) was greater for some D-diastereomers vs. L-diastereomers because the GS14X$_D$4 peptides were less structured in benign conditions. The achiral Gly substituted peptide showed inducible structure ($[\theta]_{220}$(TFE-benign)=-11300) intermediate between D- and L-diastereomers. The disruption of structure by Gly in benign solvent was also intermediate between D- and L-substitutions. There appeared to be no correlation between hydrophobicity of the substituted D-amino and the extent of inducible structure. For example, both GS14K$_D$4 and GS14L$_D$4 exhibited a disrupted structure in benign media and large induced ellipticity in 50% TFE (Table 6-1), even though they are at opposite extremes of the amino acid hydrophobicity scale (Sereda et al. 1994).

Analytical HPLC. Although reversed-phase HPLC (RP-HPLC) can be used to resolve molecules based on differences in overall hydrophobicity, the technique is also sensitive to conformational changes which alter the hydrophobicity of the preferred binding domain (nonpolar face) in an amphipathic molecule. In addition to achieving separation for peptides with different intrinsic hydrophobicities, *e.g.* those within the GS14X$_L$4 or GS14X$_D$4 series (Fig. 6-4), we also observed different retention times between D- and L-diastereomers with the same inherent hydrophobicities (Table 6-2). Figure 6-4 shows that there is a very broad range of retention times for D-diastereomers (18.1 min) *vs.* L-diastereomers (3.5 min), presumably because the D-amino acids are positioned on the GS14 nonpolar face, which forms the preferred binding domain that is the major

Table 6-2. HPLC retention times for GS14X4 peptides

Substitution[1]	t_R[2] (min)		$\Delta t_{R,\,Gly}$[3] (min)	
	L	D	L	D
Leu	49.8	55.1	0.8	6.1
Phe	50.2	54.4	1.2	5.4
Tyr	49.6	47.3	0.6	-1.7
Asn	49.7	42.1	0.7	-6.9
Lys	46.7	37.0	-2.3	-12.0
Gly	49.0		0.0	

[1] Amino acid substitution at position 4 of GS14. Side-chain stereochemistry is denoted above columns labelled L and D, with achiral Gly listed between L and D columns.

[2] Peptide retention time from a reversed-phase HPLC column eluted at 1% acetonitrile/min (see Chapter 2 for HPLC conditions).

[3] Peptide RP-HPLC retention time relative to GS14G4 retention time, calculated as Δt_R(GS14X4) - t_R(GS14G4).

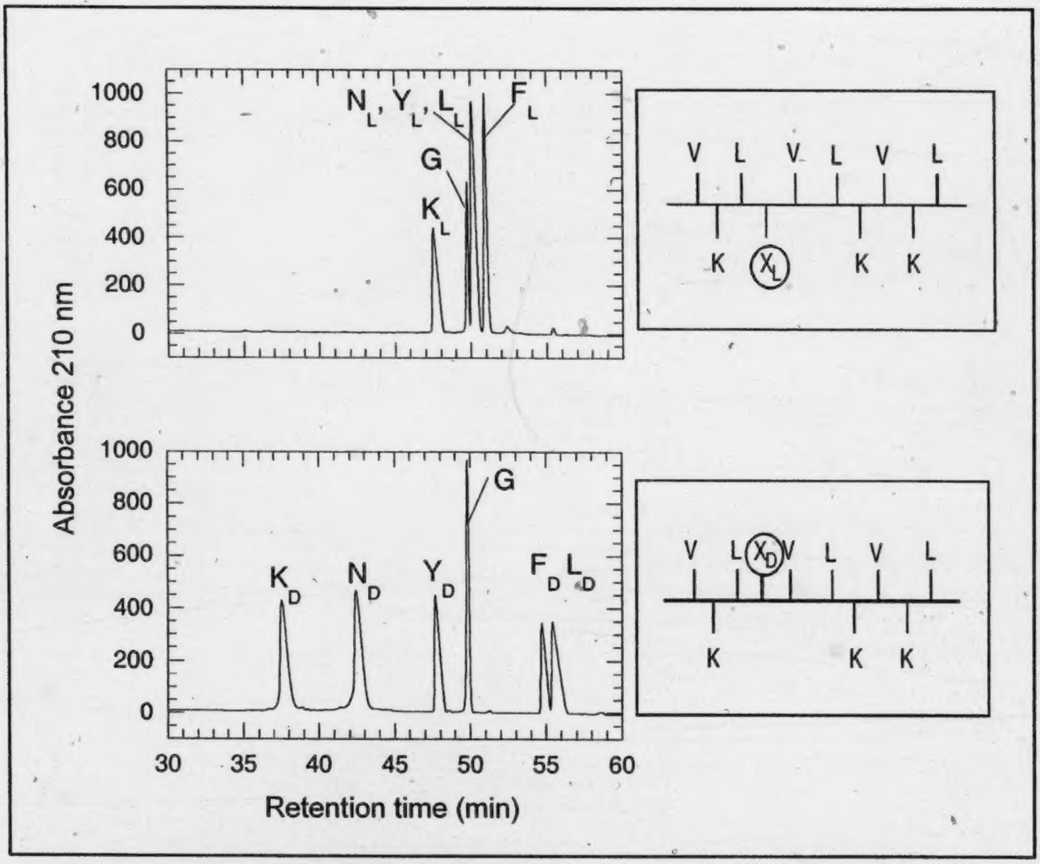

Figure 6-4. Reversed-phase HPLC separation of the 14-residue cyclic peptides with L-amino acid substitutions at position 4 (X_L, top panel) and D-amino acid substitutions at position 4 (X_D, lower panel). Inset panels show the position of substituted amino acids in relation to the peptide nonpolar and polar faces. One-letter code is used to denote the amino acid substitution, with the subscript L or D indicating the side chain stereochemistry.

interaction with the hydrophobic column matrix to determine peptide retention time. Polar D-substitutions such as D-Asn and D-Lys change the hydrophobicity of the preferred binding domain the most, thus decreasing retention time. In contrast, peptides substituted with L-Leu, L-Tyr and L-Asn were not resolved even though the intrinsic hydrophobicity of these side-chains are enormously different. The hydrophobicity of the substituted D-amino acid thus determines the relative retention time of the D-diastereomer, while substituted L-amino acids (on the GS14 polar face) have little effect on peptide retention time. In other words, substitution of amino acids on the polar face have little effect on overall peptide hydrophobicity, since they have little effect on the hydrophobicity of the preferred binding domain. The results suggest that the GS14X_D4 peptides indeed have their D-side chains positioned on the nonpolar face.

In comparing retention times between GS14X_L4 and GS14X_D4 peptides, those that the oeotudes retained more strongly than their respective diastereomers contained sequences possessing a higher amphipathic character, *i.e.* containing either nonpolar D-substitutions on the nonpolar face, or polar L-substitutions on the polar face (Table 6-2). It is interesting to note that GS14X_D4 peptides with polar D-amino acids eluted in an order generally consistent with previous hydrophobicity scales obtained by RP-HPLC (Sereda et al. 1994). In summary, peptides used in this study have a broad range of intrinsic hydrophobicities and amphipathicities, as indicated by examination of their sequences, with RP-HPLC separation achieved through differences in one or both of these parameters.

Hemolytic Activity. All L-diastereomers and GS14G4 were strongly hemolytic (Table 6-3). D-diastereomers were generally less hemolytic when the substituted amino acid was very polar (D-Asn and D-Lys), with GS14K_D4 being the most polar and the least hemolytic peptide in this study (Fig. 6-5). Hemolytic activity was strong for both D- and L-substitutions with the nonpolar amino acids Leu and Phe, possibly because these amino acids raised the overall hydrophobicity past a critical point. Although the killing mechanism of these peptides has not been determined, the increased hydrophobicity may increase specificity towards eukaryotic membranes through interactions between peptide and uncharged lipids found only in eukaryotes, such as cholesterol. Although GS14G4 exhibited a disrupted β-sheet structure in benign media, the Gly substitution also makes the polar face of GS14 less hydrophilic, increasing overall hydrophobicity and decreasing amphipathicity. Therefore, in the case of GS14G4, inducible structure was not sufficient to make this peptide active specifically against bacteria.

Antimicrobial Activity. L-diastereomers were, in general, considerably less active against all microorganisms assayed *versus* their D-counterparts (Tables 6-3 and 6-4). D-diastereomers had more complicated patterns for activity, and did not display a simple dependence on polarity of the substituted amino acid, in contrast with hemolysis results (Fig. 6-5). It is important to note that hemolytic activity and antimicrobial activity are shown in Fig. 6-5 in reciprocal units, to allow facile comparisons between hemolytic activity, antimicrobial activity and therapeutic index (higher values always correspond to higher activities). Between Gram-positive bacteria, Gram-negative bacteria, and yeast, the antimicrobial activity of GS14X_D4 peptides was generally stronger against Gram-positive bacteria (see GS14Y_D4 results, Fig. 6-5). Although GS14X_D4 peptides with nonpolar substitutions displayed some antimicrobial activity, the most active peptide against Gram-positive bacteria and yeast, GS14Y_D4, and the most active against Gram-

Table 6-3. Biological activity of GS14 analogs against yeast and Gram-negative bacteria

Substitution[1]	Hemolytic activity[2] (μg/ml)		*C. albicans* [3]					*E. coli* 1[3]					*E. coli* 2[3]					*S. typhimurium* [3]				
			MIC[4] (μg/ml)		Index[5]		Gain[6] (D/L)	MIC[4] (μg/ml)		Index[5]		Gain[6] (D/L)	MIC[4] (μg/ml)		Index[5]		Gain[6] (D/L)	MIC[4] (μg/ml)		Index[5]		Gain[6] (D/L)
	L	D	L	D	L	D		L	D	L	D		L	D	L	D		L	D	L	D	
Leu	3	5	90	40	0.03	0.1	3	>90	>80	0.02	0.04	2	45	20	0.06	0.2	3	>90	>80	0.02	0.04	2
Phe	3	2	>90	6	0.02	0.2	10	>90	>48	0.02	0.01	0.5	45	6	0.07	0.2	3	>90	>48	0.02	0.01	0.5
Tyr	8	5	>64	2.5	0.06	2	33	64	5	0.06	1	17	32	2.5	0.20	2	10	>64	5	0.06	1	17
Asn	2	62	>64	16	0.02	4	200	>64	32	0.02	2	100	32	8	0.06	8	133	>64	8	0.02	8	400
Lys	2	125	32	16	0.06	8	133	64	8	0.02	16	800	32	2	0.06	62	1033	32	2	0.06	62	1033
Gly	3		96		0.03		-	>96		0.02		-	48		0.06		-	96		0.03		-

[1] Amino acid substitution at position 4 of GS14. Side chain stereochemistry is denoted above columns labelled L and D, with achiral Gly listed between L and D columns.

[2] Minimal peptide concentration required for complete red blood cell lysis after 24 hr. at 37 C (see Methods). The peptide showing the weakest hemolytic activity is shaded.

[3] Bacterial strain assayed. *C. albicans* is wild-type *Candida albicans* ; *E. coli* 1 is wild-type *Escherichia coli* strain UB1005; *E. coli 2* is antibiotic-sensitive strain DC2; *S. typhimurium* is antibiotic-sensitive *Salmonella typhimurium* strain C610.

[4] Minimal peptide concentration required to completely inhibit bacterial growth after 24 h. Peptides showing strong (<10 μg/ml) activity are highlighted.

[5] Therapeutic index, calculated as hemolytic activity (μg/ml)/MIC (μg/ml). MIC values that exceeded the highest concentration tested were arbitrarily assigned the value 128 μg/ml for calculations.

[6] Gain or improvement in therapeutic index for GS14X$_D$4 over GS14X$_L$4 diastereomers. Gain is calculated as (therapeutic index, D-diastereomer)/(therapeutic index, L-diastereomer). The largest improvement in specificity of the D-peptide over the L-peptide is shaded.

Table 6-4. Biological activity of GS14 analogs against Gram-positive bacteria

Substitution[1]	Hemolytic activity[2] (μg/ml)		*S. aureus* 1[3]					*S. aureus* 2[3]					*S. epidermidis*[3]					*B. subtilis*[3]				
			MIC[4] (μg/ml)		Index[5]		Gain[6] (D/L)	MIC[4] (μg/ml)		Index[5]		Gain[6] (D/L)	MIC[4] (μg/ml)		Index[5]		Gain[6] (D/L)	MIC[4] (μg/ml)		Index[5]		Gain[6] (D/L)
	L	D	L	D	L	D		L	D	L	D		L	D	L	D		L	D	L	D	
Leu	3	5	45	10	0.1	0.6	6	11	5	0.2	1.2	6	22	5	0.1	1.2	12.2	90	40	0.03	0.1	3
Phe	3	2	45	3	0.1	0.7	7	11	3	0.3	0.7	2	45	1.5	0.1	1	10	90	12	0.03	0.1	3
Tyr	8	5	32	1.2	0.2	4	20	16	1.2	0.5	4	8	32	0.6	0.2	8	40	>64	1.2	0.10	4	40
Asn	2	62	32	32	0.1	2	20	16	16	0.1	4	40	16	4	0.1	16	160	>64	32	0.01	2	200
Lys	2	125	16	32	0.1	4	40	16	16	0.1	8	80	8	8	0.2	16	80	>64	8	0.01	16	1600
Gly	3		12		0.2		-	12		0.2		-	12		0.2		-	48	48	0.10	0.1	-

[1] Amino acid substitution at position 4 of GS14. Side chain stereochemistry is denoted above columns labelled L and D, with achiral Gly listed between L and D columns.

[2] Minimal peptide concentration required for complete red blood cell lysis after 24 hr. at 37 C (see Methods). The peptide showing the weakest hemolytic activity is shaded.

[3] Bacterial strain assayed. *S. aureus* 1 is wild-type *Staphylococcus aureus* strain 25923; *S. aureus* 2 is methicillin-resistant strain SAP0017; *S. epidermidis* is wild-type strain C621; *B. subtilis* is wild-type *Bacillis subtilis* .

[4] Minimal peptide concentration required to completely inhibit bacterial growth after 24 h. Peptides showing strong (<10 μg/ml) activity are highlighted.

[5] Therapeutic index, calculated as hemolytic activity (μg/ml)/MIC (μg/ml). MIC values that exceeded the highest concentration tested were arbitrarily assigned the value 128 μg/ml for calculations.

[6] Gain or improvement in therapeutic index for GS14X_D4 over GS14X_L4 diastereomers. Gain is calculated as (therapeutic index, D-diastereomer)/(therapeutic index, L-diastereomer). The largest improvement in specificity of the D-peptide over the L-peptide is shaded.

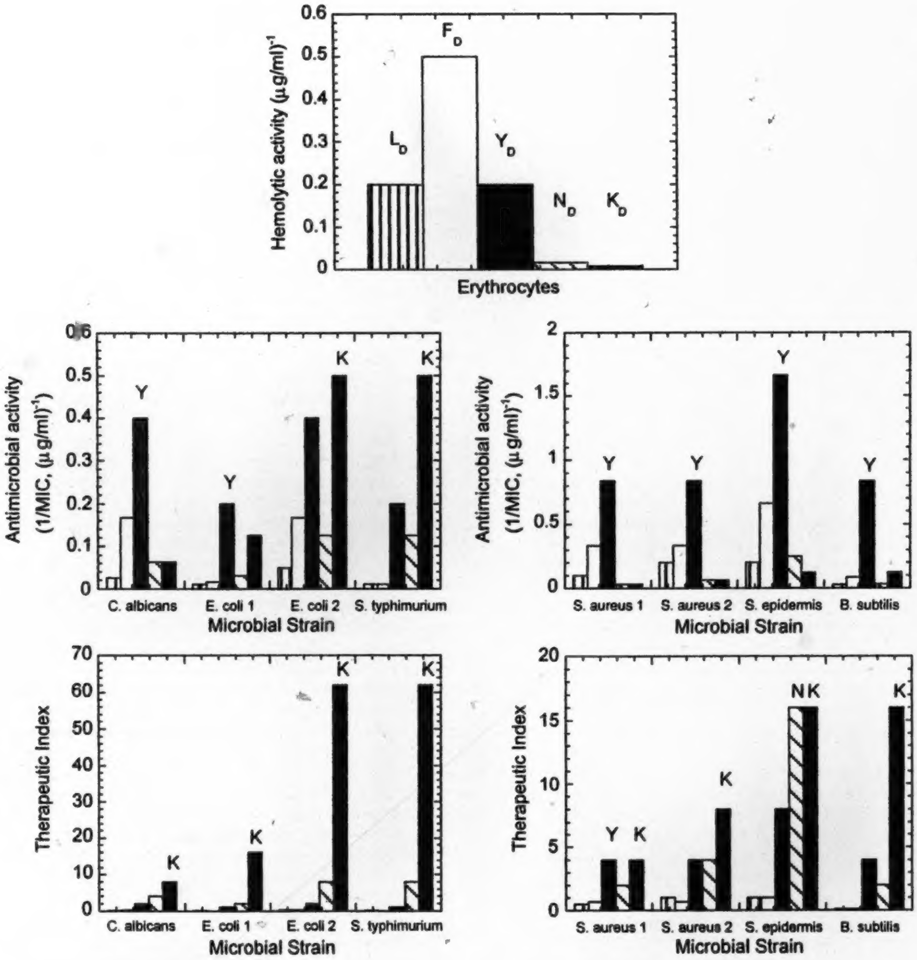

Figure 6-5. Biological activity of GS14X_D4 peptides. Top panel: hemolytic activity of peptides substituted with D-amino acids, plotted in reciprocal units, $(\mu g/ml)^{-1}$. Peptides were displayed from left to right in the order of decreasing overall hydrophobicity as follows: vertical stripes, GS14L_D4; open box, GS14F_D4; gray box, GS14Y_D4; descending diagonal stripes, GS14N_D4; black box, GS14K_D4. Second and third panels, antimicrobial activity of GS14X_D4 peptides against yeast and Gram-negative and Gram-positive bacteria, plotted in reciprocal units, $(\mu g/ml)^{-1}$. Fourth and fifth panels, therapeutic index of GS14X_D4 peptides against yeast and Gram-negative and Gram-positive bacteria. Higher values in the graphs indicate stronger hemolytic activity, more potent antimicrobial activity, and a higher therapeutic index. Microbial strains were the same as those reported in Tables 6-3 and 6-4. Peptides with L-amino acids or Gly substituted at position 4 displayed strong hemolytic activity and poor antimicrobial activity, resulting in a low therapeutic index (< 1), and were omitted from graphs (see Tables 6-3 and 6-4 for activity values).

negative bacteria, GS14K$_D$4, both contained polar substitutions (Fig. 6-5). D-Tyr was the most active peptide against six strains tested (4 Gram-positive, 1 yeast and 1 Gram-negative) and was second-most active in the other two Gram-negative strains.

Therapeutic Index. Peptides with a consistently poor therapeutic index (TI<1) against all microbial strains tested were the L-diastereomers in the GS14X$_L$4 series, as well as peptides substituted with Gly, D-Phe, and D-Leu (Tables 6-3 and 6-4). In the GS14X$_D$4 series, the value of TI *vs.* Gram negative organisms increases with increasing polarity of the D-substitution (as measured by RP-HPLC retention time, Fig. 6-6), but there is no obvious relationship between TI in Gram positive bacteria and retention time (Fig. 6-5).

The peptide with the best therapeutic index against Gram-negative bacteria and yeast was GS14K$_D$4 (Fig. 6-6, Table 6-3). We saw both improved antimicrobial activity *versus* Gram-negative bacteria and decreased hemolytic activity for GS14K$_D$4 compared with its diastereomer, GS14 (Table 6-3, Fig. 6-5). Interestingly, against Gram-positive bacteria, GS14K$_D$4 also had the best therapeutic index. Overall TI values were lower, however, compared to those *vs.* Gram-negative bacteria, because there was little or no improvement in antimicrobial activity compared to GS14 (maximum TI of 16 *vs.* 62, Tables 6-3 and 6-4).

If we turn our attention away from absolute values of therapeutic index and instead focus on relative gains in therapeutic index in switching from L- to D-diastereomers, we see that GS14X$_D$4 peptides with hydrophobic substitutions displayed little or no improvement. In contrast, GS14N$_D$4 (20 to 400-fold) and GS14K$_D$4 (40 to 1600-fold) were notable for their considerable improvement in activity over their L-diastereomers (Tables 6-3 and 6-4). GS14N$_D$4 showed a gain in TI over its diastereomer primarily

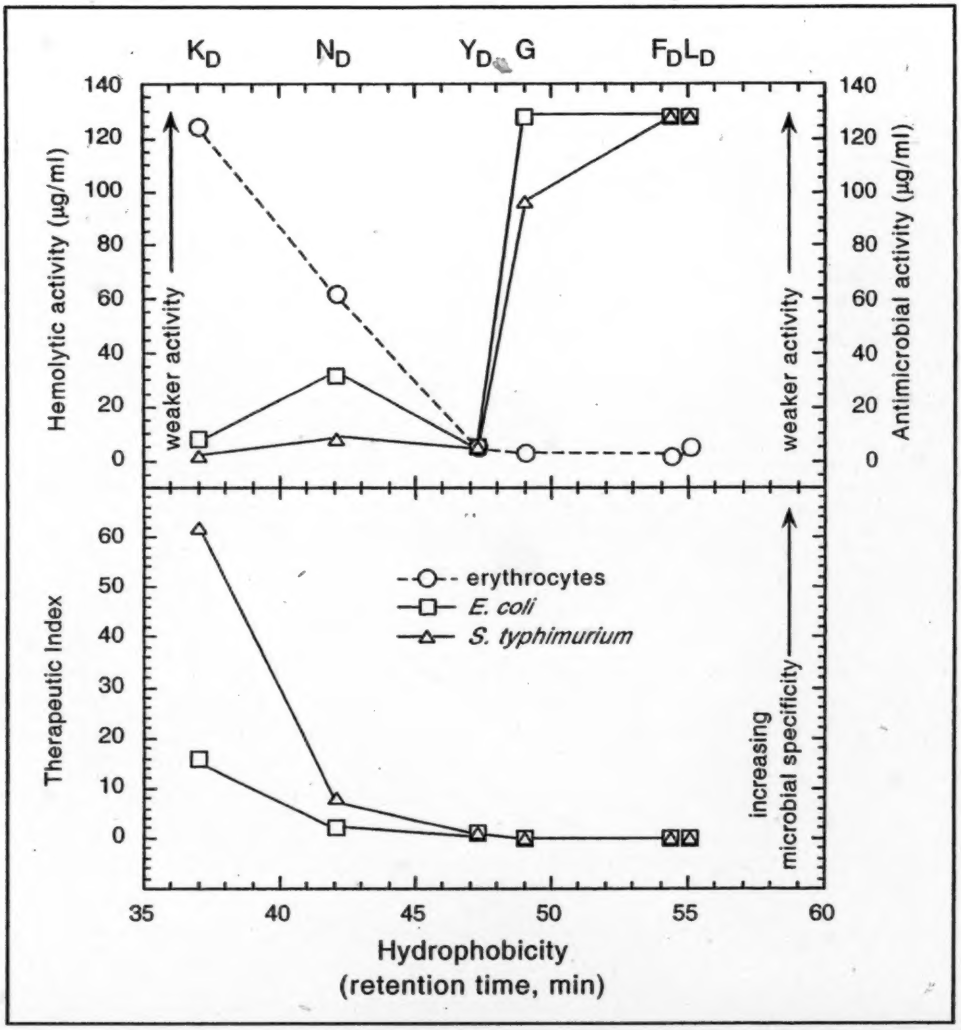

Figure 6-6. Comparison of biological activity and hydrophobicity of GS14X_D4 peptides. Upper panel: hemolytic activity against human erythrocytes (dashed line) and antimicrobial activity (solid line) against *E. coli* UB1005 (open squares) and *S. typhimurium* C610 (open triangles) were plotted *versus* reversed-phase HPLC retention times of the peptide analogs. Amino acid substitutions at position 4 are listed above their respective peptide retention times. One letter codes are used, with the subscript D denoting side-chain stereochemistry. Lower panel: therapeutic index (hemolytic activity÷antimicrobial activity) of GS14X4 peptides for *E. coli* UB1005 and *S. typhimurium* C610.

because it had reduced hemolytic activity, GS14Y_D4 improved because of its stronger antimicrobial activity, and GS14K_D4 showed the best improvement by favorably altering both antimicrobial and hemolytic activity. Therefore, in this study polar D-enantiomeric substitutions improved therapeutic index in various combinations by affecting one (GS14Y_D4, GS14N_D4) or both (GS14K_D4) of the antimicrobial and hemolytic activities.

Chapter 6-3. Discussion

Our main objective in this study was to investigate the role of the hydrophobicity of D-amino acid substitutions at position 4 of GS14 on specificity between prokaryotes and eukaryotes. The substitution of single D-amino acids at position 4 change the side-chain stereochemistry, which in turn can affect three parameters of the peptide to varying degrees: overall hydrophobicity, amphipathicity, and the degree of secondary (β-sheet) structure in benign media.

Overall Inherent Hydrophobicity. Previous studies have shown that for antimicrobial peptides in various structural categories, the hydrophobicity of the peptide must exceed a minimal value to exert antimicrobial and hemolytic activity. The differences between this minimal hydrophobicity value for prokaryotes and eukaryotes provide a window that allows the development of peptides with selectivity towards prokaryotic membranes. However, as hydrophobicity increases beyond a certain value, selectivity is lost as peptides become both strongly hemolytic and strongly antimicrobial (Wieprecht et al. 1997).

It is clear from this study that overall inherent hydropobicity is not an important consideration for amphipathic molecules. Instead, it is the hydrophobicity of the nonpolar face of the molecule that is the critical factor. For example, the range of inherent hydrophobicities in substituting L-amino acids (Lys, Asn, Tyr, Phe, and Leu) at position 4 is large, yet there was little effect on hemolytic activity. All these GS14X_L4 peptides had similar and strong hemolytic activity since the L-substitutions did not affect the hydrophobicity of the nonpolar face, only the hydrophobicity of the hydrophilic face (Fig. 6-2). The nonpolar face is identical in all these analogs, in agreement with the similar displays of strong hemolytic activities. The RP-HPLC results are in agreement with little change in hydrophobicity of the nonpolar face, because the substitutions only cause large changes in inherent hydrophobicity on the hydrophilic face. The L-analogs had similar retention times (Fig. 6-4).

Amphipathicity. Amphipathicity is a known requirement for antimicrobial activity in helical peptides (Tossi et al. 2000) and highly amphipathic molecules have been shown to increase specificity towards eukaryotic membranes. In agreement with these findings, the highly amphipathic GS14 peptide (Fig. 6-2) with four lysine residues on the hydrophilic face and six large hydrophobes (3 Val and 3 Leu residues) on the hydrophobic face had reduced antimicrobial activity, and was very hemolytic (Kondejewski et al. 1999). In addition, GS14 showed high affinity binding to LPS, a component of outer membranes of Gram negative bacteria (Kondejewski et al. 1999). This high affinity binding may prevent or inhibit the peptide from crossing the outer membrane of Gram negative bacteria to limit interaction with the inner membrane, thus weakening Gram negative antimicrobial activity.

Interestingly, GS14K_D4 (Fig. 6-2) had significantly reduced amphipathicity with the D-Lys being presented on the hydrophobic face, leaving only three lysine residues on the hydrophilic face in the absence of structural changes (McInnes et al. 2000). This peptide had weak LPS binding affinity, increased antimicrobial activity and reduced hemolytic activity. Notably, all D-analogs in this study with a hydrophilic side chain presented on the hydrophobic face (D-Tyr, D-Asn, and D-Lys) displayed reduced amphipathicity, increased antimicrobial activity and increased therapeutic index (Fig. 6-5). To further support the role of amphipathicity in biological activity and specificity, a GS14 analog containing a sequence change from Leu^3-Lys^4 to Lys^3-Leu^4 (maintains the β-sheet structure but places the L-Lys residue on the hydrophobic face and places L-Leu on the hydrophilic face to reduce amphipathicity) had very similar hemolytic and antimicrobial activity profiles to GS14K$_D$4 (McInnes et al. 2000).

Secondary Structure. The induction of secondary structure in passing from an aqueous environment to the hydrophobic membrane environment has been observed to increase microbial specificity in helical peptides (Houston et al. 1998). We have observed that D-amino acid substitution, which disrupts β-sheet structure in benign medium but allows induction of structure in hydrophobic medium, serves to reduce peptide binding affinity to LPS, reduce amphipathicity, and increase biological activity (Kondejewski et al. 1999). These results suggest that this change in structure from benign to hydrophobic media is important. However, others have shown that diastereomers of helical peptides substituted with D-amino acids displayed little or no secondary structure in benign media, and exhibited reduced hemolytic activity and retained antimicrobial activity over their L-counterparts without requiring secondary structure in a hydrophobic environment (Oren et al. 1997; Shai et al. 1996). In the same studies, preformed secondary structure in benign media can unfavorably increase specificity for eukaryotic membranes. This is exactly opposite to the result where the cyclic β-sheet peptide which is preformed in benign medium had excellent specificity (McInnes et al. 2000). These results suggest that the mode of action of antimicrobial peptides may not be the same for different classes of molecules, and the importance of structure or structure induction is dependent on the particular molecule under study. Substitution of D-amino acids is known to be disruptive to secondary structure of linear α-helical peptides (Krause et al. 1995) and cyclic peptides (McInnes et al. 2000) in benign media, but the extent of induction in hydrophobic media is larger in the former category. Although the extent of structural disruption in benign media and induction in membranes by D-amino acids is greater for linear peptides (such as melittin and pardaxin), in contrast with cyclic peptides (such as gramicidin S), we have seen that even subtle structural changes can have major effects on biological activity in both cyclic and linear structural frameworks.

How does the induction of secondary structure in hydrophobic environments relate to the model of peptide-lipid interactions? The mechanism of peptide-induced membrane destabilization by cyclic β-sheet peptides has been studied with the 10-residue peptide, gramicidin S, in liposomes and lipid films (Prenner et al. 1999a; Prenner et al. 1999b; Staudegger et al. 2000). Assuming that the peptide-lipid interaction mechanism for GS14 and analogs is similar to the behavior of GS (both have similar structures, amphipathicities, and charge per residue ratios), these peptides initially exert specificity towards bacterial membranes through long-range electrostatic interactions between the anionic cell membrane and the cationic peptide, causing association at the bilayer interface. Subsequently, the peptide molecule associates parallel to the membrane (Salgado et al.), in the interfacial region between the polar glycerol backbone and the hydrocarbon chains, whereupon a peptide conformational change in the hydrophobic media drives membrane association and bilayer penetration.

In this study, all of the D-amino acid substitutions disrupted GS14X4 structure in benign media and were inducible in trifluoroethanol, although it was not clear whether the inducible structure contributed to observed differences in activity or specificity. The most antimicrobial peptides in this study had polar D-amino acids positioned on the nonpolar face, which would likely interact with the nonpolar hydrocarbon chains in the membrane bilayer. Perhaps the polar D-amino acid on the GS14 nonpolar face increases microbial specificity by initially placing a hydrophilic side chain near the hydrophobic phospholipid acyl chains, and causes a change in peptide orientation (from parallel to the membrane surface to an oblique angle) to facilitate peptide insertion into the membrane, induction of secondary structure, and disruption of bilayer integrity. This model also helps to explain why substitutions with D-Phe and D-Leu did not increase antimicrobial activity over the polar D-Tyr, D-Asn, or D-Lys substitutions. Both D-Phe and D-Leu would increase the hydrophobicity of the nonpolar face, possibly increasing peptide binding affinity to membranes to prevent a change in peptide orientation at the bilayer interface.

We observed that $GS14K_D4$ had the best therapeutic index over other peptides substituted with polar D-amino acids, including D-Asn and D-Tyr. From a molecular standpoint, the positive charge on the ε-amino group of D-lysine 4 in $GS14K_D4$ resulted in the greatest effect on the hydrophobicity of the nonpolar face, and a lower amphipathicity than the β-carboxamide side chain of $GS14N_D4$ or the phenolic ring in $GS14Y_D4$. The positive charge on the D-Lys compared to other polar side chains at position 4 may have increased specificity towards prokaryotic membranes because of the anionic character of prokaryotic membranes (in contrast with zwitterionic eukaryotic membranes), which may partially explain its superior antimicrobial activity over Gram negative organisms. In contrast, GS14Y_D4 had excellent antimicrobial activity *vs*. Gram positive bacteria, possibly because the higher hydrophobicity in the phenolic tyrosine ring (compared to the asparagine and lysine side chain) is somehow better suited to penetrating the peptidoglycan layer of Gram positive bacteria to interact with the cell membrane. These differences in peptide activity may be due to differences between the membrane organization and composition of Gram positive and Gram negative organisms. While Gram negative organisms have a double membrane system consisting of both an outer membrane and an inner membrane, Gram positive bacteria have a single cell membrane. The components of each membrane also vary, as Gram negative bacteria have lipopolysaccharide on the outer membrane while Gram positive microorganisms have a thick peptidoglycan layer surrounding the lipid membrane.

Though there are many structural classes of antimicrobial peptides, the cyclic framework of these 14-residue β-sheet peptides has some advantages. First, cyclic peptides are more resistant to proteolysis than their linear counterparts, an important consideration in evaluating the *in vivo* stability of peptides as potential drug candidates. Second, D-amino acids are not recognized as readily as the common L-amino acids by eukaryotic enzymes, they also increase peptide stability to proteases (Hong et al. 1999), as well as allowing control of structure in benign and hydrophobic media, while maintaining the same intrinsic hydrophobicity as their L-amino acid enantiomers.

We have shown that for peptides utilizing the cyclic β-sheet structural framework of GS14, the substitution of polar D-enantiomers can improve therapeutic index through improvements in antimicrobial activity and/or through decreasing hemolytic activity. Exceeding a certain overall hydrophobicity causes an increased specificity for eukaryotic membranes and results in strong hemolytic and weak antimicrobial activity. It is possible that other polar D-substitutions at position 4 may improve therapeutic index values more than the best peptide in this study, GS14K_D4, and lead to the development of more efficacious antimicrobial therapeutics suitable for human use.

Chapter 6-4. References

Aarstad, K., Zimmer, T.L. and Laland, S.G. 1979. Replacement of phenylalanine in gramicidin S by other amino acids. *FEBS Lett* **103:** 118-121.

Ando, S., Aoyagi, H., Shinagawa, S., Nishino, N., Waki, M., Kato, T. and Izumiya, N. 1983. [4,4'-D-diaminopropionic acid]gramicidin S: a synthetic gramicidin S analog with antimicrobial activity against Gram-negative bacteria. *FEBS Lett* **161:** 89-92.

Balasubramanian, D. 1967. The conformation of Gramicidin S in solution. *J Am Chem Soc* **89:** 5445-5449.

Conti, F. 1969. 220 Mc nuclear magnetic resonance spectra of gramicidin S in solution. *Nature* **221:** 777-779.

Ganz, T. and Lehrer, R.I. 1998. Antimicrobial peptides of vertebrates. *Curr Opin Immunol* **10:** 41-44.

Hancock, R.E. and Diamond, G. 2000. The role of cationic antimicrobial peptides in innate host defences. *Trends Microbiol* **8:** 402-410.

Hong, S.Y., Oh, J.E. and Lee, K.H. 1999. Effect of D-amino acid substitution on the stability, the secondary structure, and the activity of membrane-active peptide. *Biochem Pharmacol* **58:** 1775-1780.

Houston, M.E., Jr., Kondejewski, L.H., Karunaratne, D.N., Gough, M., Fidai, S., Hodges, R.S. and Hancock, R.E. 1998. Influence of preformed alpha-helix and alpha-helix induction on the activity of cationic antimicrobial peptides. *J Pept Res* **52:** 81-88.

Jelokhani-Niaraki, M., Kondejewski, L.H., Farmer, S.W., Hancock, R.E., Kay, C.M. and Hodges, R.S. 2000. Diastereoisomeric analogues of gramicidin S: structure, biologicalactivity and interaction with lipid bilayers. *Biochem J* **349 Pt 3:** 747-755.

Katsu, T., Kobayashi, H. and Fujita, Y. 1986. Mode of action of gramicidin S on Escherichia coli membrane. *Biochim Biophys Acta* **860:** 608-619.

Kondejewski, L.H., Farmer, S.W., Wishart, D.S., Hancock, R.E. and Hodges, R.S. 1996a. Gramicidin S is active against both gram-positive and gram-negative bacteria. *Int J Pept Protein Res* **47:** 460-466.

Kondejewski, L.H., Farmer, S.W., Wishart, D.S., Kay, C.M., Hancock, R.E. and Hodges, R.S. 1996b. Modulation of structure and antibacterial and hemolytic activity by ring size in cyclic gramicidin S analogs. *J Biol Chem* **271:** 25261-25268.

Kondejewski, L.H., Jelokhani-Niaraki, M., Farmer, S.W., Lix, B., Kay, C.M., Sykes, B.D., Hancock, R.E. and Hodges, R.S. 1999. Dissociation of antimicrobial and hemolytic activities in cyclic peptide diastereomers by systematic alterations in amphipathicity. *J Biol Chem* **274:** 13181-13192.

Krause, E., Beyermann, M., Dathe, M., Rothemund, S. and Bienert, M. 1995. Location of an amphipathic alpha-helix in peptides using reversed-phase HPLC retention behavior of D-amino acid analogs. *Anal Chem* **67:** 252-258.

Lohner, K. and Staudegger, E. 2001. Are we on the threshold of the of the post-antibiotic era? In *Development of novel antimicrobial agents: emerging strategies* (K. Lohner, eds.), 1-15., Horizon Scientific Press, Wymondham.

McInnes, C., Kondejewski, L.H., Hodges, R.S. and Sykes, B.D. 2000. Development of the structural basis for antimicrobial and hemolytic activities of peptides based on gramicidin S and design of novel analogs using NMR spectroscopy. *J Biol Chem* **275:** 14287-14294.

Merrifield, R.B. 1994. In *Antimicrobial Peptides - Ciba Foundations Symposium No. 186* (H. Boman, J. Marsh and J. Goode, eds.), 21, John Wiley & Sons, New York.

Oren, Z. and Shai, Y. 1997. Selective lysis of bacteria but not mammalian cells by diastereomers of melittin: structure-function study. *Biochemistry* **36:** 1826-1835.

Oren, Z. and Shai, Y. 2001. Molecular mechanism of cell selectivity by linear amphipathic alpha-helical and diastereomeric antimicrobial peptides. In *Development of novel antimicrobial agents: emerging strategies* (K. Lohner, eds.), 183-204., Horizon Scientific Press, Wymondham.

Prenner, E.J., Lewis, R.N., Kondejewski, L.H., Hodges, R.S. and McElhaney, R.N. 1999a. Differential scanning calorimetric study of the effect of the antimicrobial peptide gramicidin S on the thermotropic phase behavior of phosphatidylcholine, phosphatidylethanolamine and phosphatidylglycerol lipid bilayer membranes. *Biochim Biophys Acta* **1417:** 211-223.

Prenner, E.J., Lewis, R.N. and McElhaney, R.N. 1999b. The interaction of the antimicrobial peptide gramicidin S with lipid bilayer model and biological membranes. *Biochim Biophys Acta* **1462:** 201-221.

Salgado, J., Grage, S.L., Kondejewski, L.H., Hodges, R.S., McElhaney, R.N. and Ulrich, A.S. 2001. Membrane-bound structure and alignment of the antimicrobial beta-sheet peptide gramicidin S derived from angular and distance constraints by solid-state ^{19}F-NMR. *J Biomol NMR* **21:** 191-208.

Sereda, T.J., Mant, C.T., Sonnichsen, F.D. and Hodges, R.S. 1994. Reversed-phase chromatography of synthetic amphipathic alpha-helical peptides as a model for ligand/receptor interactions. Effect of changing hydrophobic environment on the relative hydrophilicity/hydrophobicity of amino acid side-chains. *J Chromatogr A* **676:** 139-153.

Shai, Y. and Oren, Z. 1996. Diastereoisomers of cytolysins, a novel class of potent antibacterial peptides. *J Biol Chem* **271:** 7305-7308.

Staudegger, E., Prenner, E.J., Kriechbaum, M., Degovics, G., Lewis, R.N., McElhaney, R.N. and Lohner, K. 2000. X-ray studies on the interaction of the antimicrobial peptide gramicidin S with microbial lipid extracts: evidence for cubic phase formation. *Biochim Biophys Acta* **1468:** 213-230.

Tamaki, M., Akabori, S. and Muramatsu, I. 1996. Properties of synthetic analogs of gramicidin S containing L-serine or L-glutamic acid residue in place of L-ornithine residue. *Int J Pept Protein Res* **47:** 369-375.

Tamaki, M., Arai, I., Akabori, S. and Muramatsu, I. 1995. Role of ring size on the secondary structure and antibiotic activity of gramicidin S. *Int J Pept Protein Res* **45:** 299-302.

Tossi, A., Sandri, L. and Giangaspero, A. 2000. Amphipathic, alpha-helical antimicrobial peptides. *Biopolymers* **55:** 4-30.

van 't Hof, W., Veerman, E.C., Helmerhorst, E.J. and Amerongen, A.V. 2001. Antimicrobial peptides: properties and applicability. *Biol Chem* **382:** 597-619.

Wieprecht, T., Dathe, M., Beyermann, M., Krause, E., Maloy, W.L., MacDonald, D.L. and Bienert, M. 1997. Peptide hydrophobicity controls the activity and selectivity of magainin 2 amide in interaction with membranes. *Biochemistry* **36:** 6124-6132.

Yonezawa, H., Okamoto, K., Tomokiyo, K. and Izumiya, N. 1986. Mode of antibacterial action by gramicidin S. *J Biochem (Tokyo)* **100:** 1253-1259.

Zidovetzki, R., Banerjee, U., Harrington, D.W. and Chan, S.I. 1988. NMR study of the interactions of polymyxin B, gramicidin S, and valinomycin with dimyristoyllecithin bilayers. *Biochemistry* **27:** 5686-5692.

Chapter 7: A novel method to measure self-association of small amphipathic molecules: Temperature profiling in reversed-phase chromatography

A version of this chapter has been published. Lee, D. L., Mant, C. T., and Hodges, R. S. 2003. Journal of Biological Chemistry 278: 22918-22927.

Chapter 7-1. Introduction

The detection of molecular self-association and aggregation is an important concern for molecules intended for biological applications, such as proteins, peptides and small organic drug molecules. A plethora of biophysical techniques already exist for the detection of molecular self-association in aqueous solution, including spectroscopic (NMR, CD, FTIR, fluorescence, light scattering), chromatographic (affinity, size-exclusion/gel filtration), and other techniques (MALDI-MS, non-denaturing PAGE, sedimentation equilibrium AUC). However, some of the classical techniques commonly used for measuring self-association (sedimentation equilibrium AUC, non-denaturing PAGE, and size-exclusion chromatography) possess a lower limit to the molecular size that can be clearly resolved, such that fewer methods exist for detecting self-association in smaller molecules. With a view to solving this problem, we describe here a novel method for measuring self-association, referred to as "temperature profiling in reversed-phase chromatography", based on observation of the conformation-dependent response of peptides to RP-HPLC under changing temperature.

Much of the efficacy of RP-HPLC as a probe of polypeptide stability, folding and conformation lies in the extensive range of stationary phases and/or mobile phase conditions available to the researcher when relating polypeptide elution behavior with structural features (e.g., the amphipathicity of α-helices or cyclic β-sheet peptides; destabilization of conformation) (Benedek 1993; Chen et al. 2002; Hodges et al. 1994; Kondejewski et al. 1999; Mant et al. 1998a; Mant et al. 1998b; Mant et al. 1989; Richards et al. 1994; Rosenfeld et al. 1993; Tripet et al. 2000; Yu et al. 2000) and/or biological activity (e.g., antimicrobial potency, receptor binding) (Mant et al. 2002b, 2002c; Sereda et al. 1994). Such studies are based on the premise that the hydrophobic interactions between polypeptides and the non-polar stationary phase characteristic of RP-HPLC (Kondejewski et al. 1996; Mant et al. 1991, 2002a) mimic the hydrophobicity and interactions between non-polar residues that are the major driving forces for protein folding and stability, including those dictating the level and stability of polypeptide oligomerization. Temperature adds another dimension to such applications, with physicochemical studies of RP-HPLC of polypeptide solutes under conditions of varying temperature (hence, "temperature profiling") allowing even more insight into conformational stability and self-association of peptide solutes.

The present study demonstrates the utility of temperature profiling in RP-HPLC to monitor self-association of small cyclic peptides based on the *de novo*-designed amphipathic cytolytic peptide, GS14, through the interpretation of peptide elution behavior over a temperature range of 5°C to 80°C. This approach is shown to be simple to operate, highly sensitive, requires low sample quantities (ng to low μg) and is capable of analyzing small molecules (< 2000 Da). In addition, the applicability of this novel approach for other small molecules is also discussed.

Chapter 7-2. Results

Peptide Design and RP-HPLC Retention Behavior

Parent Peptide (GS14). GS14 is a 14-residue cytolytic amphipathic peptide designed *de novo* in our laboratory (Fig. 7-1). The sequence of GS14 was originally developed as an analog of the cationic antimicrobial peptide gramicidin S (Kondejewski et al. 1996), whose activity is thought to be a result of interaction with lipid membranes (Jelokhani-Niaraki et al. 2000; Jelokhani-Niaraki et al. 2002; Katsu et al. 1989; Kondejewski et al. 1996; Kondejewski et al. 1999; Kondejewski et al. 2002; Lewis et al. 1999; Prenner et al. 1999a; Prenner et al. 1999b; Prenner et al. 1997). GS14 has been previously studied by a number of techniques, including RP-HPLC (Jelokhani-Niaraki et al. 2001; Kondejewski et al. 1999), CD spectroscopy (Jelokhani-Niaraki et al. 2002; Jelokhani-Niaraki et al. 2001; Kondejewski et al. 1996; Kondejewski et al. 1999; Kondejewski et al. 2002), NMR spectroscopy (Kondejewski et al. 1999; McInnes et al. 2000), UV absorption and fluorescence spectroscopy (Jelokhani-Niaraki et al. 2001). It is a cyclic β-sheet molecule that contains six aliphatic residues (3 Val and 3 Leu) on the nonpolar face and four basic (Lys) residues on the polar face; the segregation of nonpolar and charged residues on opposite sides of the molecule makes it an extremely amphipathic peptide (Fig. 7-2A) (McInnes et al. 2000). GS14 is also a suitable choice for *de novo* peptide design and structure-activity studies because the cyclic nature of the peptide prevents amino acid substitutions from significantly altering secondary structure, i.e., switching the β-sheet to an α-helix or random coil. Previous studies indicated that GS14 aggregated above 50 μM peptide concentration in aqueous solution (Jelokhani-Niaraki et al. 2001). Unfortunately,

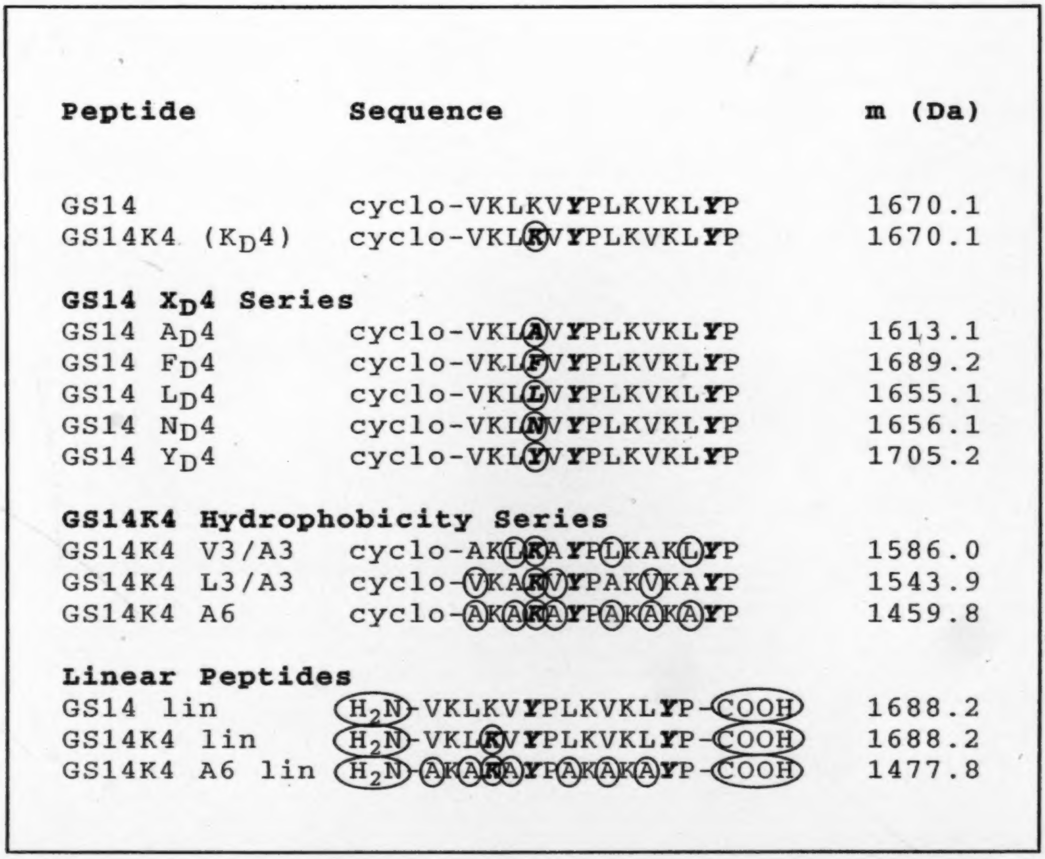

Peptide	Sequence	m (Da)
GS14	cyclo-VKLKV***Y***PLKVKL***Y***P	1670.1
GS14K4 (K_D4)	cyclo-VKL***K***V***Y***PLKVKL***Y***P	1670.1
GS14 X_D4 Series		
GS14 A_D4	cyclo-VKL***A***V***Y***PLKVKL***Y***P	1613.1
GS14 F_D4	cyclo-VKL***F***V***Y***PLKVKL***Y***P	1689.2
GS14 L_D4	cyclo-VKL***L***V***Y***PLKVKL***Y***P	1655.1
GS14 N_D4	cyclo-VKL***N***V***Y***PLKVKL***Y***P	1656.1
GS14 Y_D4	cyclo-VKL***Y***V***Y***PLKVKL***Y***P	1705.2
GS14K4 Hydrophobicity Series		
GS14K4 V3/A3	cyclo-AKL***K***A***Y***PLKAKL***Y***P	1586.0
GS14K4 L3/A3	cyclo-VKA***K***V***Y***PAKVKA***Y***P	1543.9
GS14K4 A6	cyclo-AKA***K***A***Y***PAKAKA***Y***P	1459.8
Linear Peptides		
GS14 lin	H_2N-VKLKV***Y***PLKVKL***Y***P-COOH	1688.2
GS14K4 lin	H_2N-VKL***K***V***Y***PLKVKL***Y***P-COOH	1688.2
GS14K4 A6 lin	H_2N-AKA***K***A***Y***PAKAKA***Y***P-COOH	1477.8

Figure 7-1. Sequences of peptides used in this study. The one-letter amino acid code is used. D-amino acids are in bold type and italicized; differences at N- and C-termini and amino acid substitutions relative to the parent peptide, GS14, are circled. Peptide molecular masses (m) were calculated based on average isotopic masses. In the GS14 X4 series, GS14 A_D4 denotes D-alanine substituted at position 4 in GS14. In the GS14K4 hydrophobicity series, GS14K4 L3/A3 denotes substitution of three leucine residues by three alanine residues in GS14K4.

attempts to determine the oligomerization state failed by sedimentation equilibrium analytical ultracentrifugation (due to the low molecular weight) and by size-exclusion chromatography (due to high sample load requirements and low peptide solubility), thus emphasizing the need for an alternative technique to examine self-association of this molecule. GS14 is biologically active against human red blood cells (hemolytic); however, it shows little or no antimicrobial activity against Gram-positive bacteria, Gram-negative bacteria, and yeast (Kondejewski et al. 1996).

RP-HPLC of Amphipathic Peptides

It is well documented that the formation of a hydrophobic binding domain due to peptide secondary structure can affect peptide interactions with reversed-phase matrices, this effect having been observed both for amphipathic α-helical peptides (Chen et al. 2002; Hodges et al. 1994; Mant et al. 2002b, 2002c; Mant et al. 1998b; Mant et al. 1993; Sereda et al. 1994; Yu et al. 2000; Zhou et al. 1990) and amphipathic, cyclic β-sheet peptides (Kondejewski et al. 1999; Mant et al. 1998a). Thus, peptides containing such preferred binding domains will exhibit significantly greater retention times compared to analogs with the same amino acid composition (i.e., the same intrinsic hydrophobicity) but lacking such a domain (Mant et al. 1998a; Zhou et al. 1990). Indeed, the chromatography conditions characteristic of RP-HPLC (hydrophobic stationary phase, non-polar eluting solvent) are able to induce and stabilize secondary structure in both potentially α-helical (Blondelle et al. 1995; Purcell et al. 1995; Steer et al. 1998; Steiner et al. 1991; Zhou et al. 1990) and cyclic, β-sheet (Steer et al. 1998) peptides; concomitantly, tertiary and quaternary structure is disrupted by such conditions (Ingraham et al. 1985; Lau et al. 1984a; Lau et al. 1984b; Mant et al. 1997; Mant et al.

1989; Sereda et al. 1994; Zhou et al. 1990). Due to the intimate interaction of the nonpolar faces of amphipathic cyclic analogs with a reversed-phase matrix, any differences in effective hydrophobicity of these preferred binding domains *via* amino acid substitutions in this domain will be readily monitored through subsequent differences in RP-HPLC retention time behavior.

Peptide Diastereomer (GS14K4). Because GS14 has such low specificity towards microbial membranes, analogs of GS14 have been studied in an attempt to reverse this activity profile and to create an antimicrobial peptide with minimal toxicity to human cells and high activity towards pathogens. One such analog is GS14K4 (Fig. 7-2B), a diastereomer of GS14 with the D-enantiomer of L-Lys substituted at position 4 (Kondejewski et al. 1999; Kondejewski et al. 2002). While the positively charged L-Lys 4 in GS14 is normally on the polar face, the D-Lys 4 in GS14K4 is positioned on the nonpolar face and disrupts the β-sheet structure in benign medium. GS14K4 exhibits an activity profile opposite to that of GS14 with a 10^3- to 10^4-fold improvement in therapeutic index (a measure of peptide specificity for microbial cells over human cells). Since the highly hydrophilic D-Lys is positioned on the nonpolar face of the peptide, the amphipathicity of the molecule is significantly decreased. This change decreases the retention time of the peptide in RP-HPLC relative to GS14 by over 23 minutes at 80°C (GS14, 85.6 min; GS14K4, 62.0 min, Table 7-1). While GS14 aggregates at concentrations above 50 μM (84 μg/ml) in solution due to the high hydrophobicity of its nonpolar face, no aggregation was observed in GS14K4 up to the highest concentration studied, 175 μM (292 μg/ml) (Jelokhani-Niaraki et al. 2001). Because GS14 and

Figure 7-2. NMR structures and Connolly surface representations of GS14 and GS14K4 peptides (McInnes et al. 2000). Connolly surface representations are rotated clockwise 90° along the X-axis relative to the NMR structures. Amino acid side-chains are labelled with one letter code and sequence number, with Lys 4 stereochemistry designated in subscript. Oxygen atoms are red; nitrogen atoms are blue. Panel A: structure of GS14 (left) showing the positioning of the nonpolar residues (3 Leu and 3 Val) on one face and the four Lys residues on the other face and the Connolly surface representation (right) showing the nonpolar face. Panel B: structure of GS14K4 (left) and the Connolly surface representation (right) showing the position of the D-Lys at position 4 on the nonpolar face.

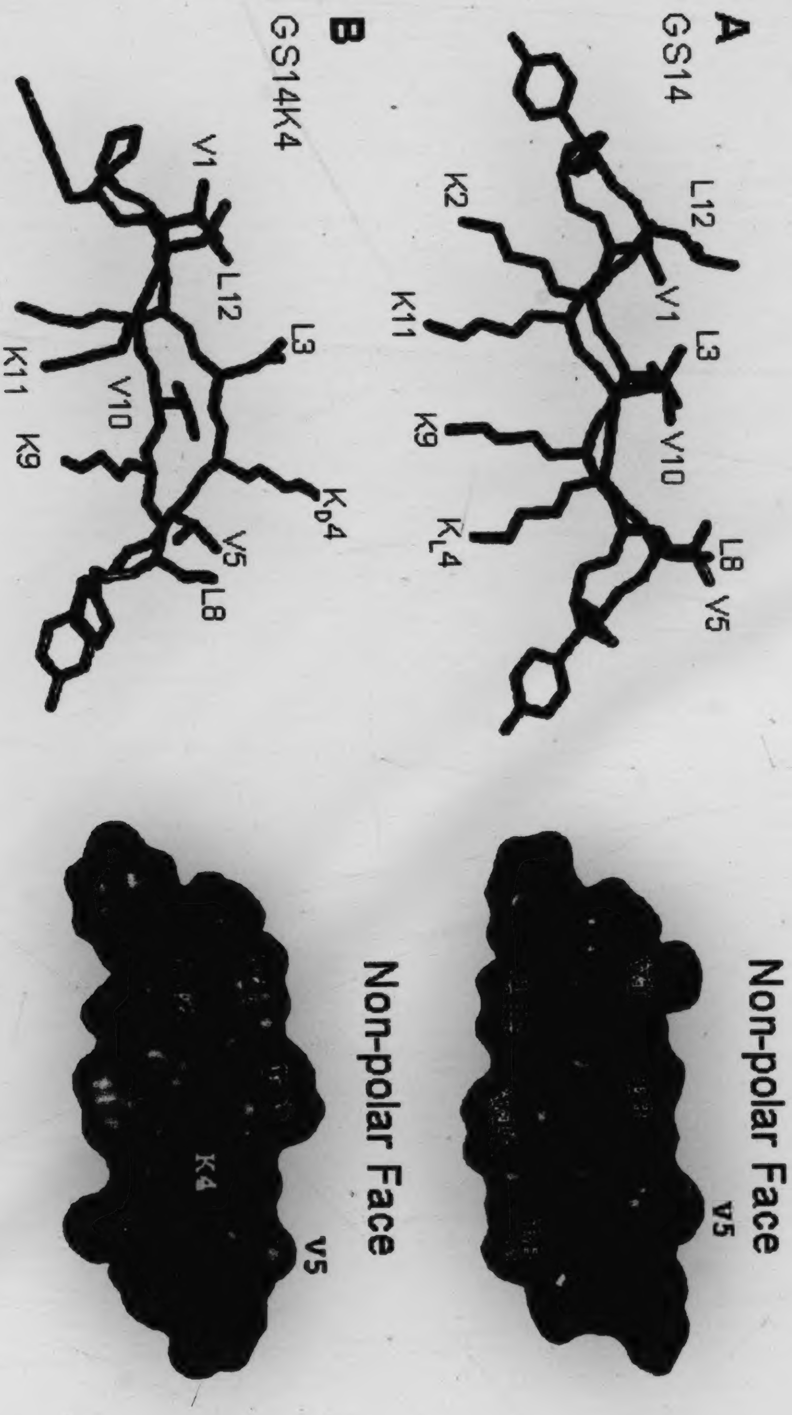
A
GS14
L12
K2
V1
K11
L3
K9
V10
K_L4
L8
V5
Non-polar Face
V5
B
GS14K4
V1
L12
L3
K2
K11
V10
K9
K_D4
V5
L8
Non-polar Face
V5
K4

[a] Peptide retention time at 80°C as determined by reversed-phase HPLC (see Methods).

[b] Peptide retention time at 5°C as determined by reversed-phase HPLC (see Methods).

[c] Temperature at which the maximum retention time is observed over the temperature range 5-80°C.

[d] Peptide retention time at temperature T_p.

[e] Difference in retention time between t_R at the T_P and t_R at 5°C.

[f] Difference in retention time between t_R at the T_P and t_R at 80°C.

[g] GS14K_D4 and GS14K4 denote the same peptide with D-Lys at position 4.

Table 7-1. HPLC data for peptides used in this study

Peptide	$t_R(80°C)$ (min)[a]	$t_R(5°C)$ (min)[b]	T_p (°C)[c]	$t_R(T_p)$ (min)[d]	$t_R(T_p)-t_R(5°C)$ (min)[e]	$t_R(T_p)-t_R(80°C)$ (min)[f]
GS14	85.6	82.5	55	86.7	4.2	1.1
GS14X$_D$4 Analogs						
GS14 L$_D$4	100.4	96.8	55	101.8	5.0	1.4
GS14 F$_D$4	98.3	94.8	55	100.0	5.2	1.7
GS14 A$_D$4	94.1	90.6	55	95.3	4.7	1.2
GS14 Y$_D$4	83.0	83.2	40	85.1	1.9	2.1
GS14 N$_D$4	73.3	73.5	40	75.3	1.8	2.0
GS14 K$_D$4[g]	62.0	65.0	20	65.3	0.3	3.3
GS14K4 Hydrophobicity Analogs						
GS14K4	62.0	65.0	20	65.3	0.3	3.3
GS14K4 V3/A3	47.4	52.5	5	52.5	0	5.1
GS14K4 L3/A3	39.8	46.4	5	46.4	0	6.6
GS14K4 A6	25.8	33.3	5	33.3	0	7.5
Linear Analogs						
GS14 lin	55.6	62.8	15	63.1	0.3	7.2
GS14K4 lin	46.2	51.6	5	51.6	0	5.4
GS14K4 A6 lin	21.3	30.7	5	30.7	0	9.4

GS14K4 possess the ability to be analyzed in a RP-HPLC system and exhibit marked differences in activity, structure, and aggregation phenomena, these *de novo*-designed cyclic peptides are ideal candidates for the investigation of relationships between molecular self-association and biological activity using the RP-HPLC technique of temperature profiling.

GS14 X_D4 Analogs. The GS14 X_D4 analogs replaced the D-Lys in GS14K4 with a series of other D-amino acids at position 4 (Fig. 7-1). The substituted amino acids ranged in hydrophobicity from D-Asn and D-Tyr (least hydrophobic) to D-Leu and D-Phe (most hydrophobic) (Monera et al. 1995; Sereda et al. 1994), and altered both the overall hydrophobicity and amphipathicity of the peptide due to position of the substituted amino acid on the nonpolar face. The analogs also had a lower net charge *vs.* GS14K4 (+3 instead of +4 from the Lys residues in GS14, Fig. 7-2). The differences in the peptide composition influenced peptide retention time in RP-HPLC, with the most hydrophobic amino acid substitution (D-Leu in GS14L_D4) producing the largest retention time, compared with GS14K4 which had the least hydrophobic amino acid (D-Lys) at position 4 and the lowest retention time within the series. Retention times at 80°C ranged from 62 min to 100 min for D-Lys and D-Leu peptides, respectively (Table 7-1).

GS14K4 Hydrophobicity Analogs. To investigate the role of peptide hydrophobicity in microbial specificity, we previously created analogs of GS14K4 with variations of the aliphatic residues in the nonpolar face (Kondejewski et al. 2002). A subset of these hydrophobicity analogs was now assessed for self-association in the present study (Fig. 7-1). The selected analogs had lower nonpolar face hydrophobicity relative to GS14K4, with valines and/or leucines in GS14K4 substituted with the less hydrophobic alanine residue (Monera et al. 1995; Sereda et al. 1994), *e.g.*, peptide GS14K4 V3/A3 had three valines substituted with three alanines, producing a peptide with one lysine, three leucine, and three alanine residues in the nonpolar face. GS14K4 and GS14K4 V3/A3 showed antimicrobial activity with minimal toxicity to human red blood cells; the other analogs selected for this study possessed insufficient hydrophobicity to exert cytolytic effects on either microbial or human cells. This series of analogs varied substantially in hydrophobicity (retention times ranged from 25 to 62 min at 80°C, Table 7-1).

Linear Analogs. The peptide analogs GS14 lin, GS14K4 lin, and GS14K4 A6 lin served as linear controls *vs.* cyclic peptides, possessing the same intrinsic hydrophobicity owing to the identical amino acid sequences but having different effective hydrophobicity due to their non-cyclic nature. For example, at 80°C, GS14 lin had a retention time of 55 min whereas its cyclic analog, GS14, had a retention time of 85 min (Table 7-1), clearly demonstrating the enhanced hydrophobicity in forming the preferred binding domain by cyclization. GS14K4 A6 lin served as the control peptide in the normalized temperature profiles for all peptides studied. This peptide lacked any defined structure and had insufficient hydrophobicity to dimerize.

Proposed Mechanism of Action

The proposed mechanism of action for temperature profiling in RP-HPLC is shown in Fig. 7-3. The mechanism is based on two assumptions, with the first based on the fact that loading the peptide onto the top of the column in aqueous conditions concentrates the peptide locally on the hydrophobic matrix bound by its hydrophobic preferred binding domain. As the acetonitrile concentration increases during gradient elution, the acetonitrile content becomes high enough to allow peptide partitioning between the matrix and the mobile phase. Thus, in the early stages of partitioning, our assumption is that the effective peptide concentration in solution is extremely high as a result of the concentration of peptide achieved on binding to the matrix during sample loading. The second assumption is that because of this concentrating effect in solution, peptides in this study that are capable of self-association during gradient elution are in equilibrium between a monomeric peptide bound to the matrix (Fig. 7-3A, top left), an unbound monomeric form in the mobile phase (Fig. 7-3A, top center), and an unbound dimeric form in the mobile phase (Fig. 7-3A, top right). As a result, peptides that dimerize in solution are eluted faster since the on-rate for the bound state is decreased, *i.e.*, retention time is lower than what would be observed if the molecule was unable to dimerize and was only in the monomeric state in the mobile phase. The dimerization is temperature-dependent, with more dimerization occurring in solution at low temperatures. As the temperature is increased, equilibrium is shifted towards the monomeric form in solution due to disruption of the dimer. The higher solution concentration of monomer during partitioning increases the on-rate for the bound state, and retention time thus increases. It should be noted that the increase in temperature also introduces other general effects on retention time because of lower mobile phase viscosity and a significant increase in mass transfer between the stationary and mobile phases. These effects decrease retention time with increasing temperature in a linear fashion. Thus, in the case of peptides that do not undergo a significant conformational change over the temperature range profiled, one would expect to see a linear decrease in retention time with increasing temperature because of the lower mobile phase viscosity and increase in mass transfer. This would be the case for a monomeric peptide with either a random coil or an undefined structure

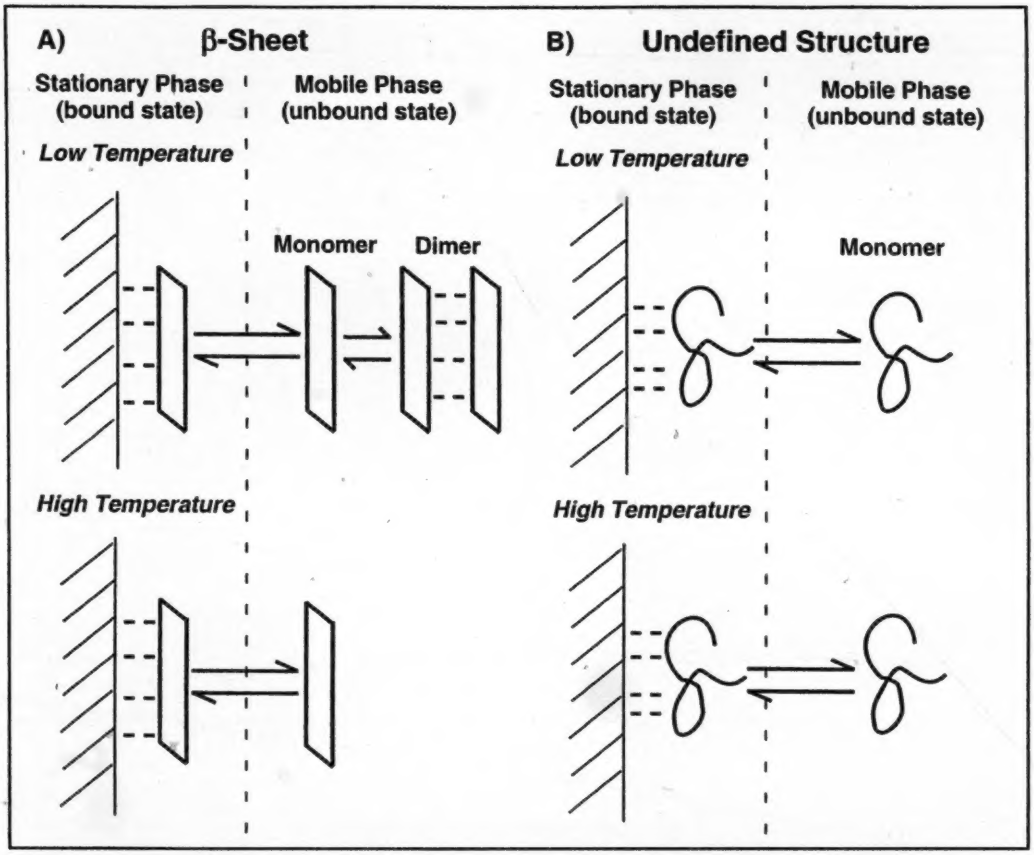
A) β-Sheet
Stationary Phase (bound state)
Mobile Phase (unbound state)
Low Temperature
Monomer
Dimer
High Temperature
B) Undefined Structure
Stationary Phase (bound state)
Mobile Phase (unbound state)
Low Temperature
Monomer
High Temperature

Figure 7-3. Proposed mechanisms of temperature profiling by RP-HPLC. Panel A: At lower temperatures, peptides capable of self-associating in aqueous solution *via* the hydrophobic effect establish equilibrium between monomer and dimer in the mobile phase. Only the monomeric form of the peptide in solution can partition with the alkyl ligands on the reversed-phase column, and retention time is decreased due to the large population of dimers in solution. At higher temperatures, the population of dimers in solution during partitioning decreases, increasing the concentration of monomeric peptide in solution and increasing retention time. At some temperature no dimer would exist in solution. Panel B: With a peptide that does not form an amphipathic structure and cannot dimerize, the peptide binds to the stationary phase and partitions in the mobile phase as a monomer with undefined structure at both low and high temperatures. Thus, the effect of temperature on retention time is linear and decreases with increasing temperature.

(Fig. 7-3B), or for a very stable peptide with a specific structure that does not change over the entire temperature range - for example, a stable amphipathic monomeric α-helix.

There are thus two opposing effects on peptide retention time as the temperature is increased: increasing retention time as dimerization is disrupted, and decreasing retention time from these general temperature effects. For molecules that dimerize, the effect of dimerization is dominant at low temperature over the general temperature effects. Thus, at low temperatures, the dimerization effect dominates and retention time increases with increasing temperature until a certain temperature is reached, which we designate T_p (the temperature at the transition point). At this temperature, the temperature effects that increase retention time (shift in the monomer/dimer equilibrium in the mobile phase favoring monomer) are equivalent to those that decrease retention time. Above the temperature, T_p, the net result is a decreased retention time as lower viscosity and higher mass transfer effects predominate.

Peptide Structure

CD Spectroscopy. The structure of peptides in this study were characterized by CD spectroscopy in aqueous buffer and in a mixture of buffer and trifluoroethanol (Fig. 7-4, Table 7-2), an organic solvent known to mimic the non-polar environment characteristic of RP-HPLC (Zhou et al. 1990). Cyclic peptides do not exhibit CD spectra of typical β-sheet character (the classic β-sheet spectrum possesses a single minimum at 215-218 nm). However, the solution structure of GS14 has previously been determined by NMR techniques and is known to be a β-sheet (Fig. 7-2) (McInnes et al. 2000); thus, the CD spectrum for GS14 shown in Fig. 7-4A, resembling that of an α-helix with minima near

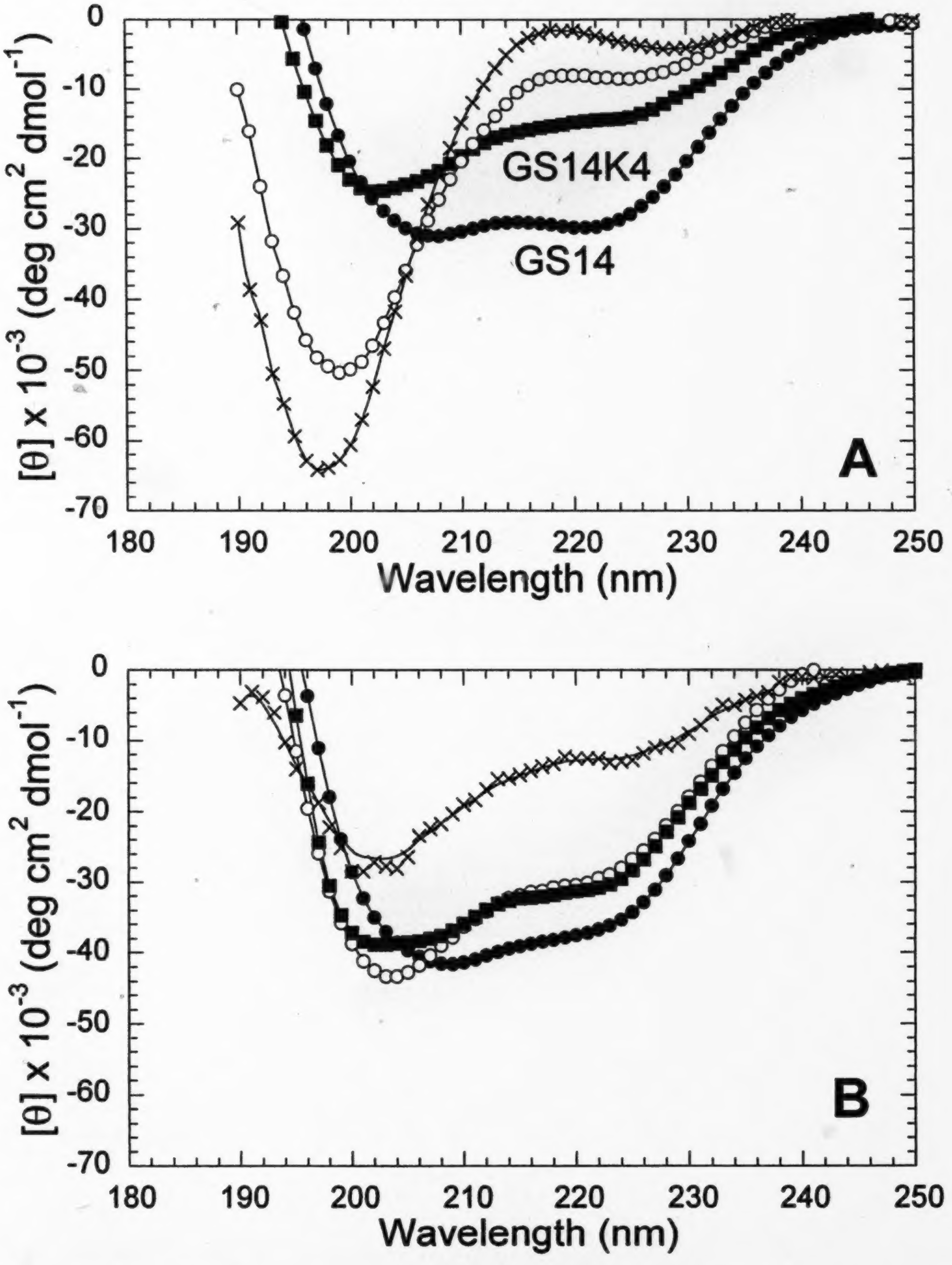

Figure 7-4. Far-UV CD spectra for cyclic and linear GS14 and GS14K4 peptides. CD spectra were obtained in 5 mM sodium acetate, pH 5.5, 25°C at ~30 μM peptide concentration in the absence (Panel A) or presence (Panel B) of 50% trifluoroethanol. Peptides in both panels were GS14 (closed circle), GS14 lin (open circle), GS14K4 (closed square) and GS14K4 A6 lin (X).

Table 7-2. Biophysical data and biological activity for representative peptides used in this study

Peptide	$[\theta]_{222}$[a]		MIC	Hemolytic activity	Therapeutic index[d]
	Benign	50% TFE	(μg/ml)[b]	(μg/ml)[c]	
GS14	-29600	-36700	284	1.5	<0.01
GS14K4	-14500	-30800	4	200	47
GS14K4 V3/A3	-8100	-22300	65	>800	25
GS14K4 L3/A3	-4900	-20200	256	>800	6
GS14K4 A6	-3700	-10500	345	>800	5

[a] Mean residue ellipticity at 222 nm, expressed in deg cm^2 $dmol^{-1}$ as determined by Kondejewksi *et al.* 2002. CD spectra were obtained at 30 μM peptide concentration in 5 mM sodium acetate pH 5.5 (Benign), or in 5 mM sodium acetate pH 5.5 in 50% trifluoroethanol (TFE) at 20°C. Cyclic β-sheet structures have a large negative $[\theta]_{222}$ value, while unstructured peptides have ellipticities near zero.

[b] Antimicrobial activity as determined by Kondejewski *et al.* 2002. Values were obtained as the average of the following microbial strains: *S. epidermidis, E. faecalis, C. xerosis, C. albicans, P. aeruginosa* H188, *E. coli* UB1005, *E. coli* DC2, *S. typhimurium* C587, and *S. typhimurium* C610.

[c] Hemolytic activity as determined by Kondejewski *et al.* 2002. Values of >800 μg/ml were listed as 1600 μg/ml for calculation of therapeutic index.

[d] Therapeutic index = hemolytic activity/MIC. Larger values indicate greater microbial specificity.

208 and 222 nm, is due to the dominating effects of the type II ′ β-turns in these small cyclic peptides. GS14K4 was known to exhibit disrupted β-sheet structure by NMR (Fig. 7-2) (McInnes et al. 2000); its CD spectrum is shown in Fig. 7-4A with a significantly less negative mean residue molar ellipticity at 222 nm ($[\theta]_{222}$) than GS14. GS14 X_D4 peptides all exhibited CD spectra similar to GS14K4 in benign and 50% TFE conditions (data not shown). GS14K4 and its hydrophobicity analogs GS14K4 L3/A3, GS14K4 V3/A3, and GS14K4 A6 all exhibited a lesser degree of β-sheet structure than GS14 in benign buffer as shown by the smaller molar ellipticity values at 222 nm, but were induced to form β-sheet structure in trifluoroethanol (Table 7-2). The linear control peptides GS14 lin and GS14K4 A6 lin both exhibited spectra typical of a random coil in aqueous conditions with a minimum below 200 nm and a maximum at 220 nm (Fig. 7-4A). But in 50% TFE, GS14 lin appeared to be induced into substantially more β-sheet structure than GS14K4 A6 lin (Fig. 7-4B). Based on GS14K4 A6 lin behavior in 50% TFE, we assume that it behaves similarly in the hydrophobic environment of the column matrix and also binds mainly in an undefined structure.

Temperature Profiles

RP-HPLC Analysis. The absolute retention times of GS14 and other cyclic peptides differed greatly because of the differences in one or more of the following properties: structure, amphipathicity, and/or intrinsic hydrophobicity (Table 7-1). To examine graphically the effect of temperature on retention time, peptide retention times were normalized relative to the values obtained at 5°C or 80°C, the lowest and highest temperature used in this study (Fig. 7-5). Normalizing at 5°C allowed determination of T_p, the transition temperature (Fig 5A), while normalizing at 80°C corrected the retention

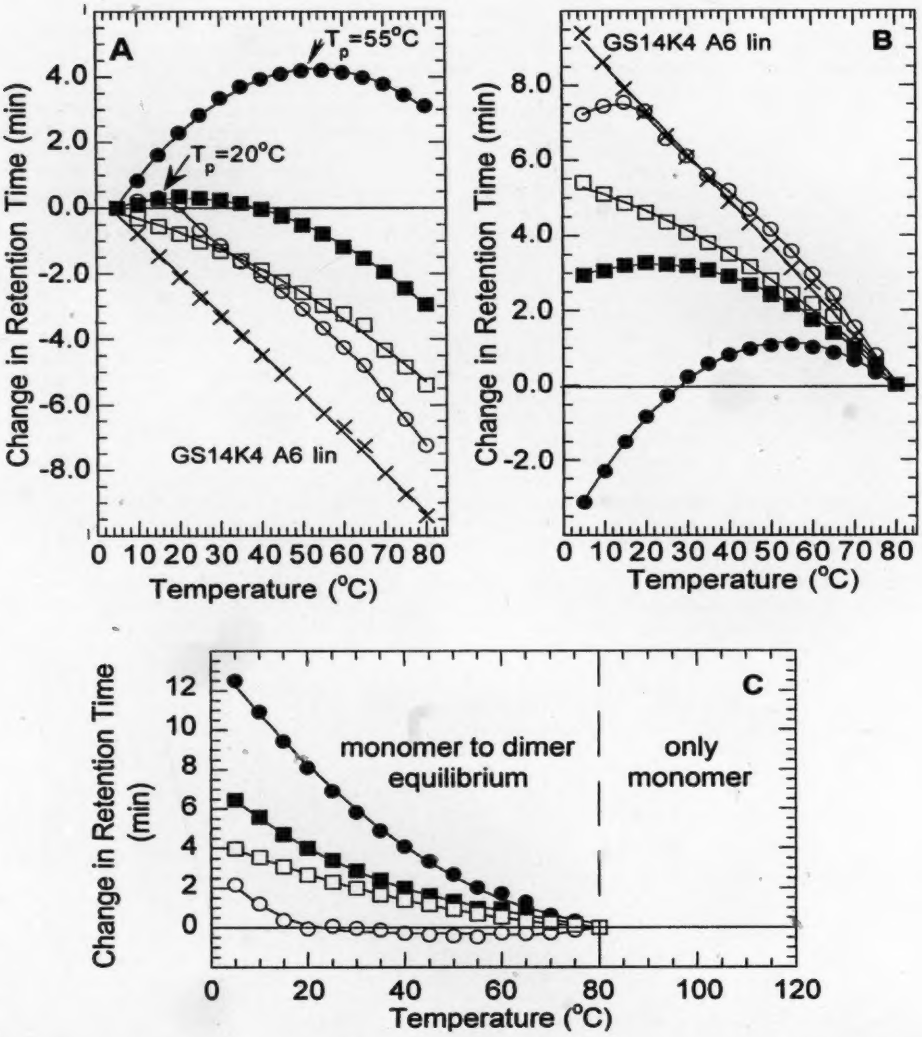

Figure 7-5. Normalized RP-HPLC temperature profiles of cyclic and linear GS14 and GS14K4 peptides. Panel A: Temperature profiles normalized to individual peptide retention times at 5°C. T_p is the temperature at which the maximum change in retention time is observed. Panel B: Temperature profiles normalized to individual peptide retention times at 80°C. Panel C: RP-HPLC temperature profiles for cyclic and linear GS14 and GS14K4 peptides normalized to retention times at 80°C and subtracted from the 80°C-normalized retention times of the control peptide, GS14K4 A6 lin. Peptides in all panels were GS14 (closed circle), GS14 lin (open circle), GS14K4 (closed square), GS14K4 lin (open square), and GS14K4 A6 lin (X).

time to a temperature where the effects of structure and self-association are minimal (Fig. 7-5B).

GS14 and GS14K4. The cyclic β-sheet peptides GS14 and GS14K4 showed a deviation from linearity in the normalized temperature profiles (Figs. 7-5A and 7-5B), indicating a change in the degree of self-association over the 5-80°C temperature range. In the temperature profile normalized to retention times at 5°C, GS14 had a T_p of 55°C, significantly higher than the T_p of GS14K4, which was 20°C (Fig. 7-5A). In contrast to the results obtained from cyclic GS14 and GS14K4, the linear peptides generally exhibited a negative relationship between RP-HPLC retention time and temperature, e.g., GS14K4 A6 lin (Fig. 7-5A). Interestingly, GS14 lin had normalized changes in retention time above 0 at temperatures of 10°, 15° and 20°C (T_p=15°C), suggesting that self-association may have occurred at these low temperatures (Fig. 7-5A). Similarly, Fig. 7-5B shows the temperature profiles normalized to retention times at 80°C. The profiles of GS14 lin and GS14K4 A6 lin were almost superimposable except at temperatures below 20°C. This indicates that additional structural effects (e.g., changes in β-sheet content or degree of self-association) did not occur from 20°C to 80°C.

The temperature profiles in Fig. 7-5C for GS14 and GS14K4 cyclic and linear peptides were zeroed at 80°C and also normalized for general temperature effects using the control peptide, GS14K4 A6 lin. Thus, these profiles showed the effects of temperature on structure formation and/or self-association, without the negative linear retention time decrease from general effects of temperature. GS14 exhibits the most self-association, with a change in retention time of 12.5 min at 5°C compared to 80°C, significantly larger than that of GS14K4 (6.5 min). It is interesting that the linear peptides GS14 lin and

GS14K4 lin also show the ability to change structure/self-associate at low temperatures. Fig. 7-5C also illustrated our hypothesis that by further increasing temperature beyond 80°C, equilibrium is completely shifted to the monomeric state in the mobile phase, and the temperature profiles of all the peptides would fall along the normalized baseline at sufficiently high temperature.

GS14 X_D4 Analogs. All peptides with D-amino acid substitutions had temperature profiles that deviated from linearity (Fig. 7-6). The change in retention time at T_p for all peptides in the series was proportional to the hydrophobicity of the D-amino acid substituted in the peptide, as determined by previous amino acid hydrophobicity scales (Monera et al. 1995; Sereda et al. 1994). The peptides GS14 F_D4, GS14 L_D4, and GS14 A_D4 had T_p values identical to GS14 (T_p of 55°C, Table 7-1). Notably, an increase in hydrophobicity of the nonpolar face (*e.g.*, with D-Phe, D-Leu, or D-Ala in addition to the three Leu residues and three Val residues of GS14) increased the magnitude of the change in retention time only slightly (5.2, 5.0, and 4.7 min, respectively, compared to GS14 with a value of 4.2 min, Table 7-1). This result showed that, above a certain nonpolar face hydrophobicity, there was no further increase in T_p for these cyclic peptides, suggesting that 55°C may represent a maximum limit for T_p in this cyclic β-sheet structural framework. Decreasing the hydrophobicity of the D-substitution at position 4 from D-Phe, D-Leu or D-Ala to D-Tyr or D-Asn dramatically decreased the T_p value to 40°C and the magnitude of the change in retention time to 1.9 and 1.8 min for D-Tyr and D-Asn, respectively, compared to GS14 (Fig. 7-6A and Table 7-1). D-Lys at position 4 had the lowest intrinsic hydrophobicity, the lowest T_p (20°C) and the lowest difference in retention time between T_p and 5°C (0.3 min, Fig. 7-6A and Table 7-1). Fig.

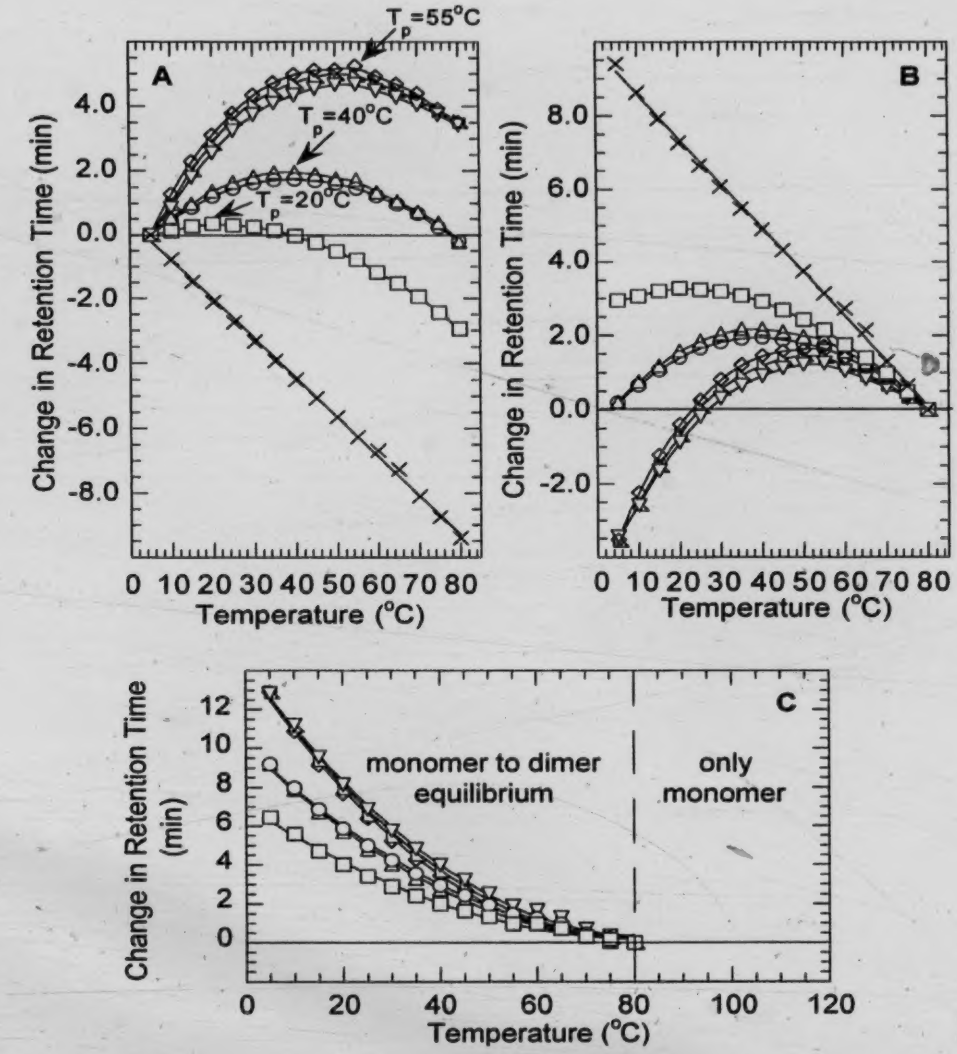

Figure 7-6. Normalized RP-HPLC temperature profiles of GS14 X4 peptides. Panel A: Temperature profiles normalized to individual peptide retention times at 5°C. T_p is the transition temperature at which the maximum change in retention time is observed. Panel B: Temperature profiles normalized to individual peptide retention times at 80°C. Panel C: Profiles normalized to individual peptide retention times at 80°C and subtracted from the 80°C-normalized retention times of the control peptide, GS14K4 A6 lin. Peptides in all panels were GS14 F_D4 (open diamond), GS14 L_D4 (open isosceles triangle), GS14 A_D4 (inverted open triangle), GS14 Y_D4 (open triangle), GS14 N_D4 (open circle), and GS14K4 (open square). GS14K4 A6 lin (X) is only in panels A and B.

7-6B shows the temperature profiles normalized to retention times at 80°C and illustrates that, despite the large change in hydrophobicity of these cyclic peptides, they all show large deviations from the linear behavior of control peptide GS14K4 A6 lin. Following normalization for general temperature effects using the GS14K4 A6 lin peptide, all these cyclic peptides show the ability to dimerize (Fig. 7-6C).

GS14K4 Hydrophobicity Analogs. The peptides with temperature profiles that were closest to the control GS14K4 A6 lin profile, GS14K4 L3/A3 and GS14K4 A6, had the lowest intrinsic hydrophobicity (Fig. 7-7A). The analogs also showed that as nonpolar face hydrophobicity decreased, β-sheet structure was diminished both in benign medium and in the presence of 50% TFE (compare $[\theta]_{222}$ in Table 7-2) and the temperature profile was closer to linearity (Fig. 7-7B). Note also that the normalized profiles all fell below that of GS14K4, showing that GS14K4 - possessing the highest hydrophobicity of the series - also had the highest degree of self-association among the hydrophobicity analogs (Fig. 7-7B). Except for GS14K4 V3/A3, the peptides that showed the smallest deviations from linearity also showed no antimicrobial or hemolytic activity (Table 7-2).

In this study, we used the differences in retention time at 80°C as a measure of the differences in apparent hydrophobicity of the various analogs. Fig. 7-8A and Fig. 7-8B show the relative hydrophobicity of the analogs using a 1% acetonitrile/min linear gradient at 80°C. The RP-HPLC retention times shown in Table 7-1 were determined at a gradient rate of 0.5% acetonitrile/min. This shallower gradient was used to amplify the differences between peptide analogs. At 80°C, the effects of dimerization are essentially eliminated, with all amphipathic molecules being in their monomeric form during partitioning in RP-HPLC. For example, compared to GS14K4 A6, the addition of 3 Leu

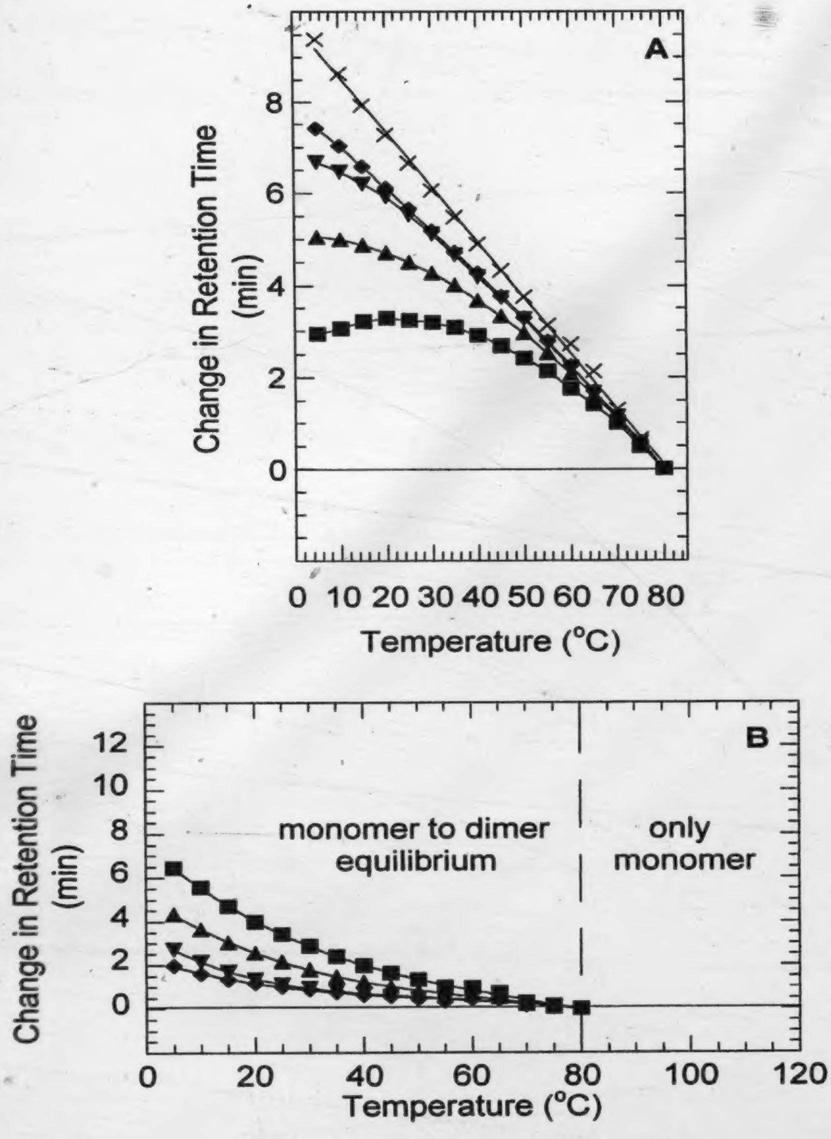

Figure 7-7. Normalized RP-HPLC temperature profiles of GS14K4 and hydrophobicity analogs. Panel A: Temperature profiles normalized to individual peptide retention times at 80°C. Panel B: Profiles normalized to individual peptide retention times at 80°C and subtracted from the 80°C-normalized retention times of the control peptide, GS14K4 A6 lin. Peptides were GS14K4 (closed square), GS14K4 V3/A3 (closed triangle), GS14K4 L3/A3 (closed inverted triangle), GS14K4 A6 (closed diamond) and GS14K4 A6 lin (X, only in panel A).

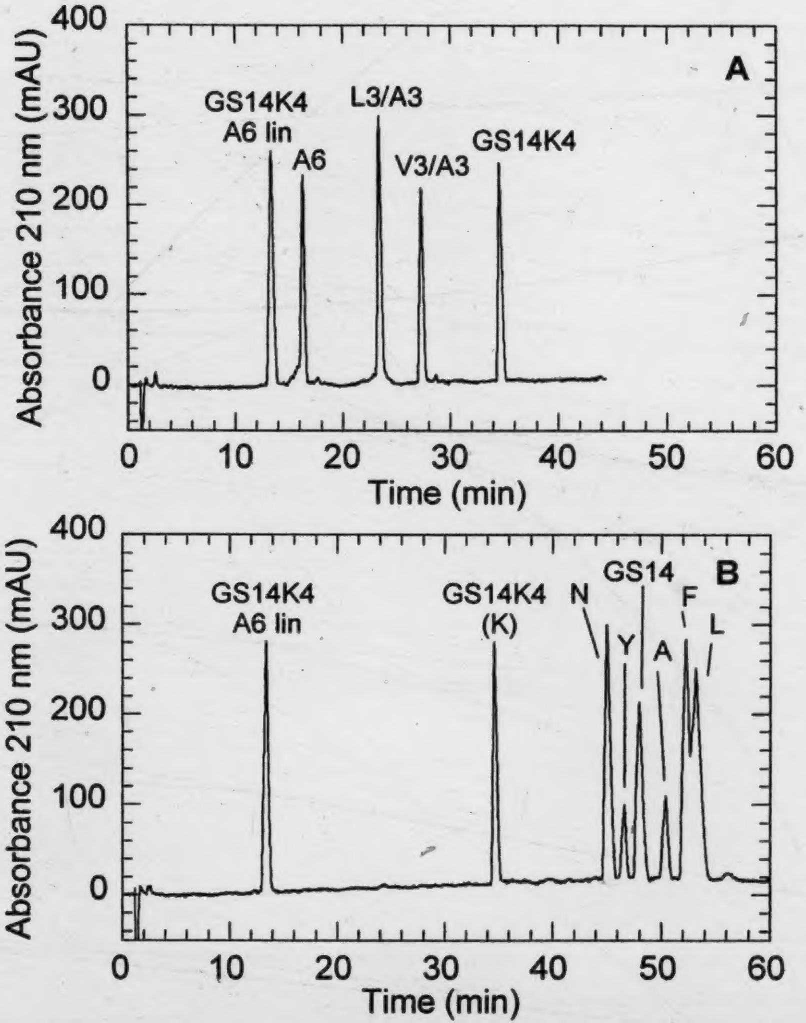

Figure 7-8. RP-HPLC elution of representative GS14 and GS14K4 analogs. Panel A: Elution of GS14K4 and representative GS14K4 hydrophobicity analogs. Panel B: Elution of GS14 and representative GS14 X_D4 analogs. Single letters denote the D-amino acid substituted at position 4 relative to GS14, *e.g.*, N corresponds to GS14 N_D4. Runs were performed on a Zorbax 300-SB C8 column (2.1x150 mm I. D.), at 1% B/min, a flow-rate of 0.35 ml/min, and a temperature of 80°C, where solvent A was 0.05% aqueous TFA and solvent B was 0.05% TFA in acetonitrile.

residues (i.e., GS14K4 V3/A3) increases retention time at 80°C by 21.6 min (47.4 – 25.8 min, Table 7-1), with each leucine residue contributing 7.2 min. In comparison, the addition of 3 Val residues (i.e., GS14K4 L3/A3) increases retention time at 80°C by 14 min (39.8 – 25.8 min, Table 7-1), with each valine residue contributing 4.7 min. Thus, the sum of 3 Val and 3 Leu residues added to GS14K4 A6 should increase retention time by 14 + 21.6 = 35.6 min, which is close to the observed value difference of 62.0-25.8 = 36.2 min (i.e., the difference between GS14K4 and GS14K4 A6 retention times at 80°C).

With the GS14X_D4 analogs the effects of substitution were in the identical order of the hydrophobicities of the substituted residues as determined by RP-HPLC from a previous study. Thus, Sereda *et al.* (Sereda et al. 1994) determined the relative hydrophobicities of amino acid side-chains in the center of the non-polar face of an amphipathic α-helix containing 6 Leu residues as 1.99, 0.96, 0, -3.94, -8.85, and –12.25 min for Leu, Phe, Ala, Tyr, Asn and Lys, respectively. Interestingly, the relative side-chain RP-HPLC-derived hydrophobicities determined in the present study from substitutions in the non-polar surface of the amphipathic cyclic β-sheet peptide containing 3 Val and 3 Leu residues were similar to those obtained from amphipathic α-helices when compared at the same gradient rate (3.1, 2.1, 0, -5.5, -10.4, and –16.0 min for Leu, Phe, Ala, Tyr, Asn and Lys, respectively).

Finally, it is worth noting that, from Table 7-1, the minimum number of hydrophobic residues required for substantial self-association of the cyclic peptide analogs appears to be six residues – specifically in this case, 3 Leu and 3 Val residues making up the hydrophobic face of GS14 (T_p = 55°C). Replacement of the 3 Leu residues (GS14K4 L3/A3) or the 3 Val residues (GS14 V3/A3) with considerably less hydrophobic Ala residues decreased self-association to almost negligible levels (T_p=5°C for the latter two analogs). This observation reflects in an interesting manner extensive work carried out in this laboratory on the role of hydrophobic residues in stabilizing amphipathic α-helical coiled-coils (Chao et al. 1996; De Crescenzo et al. 2003; Litowski et al. 2001, 2002; Su et al. 1994; Tripet et al. 2000; Wagschal et al. 1999b). Thus, it was determined that a minimum of six hydrophobic residues, capable of strong affinity interactions, were required for α-helices to dimerize in solution, i.e., two hydrophobic residues in each of the three heptads making up the seven-residue sequence repeat characteristic of α-helical coiled-coils (Su et al. 1994).

Chapter 7-3. Discussion

Reversed-Phase Chromatography and Mechanism of Elution

The time that a molecule is retained by a reversed-phase chromatography column is based on analyte partitioning between the aqueous mobile phase and the hydrophobic stationary phase. During linear gradient elution, the composition of the mobile phase changes with an increased percentage of organic solvent as a function of time. As noted previously, amphipathic molecules are generally retained longer since the hydrophobic region is localized to one side of the molecule, forming a preferred binding domain (Chen et al. 2002; Hodges et al. 1994; Kondejewski et al. 1999; Mant et al. 2002b, 2002c; Mant et al. 1998a; Mant et al. 1998b; Mant et al. 1993; Sereda et al. 1994; Yu et al. 2000; Zhou et al. 1990); also, the tertiary and quaternary structures of globular proteins are generally disrupted upon binding to the stationary phase in RP-HPLC, since hydrophobic interactions responsible for the higher order molecular structures are disrupted (Ingraham et al. 1985; Lau et al. 1984a; Lau et al. 1984b; Mant et al. 1997; Mant et al. 1989; Sereda et al. 1994; Zhou et al. 1990). If the monomeric structure of a protein is unfolded in the hydrophobic environment of the matrix and in the organic solvents used in RP-HPLC, then specific self-association cannot occur. However, both organic solvent in the mobile phase and contact with the hydrophobic matrix can stabilize the secondary structure of amphipathic molecules (α-helix and β-sheet) (Blondelle et al. 1995; Purcell et al. 1995; Steer et al. 1998; Steiner et al. 1991; Zhou et al. 1990). Though oligomerization of amphipathic molecules will be disrupted on binding to the hydrophobic matrix, the stabilization of the secondary structure by the organic solvent in the mobile phase may facilitate the potential for association of secondary structural elements. The association of amphipathic molecules in the mobile phase during partitioning will decrease the retention time of the molecule compared to the retention time of a molecule where no self-association takes place. This decrease would presumably be proportional to the molecular binding affinity of the secondary structure element in the mobile phase. Thus, this technique will work for any molecule whose structure is stabilized by the hydrophobic matrix and hydrophobic solvents in the mobile phase.

Size-Exclusion Chromatography *vs*. Reversed-Phase Chromatography

Unlike RP-HPLC, in which hydrophobic interactions between the analyte molecule and the column matrix primarily determine retention time, SEC retention time is determined by the hydrodynamic radius of the molecule in solution. Smaller molecules are retained by the SEC column and thus have longer retention times; high affinity self-association in solution increases hydrodynamic radius and decreases retention time, so that it is possible to observe multiple peaks in the case of a molecule adopting several oligomeric species if they are in slow exchange. An excellent example of SEC monitoring of the effect of amphipathic α-helical peptide concentration on oligomerization state was reported by Wagschal *et al.* (Wagschal et al. 1999a). These authors observed an equimolar mixture of trimeric and monomeric species at a peptide concentration of 500 μM which, upon dilution to 2.5 μM, was converted predominantly to monomer. Due to a slow exchange rate for interconversion of these oligomerization states relative to overall run time, two distinct peaks representing the trimeric and monomeric states were observed at high peptide concentrations. SEC has also been used to demonstrate the oligomerization state of small amphipathic α-helices that form dimeric or trimeric α-helical coiled-coils (Lau et al. 1984a; Lau et al. 1984b; Mant et al. 1997). There is an inherent separation range in all SEC columns, with the lower limit typically ~0.5 – 1 kDa for peptide columns; however, in RP-HPLC, there are no such size limitations. In SEC, the analyte concentration is diluted on the column during elution, whereas, during RP-HPLC, the analyte is eluted as a single narrow concentrated peak, regardless of initial loading concentrations. Because of the dilution effect in SEC, it is also less sensitive to detecting lower affinity self-association than RP-HPLC. Finally, since salt is typically included in the elution buffer for SEC (100-300 mM) to prevent nonspecific electrostatic interactions with the matrix (Mant et al. 1987), molecules may have different solubility limits in SEC buffer, as was the case for GS14 (insoluble in 100 mM NaCl).

Behavior of Linear Control Peptides

The temperature profiles of both GS14 lin and GS14K4 lin were not completely linear compared to the profile of GS14K4 A6 lin. The cause of the deviation from a linear temperature-dependence in GS14 lin and GS14K4 lin can best be explained by peptide self-association in aqueous solvent. GS14 lin showed deviation from linearity only at lower temperatures, suggesting that it exhibited self-association between 5-15°C. Previous molecular modeling studies of linear GS14 showed that the N- and C-termini are oriented close to one another and that the adoption of β-sheet structure was possible (Gibbs et al. 1998). By adopting a β-sheet structure, linear GS14 would become more amphipathic and increase its likelihood of dimerizing/aggregating in solution. Since secondary structure is disrupted at higher temperatures, the adoption of β-sheet structure and reduction in retention time occurred only at temperatures below 15°C for GS14 lin. This observation is not surprising considering that GS14 lin was also shown to adopt a β-sheet structure in 50% trifluorethanol (Fig. 7-4), a solvent, as noted previously, known to mimic the hydrophobic environment of the reversed-phase matrix (Zhou et al. 1990).

Role of Self-Association in Antimicrobial Peptide Activity

Based on RP-HPLC results in the present study, as well as previous biological activity data (Kondejewski et al. 2002), we observed that the GS14K4 peptides that showed the smallest temperature coefficients of retention had little or no activity against microbial or human cells. However, some peptides that showed a large extent of self-association in solution (GS14 and GS14 X_D4 analogs GS14 F_D4, GS14 L_D4, GS14 A_D4, Fig. 7-6) showed strong hemolytic activity with weak antimicrobial activity (unpublished results). It is known that antimicrobial peptides with high peptide hydrophobicity lose microbial specificity and become very hemolytic, *i.e.* toxic to red blood cells (Kondejewski et al. 2002). It is plausible that the high peptide hydrophobicity also results in greater peptide self-association in solution, as observed with GS14 and other GS14 X_D4 peptides. The most efficacious peptide studied to date, GS14K4, had a lower degree of self-association, with a T_p of 20°C, a hemolytic activity of 200 μg/ml and an average antimicrobial activity of 4 μg/ml (larger values correspond to poor activity). This suggests that high degrees of self-association may not be desirable for optimal microbial specificity. However, the role of aqueous self-association in peptide cytolytic activity has not been well studied, due to the relatively small size of peptides and the lack of suitable analytical methods to date. Temperature profiling in RP-HPLC may be a useful technique to examine other antimicrobial peptides to see if a relationship exists between the degree of self-association in solution, antimicrobial activity, and hemolytic activity.

Temperature Profiling with Other Types of Molecules

Temperature profiling in RP-HPLC in our laboratory has also been used to study the unfolding of monomeric α-helices and α-helices that dimerize (Mant et al. 2003), as well as α-helices that dimerize to form coiled-coils (Mant et al.). In all cases, we have observed similar nonlinear profiles among the two classes of structures able to dimerize (β-sheet and α-helix) and linear profiles with unstructured peptides.

The β-sheet peptides in the present study do not have an easily identifiable parameter that changes during the transition between higher-order self-association and monomer. Admittedly, the ratios of the wavelengths of the local minima appeared to shift with higher GS14 concentration, suggesting aggregation, and this hypothesis was supported by additional fluorescence studies (Jelokhani-Niaraki et al. 2001). Unlike α-helical coiled-coils, which lose both quaternary and secondary structure upon denaturation, we believe that only the quaternary structure is lost when the cyclic β-sheet peptides in our study no longer self-associate, i.e., one observes essentially the same β-sheet secondary structure over the entire denaturation range. In all cases, the control peptides with undefined structure were used to normalize profile data to account for general temperature effects associated with changes in solvent viscosity and mass transfer rates, so that we could examine the effect of temperature specifically on peptide structure.

Additional Considerations

While temperature profiling in reversed-phase chromatography is a useful technique for evaluating self-association in small amphipathic molecules, there are aspects of the technique that merit further discussion if one considers extending the methodology to analyze other kinds of molecules. Since the technique denatures proteins by exposing hydrophobic side-chains upon binding to the stationary phase and contacting organic solvent, this approach is unsuitable for assessing the self-association of native folded globular proteins stabilized by hydrophobic interactions.

On the positive side, the sensitivity of the temperature profiling described in this work could be further amplified by using narrower diameter (micro-, capillary, or nano-) reversed-phase columns, which would require less sample for analyses than the narrow bore (2.1 mm diameter) column used in the present study. Also, a complete temperature profile only requires time spent on sample preparation, since the Agilent 1100 chromatograph can be programmed to perform multiple runs, automatically regulate temperature, inject and monitor samples, and store data after each elution. Thus, although a complete set of runs may take sixteen hours of real time, the actual time the experimenter requires to set up the system is minimal. Also of significance is the point that, since the peptide oligomerization being measured is due to hydrophobic interactions and is, thus, pH-independent, this approach may be employed at any pH value suitable for chromatography – generally pH 2-8 for silica-based packing materials, although more alkaline conditions are possible with non-silica-based supports (Mant et al. 2002a).

Hence, this temperature profiling approach is not restricted to just the pH 2 conditions employed in the present study.

Chapter 7-4. Conclusions

Temperature profiling in RP-HPLC can be used to detect and measure self-association of small molecules driven together by the hydrophobic effect, due to the technique's extremely high sensitivity. By performing a series of reversed-phase elutions at a range of temperatures, we have demonstrated that self-association of small molecules in solution can be detected using extremely small (ng) quantities. One can easily identify self-association based on the nonlinear relationship between analyte retention time and temperature. The technique is applicable to association in both α-helical and β-sheet structures, cyclic and linear, and does not have either an upper or a lower size limit for detection. We envision that this technique can also be used for non-peptide analytes as well as larger biomolecules, as long as the domain responsible for self-association is hydrophobic and is stabilized by the organic modifier in the aqueous/organic solvent used in RP-HPLC.

Chapter 7-5. References

Benedek, K. 1993. Kinetics of recombinant human bran-derived neurotropic factor unfolding under reversed-phase liquid chromatography conditions. *J. Chromatogr.* **646:** 91-98.

Blondelle, S.E., Ostresh, J.M., Houghten, R.A. and Perez-Paya, E. 1995. Induced conformational states of amphipathic peptides in aqueous/lipid environments. *Biophys. J.* **68:** 351-359.

Chao, H., Houston, M.E., Jr., Grothe, S., Kay, C.M., O'Connor-McCourt, M., Irvin, R.T. and Hodges, R.S. 1996. Kinetic study on the formation of a de novo designed heterodimeric coiled-coil: use of surface plasmon resonance to monitor the association and dissociation of polypeptide chains. *Biochemistry* **35:** 12175-12185.

Chen, Y., Mant, C.T. and Hodges, R.S. 2002. Determination of stereochemistry stablity coefficients of amino acid side-chains in an amphipathic alpha-helix. *J. Peptide Res.* **59:** 18-33.

De Crescenzo, G., Litowski, J.R., Hodges, R.S. and O'Connor-McCourt, M.D. 2003. Real-time monitoring of the interactions of *de novo* designed coiled-coils using Surface Plasmon Resonance: Effect of chain length on the kinetic and thermodynamic constants of interaction. *Biochemistry* (in press).

Gibbs, A.C., Kondejewski, L.H., Gronwald, W., Nip, A.M., Hodges, R.S., Sykes, B.D. and Wishart, D.S. 1998. Unusual beta-sheet periodicity in small cyclic peptides. *Nat Struct Biol* **5:** 284-288.

Hodges, R.S., Zhu, B.-Y., Zhou, N.E. and Mant, C.T. 1994. Reversed-phase chromatography as a useful probe of hydrophobic interactions involved in protein folding and protein stability. *J. Chromatogr. A* **676:** 3-15.

Ingraham, R.H., Lau, S.Y.M., Taneja, A.K. and Hodges, R.S. 1985. Denaturation and the effects of temperature on hydrophobic interaction and reversed-phase high performance liquid chromatography of proteins: Bio-Gel TSK-Phenyl-5-PW support. *J. Chromatogr.* **327:** 77-92.

Jelokhani-Niaraki, M., Kondejewski, L.H., Farmer, S.W., Hancock, R.E., Kay, C.M. and Hodges, R.S. 2000. Diastereoisomeric analogues of gramicidin S: structure, biologicalactivity and interaction with lipid bilayers. *Biochem J* **349 Pt 3:** 747-755.

Jelokhani-Niaraki, M., Prenner, E.J., Kay, C.M., McElhaney, R.N. and Hodges, R.S. 2002. Conformation and interaction of the cyclic cationic antimicrobial peptides in lipid bilayers. *J Pept Res* **60:** 23-36.

Jelokhani-Niaraki, M., Prenner, E.J., Kondejewski, L.H., Kay, C.M., McElhaney, R.N. and Hodges, R.S. 2001. Conformation and other biophysical properties of cyclic antimicrobial peptides in aqueous solutions. *J Pept Res* **58:** 293-306.

Katsu, T., Kuroko, M., Morikawa, T., Sanchika, K., Fujita, Y., Yamamura, H. and Uda, M. 1989. Mechanism of membrane damage induced by the amphipathic peptides gramicidin S and melittin. *Biochim Biophys Acta* **983:** 135-141.

Kondejewski, L.H., Farmer, S.W., Wishart, D.S., Kay, C.M., Hancock, R.E. and Hodges, R.S. 1996. Modulation of structure and antibacterial and hemolytic activity by ring size in cyclic gramicidin S analogs. *J Biol Chem* **271:** 25261-25268.

Kondejewski, L.H., Jelokhani-Niaraki, M., Farmer, S.W., Lix, B., Kay, C.M., Sykes, B.D., Hancock, R.E. and Hodges, R.S. 1999. Dissociation of antimicrobial and hemolytic activities in cyclic peptide diastereomers by systematic alterations in amphipathicity. *J Biol Chem* **274:** 13181-13192.

Kondejewski, L.H., Lee, D.L., Jelokhani-Niaraki, M., Farmer, S.W., Hancock, R.E. and Hodges, R.S. 2002. Optimization of microbial specificity in cyclic peptides by modulation of hydrophobicity within a defined structural framework. *J Biol Chem* **277:** 67-74.

Lau, S.Y., Taneja, A.K. and Hodges, R.S. 1984a. Synthesis of a model protein of defined secondary and quaternary structure. Effect of chain length on the stabilization and formation of two-stranded alpha-helical coiled-coils. *J Biol Chem* **259:** 13253-13261.

Lau, S.Y.M., Taneja, A.K. and Hodges, R.S. 1984b. Effects of HPLC solvents and hydrophobic supports on the secondary and quaternary structure of a model protein: Reversed-phase and size-exclusion high performance liquid chromatography. *J. Chromatogr.* **317:** 129-140.

Lewis, R.N., Prenner, E.J., Kondejewski, L.H., Flach, C.R., Mendelsohn, R., Hodges, R.S. and McElhaney, R.N. 1999. Fourier transform infrared spectroscopic studies of the interaction of the antimicrobial peptide gramicidin S with lipid micelles and with lipid monolayer and bilayer membranes. *Biochemistry* **38:** 15193-15203.

Litowski, J.R. and Hodges, R.S. 2001. Designing heterodimeric two-stranded alpha-helical coiled-coils: the effect of chain length on protein folding, stability and specificity. *J Pept Res* **58:** 477-492.

Litowski, J.R. and Hodges, R.S. 2002. Designing heterodimeric two-stranded alpha-helical coiled-coils. Effects of hydrophobicity and alpha-helical propensity on protein folding, stability, and specificity. *J Biol Chem* **277:** 37272-37279.

Mant, C.T., Chao, H. and Hodges, R.S. 1997. Effect of mobile phase on the oligomerization state of alpha-helical coiled-coil peptides during high-performance size-exclusion chromatography. *J. Chromatogr. A* **791:** 85-98.

Mant, C.T., Chen, Y. and Hodges, R.S. Temperature profiling of polypeptides in reversed-phase chromatography: I. Monitoring of dimerization and unfolding of amphipathic alpha-helical peptides. *J. Chromatogr. A* (submitted).

Mant, C.T. and Hodges, R.S. 2002b. Reversed-phase liquid chromatography as a tool in the determination of the hydrophilicity/hydrophobicity of amino acid side-chains at a ligand-receptor interface in the presence of different aqueous environments: I. Effect of varying peptide ligand hydrophobicity. *J. Chromatogr. A* **972:** 45-60.

Mant, C.T. and Hodges, R.S. 2002c. Reversed-phase liquid chromatography as a tool in the determination of the hydrophilicity/hydrophobicity of amino acid side-chains at a ligand-receptor interface in the presence of different aqueous environments: II. Effect of varying peptide ligand hydrophobicity. *J. Chromatogr. A* **972:** 61-75.

Mant, C.T., Kondejewski, L.H. and Hodges, R.S. 1998a. Hydrophilic interaction/cation-exchange chromatography for separation of cyclic peptides. *J. Chromatogr. A* **816:** 79-88.

Mant, C.T., Litowski, J.R. and Hodges, R.S. 1998b. Hydrophilic interaction/cation exchange chromatography for separation of amphipathic alpha-helical peptides. *J. Chromatogr. A* **816:** 65-78.

Mant, C.T., Parker, J.M.R. and Hodges, R.S. 1987. Size-exclusion HPLC of peptides: Requirement for peptide standards to monitor non-ideal behavior. *J. Chromatogr.* **397:** 99-112.

Mant, C.T., Zhou, N.E. and Hodges, R.S. 1989. Correlation of protein retention times in reversed-phase chromatography with polypeptide chain length and hydrophobicity. *J. Chromatogr.* **476:** 363-375.

Mant, T.C., Tripet, B. and Hodges, R.S. 2003. Temperature profiling of polypeptides in reversed-phase chromatography: II. Monitoring of folding and stability of two-stranded alpha-helical coiled-coils. *J. Chromatogr. A* (submitted).

McInnes, C., Kondejewski, L.H., Hodges, R.S. and Sykes, B.D. 2000. Development of the structural basis for antimicrobial and hemolytic activities of peptides based on gramicidin S and design of novel analogs using NMR spectroscopy. *J Biol Chem* **275:** 14287-14294.

Monera, O.D., Sereda, T.J., Zhou, N.E., Kay, C.M. and Hodges, R.S. 1995. Relationship of side-chain hydrophobicity and alpha-helical propensity on the stability of the single-stranded amphipathic alpha-helix. *J. Pept. Sci.* **1:** 319-329.

Prenner, E.J., Lewis, R.N., Kondejewski, L.H., Hodges, R.S. and McElhaney, R.N. 1999a. Differential scanning calorimetric study of the effect of the antimicrobial peptide gramicidin S on the thermotropic phase behavior of phosphatidylcholine, phosphatidylethanolamine and phosphatidylglycerol lipid bilayer membranes. *Biochim Biophys Acta* **1417:** 211-223.

Prenner, E.J., Lewis, R.N. and McElhaney, R.N. 1999b. The interaction of the antimicrobial peptide gramicidin S with lipid bilayer model and biological membranes. *Biochim Biophys Acta* **1462:** 201-221.

Prenner, E.J., Lewis, R.N., Neuman, K.C., Gruner, S.M., Kondejewski, L.H., Hodges, R.S. and McElhaney, R.N. 1997. Nonlamellar phases induced by the interaction of gramicidin S with lipid bilayers. A possible relationship to membrane-disrupting activity. *Biochemistry* **36:** 7906-7916.

Purcell, A.W., Aguilar, M.I., Wettenhall, R.E.W. and Hearn, M.T.W. 1995. The induction of amphipathic alpha-helical structures in peptides during RP-HPLC. *Peptide Res.* **8:** 160-170.

Richards, K.L., Aguilar, M.I. and Hearn, M.T.W. 1994. A comparative study of the retention behaviour and stability of cytochrome c in reversed-phase high-performance liquid chromatography. *J. Chromatogr.* **676:** 17-31.

Rosenfeld, R. and Benedek, K. 1993. Conformational changes of brain-derived neurotrophic factor during reversed-phase high-performance liquid chromatography. *J. Chromatogr.* **632:** 29-36.

Sereda, T.J., Mant, C.T., Sonnichsen, F.D. and Hodges, R.S. 1994. Reversed-phase chromatography of synthetic amphiptahic alpha-helical peptides as a model for ligand-receptor interactions: Effect of changing hydrophobic environment on the relative hydrophilicity/hydrophobicity of amino acid side-chains. *J. Chromatogr. A* **676:** 139-153.

Steer, D.L., Thompson, P.E., Blondelle, S.E., Houghten, R.A. and Aguilar, M.I. 1998. Comparison of the binding of α-helical and β-sheet peptides to a hydrophobic surface. *J. Peptide Res.* **51:** 401-412.

Steiner, V., Scharr, M., Bornsen, K.O. and Mutter, M. 1991. Retention behaviour of a template-assembled synthetic protein and its amphiphilic building blocks on reversed-phase columns. *J. Chromatogr.* **586:** 43-50.

Su, J.Y., Hodges, R.S. and Kay, C.M. 1994. Effect of chain length on the formation and stability of synthetic alpha-helical coiled coils. *Biochemistry* **33:** 15501-15510.

Tripet, B., Wagschal, K., Lavigne, P., Mant, C.T. and Hodges, R.S. 2000. Effects of side-chain characteristics on stability and oligomerization state of a de novo-designed model coiled-coil: 20 amino acid substitutions in position "d". *J Mol Biol* **300:** 377-402.

Wagschal, K., Tripet, B. and Hodges, R.S. 1999a. De novo design of a model peptide sequence to examine the effects of single amino acid substitutions in the hydrophobic core on both stability and oligomerization state of coiled-coils. *J Mol Biol* **285:** 785-803.

Wagschal, K., Tripet, B., Lavigne, P., Mant, C. and Hodges, R.S. 1999b. The role of position a in determining the stability and oligomerization state of alpha-helical coiled coils: 20 amino acid stability coefficients in the hydrophobic core of proteins. *Protein Sci* **8:** 2312-2329.

Yu, Y.B., Wagschal, K.C., Mant, C.T. and Hodges, R.S. 2000. Trapping the monomeric alpha-helical state during unfolding of coiled-coils by reversed-phase chromatography. *J. Chromatogr. A* **890:** 81-94.

Zhou, N.E., Mant, C.T. and Hodges, R.S. 1990. Effect of preferred binding domains on peptide retention behavior in reversed-phase chromatography: Amphipathic Alpha-Helices. *Pept. Res.* **3:** 8-20.

Appendix 1: Structure-activity relationships of *de novo* designed cyclic antimicrobial peptides based on gramicidin S

A version of this chapter has been published. Lee, D. L. & Hodges, R. S. 2003. Biopolymers. 71: 28-48. This manuscript was part of the Vincent du Vigneaud Award lecture by Robert Hodges at the Gordon Research Conference on the Chemistry and Biology of Peptides, 2002.

Chapter I-1. Introduction

Antimicrobial peptides (AMPs) are a large class of biomolecules that form part of the biological defense system of a broad range of multicellular and single-celled organisms (Hancock et al. 2000a; van 't Hof et al. 2001; Zasloff 2002). They act rapidly in a concentration-dependent manner, and their mode of action has been proposed to include targets such as the microbial membrane and/or intracellular components such as heat shock proteins (Otvos et al. 2000), DNA, and RNA (Hancock et al. 2002). Since the discovery of the first nonhemolytic antimicrobial peptides in frog skin (Zasloff 1987), hundreds have been discovered and recorded in databases and characterized in terms of structure and function (Tossi et al. 2000). Though varying widely in structural categories, general subcategories include the linear α-helical class, the linear extended peptides with one or two amino acids in high abundance, the looped structures, the disulfide-bridged β-strands and cyclic β-sheet peptides (Epand et al. 1999).

In spite of the variation among structural subclasses, some general commonalities have emerged among the majority of antimicrobial peptides that provide them with their biological activity. These include a net positive (cationic) charge, a certain hydrophobicity and amphipathicity (localization of polar and nonpolar faces), and some kind of structure formed in interactions with the lipid components of membranes. AMPs have been the focus of both academic and industrial research endeavors because of their potential as novel broad-spectrum antimicrobial therapeutics to be used against the rapidly growing numbers of antibiotic-resistant microorganisms (Hancock et al. 2000b; van't Hof et al. 2001; Zasloff 2002). The microbial membrane is the target of choice for *de novo* designed AMPs, since it is believed that bacteria are less capable of developing resistance mechanisms involving a change in the composition of their lipid bilayers. In contrast, conventional antibiotics usually must enter the intracellular compartment of microorganisms and inhibit a specific macromolecule to be effective. Resistance develops as bacterial populations mutate to counteract the effects of the antibiotic through degradation, inactivation, or physical removal of the antibiotic from the site of action, or by alteration of the molecule targeted by the antibiotic to reduce binding affinity. Moreover, these bacteria can then pass resistance genes onto other bacterial strains, thereby accelerating the threat of pathogenic infections to the global human population.

Because of the broad scope of literature already published on antimicrobial peptides, we will focus only on the work done in our laboratory detailing the research centering around the cyclic β-sheet structural framework found in the peptide antibiotic, gramicidin S (GS). Our objective with this project was to design *de novo* a cyclic β-sheet peptide with excellent broad-spectrum antimicrobial activity, negligible hemolytic activity (a measure of toxicity to red blood cells), and a high therapeutic index (therapeutic index is the hemolytic activity in μg/ml divided by the antimicrobial activity in μg/ml, resulting in a unitless value). Although the interaction of a peptide with the lipid membrane is of fundamental importance in understanding the mode of action of the various classes of antimicrobial peptides, the majority of the peptide-lipid interaction studies on gramicidin S and analogs established in collaboration with the McElhaney laboratory (Jelokhani-Niaraki et al. 2002; Jelokhani-Niaraki et al. 2001; Krivanek et al. 2001; Lewis et al. 1999; Prenner et al. 2001; Prenner et al. 1999a; Prenner et al. 1999b; Prenner et al. 1997; Salgado et al. 2001; Staudegger et al. 2000) and those performed in the Hancock laboratory (Hancock et al. 2002; Wu et al. 1999; Zhang et al. 2000; Zhang et al. 2001) will also not be discussed in detail here. Instead, emphasis will be placed on the relationship between modification of peptide structural characteristics and effects on biological activity against microbes and human cells.

Though the antibiotic gramicidin S was isolated from *Bacillus brevis* in 1944 (Gause et al. 1944) and has been studied to date for almost sixty years, its therapeutic value has been limited to topical applications because of its strong toxicity to human red blood cells (hemolysis occurring at μg/ml concentrations (Kondejewski et al. 1996a)). The peptide sequence is cyclo-FPVOLFPVOL, where underlined residues represent D-enantiomers and O denotes ornithine. Gramicidin S forms a cyclic amphipathic antiparallel β-sheet structure with a net +2 charge from the ornithine residues, a hydrophobic face of two valine and two leucine residues, and two type II′ β-turns at the Leu-D-Phe-Pro-Val positions (Fig. 1). It is hypothesized that the mode of action is primarily, but not limited to, the peptide interacting with the microbial membrane. The consequences of this peptide-lipid interaction include dissipation of the chemiosmotic potential (Wu et al. 1999; Zhang et al. 2000) and inhibition of respiratory enzymes found in the cell

Figure 1. Model of gramicidin S based on high-resolution ^{1}H-NMR structural analysis (Gibbs et al. 1998; Wishart et al. 1995b; Xu et al. 1995). Top: C_α backbone with Pro side-chains shown. Red atoms denote oxygen; blue atoms denote nitrogen. Dashed lines denote hydrogen bonds. Bottom: Representation with hydrophobic side-chains shown in green (Leu, Val, Pro and D-Phe) and basic side-chains (Orn) shown in blue.

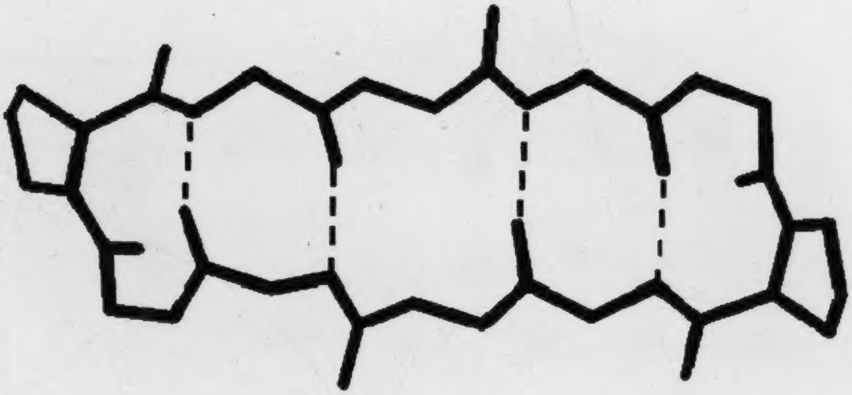

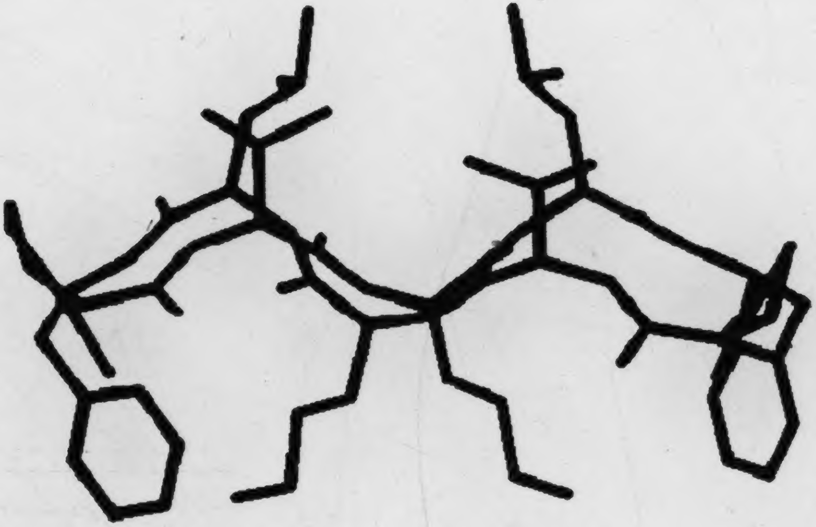

membrane (Prenner et al. 1999b). However, since maximal depolarization of electrochemical gradients has been observed at peptide concentrations below the minimal inhibitory concentration (MIC), it has been suggested that perhaps a 'multiple hit hypothesis' involving additional cytoplasmic targets is the case for GS (Zhang et al. 2001).

Interestingly, in 1995 when we began this project, there had been 50 years of extensive studies on gramicidin S and synthetic analogs without any significant breakthroughs. We were also of the opinion that, considering the lack of success over such a long period of time, no granting agency would support this project. Nevertheless, we considered the project a viable one and worthy of the challenge. We had observed that prior to our work, no thorough structure-function study of gramicidin S had been conducted. Furthermore, there were many advantages to studying this molecule in terms of the key features of GS that made it an attractive drug design candidate over other antimicrobial peptides. First, a rigid defined structure (such as the β-sheet in GS) is more amenable to structure-function studies since differences in both the structure and activity of peptide analogs could be easily compared to the parent molecule. Second, its small size should allow easy synthesis and ultimately should require fewer analogs to achieve the desired biological activities due to the smaller number of theoretical amino acid substitution sites. Third, the cyclic nature of the peptide made it resistant to proteolysis, an important aspect for future drug stability studies *in vivo*. The fourth advantage, from our perspective, was the possibility of a “lipid-only” mechanism, an idea that brought the possibility of achieving microbial specificity based only on differences in lipid composition between microbes and eukaryotic cells. However, at the time, the "lipid-only" mechanism instead brought the criticism that specificity could not be achieved if this were the case. In the following presentation we will show that not only were we able to achieve specificity for microbial cells, *i.e.* high antimicrobial activity with negligible hemolytic activity, but also that we can explain this specificity based on the difference in composition between the lipid membranes of microbes and human cells.

In order to prepare for a meaningful structure-function study, we identified five major areas that had to be addressed prior to beginning the synthesis of a series of analogs. First, was the methodology for synthesis robust and would it ensure racemization-free cyclization of the peptides? Second, does the lead compound have excellent solubility to ensure that we would not encounter solubility issues with a wide range of analogs? Third, do we have the NMR methodology for rapid evaluation of structure? Fourth, do we have the correct biological assays and enough sensitivity to accurately evaluate activity, which would allow us to distinguish between subtle changes in sequence? Finally, were there other methodologies required to improve our evaluation of various analogs?

Chapter I-2. Improvement of synthesis methodology for cyclic peptides

We developed a simple method for the facile synthesis of GS and analogs, using standard solid-phase technology and a single solution-phase cyclization step (Wishart et al. 1995b; Wishart et al. 1996). This approach was a significant improvement over previous protocols, which were based on labor-intensive and time-consuming solution-phase peptide syntheses at all stages of production. Our newer approach proved to be simple, easily automated, rapid (< 3 days), capable of producing high yields (>80%), and generally applicable to the preparation of a variety of related head-to-tail cyclic peptides. Significantly, NMR studies confirmed that cyclic peptides could be prepared with no indication of racemization. Subsequently, we utilized the formyl group for side-chain protection of lysine and ornithine residues to further improve the synthesis (Kondejewski et al. 1996b) (Fig. 2).

All peptides were synthesized by solid-phase peptide synthesis using precoupled Boc-Pro-phenylacetamidomethyl resin (PAM-resin) on an Applied Biosystems model 430A peptide synthesizer using standard t-butyloxycarbonyl (Boc) chemistry. The use of a C-terminal proline on the peptide was to prevent racemization during cyclization. This is a critical step since we believe that many of the analogs previously reported were actually racemized, which makes the interpretation of results in the literature extremely difficult. Side-chain protecting groups were 2-bromobenzyloxycarbonyl for tyrosine and formyl (CHO) for lysine and ornithine. The formyl group was utilized to produce a linear peptide with Lys or Orn side-chains still blocked after peptide cleavage from resin, ensuring that subsequent cyclization would not occur through the side-chain amino groups. Peptides were cleaved from the resin using anhydrous hydrogen fluoride in the presence of 10% anisole for 1 h at –5°C. The crude linear peptides were purified by reversed-phase chromatography (RP-HPLC). The pure linear formylated peptides were cyclized at a concentration of 2 mg/ml in N, N-dimethylformamide (DMF) using three molar equivalents of benzotriazolyl N-oxytri-dimethylamino-phosphonium hexafluorophosphate (BOP), 1-hydroxybenzotriazole (HOBt), and diisopropylethylamine (DIEA). The progress of the cyclization reaction was monitored by analytical reversed-phase HPLC and was typically complete after 12 h. Cyclic peptides were deformylated (10% HCl in methanol, 37°C for 24 h) and purified by preparative reversed-phase HPLC. Purified cyclic peptides were homogeneous by analytical reversed-phase HPLC and gave

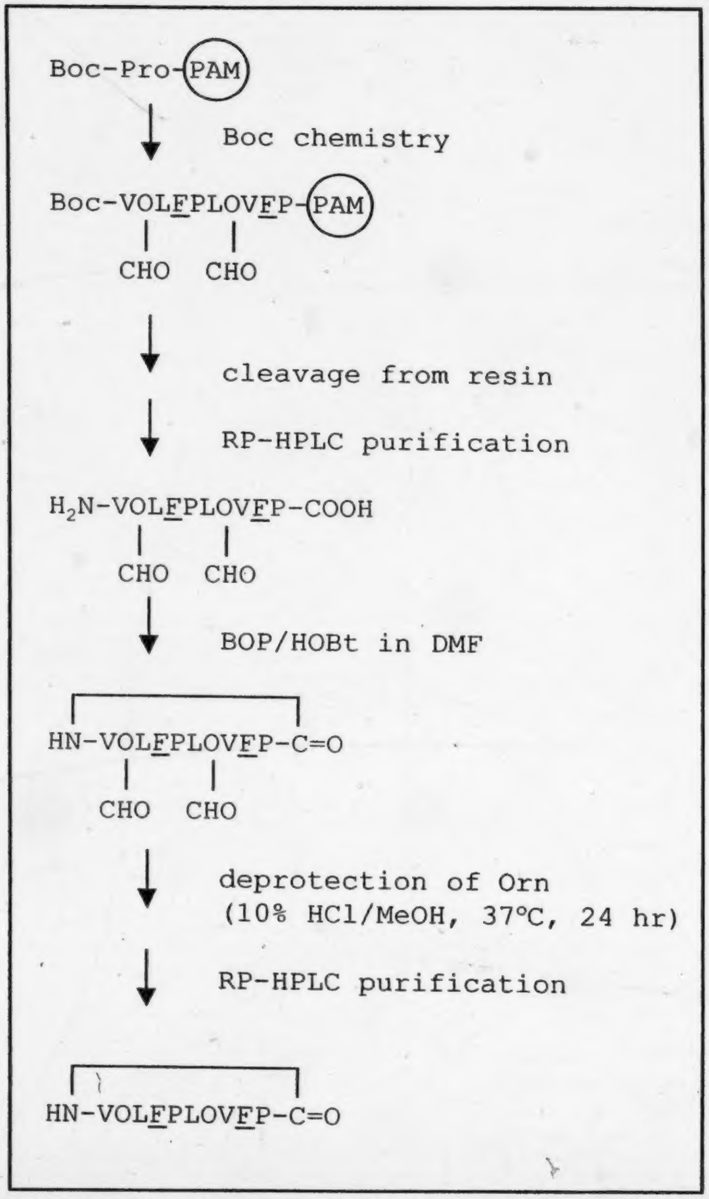
Boc-Pro-PAM
Boc chemistry
Boc-VOLFPLOVFP-PAM
CHO CHO
cleavage from resin
RP-HPLC purification
H2N-VOLFPLOVFP-COOH
CHO CHO
BOP/HOBt in DMF
HN-VOLFPLOVFP-C=O
CHO CHO
deprotection of Orn
(10% HCl/MeOH, 37°C, 24 hr)
RP-HPLC purification
HN-VOLFPLOVFP-C=O

Figure 2. Synthesis scheme of cyclic β-sheet peptides (Kondejewski et al. 1996b). One-letter amino acid code is used; D-amino acids are underlined. PAM denotes phenylacetamidomethyl polystyrene resin for solid-phase peptide synthesis (see text for definitions of other abbreviations).

correct primary ion molecular masses by mass spectrometry as well as appropriate amino acid analysis ratios. For further details of the synthesis protocol, refer to our publication (Kondejewski et al. 1996b).

Chapter I-3. Improvement of aqueous solubility of cyclic peptides

GS is not readily soluble in water and often precipitates in the presence of divalent counterions. In order to design β-sheet analogs that were much more water-soluble and much less sensitive to salt or pH, we investigated the effect of replacing the hydrophobic amino acid in the two β-turns of GS (Fig. 1, bottom) with a series of polar amino acids (Wishart et al. 1995b). Thus, analogs were synthesized with polar or charged amino acids D-Tyr, D-Ser, D-Asn and D-His in the turn positions containing D-Phe in GS. Both the D-Tyr and D-Ser analogs exhibited considerably improved solubility over GS, while, importantly, maintaining both β-sheet structure (as confirmed by NMR and far-UV CD spectroscopy) and biological activity (Kondejewski et al. 1996a; Wishart et al. 1995b; Wishart et al. 1996).

Chapter I-4. Development of NMR methodology to evaluate structure of cyclic β-sheet peptides

Unequivocal confirmation of β-sheet conformation of a particular GS analog or, indeed, detection of periodic variation in secondary structural content due to subtle changes in sequence or sequence length is immensely important for interpretation of subsequent structure/function studies. We set out to characterize GS analogs by NMR, generally assigning NMR spectra using conventional ^{1}H homonuclear techniques (Gibbs et al. 1998). However, as noted by other researchers (Sefler et al. 1996) we also discovered that cyclic peptides in aqueous conditions tend to exhibit relatively few interresidue Nuclear Overhauser Effects (NOEs). In addition, resonance degeneracy arising from molecular C_2 symmetry, combined with the limited variation in amino acid composition of many of the GS analogs under investigation in our laboratory, further reduced the number of useful NOEs. Thus, three-dimensional structural determination through conventional NOE-based techniques proved somewhat difficult. However, using a protocol similar to that described by Sefler *et al.*, (Sefler et al. 1996) we were able to overcome these difficulties by supplementing the sparse NOE data with detailed $^3J_{HNH\alpha}$ coupling constant measurements, ^1H chemical shift values, amide exchange rates and amide temperature coefficients (for additional dihedral and hydrogen bond constraints). To overcome the problems of molecular symmetry associated with specific analogs, we used the crystal structure of native GS to assign the hydrogen bonds from amide exchange data (Gibbs et al. 1998). Furthermore, by concentrating on the backbone conformation only and making use of an efficient genetic algorithm, we were able to reduce the computational complexity of multiple structure determinations to a manageable level, thus allowing us to determine the three-dimensional NMR structures for our β-sheet peptides.

Chapter I-5. Investigation of methods for evaluating antimicrobial activity of cyclic peptides

One of the central dogmas of GS research at the time that our laboratory entered this field was the long-held belief that GS was active only against Gram-positive bacteria. We noted that for 30 years, agar-based (*i.e.*, solid-phase) assays had been used almost exclusively to measure antibacterial activity of GS and its analogs. We published an important paper in 1996 in collaboration with Dr. Robert Hancock, where we switched

Table 1. Antibacterial and antifungal activity of gramicidin S and analogs in agar-based and liquid-based assays

Peptide or Antibiotic	Minimal Inhibitory Concentration (μg/ml)[a]								
	Gram-negative[b]					Gram-positive[c]			Yeast
	E. coli UB1005	*E. coli* DC2	*E. coli* SC9251	*E. coli* SC9252	*P. aeruginosa* H187	*S. aureus* SAP0017	*S. aureus* K147	*B. subtilis* Vernon	*C. albicans* CAND105[d]
Gramicidin S (Agar)	>200	200	200	200	>200	3.1	3.1	6.2	200
Gramicidin S (Liquid)	12.5	3.1	6.2	3.1	12.5	3.1	3.1	3.1	6.2
Polymixin B	0.1	0.1	0.1	64	0.3	>64	>64	>64	>64
Gentamicin	0.3	0.3	1	4	0.3	64	2	1	>64
Ceftazidime	0.3	0.03	0.1	4	0.5	2	2	32	>64
Methicillin	>512	0.5	256	128	256	16	0.5	32	>512
Fungizone	>5	>5	>5	>5	>5	>5	>5	>5	1.3

[a] Minimal inhibitory concentration of peptide or antibiotic required for 100% microbial growth inhibition, incubated overnight at 37 °C. Lower values indicate stronger antimicrobial activity.

[b] The bacterial strains are wild-type *Escherichia coli* UB1005, antibiotic supersusceptible derivative DC2, *Escherichia coli* SC9251 and its polymyxin B resistant mutant pmrA SC9252, and wild-type *Pseudomonas aeruginosa* H187.

[c] The bacterial strains are methicillin-resistant *Staphylococcus aureus* SAP0017, methicillin-resistant strain K147 from Dr. A. Chow (University of British Columbia), and wild-type *Bacillus subtilis*.

[d] Clinical lab isolate of *Candida albicans*.

from a solid-phase (agar) assay to a liquid-phase (broth) assay and clearly showed that GS and GS-related analogs were active against both Gram-positive and Gram-negative microorganisms as well as fungi (Table 1) (Kondejewski et al. 1996a). We postulated that the differences between the two assays might be a reflection of peptide solubility and diffusion in the different media or possibly a function of the water activity in the media. This discovery of broad-spectrum antimicrobial activity in broth added further support to our efforts to develop a gramicidin S-based therapeutic.

Chapter I-6. Effect of ring size in cyclic gramicidin S analogs in dissociating hemolytic and antibacterial activity

Although a number of reports published prior to 1996 detailed the properties of GS analogs with various ring sizes (Ando et al. 1995; Ando et al. 1993; Aoyagi et al. 1988; Tamaki et al. 1991; Tamaki et al. 1995; Tamaki et al. 1988) the assays used to determine antibacterial activity in all cases had been agar-based. Since we had shown that such assays severely underestimate antifungal and Gram-negative antibacterial activity compared with solution-based assays (Kondejewski et al. 1996a), we set out to synthesize a complete set of ring-size analogs (ranging from 4 - 16 residues) and to evaluate the effect of ring size on peptide secondary structure, lipid binding, lipid disruption, antibacterial activity (solution-based assays) and hemolytic activity.

The ring-size analogs varied in both the number of positively charged residues (2 Lys residues in ring sizes of 6, 8 and 10 residues; 4 Lys residues in ring sizes of 12 and 14 residues; 6 Lys residues in the ring size of 16 residues) and the number of hydrophobic residues (0, 2, 4, 4, 6 and 6 hydrophobes with ring sizes of 6, 8, 10, 12, 14 and 16 residues, respectively), increasing as the total number of residues in the cyclic peptide

Figure 3. Proposed β-sheet structures of gramicidin S ring-size analogs (6, 8, 10, 12, 14 and 16 residues), assuming that all analogs adopt the β-sheet conformation. As the ring-size analogs increase in size, the number of positively charged residues increases from 2 (in the ring sizes 6, 8 and 10) to 4 (in ring sizes 12 and 14) to 6 (in ring size 16). Similarly, the number of hydrophobic residues increases with ring size from 2 (in ring size 8) to 4 (in ring sizes 10 and 12) to 6 (in ring sizes 14 and 16).

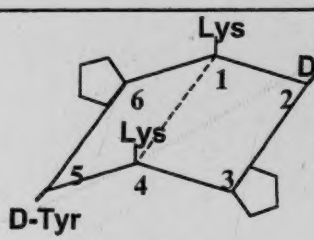
Lys
D-Tyr
Lys
D-Tyr

6

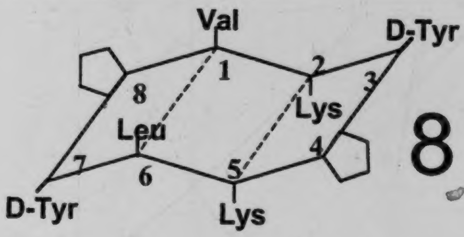
Val
D-Tyr
1
2
3
8
Lys
Leu
4
5
7
6
D-Tyr
Lys

8

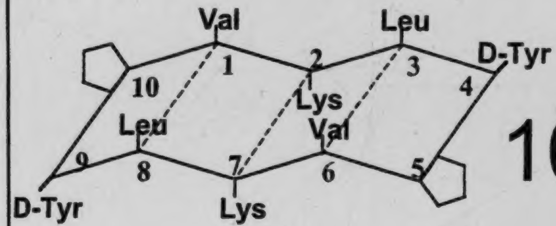
Val
Leu
D-Tyr
1
2
3
4
10
Lys
Leu
Val
9
8
7
6
5
D-Tyr
Lys

10

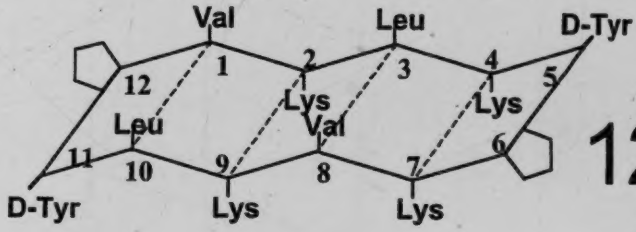
Val
Leu
D-Tyr
1
2
3
4
5
12
Lys
Leu
Val
Lys
11
10
9
8
7
6
D-Tyr
Lys
Lys

12

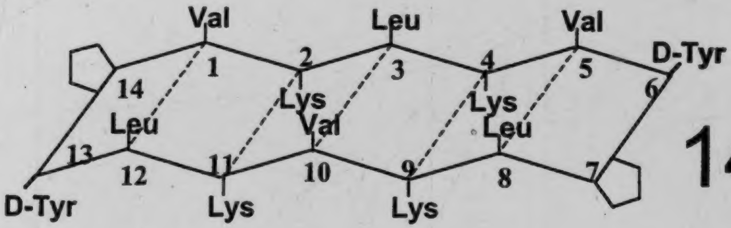
Val
Leu
Val
D-Tyr
1
2
3
4
5
6
14
Lys
Lys
Leu
Val
Leu
13
12
11
10
9
8
7
D-Tyr
Lys
Lys

14

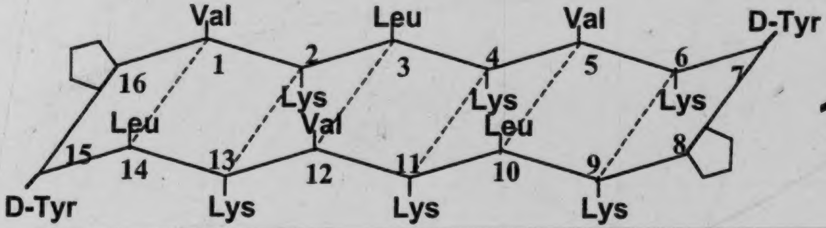
Val
Leu
Val
D-Tyr
1
2
3
4
5
6
7
16
Lys
Lys
Lys
Leu
Val
Leu
15
14
13
12
11
10
9
8
D-Tyr
Lys
Lys
Lys

16

Table 2. Peptides used in structure-activity studies of gramicidin S analogs

Peptide Name	Linear Sequence[a]	Hemolytic Activity[b]	Gram - Activity[c]	Gram + Activity[d]	Gram - Index[e]	Gram + Index[f]
GS Ring Size Analogs						
GS	VOLFPVOLFP	+++	++++	++++	2	8
GS4	YPYP	-	-	-	nd[g]	nd[g]
GS6	KYPKYP	-	-	-	nd[g]	nd[g]
GS8	VKYPKLYP	-	-	-	nd[g]	nd[g]
GS10	VKLYPVKLYP	++	+++	++++	4	8
GS12	VKLKYPKVKLYP	-	+++	-	8	1
GS14	VKLKVYPLKVKLYP	++++	-	-	0.01	0.01
GS14 Diastereomers						
GS14V1	VKLKVYPLKVKLYP	+++	+++	+++	8	14
GS14K2	VKLKVYPLKVKLYP	+++	+++	+++	12	27
GS14L3	VKLKVYPLKVKLYP	++++	-	+	<1	5
GS14K4	VKLKVYPLKVKLYP	-	++++	+++	39	63
GS14V5	VKLKVYPLKVKLYP	+	+++	++	16	42
GS14Y6	VKLKVYPLKVKLYP	+++	+	+	2	6
GS14P7	VKLKVYPLKVKLYP	++++	-	+	<1	3
GS14L8	VKLKVYPLKVKLYP	+++	++++	+++	9	20
GS14K9	VKLKVYPLKVKLYP	++	+++	+++	13	27
GS14V10	VKLKVYPLKVKLYP	++++	-	++	<1	2
GS14K11	VKLKVYPLKVKLYP	+	++++	++++	24	59
GS14L12	VKLKVYPLKVKLYP	+++	++	++	3	11
GS14Y13	VKLKVYPLKVKLYP	++++	+	+	<1	<1
GS14P14	VKLKVYPLKVKLYP	++++	+	+	<1	2
GS14 Amphipathicity Analog						
GS14 K3L4	VKKLVYPLKVKLYP	+[h]	++++	++++	19[h]	28[h]
GS14K4 Hydrophobicity Analogs						
GS14K4 Y2/F2, V3/L3	LKLKLFPLKLKLFP	++++	++++	++++	2	5
GS14K4 V3/L3	LKLKLYPLKLKLYP	+++	+++	++++	4	10
GS14K4 Y2/F2	VKLKVFPLKVKLFP	+++	++++	++++	14	13
GS14K4	VKLKVYPLKVKLYP	-	++++	+++	40	61
GS14K4 V3/A3	AKLKAYPLKAKLYP	-	+++	+	118	95
GS14K4 L3/A3	VKAKVYPAKVKAYP	-	-	-	9	6
GS14K4 V3L3/A6	AKAKAYPAKAKAYP	-	-	-	5	5

increased (Fig. 3). Biological activity was dependent on exceeding a minimal size, as peptides of less than 10 residues showed no ability to disrupt human or microbial membranes (Table 2). Our previous results with gramicidin S analogs showed that hemolytic activity was correlated with antimicrobial activity (Kondejewski et al. 1996a); however, by altering ring size we observed large differences between hemolytic and antimicrobial activities (Kondejewski et al. 1996b).

Cyclic peptides containing 6, 10 or 14 residues exhibited GS-like CD spectra under aqueous conditions and, thus, were shown to contain β-sheet structure; however, cyclic peptides containing either 8, 12 or 16 residues exhibited completely different CD spectra characteristic of a largely disordered structure (Fig. 4A). This periodicity of β-sheet content dependent on ring size was confirmed in our laboratory by ^{1}H-NMR spectroscopy using the chemical shift index (Gibbs et al. 1998; Kondejewski et al.; Wishart et al. 1995a; Wishart et al. 1992) and detailed analysis of coupling constants. Modelling of the ring structures of the linear peptides made it apparent that the N- and C-termini of the 10- and 14-residue peptides were in close proximity, thus likely maintaining the specified β-structure upon cyclization of the termini, consistent with both CD (Fig. 4A) (Kondejewski et al. 1996b) and NMR analysis (Gibbs et al. 1998). Although the widely spaced N- and C-termini of the 12-residue analog could be chemically linked during cyclization, this would lead to severe distortion of the β-sheet structure, again consistent with CD and NMR analysis. These results confirmed an absolute requirement for an odd number of residues in each strand between residues i + 1 and i + 2 of each turn to maintain β-strand character in cyclic peptides.

Schwyzer and coworkers predicted over 40 years ago that the number of amino acids within a cyclic peptide would influence the type of secondary structure adopted by the molecule (Schwyzer 1958; Schwyzer et al. 1964). Based on stereochemical considerations, Robert Schwyzer hypothesized that cyclic peptides would form β-hairpin structures if they contained 2(2n+1) residues where n = 1, 2, 3, etc. This is exactly what we observed for the cyclic peptides containing 6, 10 or 14 residues by CD and NMR analysis, where n = 1,2, or 3 respectively (Gibbs et al. 1998; Kondejewski et al. 1996b).

We also proposed some important refinements to the Schwyzer hypothesis. First, and most importantly, β-sheet formation in cyclic peptides can only take place in those molecules containing two and only two equally separated type I′ or type II′ β-turns (Gibbs et al. 1998). Thus, if a cyclic peptide that satisfies the 2(2n+1) rule does not have the appropriate sequence or the appropriate placement of these specific β-turns, it will not form a cyclic β-sheet peptide. As is the case with these peptides with type II′ turns, β-sheet formation is dictated by the appropriate placement of D-amino acids (or glycine) in the i + 1 position and a moderately strong preference for proline in the i + 2 position (Hutchinson et al. 1994). Thus, gramicidin S has Xxx-D-Phe-Pro-Xxx and our *de novo* designed molecules have Xxx-D-Tyr-Pro-Xxx in each of the turns. Second, the sequence and amino acid composition of both the turns and the β-strands is important for β-sheet periodicity. For example, substitution of glycine for isoleucine into the β-strand region or the substitution of D-His for D-Tyr in the β-turns of peptides that satisfy the 2(2n+1) rule have been shown by CD and NMR spectroscopy to disrupt the β-sheet content (Wishart et al. 1995b). These results suggest that intrinsic secondary structural propensities of individual amino acids can play a significant role in the formation of β-sheets in cyclic peptides. Third, cyclic peptides that satisfy the 2(2n+1) rule but which contain even a single D-amino acid in one of the β-strands will disrupt β-sheet structure (Kondejewski et al. 1999). This arises because the insertion of the D-amino acid will disrupt the hydrogen-bonding pattern typically associated with antiparallel β-strands. Fourth, cyclic peptides that do not contain 2(2n+1) residues will not form stable β-sheet peptides. That is, cyclic peptides containing two evenly spaced type I′ or type II′ turns will always form a disordered or random-coil structure if they contain 4n residues (where n = 1, 2, 3...). In addition, cyclic peptides containing an odd number of residues are also incapable of forming cyclic β-sheet peptides (Morita et al. 1996). Thus, in addition to the fundamental stereochemical requirements for cyclic β-sheet peptides (described previously by Schwyzer), sequence, composition and secondary structural propensities of individual amino acids are also extremely important (Gibbs et al. 1998).

The ring-size analogs showed a trend of increasing binding affinity for lipopolysaccharide (LPS) with increasing length (Fig. 4B). GS14 bound to LPS with the highest affinity of the ring-size analogs and had similar affinity to polymyxin B. An extremely significant observation was that a 14-residue analog (GS14) showed a dissociation of hemolytic *versus* antimicrobial activity, *i.e.*, GS14 showed weak antibiotic activity but extremely strong hemolytic activity for a very low therapeutic index. Thus, this analog represented an important milestone of our rational drug design. However, a true test of our ability to design an analog with potential clinical applications would be to invert the properties of GS14 and to produce a compound with very strong antimicrobial activity but weak hemolytic activity (high therapeutic index). Nevertheless, this important study represented the first systematic attempt to dissociate antimicrobial and hemolytic activity in GS analogs, demonstrating that modulation of the biological activity of cyclic

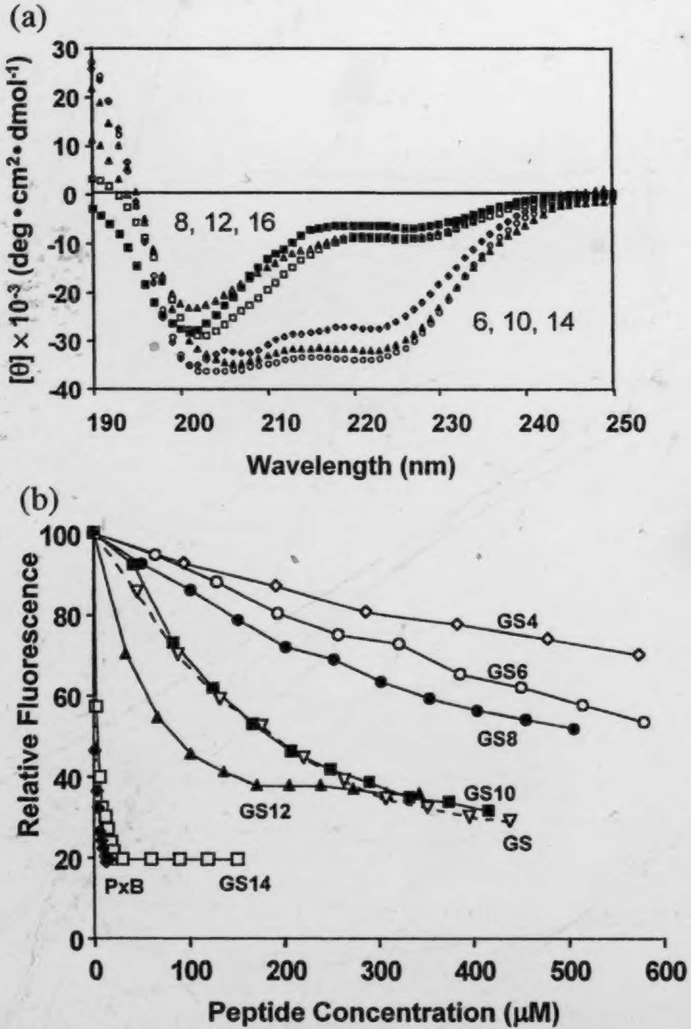

Figure 4. Panel A, far-UV circular dichroism spectra of GS ring-size analogs. Spectra were recorded in 10 mM sodium acetate buffer, pH 5.5 at 20°C (Kondejewski et al. 1996b). Note that ring-size analogs 8, 12 and 16 display significantly different spectra compared to ring-size analogs 6, 10 and 14. Panel B, displacement by GS ring-size analogs of fluorescent dansyl-polymyxin B bound to *E. coli* lipopolysaccharide (LPS). Solutions containing LPS-bound dansyl-polymyxin B were titrated with peptides and the decrease in fluorescence was monitored; polymyxin B (PxB) served as a positive control (Kondejewski et al. 1996b).

GS analogs could be achieved by variations in ring size.

Chapter I-7. Dissociation of antimicrobial and hemolytic activities using diastereomeric substitutions which alter amphipathicity

Building upon our previous demonstration that it was possible to dissociate antimicrobial and hemolytic activities through gross manipulation of β-sheet structure (ring size), we then investigated the effect of small incremental changes in amphipathicity (effective hydrophobicity and positive charge) on the antimicrobial and hemolytic properties of cyclic peptides. Specifically, we employed GS14 as the lead compound, reasoning that, since amphipathicity is intimately linked to β-sheet structure in GS14, any change in β-sheet structure, *e. g.*, through disruption by substitution of residues with their enantiomers, would directly affect the amphipathicity of the molecule. Our approach was to create a series of GS14 diastereomers in which each peptide contained a different single enantiomeric residue substitution at each position within the framework of GS14, resulting in a series of 14-residue cyclic peptides possessing gradated disruption of β-sheet structure and amphipathicity depending on the amino acid substituted. This approach had the advantage that all peptides retained the same sequence, intrinsic hydrophobicity and basicity, and differed only in structure.

The extent of disruption of the β-sheet structure in the GS14 diastereomers was evaluated by both NMR and CD analyses of GS14 and GS14 analogs (Kondejewski et al. 1999). The CD spectra of representative single residue diastereomers under aqueous conditions indicated disruption of the β-sheet structure of GS14 (Fig. 5A). The CD spectra of GS14 and representative diastereomers recorded in the presence of the lipid-mimicking solvent trifluoroethanol (TFE) (data not shown), which can stabilize β-hairpin and β-turn structures, indicated an enhancement or stabilization of β-sheet structure in the peptides (Jelokhani-Niaraki et al. 2001; Kondejewski et al. 1999). β-sheet structure in GS14 has also been observed in SDS micelles and phospholipid bilayers (Jelokhani-Niaraki et al. 2002).

Reversed-phase HPLC retention time of the GS14 diastereomers was a measure of their ability to form a large hydrophobic binding domain, a domain that was segregated to varying degrees from the hydrophilic side-chains on the opposite side of the molecule. Thus, lower retention time of a GS14 diastereomer relative to the parent, highly amphipathic GS14 molecule indicated lower nonpolar face hydrophobicity and, hence, lower amphipathicity relative to GS14 (Fig. 5B). That is, measurement of retention time of the diastereomers in RP-HPLC produced a convenient means for ranking and comparing peptide amphipathicity in this homologous series of peptides.

Significantly, we demonstrated a relationship between peptide amphipathicity (as expressed by RP-HPLC retention time) and antimicrobial activity and specificity for both Gram-negative and Gram-positive microorganisms. Table 2 and Fig. 6A demonstrate this correlation for the GS14 diastereomers, where the antimicrobial activity increased and hemolytic activity decreased with decreasing retention time in RP-HPLC (decreasing peptide amphipathicity), resulting in substantial increases in the therapeutic indices compared with GS14. To complement these results, there was also a good correlation between affinity of binding to bacterial lipopolysaccharide (LPS) and peptide retention time on RP-HPLC, with those peptides having a longer retention time (*i.e.*, more amphipathic and, hence, containing more hydrophobic and charged preferred binding domains) exhibiting higher affinity for LPS (Fig. 6B).

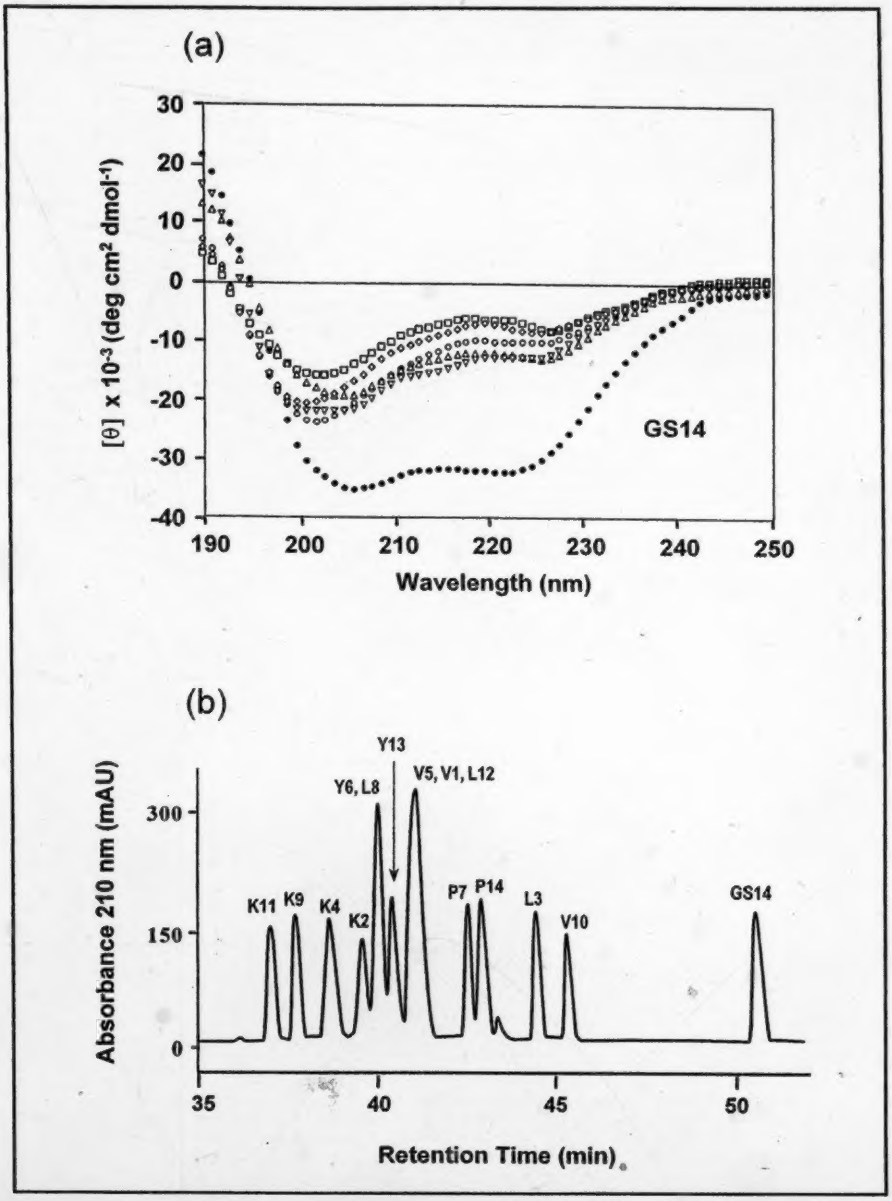

Figure 5. Panel A, CD spectra of GS14 and representative GS14 diastereomers. Spectra were recorded in 5 mM sodium acetate buffer, pH 5.5 at 20°C at a peptide concentration of approximately 0.3 mM. Samples were GS14 (●), GS14V1 (O), GS14K2 (□), GS14L3 (Δ), GS14K4 (∇) and GS14V5 (◊) (Kondejewski et al. 1999). Panel B, reversed-phase (RP) HPLC separation of GS14 and single residue substitution diastereomers. A mixture of GS14 and the 14 diastereomers was separated by RP-HPLC at 70°C using a 1% B/min gradient, where solvent A is 0.05% aqueous TFA and solvent B is 0.05% TFA in acetonitrile. The position of the enantiomeric substitution is shown for each peak on the chromatogram (Kondejewski et al. 1999).

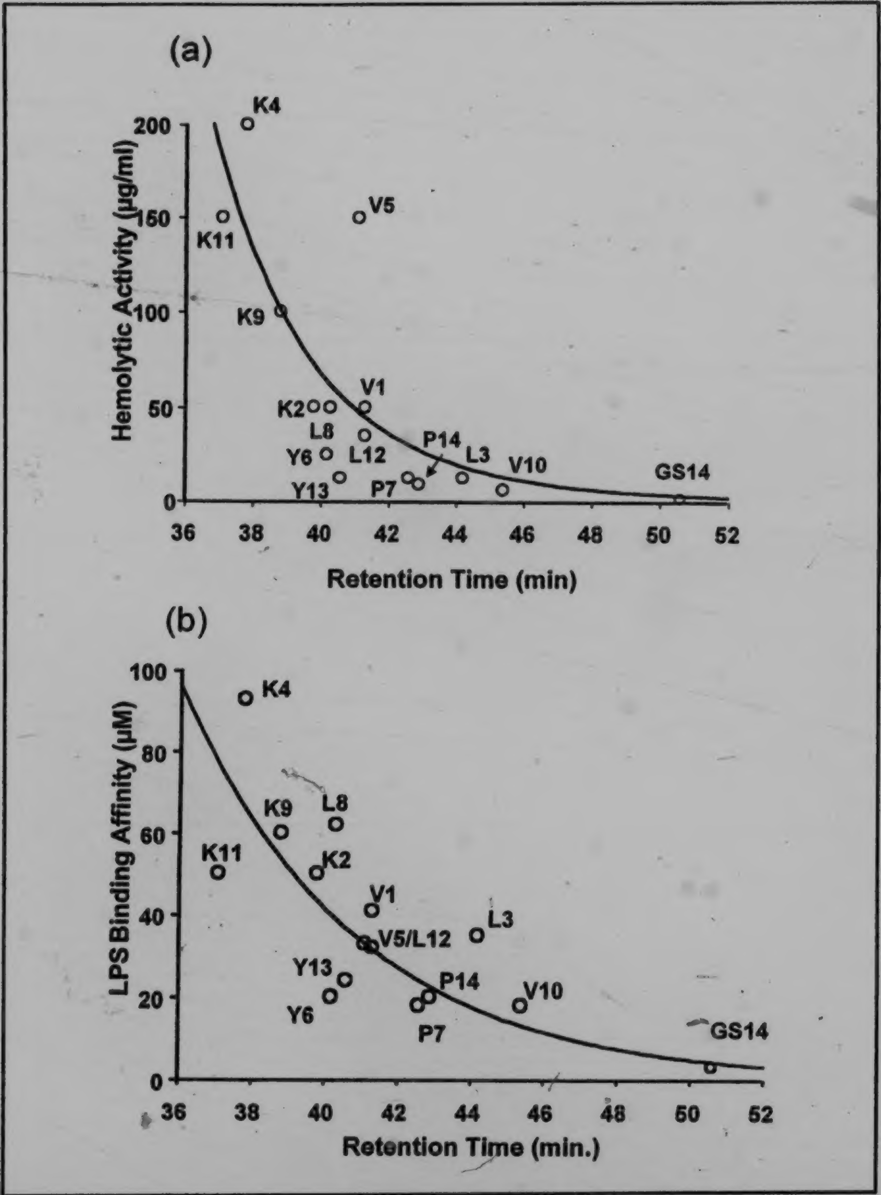

Figure 6. Panel A, correlation between amphipathicity and hemolytic activity in GS14 diastereomers. Panel B, correlation between amphipathicity and LPS binding affinity in GS14 diastereomers. Retention times on RP-HPLC were determined for each diastereomer as described in Fig. 5. Hemolytic activity and LPS binding affinity were measured as described by Kondejewski *et al*. (Kondejewski et al. 1999). The position of the enantiomeric substitution is shown for each point. The lines are drawn to guide the eye.

This study was significant in demonstrating that a highly amphipathic nature in benign medium is not desirable in these cyclic peptides, since this results in decreased specificity (low therapeutic index of GS14, <0.01 against *P. aeruginosa*) as well as increased interactions with outer membrane components, namely LPS (Fig. 6B). In addition, by systematically manipulating the amphipathicity of GS14 (by D-amino acid substitution), we were able to identify peptides with high therapeutic indices. GS14K4 had a therapeutic index of 65 against *P. aeruginosa*, which is a 6500-fold improvement over GS14; similarly, GS14K11 had a therapeutic index of 30 against *P. aeruginosa* which is a 3000-fold improvement over GS14 (Kondejewski et al. 1999). In other words, we were able to reverse the activity profile of GS14, to increase microbial specificity and decrease hemolytic activity through a reduction of peptide amphipathicity in GS14 diastereomers.

Chapter I-8. NMR structures of cyclic peptides

The solution structures of GS14 and two analogs were determined by NMR spectroscopy (Figs. 7 & 8) (McInnes et al. 2000). While GS14 forms a cyclic amphipathic β-sheet with three valine and three leucine residues on the nonpolar face and four lysines on the polar face, the diastereomer GS14K4 showed a less amphipathic disrupted cyclic β-sheet structure, with three valines, three leucines and a lysine on the nonpolar face and three lysines on the polar face (Fig. 7). Notably, one valine (Val 5) did not project onto the nonpolar face in GS14K4 but rather was rotated away from the nonpolar face to accommodate the D-Lys projecting onto this surface, thus giving further insight into the reduction in the amphipathicity and directed hydrophobicity of this analog.

Figure 7. NMR structures of GS14 (top), GS14K4 (middle), and GS14 K3L4 (bottom). The peptide backbone is colored black. Oxygen atoms are colored red (D-Tyr), hydrophobic side-chains are shown in green (Leu, Val, Pro, and D-Tyr), and basic side-chains (Lys and D-Lys) are shown in blue. The D- and L- subscripts denote amino acid side-chain stereochemistry, *e.g.* K_D4 is D-Lys4.

GS14

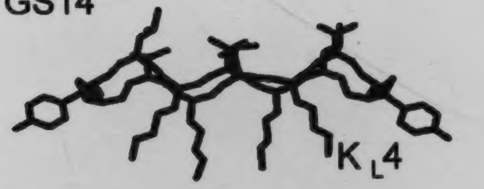

GS14K4

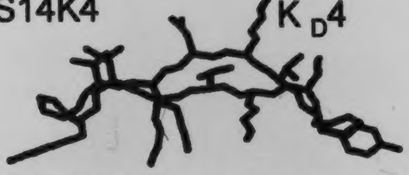

GS14 K3L4

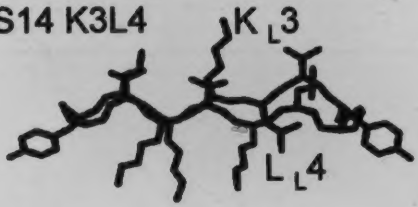

Because the CD spectra of cyclic peptides such as GS14 and its analogs are completely different from the representative spectra for β-sheet proteins, it is often difficult to interpret variations in the spectra of GS14 peptides in terms of structural changes. NMR analysis and structure determination greatly assisted in the characterization of structural variations observed from CD data, especially in the presence of the lipid-mimicking solvent, trifluoroethanol. GS14K4 appeared to possess a disrupted β-sheet structure in aqueous conditions by CD and NMR, but was demonstrated to be highly inducible in 30% TFE (McInnes et al. 2000). Since the secondary structure induced by TFE resulted in stabilization of the β-sheet and the side-chain presentation of the hydrophobic face, it is probable that GS14K4 in the environment of the biological membrane also adopts a β-sheet conformation similar to the one observed in TFE, a lipid-mimetic solvent. Because the positioning of D-Lys on the nonpolar face of GS14K4 both disrupts β-sheet structure and reduces amphipathicity it was not known which of these effects weakened hemolytic activity and improved antimicrobial activity over GS14. To address this question, a GS14 peptide analog was designed to retain β-sheet structure but have reduced amphipathicity (GS14 K3L4). In the K3L4 sequence, the positions of lysine 4 and leucine 3 in the GS14 sequence were switched so that a lysine appears on the nonpolar face and a leucine appears on the polar face (Fig. 8 and Table 2).

Although the amphipathicity of K3L4 is not identical to GS14K4, which does not have a leucine on its polar face, GS14 K3L4 also had weak hemolytic activity and strong antimicrobial activity, albeit with a lower therapeutic index than GS14K4 due to slightly stronger hemolytic activity. The increased hemolytic activity relative to GS14K4 is likely due to the somewhat higher overall hydrophobicity, as is evident by the slightly higher

GS14

GS14K4

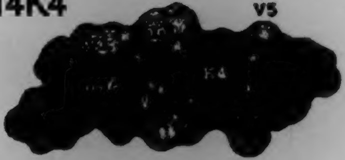

GS14 K3L4

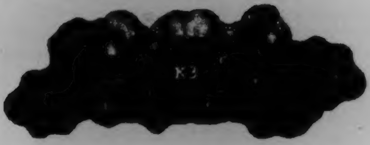

retention time on RP-HPLC (recall also the positioning of Val 5 on the nonpolar face of GS14K4) (McInnes et al. 2000). With respect to hemolytic activity, it is presumed that the presentation of a large hydrophobic face is the impetus for lysis of eukaryotic membranes. The placement of the lysine on the hydrophobic face of both GS14K4 and GS14 K3L4 (Fig. 8) consequently reduces the directed hydrophobicity of these molecules and therefore diminishes the ability of the peptide to interact with human erythrocytes. This occurs since the exterior of these cells tends to be less ionic in nature than the anionic lipids present on the external region of bacterial cell walls, and therefore, greater selectivity for the microbial membranes is obtained.

Previously, it was suggested that the high antimicrobial activity of GS14K4 was the consequence of decreased high affinity binding to outer membrane components, which in turn facilitates peptide accumulation at the inner membrane and propagation of the effects leading to subsequent lysis of the bacterial cell membrane. In an analogous manner to GS14K4, the disruption of the directed hydrophobicity through the placement of the charged residue on the hydrophobic binding face in GS14 K3L4 probably decreases the interaction with bacterial outer membranes, allowing the peptide to penetrate into the inner membrane to exert its antimicrobial effects.

Chapter I-9. Modulation of hydrophobicity of the GS14K4 nonpolar face

By changing the ring size of gramicidin S analogs, parameters including β-sheet structure, overall hydrophobicity, net charge, and ratios of hydrophobic:charged residues were altered. GS14 had the largest overall hydrophobicity and the strongest hemolytic activity, with three leucine and three valine residues on the nonpolar face. Reducing amphipathicity by placing a lysine on the nonpolar face of GS14K4 weakened hemolytic activity, suggesting that further alterations of the hydrophobicity of the nonpolar face might result in further differences in activities against microbial and eukaryotic membranes.

Based on the results from previous experiments indicating that GS14K4 had the highest therapeutic index of the cyclic peptides studied thus far, we studied a peptide series of GS14K4 analogs with a range of hydrophobicities above and below that of GS14K4 (Table 2) (Kondejewski et al. 2002). All analogs had different hydrophobic residues on the nonpolar face (in addition to the D-Lys 4), while the polar face always had three lysines. The peptides were named according to the type and number of amino acids being substituted, *e.g.* V3/L3 substituted three valines in GS14K4 with three leucines, thus increasing hydrophobicity. As evidenced by retention time on RP-HPLC, the most hydrophobic peptide substituted three valines with three leucines as well as two D-tyrosines with D-phenylalanines (peptide V3/L3, Y2/F2). The peptide with intermediate hydrophobicity was GS14K4, and the least hydrophobic peptide had the three leucines and three valines substituted with six alanine residues (peptide V3L3/A6).

In agreement with the results from the previous study of GS14 diastereomers (Kondejewski et al. 1999), there was a direct correlation (r = 0.99) between peptide hydrophobicity and LPS binding affinity for the GS14K4 hydrophobicity analogs (Fig. 9), indicating that increased peptide hydrophobicity resulted in higher binding affinity to LPS. Although the previous study used RP-HPLC retention times as a measure of amphipathicity rather than peptide hydrophobicity as in this study, both parameters are indicative of the size of the preferred binding domain on the peptide and thus can be

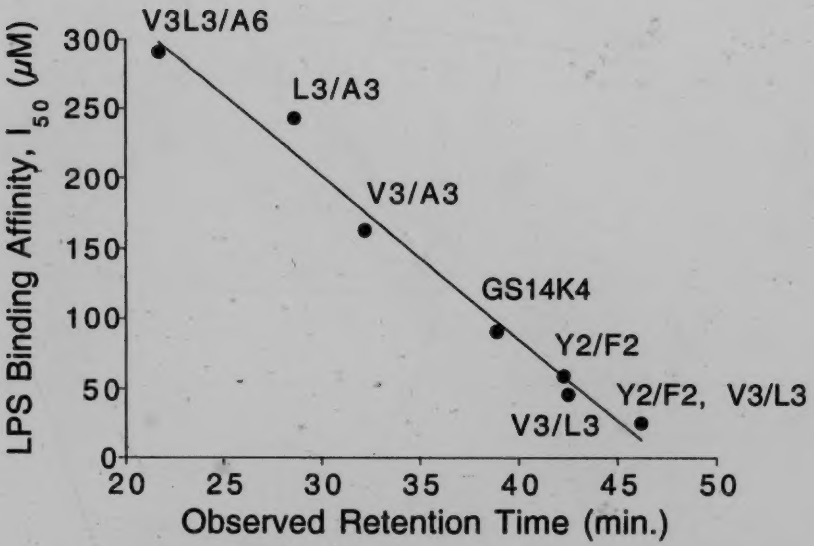

Figure 9. Correlation between peptide hydrophobicity and LPS-binding affinity in GS14K4 hydrophobicity analogs. Peptides are labelled as in Table 2. The RP-HPLC-derived retention times and LPS binding affinity were measured as described by Kondejewski *et al.* (Kondejewski et al. 2002).

compared. This was the first demonstration that peptide binding affinity to LPS was affected not only by positive charge, but also by peptide hydrophobicity.

The GS14K4 peptide analogs with the highest hydrophobicities (peptides Y2/F2, V3/L3; V3/L3; and Y2/F2) lost specificity between microbial and eukaryotic membranes, and were highly active against both. Peptides with lower hydrophobicity than GS14K4 tended to have lower activities against both microorganisms and red blood cells (Table 2). The plots of therapeutic index against peptide hydrophobicity indicated that a 'hydrophobicity window' exists, with optimal hydrophobicity dependent on the type of microorganism (Figs. 10 & 11). Again, peptide retention time on reversed-phase HPLC was used here to determine relative peptide hydrophobicity, as the amino acid substitutions on the nonpolar face of the molecule altered the overall hydrophobicity of the molecule. This is slightly different from the case of the GS14 diastereomers, where the overall hydrophobicity of the molecules did not change with enantiomeric substitution but the amphipathicities did change and HPLC retention times were used to indicate relative amphipathicity (Fig. 5B). In the GS14K4 hydrophobicity analogs, Gram-negative bacteria had an optimal peptide hydrophobicity that was lower than the optimal hydrophobicity against Gram-positive microorganisms; the best peptide (highest therapeutic index) against Gram-negative bacteria was GS14K4 V3/A3 (Fig. 10 & Table 3), while against Gram-positive microorganisms the best peptide was the more hydrophobic GS14K4 (Fig. 11 & Table 4). Against the yeast *C. albicans*, both GS14K4 V3/A3 and GS14K4 had equally high therapeutic index values and were the best two peptides in the series (Fig. 11 & Table 4).

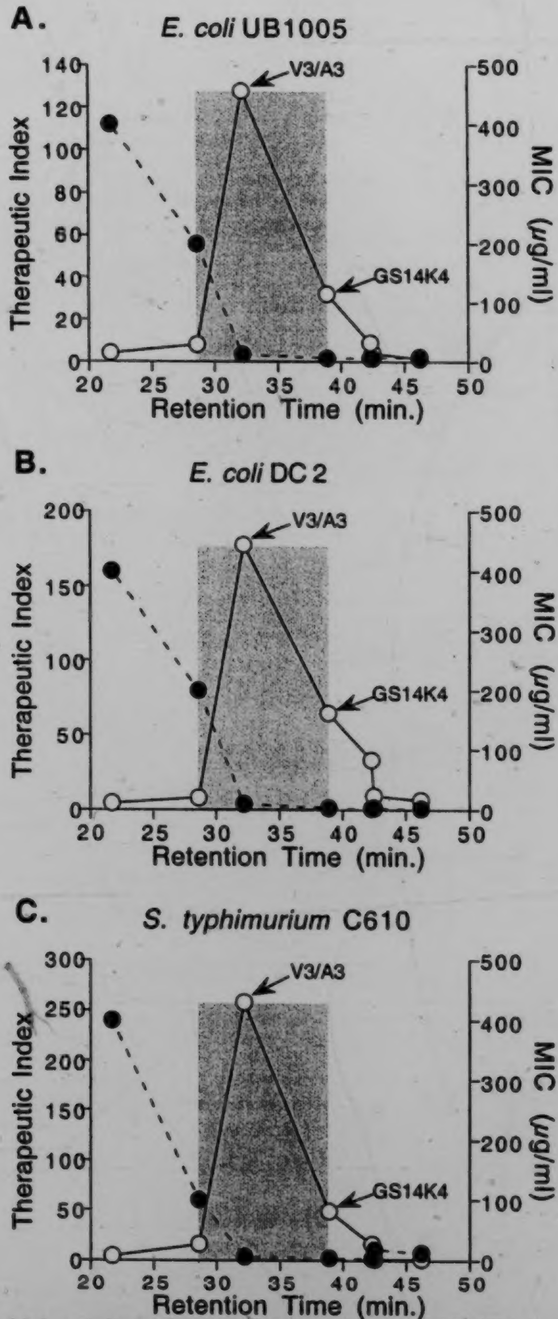

Figure 10. Antimicrobial activity and microbial specificity of GS14K4 hydrophobicity analogs against Gram-negative microorganisms. The minimal inhibitory concentration (MIC, closed circle) and the therapeutic index (open circle) of the GS14K4 analogs are plotted as a function of peptide hydrophobicity as determined by RP-HPLC (observed retention time). A, *Escherichia coli* UB 1005; B, *Escherichia coli* DC2; C, *Salmonella typhimurium* C610. A value of 400 μg/ml was used for MIC values reported as >200 μg/ml, and a value of 1600 μg/ml was used for hemolytic activities reported as >800 μg/ml to allow calculation of the therapeutic index (Kondejewski et al. 2002).

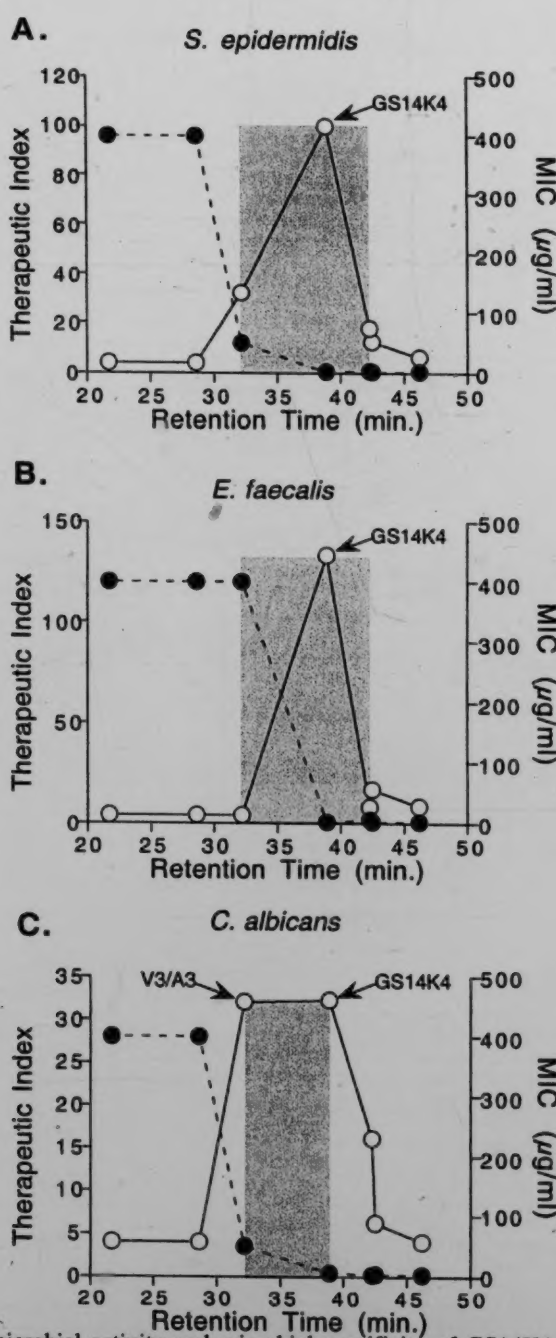

Figure 11. Antimicrobial activity and microbial specificity of GS14K4 hydrophobicity analogs against Gram-positive microorganisms and yeast. The minimal inhibitory concentration (MIC, closed circle) and the therapeutic index (open circle) of the GS14K4 analogs are plotted as a function of peptide hydrophobicity as determined by RP-HPLC (observed retention time). A, *Staphylococcus epidermis*; B, *Enterococcus faecalis*; C, *Candida albicans*. A value of 400 µg/ml was used for MIC values reported as >200 µg/ml, and a value of 1600 µg/ml was used for hemolytic activities reported as >800 µg/ml to allow calculation of the therapeutic index (Kondejewski et al. 2002).

Table 3. Comparison of biological activity of GS, GS14, GS14K4, and GS14K4 V3/A3 against Gram-negative microorganisms

Peptide	Minimal Inhibitory Concentration (μg/ml) and Therapeutic Index[a]											
	P. aeruginosa H187[b]		*P. aeruginosa* H188[b*]		*E. coli* UB1005[b]		*E. coli* DC2[b*]		*S. typhimurium* C587[b]		*S. typhimurium* C610[b*]	
	MIC	Index	MIC	Index	MIC	Index	MIC	Index	MIC	Index	MIC	Index
GS	20	0.6	6.2	2	6.2	2	3.1	4	20	0.6	10	1.3
GS14	>200	<0.01	>200	<0.01	>200	<0.01	200	0.01	>200	<0.01	>200	<0.01
GS14K4	25	8	3.1	65	6.2	32	3.1	65	11	18	4.1	49
GS14K4 V3/A3	150	11	18	89	13	128	9	178	38	42	6.2	258
Fold Improvement GS14K4:GS14[c]		800		6500		3200		6500		1800		4900
Fold Improvement GS14K4:GS[d]		13		33		16		17		30		38
Fold Improvement GS14K4 V3/A3:GS[e]		18		45		64		45		70		198

[a] Therapeutic index = hemolytic activity/minimal inhibitory concentration. For the calculation of the therapeutic index, values of 400 μg/ml were used for MIC values reported as >200 μg/ml and values of 1600 μg/ml were used for hemolytic activity values reported as >800 μg/ml. The hemolytic activities for GS, GS14, GS14K4, and GS14K4 V3/A3 were 12.5 μg/ml, 1.5 μg/ml, 200 μg/ml, and >800 respectively. Larger therapeutic index values indicate greater microbial specificity. Highest values for therapeutic index and improvement in therapeutic index for each microorganism are underlined.

[b] Microbial strains used were wild-type and antibiotic-sensitive strains of *Pseudomonas aeruginosa*, *Escherichia coli*, and *Salmonella typhimurium* (Kondejewski *et al.* 2002); an asterisk (*) denotes an antibiotic-sensitive strain.

[c] Improvement of the therapeutic index in GS14K4 *vs.* GS14 was calculated as (therapeutic index, GS14K4)/(therapeutic index, GS14). For therapeutic index values of GS14 less than 0.01, the value 0.01 was used for the calculation.

[d] Improvement of the therapeutic index in GS14K4 *vs.* GS was calculated as (therapeutic index, GS14K4)/(therapeutic index, GS).

[e] Improvement of the therapeutic index in GS14K4 V3/A3 *vs.* GS was calculated as (therapeutic index, GS14K4 V3/A3)/(therapeutic index, GS).

Table 4. Comparison of biological activity of GS, GS14, GS14K4, and GS14K4 V3/A3 against Gram-positive microorganisms

Peptide	Minimal Inhibitory Concentration (μg/ml) and Therapeutic Index[a]							
	S. epidermidis[b]		*E. faecalis*[b]		*C. xerosis*[b]		*C. albicans*[b]	
	MIC	Index	MIC	Index	MIC	Index	MIC	Index
GS	1.5	8.3	2.8	4.5	0.7	18	3.1	4
GS14	113	0.01	2.3	0.7	6.2	0.2	175	0.01
GS14K4	2	100	1.5	133	1.7	118	6.2	32
GS14K4 V3/A3	50	32	>200	4	3.1	520	50	32
Fold Improvement GS14K4:GS14[c]		10 000		190		590		3200
Fold Improvement GS14K4:GS[d]		12		30		7		8
Fold Improvement GS14K4 V3/A3:GS		4		0.9		29		8

[a] Therapeutic index = hemolytic activity/minimal inhibitory concentration. For the calculation of the therapeutic index, values of 400 μg/ml were used for MIC values reported as >200 μg/ml and values of 1600 μg/ml were used for hemolytic activity values reported as >800 μg/ml. The hemolytic activities for GS, GS14, GS14K4, and GS14K4 V3/A3 were 12.5 μg/ml, 1.5 μg/ml, 200 μg/ml, and >800 respectively. Larger therapeutic index values indicate greater microbial specificity. Highest values for therapeutic index and improvement in therapeutic index for each microorganism are underlined.

[b] Microbial strains used were wild-type *Staphylococcus epidermidis, Enterococcus faecalis, Corynebacterium xerosis,* and the yeast *Candida albicans* (Kondejewski *et al.* 2002).

[c] Improvement of the therapeutic index in GS14K4 *vs.* GS14 was calculated as (therapeutic index, GS14K4)/(therapeutic index, GS14).

[d] Improvement of the therapeutic index in GS14K4 *vs.* GS was calculated as (therapeutic index, GS14K4)/(therapeutic index, GS).

[e] Improvement of the therapeutic index in GS14K4 V3/A3 *vs.* GS was calculated as (therapeutic index, GS14K4 V3/A3)/(therapeutic index, GS).

Utilizing a rational approach to antimicrobial peptide design, we continued to use the structural framework of GS14K4 to further optimize activity and specificity through incremental changes in the intrinsic peptide hydrophobicity. These changes in hydrophobicity were accomplished through manipulation of the nature of the hydrophobic residues on the nonpolar face. The combination of disrupted structure, moderate amphipathicity and varying hydrophobicity in GS14K4 analogs yielded a peptide with a 198-fold improvement in therapeutic index over GS, and a five-fold improvement over GS14K4 (peptide GS14K4 V3/A3 against Gram-negative *S. typhimurium* C610, Table 3). Yet against Gram-positive bacteria, although the same peptide showed a four-fold improvement over GS14K4 against *C. xerosis*, it was equally or less effective against all other bacteria and fungi (Table 4). Therefore, since peptide hydrophobicity has been demonstrated here to have different optimal levels depending on the microorganism in question, modulation of peptide hydrophobicity can be used to "fine tune" the peptide specificity for microbial membranes depending on the targeted microorganism.

Chapter I-10. Other studies

Together with the McElhaney laboratory we have examined the peptide-lipid interactions between gramicidin S and related analogs and model membrane systems (see review by Prenner *et al.* (Prenner et al. 1999b) and Jelokhani-Niaraki *et al.* (Jelokhani-Niaraki et al. 2002)). The temperature of gel to liquid-crystalline lipid phase transitions was dependent on both peptide:lipid ratios and lipid composition of membranes. Importantly, vesicles containing anionic lipids found in bacterial membranes but not eukaryotic membranes (*e.g.* phosphatidylglycerol, PG) showed a greater reduction in the gel to liquid-crystalline phase transition with GS *vs.* vesicles containing lipids that are a major component of eukaryotic (*e.g.* human) cell membranes (*e.g.* phosphatidylcholine, PC) (Prenner et al. 1999a). However, in both cases the addition of GS decreased the main phase transition temperature, consistent with the strong antimicrobial *and* strong hemolytic activity exhibited by this peptide. The enhanced specificity for bacterial lipids is partially explained by electrostatic interactions between cationic peptide and anionic lipid (in the case of PG). Also, the presence of cholesterol, another major lipid component of eukaryotic membranes but not bacterial membranes, decreased permeability of PC vesicles and increased the gel to liquid-crystalline phase transition temperature in GS/PC studies, suggesting that cholesterol also helps to decrease GS toxicity in human erythrocytes and thus contributes to the slight GS specificity for microbial *vs.* eukaryotic membranes (Table 2) (Prenner et al. 2001). These studies lend support to the role that membrane lipid composition plays in microbial and eukaryotic membrane specificity as a primary target in the mode of action of GS and related analogs.

We also determined the membrane-bound structure and alignment of a gramicidin S analog substituting leucine with ^{19}F-phenylglycine for ^{19}F-NMR structure determination (Fig. 12) (Salgado et al. 2001). The analog exhibited similar antimicrobial properties to GS, within a two-fold dilution against all microorganisms tested. The peptide was found to possess a similar backbone conformation to gramicidin S, and lies parallel to the plane of the dimyristoylphosphatidylcholine (DMPC) bilayer at peptide:lipid ratios 1:80 and 1:200. In the lipid gel state, the peptide is immobilized, but in the liquid-crystalline phase the peptide becomes highly mobile and exhibits fast rotation around the bilayer normal and further wobbling with a molecular order parameter (S_{mol}) of ~0.34 (0 indicates

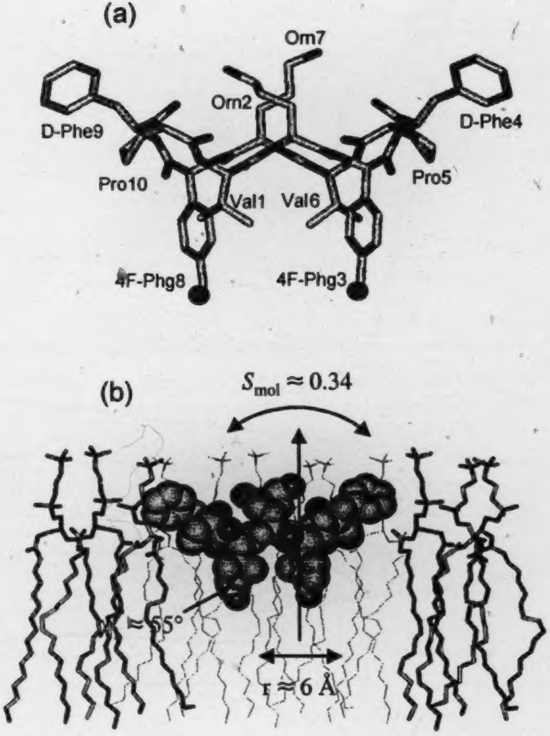
(a)
Orn7
Orn2
D-Phe9
D-Phe4
Pro10
Pro5
Val1
Val6
4F-Phg8
4F-Phg3
(b)
$S_{mol} \approx 0.34$
≈55°
r ≈ 6 Å

Figure 12. Panel A shows a model of the ^{19}F-labelled analog based on the structure of gramicidin S where the two original Leu side-chains are replaced by 4F-phenylglycine (4F-Phg). Panel B is the proposed structure and flat alignment of 4F-phenylglycine-substituted gramicidin S analog (F-GS) in liquid-crystalline DMPC bilayers for lipid:peptide molar ratios between 80:1 and 200:1. The values for the ^{19}F-^{19}F distance r, for the molecular order parameter S_{mol}, and for the 4F-Phg side-chain torsion angle χ_1, were determined as a self-consistent solution from the solid-state ^{19}F-NMR data (adapted from Salgado *et al.* (Salgado et al. 2001)).

complete freedom about the bilayer normal while 1 indicates complete rigidity). The intramolecular distance between the two 4F-phenylglycine probes (r) was 6±1 Å, similar to the calculated results for gramicidin S in solution (7.3 Å). Also, the torsion angle χ_1 of the 4F-phenylglycine side-chain was 55°, close to the value typical of β-sheets, 60°±10°. The study represented the first direct observation of an antimicrobial β-sheet peptide in its membrane-associated state, and illustrated one of the first applications of solid-state ^{19}F-NMR to a membrane-bound peptide.

Biophysical studies of various cyclic peptides related to gramicidin S indicate that GS14 (β-sheet) aggregated at concentrations greater than 50 μM in benign media and in lipid bilayers, while GS14K4 (disrupted β-sheet) did not (Jelokhani-Niaraki et al. 2002; Jelokhani-Niaraki et al. 2001). The reduction in amphipathicity and/or structural disruption in GS14K4 is thus beneficial not only in improving therapeutic index, but also by increasing peptide solubility over GS14.

Since amphipathic molecules with significant hydrophobicity of the nonpolar face would be expected to dimerize in aqueous benign media, it became obvious that a simple and sensitive method to measure dimerization ability of small amphipathic molecules would be critical in any rational design approach. Thus, we have developed a novel method referred to as "temperature profiling in reversed-phase chromatography" to measure the tendency for dimerization of amphipathic molecules.

This method relies on the assumptions that 1) during partitioning of the molecule in gradient elution, the molecule in solution is in equilibrium between dimer and monomer, and that 2) the amount of dimer in solution is dependent on temperature. Based on the second assumption, at low temperature, low retention time is attributed to dimerization;

as the temperature is increased, dimerization is disrupted and retention time increases as the concentration of monomer in solution during partitioning increases. The increase in monomer concentration means that the hydrophobic face of the molecule is more exposed in solution *vs.* the dimer form, allowing for greater partitioning with the hydrophobic stationary phase and giving a longer elution time. At even higher temperatures, the amount of dimer in solution becomes minimal and retention time no longer increases, but decreases with increasing temperature because of increased diffusion rates and peptide entropy in solution. The molecule GS14 can dimerize in aqueous solution, as indicated by the large T(Δt_Rmax) value (Fig. 13A). Reversed-phase gradient elution is carried out every 5°C, ranging from 5°C to 80°C, and the results are plotted as the change in retention time at temperature T ($\Delta t_R = t_{R,\,T} - t_{R,\,5°C}$) *versus* temperature. T(Δt_Rmax) is the temperature at which the maximum Δt_R value is obtained for each molecule. GS14 (β-sheet amphipathic peptide with six large hydrophobes) exhibits behavior consistent with dimerization at lower temperatures as indicated by the changes in Δt_R at increasing temperatures. GS14K4 (disrupted β-sheet with lysine on the nonpolar face) shows insignificant ability to dimerize and linear GS14K4 lin shows no dimerization ability throughout the entire temperature range used in this study.

Fig. 13B shows the elution profile of the three peptides at 80°C, a temperature at which all peptides are monomeric in solution. The elution order GS14K4 lin<GS14K4<GS14 is consistent with the order of amphipathicity of the three peptides, with the least amphipathic GS14K4 lin eluting first. These profiles further illustrate that GS14, which

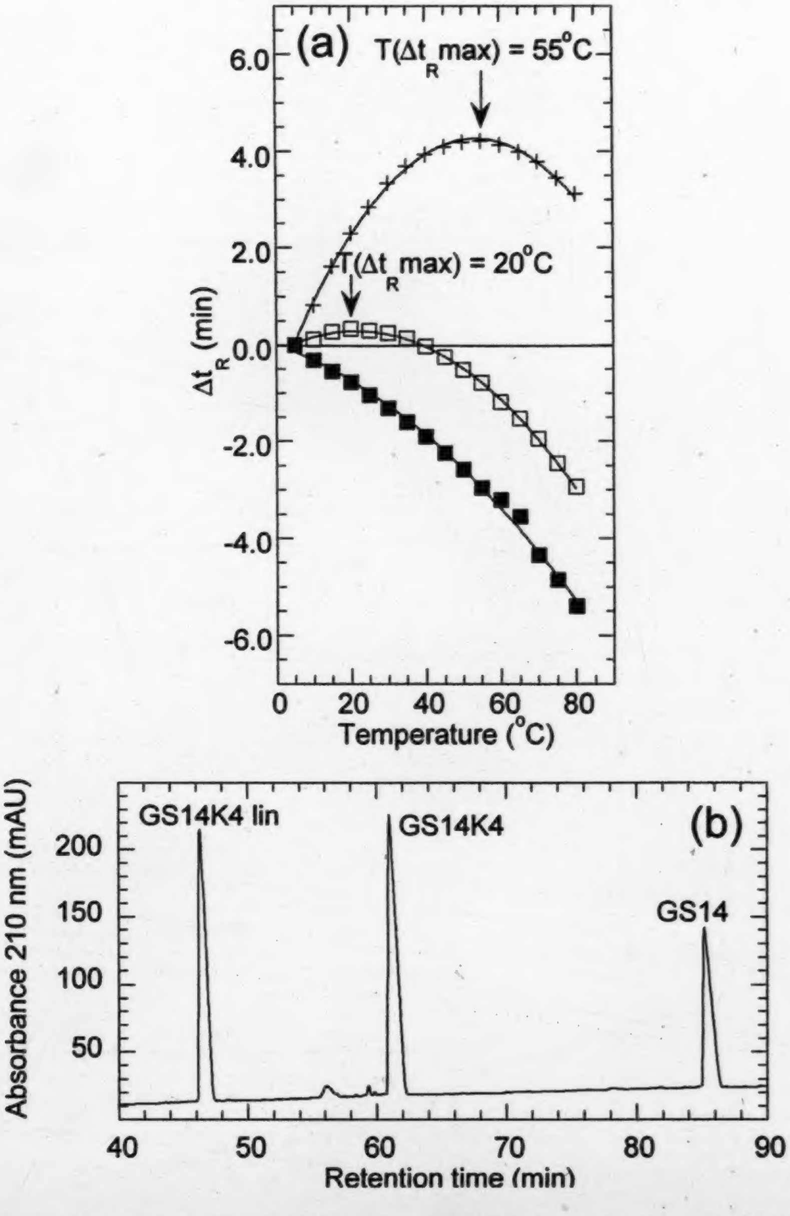

Figure 13. Panel A: Temperature profiling in reversed-phase chromatography. Cyclic peptides GS14 (+), GS14K4 (□), and the linear peptide GS14K4 lin (■) were analyzed at temperatures between 5°C and 80°C. The change in retention time (Δt_R) was the difference between retention time at temperature T and the retention time at 5°C ($t_{R,T} - t_{R,5°C}$). T(Δt_Rmax) was the temperature at which the maximum Δt_R was observed. Panel B: Reversed-phase elution profiles of GS14K4 lin, GS14K4, and GS14 at 80°C. Reversed-phase chromatography was performed with a linear AB gradient, where A is aqueous 0.05% TFA and B is 0.05% TFA in acetonitrile; gradient rate 0.5 %B/min (0.5% acetonitrile/min); flow rate 0.35 ml/min; column used was a Zorbax 300SB-C8, 2.1 mm I.D x 150 mm.

dimerizes in solution more than the other two peptides, does so because it possesses the largest nonpolar face of the three molecules. Also, the D-Lys residue on the hydrophobic face of GS14K4 significantly decreases the ability of the peptide to dimerize. The results of the linear GS14K4 lin peptide show that cyclization is required to maintain the nonpolar face, which then enhances the ability to dimerize.

Chapter I-11. Conclusions

We have taken a naturally occurring cyclic peptide antibiotic, gramicidin S, developed a facile protocol for a soluble, racemization-free chemical synthesis of gramicidin S and analogs, and systematically altered ring size, amphipathicity, structure, and overall hydrophobicity to examine the effect of these parameters on activity against microbial and eukaryotic membranes. The most efficacious peptide we have studied to date, GS14K4, showed significant favorable dissociation between antimicrobial and hemolytic activity, displaying broad-spectrum activity against Gram-negative bacteria, Gram-positive bacteria, and fungi with low toxicity to human cells in a marked improvement over the specificity of GS. Based on the results of these studies, it is our belief that a clinically useful broad-spectrum cyclic antimicrobial peptide can be rationally designed in our laboratory.

Chapter I-12. References

Ando, S., Nishihama, M., Nishikawa, H., Takiguchi, H., Lee, S. and Sugihara, G. 1995. Drastic reduction in antimicrobial activity by replacement of Orn residues with Lys in cyclized amphiphilic beta-structural model peptides. *Int J Pept Protein Res* **46:** 97-105.

Ando, S., Nishikawa, H., Takiguchi, H., Lee, S. and Sugihara, G. 1993. Antimicrobial specificity and hemolytic activity of cyclized basic amphiphilic beta-structural model peptides and their interactions with phospholipid bilayers. *Biochim Biophys Acta* **1147:** 42-49.

Aoyagi, H., Ando, S., Lee, S. and Izumiya, N. 1988. Synthesis of antibacterial peptides, gramicidin S analogs and designed amphiphilic oligopeptides. *Tetrahedron* **44:** 877-886.

Epand, R.M. and Vogel, H.J. 1999. Diversity of antimicrobial peptides and their mechanisms of action. *Biochim Biophys Acta* **1462:** 11-28.

Gause, G.F. and Brazhnikova, M.G. 1944. Gramicidin S and its use in the treatment of infected wounds. *Nature* **154:** 703.

Gibbs, A.C., Kondejewski, L.H., Gronwald, W., Nip, A.M., Hodges, R.S., Sykes, B.D. and Wishart, D.S. 1998. Unusual beta-sheet periodicity in small cyclic peptides. *Nat Struct Biol* **5:** 284-288.

Hancock, R.E. and Diamond, G. 2000a. The role of cationic antimicrobial peptides in innate host defences. *Trends Microbiol* **8:** 402-410.

Hancock, R.E. and Rozek, A. 2002. Role of membranes in the activities of antimicrobial cationic peptides. *FEMS Microbiol Lett* **206:** 143-149.

Hancock, R.E. and Scott, M.G. 2000b. The role of antimicrobial peptides in animal defenses. *Proc Natl Acad Sci U S A* **97:** 8856-8861.

Hutchinson, E.G. and Thornton, J.M. 1994. A revised set of potentials for beta-turn formation in proteins. *Protein Sci* **3:** 2207-2216.

Jelokhani-Niaraki, M., Prenner, E.J., Kay, C.M., McElhaney, R.N. and Hodges, R.S. 2002. Conformation and interaction of the cyclic cationic antimicrobial peptides in lipid bilayers. *J Pept Res* **60:** 23-36.

Jelokhani-Niaraki, M., Prenner, E.J., Kondejewski, L.H., Kay, C.M., McElhaney, R.N. and Hodges, R.S. 2001. Conformation and other biophysical properties of cyclic antimicrobial peptides in aqueous solutions. *J Pept Res* **58:** 293-306.

Kondejewski, L.H., Farmer, S.W., Wishart, D.S., Hancock, R.E. and Hodges, R.S. 1996a. Gramicidin S is active against both gram-positive and gram-negative bacteria. *Int J Pept Protein Res* **47:** 460-466.

Kondejewski, L.H., Farmer, S.W., Wishart, D.S., Kay, C.M., Hancock, R.E. and Hodges, R.S. 1996b. Modulation of structure and antibacterial and hemolytic activity by ring size in cyclic gramicidin S analogs. *J Biol Chem* **271:** 25261-25268.

Kondejewski, L.H., Jelokhani-Niaraki, M., Farmer, S.W., Lix, B., Kay, C.M., Sykes, B.D., Hancock, R.E. and Hodges, R.S. 1999. Dissociation of antimicrobial and hemolytic activities in cyclic peptide diastereomers by systematic alterations in amphipathicity. *J Biol Chem* **274:** 13181-13192.

Kondejewski, L.H., Lee, D.L., Jelokhani-Niaraki, M., Farmer, S.W., Hancock, R.E. and Hodges, R.S. 2002. Optimization of microbial specificity in cyclic peptides by modulation of hydrophobicity within a defined structural framework. *J Biol Chem* **277:** 67-74.

Krivanek, R., Rybar, P., Prenner, E.J., McElhaney, R.N. and Hianik, T. 2001. Interaction of the antimicrobial peptide gramicidin S with dimyristoyl-- phosphatidylcholine bilayer membranes: a densitometry and sound velocimetry study. *Biochim Biophys Acta* **1510:** 452-463.

Lewis, R.N., Prenner, E.J., Kondejewski, L.H., Flach, C.R., Mendelsohn, R., Hodges, R.S. and McElhaney, R.N. 1999. Fourier transform infrared spectroscopic studies of the interaction of the antimicrobial peptide gramicidin S with lipid micelles and with lipid monolayer and bilayer membranes. *Biochemistry* **38:** 15193-15203.

McInnes, C., Kondejewski, L.H., Hodges, R.S. and Sykes, B.D. 2000. Development of the structural basis for antimicrobial and hemolytic activities of peptides based on gramicidin S and design of novel analogs using NMR spectroscopy. *J Biol Chem* **275:** 14287-14294.

Morita, H., Kayashita, T., Takeya, K. and Itokawa, H. 1996. Conformational analysis of a cyclic heptapeptide, pseudostellarin D by molecular dynamics and Monte Carlo simulations. *Chem Pharm Bull (Tokyo)* **44:** 2177-2180.

Otvos, L., Jr., O, I., Rogers, M.E., Consolvo, P.J., Condie, B.A., Lovas, S., Bulet, P. and Blaszczyk-Thurin, M. 2000. Interaction between heat shock proteins and antimicrobial peptides. *Biochemistry* **39:** 14150-14159.

Prenner, E.J., Lewis, R.N., Jelokhani-Niaraki, M., Hodges, R.S. and McElhaney, R.N. 2001. Cholesterol attenuates the interaction of the antimicrobial peptide gramicidin S with phospholipid bilayer membranes. *Biochim Biophys Acta* **1510:** 83-92.

Prenner, E.J., Lewis, R.N., Kondejewski, L.H., Hodges, R.S. and McElhaney, R.N. 1999a. Differential scanning calorimetric study of the effect of the antimicrobial peptide gramicidin S on the thermotropic phase behavior of phosphatidylcholine, phosphatidylethanolamine and phosphatidylglycerol lipid bilayer membranes. *Biochim Biophys Acta* **1417:** 211-223.

Prenner, E.J., Lewis, R.N. and McElhaney, R.N. 1999b. The interaction of the antimicrobial peptide gramicidin S with lipid bilayer model and biological membranes. *Biochim Biophys Acta* **1462:** 201-221.

Prenner, E.J., Lewis, R.N., Neuman, K.C., Gruner, S.M., Kondejewski, L.H., Hodges, R.S. and McElhaney, R.N. 1997. Nonlamellar phases induced by the interaction of gramicidin S with lipid bilayers. A possible relationship to membrane-disrupting activity. *Biochemistry* **36:** 7906-7916.

Salgado, J., Grage, S.L., Kondejewski, L.H., Hodges, R.S., McElhaney, R.N. and Ulrich, A.S. 2001. Membrane-bound structure and alignment of the antimicrobial beta-sheet peptide gramicidin S derived from angular and distance constraints by solid state 19F-NMR. *J Biomol NMR* **21:** 191-208.

Schwyzer, R. 1958. *Chimia* **12:** 53-68.

Schwyzer, R., Garrion, J.P., Gorub, B., Nolting, H. and Tun-Kyi, A. 1964. *Helv Chim Acta* **47:** 441-464.

Sefler, A.M., Lauri, G. and Bartlett, P.A. 1996. A convenient method for determining cyclic peptide conformation from 1D 1H-NMR information. *Int J Pept Protein Res* **48:** 129-138.

Staudegger, E., Prenner, E.J., Kriechbaum, M., Degovics, G., Lewis, R.N., McElhaney, R.N. and Lohner, K. 2000. X-ray studies on the interaction of the antimicrobial peptide gramicidin S with microbial lipid extracts: evidence for cubic phase formation. *Biochim Biophys Acta* **1468:** 213-230.

Tamaki, M., Arai, I., Akabori, S. and Muramatsu, I. 1995. Role of ring size on the secondary structure and antibiotic activity of gramicidin S. *Int J Pept Protein Res* **45:** 299-302.

Tossi, A., Sandri, L. and Giangaspero, A. 2000. Amphipathic, alpha-helical antimicrobial peptides. *Biopolymers* **55:** 4-30.

van 't Hof, W., Veerman, E.C., Helmerhorst, E.J. and Amerongen, A.V. 2001. Antimicrobial peptides: properties and applicability. *Biol Chem* **382:** 597-619.

Wishart, D.S., Bigam, C.G., Holm, A., Hodges, R.S. and Sykes, B.D. 1995a. 1H, 13C and 15N random coil NMR chemical shifts of the common amino acids. I. Investigations of nearest-neighbor effects. *J Biomol NMR* **5:** 67-81.

Wishart, D.S., Kondejewski, L.H., Semchuk, P.D., Sykes, B.D. and Hodges, R.S. 1996. A method for the facile solid-phase synthesis of gramicidin S and its analogs. *Lett Pept Sci* **3:** 53-60.

Wishart, D.S., Sykes, B.D. and Richards, F.M. 1992. The chemical shift index: a fast and simple method for the assignment of protein secondary structure through NMR spectroscopy. *Biochemistry* **31:** 1647-1651.

Wu, M., Maier, E., Benz, R. and Hancock, R.E. 1999. Mechanism of interaction of different classes of cationic antimicrobial peptides with planar bilayers and with the cytoplasmic membrane of Escherichia coli. *Biochemistry* **38:** 7235-7242.

Xu, Y., Sugar, I.P. and Krishna, N.R. 1995. A variable target intensity-restrained global optimization (VARTIGO) procedure for determining three-dimensional structures of polypeptides from NOESY data: application to gramicidin S. *J Biomol NMR* **5:** 37-48.

Zasloff, M. 1987. Magainins, a class of antimicrobial peptides from Xenopus skin: isolation, characterization of two active forms, and partial cDNA sequence of a precursor. *Proc Natl Acad Sci U S A* **84:** 5449-5453.

Zasloff, M. 2002. Antimicrobial peptides of multicellular organisms. *Nature* **415:** 389-395.

Zhang, L., Dhillon, P., Yan, H., Farmer, S. and Hancock, R.E. 2000. Interactions of bacterial cationic peptide antibiotics with outer and cytoplasmic membranes of Pseudomonas aeruginosa. *Antimicrob Agents Chemother* **44:** 3317-3321.

Zhang, L., Rozek, A. and Hancock, R.E. 2001. Interaction of cationic antimicrobial peptides with model membranes. *J Biol Chem* **276:** 35714-35722.